Aronne Armanini

Principles of River Hydraulics

Principles of River Hydraulics

Aronne Armanini

Principles of River Hydraulics

Aronne Armanini
Department of Civil, Mechanical and
    Environmental Engineering
University of Trento
Trento
Italy

Translated by Giusi Zummo

To my family

Preface

The intention is to collect my lecture notes for the introduction to River Engineering, a subject I have been teaching to master's students in Environmental and Land Engineering at the University of Trento since 1987. This course is divided into two parts: the former is devoted to the fundamentals of river hydraulics, and the latter deals with calculation and design tools used for river restoration. In full regard to the location, the course especially focuses on mountain and piedmont streams which are subject to intense sediment transport and continuous morphological variations. This first volume contains the key topics of natural watercourse hydraulics. I deliberately left out, and took for granted, the topics conventionally dealt with in manuals of hydraulics, hydrodynamics and hydrology, as well as the problem of unsteady river flows addressed with the traditional fixed-bed approach. On the other hand, some hydraulics topics usually neglected in traditional text-books, for example, vegetation and macro-roughness effects on flows, are considered in the first chapter, in that they are typical of several gravel bed rivers. The other chapters are entirely devoted to mobile-bed river hydraulics. I also tried to emphasize a few aspects which in the past may have been neglected for a limited knowledge of phenomena but currently required to identify and solve some problems, for example, the effect of nonuniform sediments and mathematical modeling. The structure of the book is the same as many river hydraulics or sediment transport manuals, both classical like those by H. Walter Graf, M. Yalin, and Pieter Ph. Jansen et al., and most recent like Pierre Julien's; it also takes some important internet contributions by Gary Parker into account. Sometimes, the formulation of the problems may appear too analytical, which is undoubtedly helpful for engineering students but rather complex for those who will use it as a reference book for applications. In my opinion, however, the study of sediment transport and fluvial morphology has always been too empirical, without any attempt to take a theoretical look at the subject. Nowadays, such a method is outdated: as a matter of fact, design choices demonstrated a reckless disregard of long-term consequences on watercourse dynamics and, last but not least, hydraulic engineers were highly competent in the fixed-bed hydraulics, but somewhat reluctant to replace their conceptual frameworks inadequate for the study of natural water streams which are

simply mobile-boundary flows. This book first appeared in Italian in 1999 under the title *Principi di idraulica fluviale (Principles of River Hydraulics)*; this is the English version, revised and expanded. Special thanks are due to Giuseppina Zummo for her professional competence and accuracy in the English translation. I would like to thank Paolo Scarfiello for his valuable help with several graphs and charts of the book. I am deeply grateful to my colleagues of the Department of Civil and Environmental Engineering at the University of Trento for the precious moments of discussion on nearly all the topics covered in the book, especially to Michele Larcher, Giorgio Rosatti, and Luigi Fraccarollo. Finally, thank to Giulia Rossi for her precious help in reviewing the page proofs of the book.

Trento, Italy   Aronne Armanini
August 2017

Contents

Symbols

A	Cross-sectional area; area [L^2]
$\mathbf{F}$	Interparticle friction force [MLT^{-2}]
A_n	Coefficient (Chaps. 3 and 8) [$-$]
A_{pj}	Projected section of a plant (Chap. 1) [L^2]
$\mathbf{A_U}$	Matrix of coefficients (Chap. 7)
A_v	Coefficient [$-$]
A_λ	Coefficient (Chap. 7) [$-$]
A_τ	Coefficient related to the secondary circulations in a channel bend [$-$]
A_1	Coefficient [$-$]
A_*	Coefficient (Einstein, Chap. 5) [$-$]
a	Reference level for suspended load [L]
$a = (\mathbf{G} - \mathbf{B})/\overline{\mathbf{P}}$	Dimensionless threshold value (Einstein, Chap. 5) [$-$]
b	Length of a bridge abutment (Chap. 8) [L]
B, B_o	Width of the cross section [L]
B_r	Width of the cross section in a contraction (Chap. 8) [L]
B_g	Length of a groyne (Chap. 8) [L]
B_v	Coefficient [$-$]
$\mathbf{B}$	Buoyancy of a particle [MLT^{-2}]
B_λ	Coefficient (Chap. 7) [$-$]
B_1	Coefficient [$-$]
B_*	Coefficient (Einstein, Chap. 5) [$-$]
C	Areal or depth average solid concentration [$-$]
C_L	Particle lift coefficient [$-$]
C_D	Particle drag coefficient [$-$]
c	Local value of the particles volume concentration [$-$]
c_Z	Celerity of a simple wave (Chap. 7) [LT^{-1}]
c_w	Coefficient of the local scour (Chap. 8) [$-$]
d	Particle diameter [L]
d_j	Diameter of the jth grain size class [L]

d_n	Sieve diameter [L]
d_p	Average plant diameter (Chap. 1) [L]
d_s	Sedimentological diameter [L]
D	Drag force of a particle [MLT^{-2}]
D_{pj}	Drag of a single plant (Chap. 1) [MLT^{-2}]
D_p	Diameter of a bridge pile (Chap. 8) [L]
D_t	Triaxial diameter [L]
d_1, d_2, d_3	Longest, intermediate, and shorter dimensions of a particle (Chap. 1) [L]
$\overline{d}$	Mean particle diameter [L]
$D_* = d(g\,\Delta/v^2)^{1/3}$	Dimensionless particle diameter [L]
e_s	Nikuradse's equivalent roughness [L]
f	Darcy-Weisbach friction coefficient (or friction factor) $[-]$
F_r, F_{ro}	Froude number and undisturbed Froude number $[-]$
g	Gravity acceleration [LT^{-2}]
G	Weight of a particle [MLT^{-2}]
g_b	Weight sediment discharge per unit width [MT^{-3}]
H	Specific energy [L]
H_o, H_r	Undisturbed specific energy, specific energy in a contraction [L]
H_u, H_d	Upstream and downstream specific energy [L]
H_B	Height of alternated bars (Chap. 8) [L]
H_{dune}	Height of bed forms or dunes [L]
h, h_o	Flow depth; flow depth in uniform condition [L]
h_r	Flow depth in a contraction (Chap. 8) [L]
h_u, h_d	Flow depth in upstream or downstream section (Chap. 8) [L]
h_v	Vegetation height (Chap. 1) [L]
I	Identity matrix (Chap. 7) $[-]$
i_E	Energy gradient or energy slope $[-]$
i_b	Bed slope $[-]$
k_e	Equivalent roughness [L]
k_s	Strickler roughness coefficient [L$^{1/3}$T^{-1}]
$k_{s_{eq}}$	Equivalent Strickler roughness coefficient [L$^{1/3}$T^{-1}]
k_{so}	Strickler coefficient of bed roughness [L$^{1/3}$T^{-1}]
k_{s-veg}	Strickler coefficient of equivalent vegetation roughness [L$^{1/3}$T^{-1}]
k_v	Equivalent roughness of vegetation (Chap. 1) [L]
K_p, K_1, K_2, K_3	Shape coefficients for localized scours (Chap. 8) $[-]$
$K_{Fr}, K_h, K_d, K_{Sf}, K_\sigma$	Correction factors on the local scour for influence of the subscript parameters (Chap. 8) $[-]$
l	Length of a bridge pier or abutment (Chap. 8) [L]
L	Lift force on a particle [MLT^{-2}]
L_p	Average particle hop distance (Einstein) [L]

L_g	Distance between two consecutive groynes (Chap. 8) [L]
L_s, L_s'	Length of a scour hole (Chap. 8) [L]
L_*	Adaptation length (Chap. 7) [L]
n	Exponent (Chap. 8) $[-]$
m	Exponent (Chap. 8) $[-]$
MEI	Vegetation stiffness parameter (Chap. 1) $[\mathrm{ML}^{-1}\mathrm{T}^{-2}]$
n	Exponent $[-]$
n	Number of bedload layers according to Du Boys (Chap. 5) $[-]$
p	Bed porosity $[-]$
P_e	Wetted perimeter [L]
P_j	Probability $[-]$
p_n	Probability for a particle to be detached at least n times in the exchange time T_p (Einstein) $[-]$
P_r	Non-detachment probability of a particle (Einstein, Chap. 5) $[-]$
P_0	Probability $[-]$
Q	Liquid volumetric discharge $[\mathrm{L}^3\mathrm{T}^{-1}]$
Q_j	Liquid volumetric discharge of a sub-area $[\mathrm{L}^3\mathrm{T}^{-1}]$
Q_s	Solid volumetric discharge $[\mathrm{L}^3\mathrm{T}^{-1}]$
Q_s^*	Transport capacity (in adaptive models, Chap. 7) $[\mathrm{L}^3\mathrm{T}^{-1}]$
q	Liquid discharge per unit width $[\mathrm{L}^2\mathrm{T}^{-1}]$
q_{bj}^*	Transport capacity of the jth grain size class $[\mathrm{L}^2\mathrm{T}^{-1}]$
$q_s = q_b + q_{ss}$	Solid discharge per unit width $[\mathrm{L}^2\mathrm{T}^{-1}]$
q_s^*	Total transport capacity per unit width $[\mathrm{L}^2\mathrm{T}^{-1}]$
q_{ss}	Solid discharge in suspension (suspended load) per unit width $[\mathrm{L}^2\mathrm{T}^{-1}]$
$R = B_o/B_r$	Contraction ratio (Chap. 8) $[-]$
R_e	Reynolds number $[-]$
$Re_w = (w_s d)/v$	Grain Reynolds number (relative to the particle fall velocity) $[-]$
$Re_* = (u_* d)/v$	Grain Reynolds number (relative to the friction velocity) $[-]$
R_h	Hydraulic radius [L]
$r = \mathbf{P}/\overline{\mathbf{P}}$	Ratio between the instantaneous and the average particle lift (Einstein, Chap. 5) $[-]$
r_m, r_e, r_i	Curvature radius: average, on the extrados and on the intrados of a channel bend [L]
SF	Particle shape factor $[-]$
Sf_p	Shape factor of a bridge pier (Chap. 8) $[-]$
T	Transport stage parameter by Van Rijn $[-]$
T_p	Exchange time (Einstein, Chap. 5) [T]
$\mathbf{T}$	Matrix of coefficients of the system of equations of the bed evolution in canonical form $[-]$

t	Time
$\mathbf{U} = \{h, U, z_b\}$	Vector of variables (Chap. 7)
u	Velocity at distance y from the bed $[\mathrm{LT}^{-1}]$
U	Depth or areal average velocity $[\mathrm{LT}^{-1}]$
U_o, U_r	Average velocity in uniform flow condition or inside a contraction (Chap. 8) $[\mathrm{LT}^{-1}]$
U_u, U_d	Upstream and downstream average velocity (Chap. 8) $[\mathrm{LT}^{-1}]$
U_{cr}	Critical (incipient) particle velocity $[\mathrm{LT}^{-1}]$
u_s	Local velocity of the solid phase $[\mathrm{LT}^{-1}]$
$u_* = \sqrt{\tau_o/\rho}$	Friction velocity $[\mathrm{LT}^{-1}]$
$u_i, i = 1, 2, 3$	x_i component of the velocity vector $[\mathrm{LT}^{-1}]$
v_s	Difference in velocity between two consecutive layers in Du Boys's model (Chap. 5) $[\mathrm{LT}^{-1}]$
$w_i, i = 1, 2, 3$	x_i component of the fall velocity of a particle $[\mathrm{LT}^{-1}]$
w_s	Module of particle fall velocity $[\mathrm{LT}^{-1}]$
x	Longitudinal coordinate $[\mathrm{L}]$
$x_i, i = 1, 2, 3$	Generic coordinate $[\mathrm{L}]$
X_E	Einstein's roughness parameter (Chap. 5) $[\mathrm{L}]$
$Y = h/k_e$	Dimensionless submergence $[-]$
Y_E	Einstein's hiding parameter (Chap. 5) $[-]$
y	Vertical (or normal to the bed) coordinate $[\mathrm{L}]$
y_o	Reference level for the logarithmic velocity distribution $[\mathrm{L}]$
y_{sm}	Maximum scour depth (Chap. 8) $[\mathrm{L}]$
$y_s(t)$	Time evolution of local scour (Chap. 8) $[\mathrm{L}]$
y_{su}, y_{sd}	Maximum scour depth upstream and downstream of a contraction (Chap. 8) $[\mathrm{L}]$
$Z = w/(\beta_\varepsilon u_* \kappa)$	Rouse's exponent concentration distribution $[-]$
z	Transversal coordinate (in suspended load) $[\mathrm{L}]$
z_b	Bed level $[\mathrm{L}]$
α_b	Slope angle of the bed $[\mathrm{rad}]$
α_{cu}	Correction coefficient for solid discharge $[-]$
α_D	Coefficient $[-]$
α_l	Slope angle of the banks $[\mathrm{rad}]$
$\alpha_2, \alpha_3, \alpha_f, \alpha_y, \alpha_k$	Shape factors $[-]$
α_w	Coefficient (Einstein, Chap. 5) $[-]$
α_Ψ	Coefficient (Einstein, Chap. 5) $[-]$
$\beta = B/(2h), \beta_c$	Semi-aspect ratio, and its critical value for fluvial bar formation (Chap. 8) $[-]$
β_j	jth grain size percentage on the bed surface composition $[-]$
β_2	Correction coefficient for liquid (or total) momentum $[-]$
β_{c2}	Correction coefficient for solid momentum $[-]$
β_ε	Coefficient $[-]$

$\Delta = (\rho - \rho_s)/\rho$	Relative submerged density of sediment $[-]$
Δ_D	Dune height $[L]$
δ	Thickness of Hirano's mixing layer $[L]$
$\delta' = 11.6v/u_*$	Thickness of viscous sub-layer $[L]$
ε	Coefficient (Du Boys) $[-]$
ε	Turbulent diffusion coefficient $[-]$
$\varepsilon_1, \varepsilon_2$	Coefficients (Chap. 7)
$\eta = y/h$	Dimensionless normal (or vertical) coordinate $[-]$
η_o	Dimensionless thickness of the bedload layer $[-]$
θ	Shields mobility parameter $[-]$
θ_c, θ_{co}	Critical shields mobility parameter (quasi-horizontal straight bed) $[-]$
θ_{cb}	Critical mobility parameter in a sloping bed $[-]$
θ_{c-ls}	Critical mobility parameter in low submergence $[-]$
θ_{ccb}	Critical mobility parameter in a channel curve $[-]$
θ_{csb}	Critical mobility parameter in a channel side bank $[-]$
θ_o	Mobility parameter of the undisturbed (uniform) flow (Chap. 8) $[-]$
$\kappa = 0.41$	von Kármán constant $[-]$
κ_Z	Diffusion coefficient (Chap. 7) $[-]$
Λ_D	Length of the dunes $[L]$
Λ_v	Density of vegetation (Chap. 1) $[-]$
Λ_B	Average length of alternate bars (Chap. 8) $[L]$
λ	Shen parameter of the bed form resistance $[-]$
λ_i	Eigenvalues of the system of equations of the flow and bed evolution $[LT^{-1}]$
$\tilde{\lambda}_i = \lambda_i/\sqrt{gh}$	Dimensionless eigenvalues of the system of equations of the flow and bed evolution $[-]$
μ	Dynamic viscosity of water $[ML^{-1}T^{-1}]$
μ_f	Interparticle friction coefficient (Chaps. 3 and 5) $[-]$
$v = \mu/\rho$	Kinematic viscosity of water $[L^2T^{-1}]$
$\xi_j; \xi_{Ej}; \xi_{uj}$	Hiding factor of the jth grain size class $[-]$
ρ	Density of water $[ML^{-3}]$
ρ_s	Density of sediments $[ML^{-3}]$
σ	Standard deviation of lift fluctuations $[-]$
σ_g	Standard deviation of the grain size distribution $[-]$
τ	Shear stress $[ML^{-1}T^{-2}]$
τ_o	Bed shear stress $[ML^{-1}T^{-2}]$
τ_*	Adaptation time $[T]$
φ	Friction angle $[°]$
ϕ	Shape factor of a channel cross section (Chap. 1) $[-]$
ϕ	Index of the grain size distribution $[-]$

Φ	Dimensionless solid discharge (Einstein) $[-]$
Ψ	Flow intensity parameter (Einstein) $[-]$
χ	Chézy's roughness coefficient $[L^{1/2}T^{-1}]$

Superscripts or Subscripts

$()_b$	Bedload
$()_c$	Critical condition (incipient motion condition)
$()_D$	Dune
$()_j$	jth size class of sediments
$()_s$	Solid phase
$()_i$	x_i, $i = 1, 2, 3$ component
$()'$	Fluctuating component
$()^{\prime}$	Grain roughness
$()^{\prime\prime}$	Bed forms roughness
$()^{\prime\prime\prime}$	Interaction among grains
$\tilde{()}$	Instantaneous and local component

Chapter 1
Roughness in Fixed-Bed Streams

1.1 Introduction

The solid boundaries of a natural watercourse are usually composed of earth, sediments, and vegetation of different species, which together determine the resistance to the flow of water. From a hydraulic point of view, these parameters are treated as equivalent roughness. However, the hydraulic roughness is a major source of uncertainty in predicting the hydraulic parameters (velocity and depth) of the stream. On the other hand, the determination of hydrodynamic resistance of a natural stream is a rather complex operation.

When dealing with a flow resistance formula, in fact, it is worth referring to a uniform flow condition, i.e., a flow steady in time and homogeneous in the flow direction, although an exact condition of uniform flow is quite unlikely to occur in a natural stream, especially because of longitudinal variations in cross sections. Therefore, useful results for hydraulic engineering can be achieved only after making a number of sometimes significant simplifications.

In some cases in the natural watercourses, we can refer approximately to a quasi-uniform condition as the condition which would take place if we considered a straight prismatic channel with the same cross section as that in question.

Assuming that the fundamentals of the laminar and turbulent flow in cylindrical pipes are known, in that they are usually dealt with in standard textbooks on hydraulic or fluid mechanics, in this chapter we will summarize some results that can be used as reference for uniform motion in channels with *compact section* and *homogenous roughness* of small size compared to the water depth, and will focus some of the most common uniform flow formulae.

In Sect. 1.3.2, we will deal with motion problems in channels with roughness comparable to the water depth (*low submergence*).

We will then address the theme of the resistance due to vegetation, distinguishing between herbaceous vegetation, submerged shrubs, and emerging arboreal vegetation (Sect. 1.4).

In Sect. 1.5 we will describe how to treat compound channels and channels with floodplains.

Finally, we will describe some methods for calculating channel resistance with nonhomogeneous roughness along the perimeter (Sect. 1.6).

1.2   Uniform Flow in Circular Pipes

The conditions of uniform flow in a prismatic channel of any cross section are usually obtained by referring to the uniform flow in circular pipes (Fig. 1.1).

In this case, like in the two-dimensional plane flow, the symmetry of the flow allows to make considerable simplifications. Details of these topics can be found in traditional fluid mechanics and hydraulics books. Table 1.1 shows the main characteristics of the pipe flows: velocity distribution in the different regions and the resistance relations.

In Table 1.1, e_s denotes the Nikuradse equivalent sand grain roughness. The resistance law is thus obtained by integrating the velocity over the cross section.

The Darcy-Weisbach formula illustrated in Table 1.1 is the rational law of resistance. The friction factor f is a function of the Reynolds number $Re = UD/\nu$ and the relative equivalent roughness e_s/D. In addition to the rational formulae shown in Table 1.1, such a dependence can be derived from the empirical Moody diagram.

1.3   Uniform Flow in Compact Cross-Sectional Channels

The formulae on resistance, illustrated in Table 1.1, are usually extended to prismatic channels with a relatively compact cross section, that is, with cross sections whose water depth has the same order of magnitude as the surface width and whose roughness is more or less evenly distributed along the wetted perimeter. In these cases, the effective hydraulic radius is at most modified by multiplying it by an appropriate empirical shape coefficient (Marchi 1961) (Table 1.2) (Fig. 1.2).

Fig. 1.1 Scheme of velocity and shear stress distributions in a circular pipe
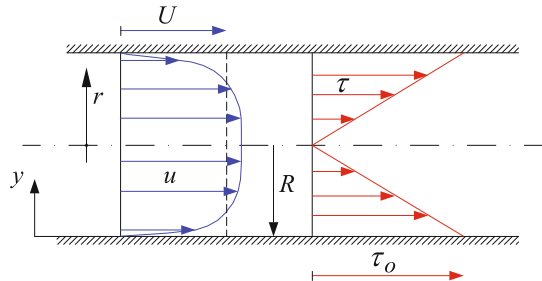
Table 1.1 Velocity distributions and resistance law in a circular pipe in uniform flow condition. y is the distance from the wall, and r is the radial distance from the center

smooth wall pipe

$$\frac{u}{u_*} = \frac{u_* y}{\nu} \qquad\qquad \text{for} \qquad \frac{u_* y}{\nu} \le 11.6$$

$$\frac{u}{u_*} = \frac{1}{\kappa} \ln \frac{u_* y}{\nu} + 5.62 \qquad \text{for} \qquad 11.6 \ge \frac{u_* y}{\nu} \le 70 \sim 100$$

$$\frac{u_{max} - u}{u_*} = \left(\frac{r}{R}\right)^2 \qquad \text{for} \qquad \frac{u_* y}{\nu} > 100 \qquad \frac{r}{R} \le 0.85$$

rough wall pipe

$$\frac{u}{u_*} = \frac{1}{\kappa} \ln \frac{y}{e_s} + 8.5 \qquad \text{for} \qquad \frac{u_* y}{\nu} \le 70 \sim 100$$

$$\frac{u_{max} - u}{u_*} = \left(\frac{r}{R}\right)^2 \qquad \text{for} \qquad \frac{u_* y}{\nu} > 100 \qquad \frac{r}{R} \le 0.85$$

$$\kappa = 0.4 \qquad\qquad \text{von Kármán constant}$$

resistance law

smooth pipes $\qquad\qquad \dfrac{U}{u_*} = \sqrt{\dfrac{8}{f}} = \dfrac{1}{\kappa} \ln \dfrac{u_* R}{\nu} + 1.75$

rough wall pipes $\qquad \dfrac{U}{u_*} = \sqrt{\dfrac{8}{f}} = \dfrac{1}{\kappa} \ln \dfrac{R}{e_s} + 4.75$

in general $\qquad\qquad \dfrac{U}{u_*} = \sqrt{\dfrac{8}{f}} = \dfrac{1}{\kappa} \ln \dfrac{R}{e_s} + \bar{B}\left(\dfrac{u_* e_s}{\nu}\right)$

Darcy-Weisbach formula: $\qquad i_E = \dfrac{f}{D} \dfrac{U^2}{2g}$
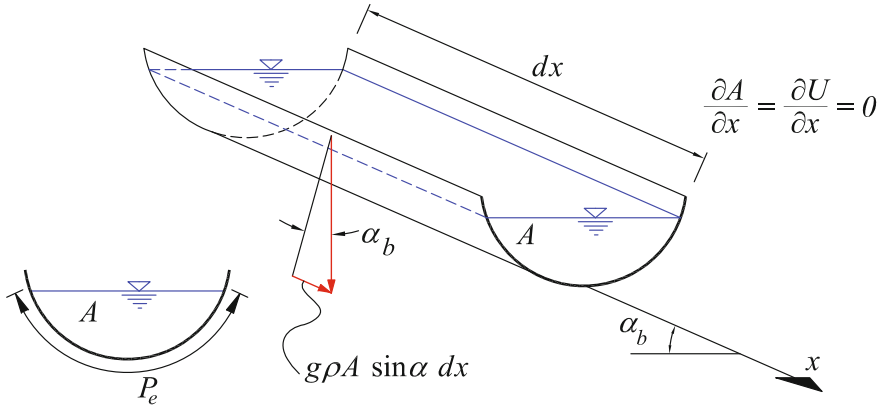
Fig. 1.2 Scheme of a channel in uniform flow

The velocity distribution and the formulae for resistance can also be applied to wide rectangular channels ($B >\sim 5$), by simply substituting the radial distance r with the distance from the wall y and the pipe diameter D with the hydraulic radius R_h or often with the water depth h multiplied by 4. By definition, the hydraulic radius is the ratio between the cross-sectional area A and the wetted perimeter P_e:

$$\int_{P_e} \tau_o \, dp_e = \overline{\tau_0} \, P_e = g \, \rho \, A \, \sin \alpha_b$$

$$\overline{\tau_0} = g \, \rho \, \frac{A}{P_e} \, \sin \alpha_b = g \, \rho \, R_h \, \sin \alpha_b$$

where α_b denotes the slope angle of the bed, P_e the wetted perimeter, and $R_h = A/P_e$ the hydraulic radius of the cross section.

Along with the Darcy-Weisbach equation, which can be considered a rational formula, empirical formulae are commonly used, which consider the resistance coefficient as only dependent either on the absolute roughness (Gauckler-Strickler's and Manning formulae) or on the relative roughness (Chézy's formula) (Table 1.2). Notwithstanding their purely empirical derivation, these formulae can well be applied to natural watercourses in that, on the one hand, the established regime is generally referred to a rough wall and, on the other, the uncertainty about determining the equivalent roughness makes some conceptual sophistications on the subject virtually useless. Strickler's formula can be converted into Chézy's:

$$k_s = \chi \, R_h^{-1/6} \qquad [\text{m}^{1/3}\text{s}^{-1}] \tag{1.1}$$

and, similarly, into Darcy-Weisbach's:

Table 1.2   Uniform flow relations in compact cross section open channels. $i_b = \tan \alpha_b \simeq \sin \alpha_b$ is the slope of the bed

compact-section channels
average tangential stress across the wall $\overline{\tau_0} = \dfrac{1}{P_e} \displaystyle\int_{P_e} \tau_0 \, dp_e$
uniform flow condition $\qquad\qquad \dfrac{1}{P_e} \displaystyle\int_{P_e} \tau_0 \, dp_e = \rho \, g \dfrac{A}{P_e} \sin \alpha_b \simeq \rho \, g R_h \, i_b$
friction velocity $\qquad\qquad\qquad u_* = \sqrt{\overline{\tau_0}/\rho}$

uniform flow formulae		
$\dfrac{\overline{\tau_0}}{\rho} = u_*^2 = U^2 \dfrac{f}{8}$	$Q = A \sqrt{\dfrac{8g}{f}} \, R_h^{1/2} \, i_b^{1/2}$	*Darcy-Weisbach*
$\dfrac{\overline{\tau_0}}{\rho} = u_*^2 = U^2 \dfrac{g}{\chi^2}$	$Q = A \chi \, R_h^{1/2} \, i_b^{1/2}$	*Chézy-Tadini*
$\dfrac{\overline{\tau_0}}{\rho} = u_*^2 = U^2 \dfrac{g}{k_s^2 \, R_h^{1/3}}$	$Q = A \, k_s \, R_h^{2/3} \, i_b^{1/2}$	*Gauckler-Strickler*
$\dfrac{\overline{\tau_0}}{\rho} = u_*^2 = U^2 \dfrac{n^2 g}{R_h^{1/3}}$	$Q = A \dfrac{1}{n} R_h^{2/3} \, i_b^{1/2}$	*Manning*

Darcy-Weisbach friction coefficient	
smooth wall	$\dfrac{1}{\sqrt{f}} = \dfrac{1}{\sqrt{8}} \left(\dfrac{1}{\kappa} \ln \dfrac{U R_h}{\nu} \sqrt{f} + 1.14 \right)$
	$\dfrac{1}{\sqrt{f}} = 2 \log_{10} \dfrac{U R_h}{\nu} \sqrt{f} + 0.4$
rough wall	$\dfrac{1}{\sqrt{f}} = \dfrac{1}{\sqrt{8}} \left(\dfrac{1}{\kappa} \ln \dfrac{R_h}{e_s} + 5.77 \right)$
	$\dfrac{1}{\sqrt{f}} = 2 \log_{10} \dfrac{R_h}{e_s} + 2.34$
in general	$\dfrac{1}{\sqrt{f}} = -2 \log_{10} \left(\dfrac{0.63}{\dfrac{U R_h}{\nu} \sqrt{f}} + \dfrac{e_s}{14.8 R_h} \right)$

channel shape effect	
shape factor (Marchi, 1961)	$R_h = \phi \, A/P_e$
equilateral triangle	$\phi = 1.25 \sim 1.3$
right-angled triangle	$\phi = 1.15 \sim 1.20$
semicircle	$\phi = 0.9$
semi-hexagonal trapezoid	$\phi = 0.9 \sim 1.0$
large trapezoid	$\phi = 0.80$
rectangle (B = 2h)	$\phi = 0.95$
arrow rectangle (B = 0.66h)	$\phi = 0.80$

Table 1.3 Gauckler-Strickler coefficients for natural streams (Chow 1959)

Strickler coefficient $[m^{1/3}s^{-1}]$	Max.	Norm.	Min.
Natural streams:			
Minor streams $(h < 3.5\,m)$			
(a) *Streams on plain*			
1. clean, straight, full stage, no rifts, or deep pools	40	33	30
2. same as above, but more stones and weeds	33	29	25
3. clean, winding, some pools, and shoals	30	25	22
4. same as 3, but some weeds and stones	29	22	20
5. same as 4, lower stages; more ineffective slopes, sections	25	21	18
6. same as 4, but more stones	22	20	17
7. sluggish reaches, weedy, deep pools	20	14	12
8. very weedy reaches, deep pools, or floodways with heavy stand of timber and underbrush	13	10	7
(b) *Mountain watercourses, no vegetation in channel, bank usually steep, trees and brush along banks submerged at high stages*			
1. bottom: gravels, cobbles, and few boulders	33	25	20
2. bottom: cobbles, large boulders	25	20	14

$$k_s = \sqrt{\frac{8\,g}{f}}\, R_h^{-1/6} \qquad [m^{1/3}s^{-1}] \tag{1.2}$$

In English-speaking countries, the Manning formula is preferred to Gauckler-Strickler's. The Manning coefficient n is the reciprocal of the Strickler coefficient. The Manning formula is often expressed in British metric units still today; in this case, it is written as:

$$Q = A\frac{k_n}{n} R_h^{2/3} i_b^{1/2} \tag{1.3}$$

where k_n is a conversion factor: $k_n = 1.486$ for English units and $k_n = 1.0$ for SI units.

There is no criterion which allows to establish that one formula is better than another. However, in applications to channel flows, the recourse to Gauckler-Strickler's or to Manning formula is quite frequent, in that the respective coefficient depends to a lesser extent on the hydraulic radius and thus, basically, on the absolute roughness of the wall, at least under high submergence condition.

Tables 1.3 and 1.4 show some values of the Strickler coefficient for different types of roughness taken from Chow (1959). Chow's original tables are related to the Manning coefficient n $[m^{-1/3}\,s^1]$, which has been converted to a Strickler coefficient $k_s = 1/n$ $[m^{1/3}\,s^{-1}]$, whose values are truncated to the unit.

Table 1.4 Gauckler-Strickler coefficients for artificial watercourses (Chow 1959)

Strickler coefficient $[\mathrm{m}^{1/3}\mathrm{s}^{-1}]$	Max.	Norm.	Min.
Excavated or dredged channels			
(a) *Earth, straight and uniform*			
1. clean, recently completed	62	56	50
2. clean, after weathering	56	45	40
3. gravel, uniform section, clean	45	40	33
4. with short grass, few weeds	45	37	30
(b) *Earth, winding and sluggish*			
1. no vegetation	43	40	33
2. grass, some weeds	40	33	30
3. dense weeds or aquatic plants in deep channel	33	29	25
4. earth bottom and rubble sides	36	33	29
5. stony bottom and weedy banks	40	29	25
6. cobble bottom and clean sides	33	25	20
(c) *Excavated or dredged channels*			
1. no vegetation	40	36	30
2. light brush on banks	29	20	17
(d) *Rock cuts*			
1. smooth and uniform	40	29	25
2. jagged and irregular	29	25	20
(e) *Channels not maintained, weeds and brush uncut*			
1. dense weeds, high as flow depth	20	12	8
2. clean bottom, brush on sides	25	20	12
3. same, highest stage of flow	22	14	9
4. dense brush and high stage	12	10	7

1.3.1   Secondary Circulations

A particular aspect of flow in open channels is represented by secondary circulations that appear in proximity to angles and to the free surface. One of the most evident effects produced by these secondary circulations is the maximum velocity occurring below the free surface. If, according to the Boussinesq diffusive model, the tangential stresses went to zero in proximity to the velocity maxima, the longitudinal component of the weight of the fluid volume comprised between the line connecting the velocity maxima and the free surface (dotted area in Fig. 1.3) would not be balanced by any force. This inconsistency is explained by the presence of a secondary circulation, in other words by a positive net momentum flux across the line of maxima, as well as by the fact that the Boussinesq diffusive model is likely to be inadequate in those conditions.
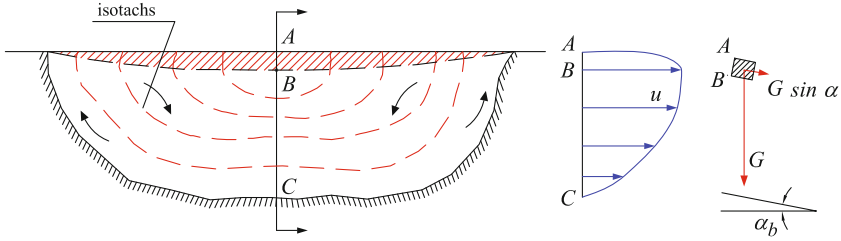
Fig. 1.3 Effect of secondary circulations in proximity to the free surface

1.3.2 Low Submergence Flow

One of the characteristics of mountain streams is the relatively elevated size of the roughness elements. In some cases, roughness k_e and water depth h are even nearly the same size:

$$Y = \frac{h}{k_e} = O(1) \quad (<\sim 4)$$

This is known as a situation of *low submergence*. In this case, in proximity to the bed there is a *macro-roughness layer*, where the velocity distribution along the depth tends to become more uniform than in case of high submergence. At the same time, the Reynolds stress tends to be suppressed (Nakagawa et al. 1991), which is accounted for by the existence of a series of secondary circulations generated by the roughness elements.

A more convincing explanation (Nikora et al. 2001) is that in case of low submergence, the spatial heterogeneities due to roughness elements affect the flow field so greatly that the flow cannot be considered any longer as homogeneous at the depth scale, since the flow depth is of the same order of magnitude as the roughness elements.

It is also convenient to perform a space average of the velocity over bed-parallel planes (*double averaging*), in addition to the time average. This double average is indicated with the symbol $< \overline{u} >$.

The double-averaged velocity $< \overline{u} >$ follows a nearly linear distribution within the macro-roughness layer and a logarithmic distribution in the layer immediately above (Fig. 1.4).

$$\frac{< \overline{u} >}{u_*} = C_1 \frac{y}{\delta_R} \quad \text{for } 0 \leq y \leq \delta_R \tag{1.4}$$

while the logarithmic sub-layer is characterized by the following distribution:

$$\frac{< \overline{u} >}{u_*} = \frac{1}{\kappa} \ln \frac{y}{\delta_R} + C_1 \text{ for } y \geq \delta_R \tag{1.5}$$

Fig. 1.4 Velocity distribution in case of low submergence, according to Nikora et al. (2001)
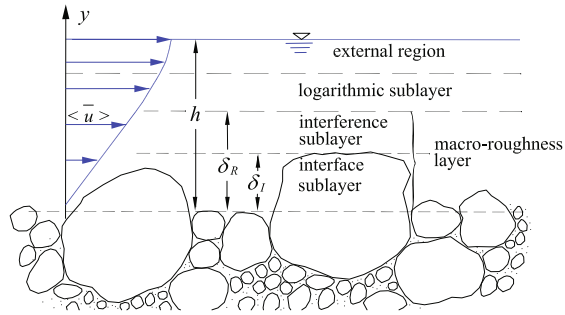
where $\delta_R \simeq \delta_I$ represents the thickness of the macro-roughness layer, while δ_I is the thickness of the interface sub-layer occupied by the grains, and C_1 a constant that takes values between 3 and 7.

As a result of the process of double averaging, in the momentum balance additional stresses appear: they are called *dispersive stresses* and, when added to the Reynolds stresses, they lead to a triangular distribution of the total stress in uniform flow conditions.

Under slightly larger submergence ($\sim 10 > h/d_{85} > \sim 5$), as a first approximation we can extend the validity of the logarithmic law to the entire water depth h:

$$\frac{u}{u_*} = \frac{1}{\kappa} \ln \frac{y}{d_s} + B_r \tag{1.6}$$

where d_s is the size of bed grains. In case of low submergence, constant B_r (Keulegan's constant) was observed (Graf 1991) to assume lower values ($B_r = 3.26$) than 8.5 which characterizes high submergence. However, we should remind that the constant of the logarithmic law practically depends on the definition of equivalent roughness: the above considerations are to be taken into account when we assume the Nikuradse criterion to define the equivalent roughness.

The formula for bed uniform flow under these conditions is obtained by generalizing the resistance law for circular pipes:

$$\frac{U}{u_*} = \sqrt{\frac{8}{f}} = A_1 \ln X + B_1 \tag{1.7}$$

In the literature, diverse numerical values and parameters have been suggested for this expression. The most used are given in Table 1.5.

The diversity of the parameters used to express the relative roughness and of the numerical values in the formulae is often due to the difference in operating conditions used by authors, especially with regard to the different level of imbrication or exposure of single particles, as well as to the uncertainty about defining the bed level of reference. The logarithmic law is often substituted with a power law:

Table 1.5 Parameter values of Eq. (1.7) proposed by various authors

A_1	B_1	X	Range of application	Authors	
2.90	0.70	$\dfrac{h}{d_{50}}$	$2.2 \leq \dfrac{h}{d_{90}} \leq 31$	Bray (1982)	
2.80	1.72	$\dfrac{h}{d_{65}}$			
2.49	3.02	$\dfrac{h}{d_{84}}$	$1 \leq \dfrac{R_h}{d_{65}} \leq 14$	Hey (1979)	
$2.457 \left(1 - \dfrac{0.1\,k_e}{R_h}\right)$	0	$12\dfrac{R_h}{k_e}$	$\dfrac{h}{d_{84}} > 1.2$	Thompson and Campbell (1979)	(1)
2.43	2.15	$\dfrac{R_h}{d_{50}}$	$1 \leq \dfrac{R_h}{d_{50}} \leq 200$	Griffiths (1981)	
2.5	2.88	$\dfrac{R_h}{d_{84}}\left(\dfrac{h_m}{R_h}\right)^{0.314}$	$0.3 \leq \dfrac{R_h}{d_{84}} \leq 1$	Bathurst (2002)	(2)
2.48	3.1	$\dfrac{R_h}{d_{84}}$	$\dfrac{h}{d_{50}} > 1$	Bray (1979)	
2.80		$\dfrac{h_m}{M\,d_{84}}$	$\dfrac{h}{d_{50}} > 1$	Colosimo et al. (1988)	(3)
3.28	2.43	$\dfrac{R_h}{d_{84}}$	Gravel bed	Limerinos (1970)	
2.5	3.25	$\dfrac{R_h}{d_{50}}$	$1 \leq \dfrac{R_h}{d_{50}} \leq 50$	Graf et al. (1987)	

(1) Authors suggest: $k_e = 4.5\,d_{50}$

(2) h_m = maximum water depth in the cross section;

(3) The formula suggested by Colosimo et al. (1988) also takes into account both cross-sectional shape by means of parameter b and particle size composition of the material by means of parameter M $B_1 = 1.12\,(8.5 - 2.5(1 - b))$ with $b = \ln(1 + 2\dfrac{h_m}{w} - \dfrac{h_m}{w})$; h_m and w are, respectively, the average water depth and the average cross-sectional width. M, the uniformity module of the granulometric curve, is defined as $M = (A_1 + A_2)/A_2$, where A_1 and A_2 are the areas subtended by the particle size curve (Chap. 2)

$$\frac{U}{u_*} = \sqrt{\frac{8}{f}} = a\ Y^b \tag{1.8}$$

By comparing Eq. (1.8) with the Gauckler-Strickler formula (Table 1.2) with the coefficient expressed by Eq. (1.2), we deduce that exponent b is equivalent to $1/6 \simeq 0.167$. On the other hand, the values observed experimentally have higher

Table 1.6 Parameter values of the power formula (1.8) suggested by various authors

a	b	Y	Validity field	Authors
8.30	0.167	$\dfrac{R_h}{d_{90}}$	gravel bed and cobbled bed	Meyer-Peter and Müller (1948)
6.74	0.167	$\dfrac{R_h}{d_{50}}$	gravel bed and cobbled bed	Strickler (1923)
3.85	0.281	$\dfrac{h}{d_{50}}$	$2.2 \leq \dfrac{h}{d_{90}} \leq 31$	Bray (1979)
4.19	0.277	$\dfrac{h}{d_{65}}$	,,	,,
5.03	0.268	$\dfrac{h}{d_{90}}$	,,	,,
5.4	0.26	$\dfrac{R_h}{d_{84}}$	$\dfrac{h}{d_{50}} > 1$	Bray and Davar (1987)
4.19	1.80	$\dfrac{R_h}{d_{84}}$	$i \sim 0.06$ step-pool	Lee and Ferguson (2002)
3.84	0.547	$\dfrac{R_h}{d_{84}}$	$0.002 < i < 0.008$ $\dfrac{h}{d_{84}} < 11$	Bathurst (2002)
3.10	0.93	$\dfrac{R_h}{d_{84}}$	$0.008 < i < 0.04$ $\dfrac{h}{d_{84}} < 11$	Bathurst (2002)

exponents, as can be seen in the table below. Table 1.6 shows the literature values for the parameters of Eq. (1.8).

Among those mentioned, some formulae were worked out in conditions of not extremely low submergence, that is, in gravel beds and cobbled beds; they are also widely used in fluvial beds, still nowadays. They are rewritten below with reference to coefficient k_s of the Gauckler-Strickler formula:

$$Q = A \; k_s \; R_h^{2/3} \; i_E^{1/2}$$

- *Strickler formula* (Strickler 1923), with reference to d_{50} of the bed material:

$$k_s = \frac{21.1}{d_{50}^{1/6}} \quad [d_{50}] = [\,\mathrm{m}\,]; \quad [k_s] = [\,\mathrm{m}^{1/3}\mathrm{s}^{-1}\,] \tag{1.9}$$

- *Meyer-Peter and Müller formula* (Meyer-Peter and Müller 1948), referred to d_{90}, diameter which best represents the roughness compared to d_{50}:

$$k_s = \frac{26}{d_{90}^{1/6}} \quad [d_{90}] = [\,\mathrm{m}\,]; \quad [k_s] = [\,\mathrm{m}^{1/3}\mathrm{s}^{-1}\,] \tag{1.10}$$

• *Limerinos formula* (Limerinos 1970), calibrated on a great number of Californian watercourses:

$$k_s = \frac{1.16 + 0.86 \ln \dfrac{R_h}{d_{84}}}{0.113 R_h^{1/6}} \quad [d_{84}] = [\,\mathrm{m}\,]; \quad [k_s] = [\,\mathrm{m}^{1/3}\mathrm{s}^{-1}\,] \tag{1.11}$$

If, instead of Strickler's, we used Chézy's, according to Limerinos the Chézy coefficient would become:

$$\chi = \frac{1.16 + 0.86 \ln \dfrac{R_h}{d_{84}}}{0.113} \quad [\,\mathrm{m}^{1/2}\mathrm{s}^{-1}\,] \tag{1.12}$$

1.4 Resistance Due to Vegetation

The resistance offered by vegetation needs to be dealt with specifically, in that this roughness type is flexible and permeable.

The presence of vegetation on the wetted perimeter of a stream can imply a considerable increase in the equivalent roughness, and thus an appreciable rise in flow resistance, as is shown from the following figures concerning flexible herbaceous vegetation.

In Fig. 1.5, the first part of the solid line ($h \leq\sim 0.6\,\mathrm{m}$) corresponds to a flow between the grass interstices, whereby the resistance to motion is very large. The second part of the same curve ($\sim 0.6 \geq h \leq\sim 0.8\,\mathrm{m}$) corresponds to a flow partially through the vegetation and partially above the vegetation. In the third section ($h \geq\sim 0.8\,\mathrm{m}$), water flows mainly above the grass, thus making the river bed wall smoother.

Figure 1.6 shows the same phenomenon in terms of equivalent roughness variation.

The technical literature on the subject is rather unsystematic. To deal systematically with the problem, we should distinguish between flexible grassy vegetation and inflexible vegetation or bushy shrub type. We still need to discriminate between completely submerged vegetation and emergent vegetation with respect to the free surface.

1.4.1 Channels with Fully Submerged Flexible Vegetation

Also in case of fully submerged vegetation, a layer was observed close to the wall and dominated by the roughness offered by vegetation (Fig. 1.7).

Fig. 1.5 Bermudagrass effect on the average velocity in an agricultural drainage channel. The continuous curve represents the vegetated channel, and the dotted curve indicates the same channel without vegetation ($k_s = 33 \text{ m}^{1/3}\text{s}^{-1}$) (Przedwojski et al. 1995)

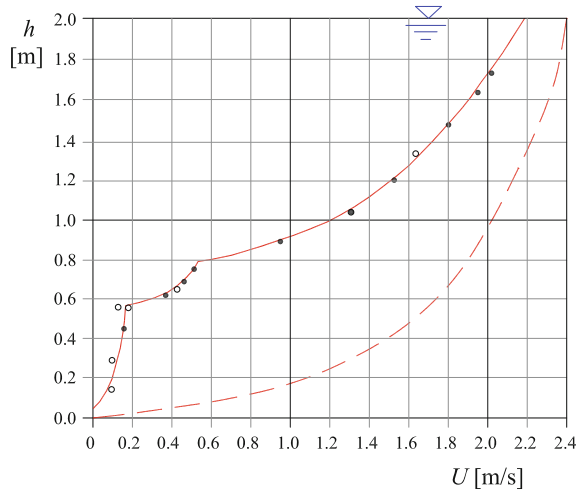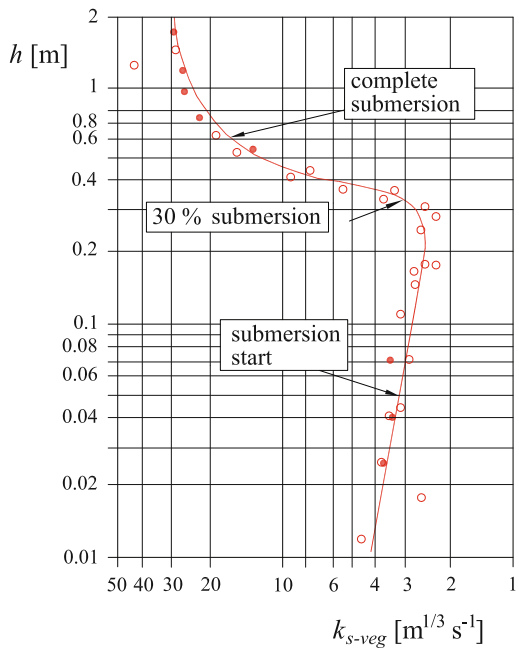**Fig. 1.6** Bermudagrass effect ($h_{veg} = 0.2$ m) on the roughness coefficient as the level varies (Przedwojski et al. 1995)

In order to estimate effects of vegetation on flow resistance, it is worth referring to the Darcy-Weisbach expression, by supposing the existence of a layer dominated by wall turbulence, and consequently by a logarithmic resistance law.
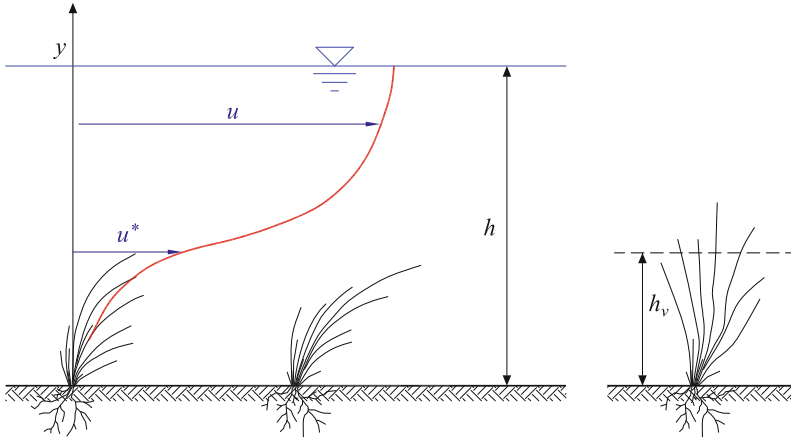
Fig. 1.7 Scheme of velocity profiles observed over flexible vegetation

$$\sqrt{\frac{1}{f}} = A_v \ln \frac{h}{k_v} + B_v \tag{1.13}$$

Coefficients A_v and B_v depend on the type and state of vegetation. Various parameter values have been suggested for agricultural drainage channels. The following Table 1.7 shows some literature values for the roughness coefficient: k_v denotes the equivalent roughness due to vegetation. The choice for this parameter clearly affects the value of constants (especially B_v). In fact, a possibility of defining vegetation roughness is to assume the same vegetation height as k_v value.

For wide channels, the ratio h/k_v is equivalent to the ratio between the area of the wetted cross section S and that occupied by vegetation S_v. Thus, (1.13) can be rewritten as such:

$$\sqrt{\frac{1}{f}} = A_{1v} \ln \frac{S}{S_v} + B_{1v} \tag{1.14}$$

Kouwen (Kouwen and Unny 1973; Kouwen 1988) proposed a criterion for defining the equivalent roughness, which takes vegetation flexibility into account; k_v is made dependent on vegetation stiffness by means of parameter *MEI*, which implicitly considers the spatial vegetation density as well (Fig. 1.8):

$$k_v = 0.14\, h_{veg} \left(\frac{\left(\frac{MEI}{\tau_o} \right)^{0.25}}{h_{veg}} \right)^{1.59} \tag{1.15}$$

h_{veg} denotes the average plant height. As to the *stiffness parameter MEI*, for the *green vegetation* we have:

Table 1.7 Values of parameters of Eq. (1.13) proposed by various authors

Vegetation type	A_v	B_v	Authors
aquatic plants (*alisma plantago*)	4.28	1.24	Keulegan (1938)
elodea (*elodea canadensis*), cerastium (*callitriche*), and algae	1.61	0.32	Plate and Quraishi (1965)
grass-wrack pondweed (*potamogeton compressus*), aquatic plants (*alisma plantago*), algae (*cladophora*), elodea	5.22	1.19	Keulegan (1938)
floating sweet grass (*glyceria fluitans*), curlyleaf pondweed (*potamogeton crispus*) and sago pondweed (*potagemon pectinatus*)	2.55	1.45	Plate and Quraishi (1965)
floating sweet grass (*glyceria fluitans*), curlyleaf pondweed (*potamogetoncris-pus*)	2.09	0.70	Plate and Quraishi (1965)

Table 1.8 Suggested values for the parameters in Eq. (1.14)

Vegetation type	B_{1v}	A_{1v}
Erect vegetation	0.15	1.85
Prone vegetation	2.69–3.50	0.20–0.29

$$MEI = 319\, h_{veg}^{3.3} \quad [MEI] = [\,\mathrm{N/m^2}\,]\; ;\; [h_{veg}] = [\,\mathrm{m}\,] \tag{1.16}$$

while for the *dormant vegetation* we have:

$$MEI = 25.4 h_{veg}^{2.26} \quad [MEI] = [\,\mathrm{N/m^2}\,]\; ;\; [h_{veg}] = [\,\mathrm{m}\,] \tag{1.17}$$

No indications being given on the state of vegetation, Kouwen (1988) suggested the following expression averaging the two cases:

$$MEI = 233\, h_{veg}^{3.125} \quad [MEI] = [\,\mathrm{N/m^2}\,]\; ;\; [h_{veg}] = [\,\mathrm{m}\,] \tag{1.18}$$

The constants A_{1v} and B_{1v} of Eq. (1.13) basically depend on the fact that the vegetation is *erect* or *prone* (Table 1.8).
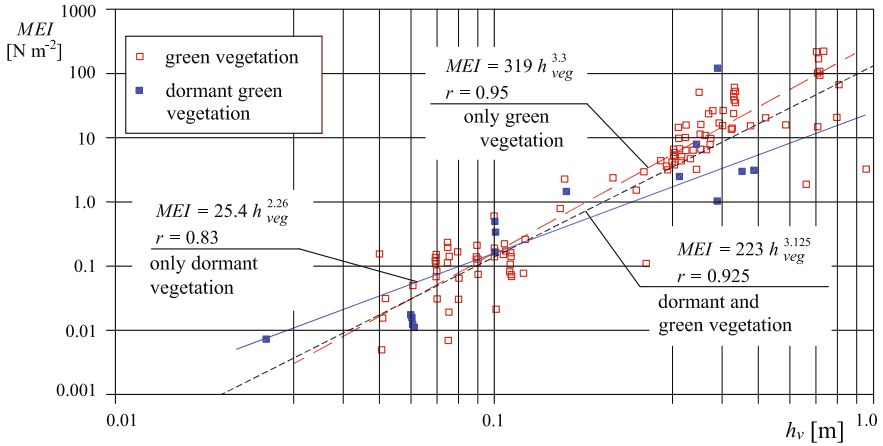
Fig. 1.8 Stiffness parameter value as a function of vegetation height (Kouwen 1988)
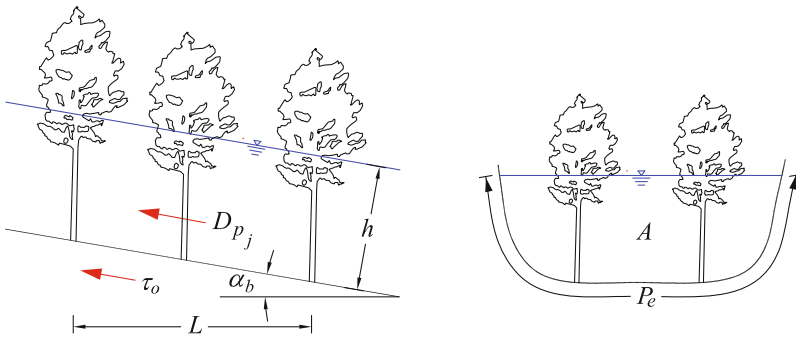

Fig. 1.9 Scheme of the roughness calculation in the presence of rigid emergent stems

It is worth reminding that Kouwen's formula cannot be applied to higher vegetation than the water depth.

1.4.2   Channels with Emergent Vegetation

In case of rigid plants or bushes, unevenly distributed along the watercourse wall, the total resistance is worked out by analyzing the resistance provided by the single plants.

Let then a stream section of length L be considered and the wetted perimeter be denoted with P_e (Fig. 1.9).

In uniform flow, the component in the longitudinal direction of the weight of the fluid contained in the control volume $\rho\, gALi_E$ is balanced by the stresses acting on

Fig. 1.10 Scheme of a plant
section
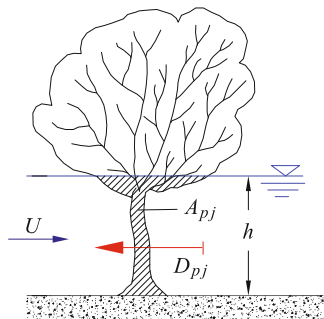
the wetted perimeter $\tau_o \, P_e \, L$, and by the sum of hydrodynamic resistances offered
by the plants present in the control volume $\sum D_{pj}$:

$$\rho \, gALi_E = \tau_o \, P_e \, L + \sum D_{pj} \tag{1.19}$$

where $i_e = i_b = \tan \alpha_b \simeq \sin \alpha_b$ is the energy slope, which in uniform flow is parallel
to the bed slope (Fig. 1.10).

The resistance offered by a single plant can be expressed in function of the drag
coefficient C_D, the average plant section A_{pj}, and the averaged velocity on the cross
section U:

$$D_{pj} = C_D \, \rho \, A_{pj} \frac{U^2}{2} \tag{1.20}$$

By substituting, we have:

$$\rho \, g \, A \, L \, i_E = \tau_o \, P_e \, L + \sum C_D \, \rho \, A_{pj} \frac{U^2}{2}$$

$$i_E = \frac{\tau_o}{\rho \, g} \frac{P_e}{A} + \frac{1}{g \, A \, L} \frac{U^2}{2} \sum C_D \, A_{pj} \tag{1.21}$$

The energy slope i_E is expressed by using the Strickler formula, in which an
equivalent friction coefficient $k_{s_{eq}}$ is introduced:

$$i_E = \frac{U^2}{k_{s_{eq}}^2 \, R_h^{4/3}} \tag{1.22}$$

and, by means of the same formula, τ_o is expressed in function of Strickler's coeffi-
cient for unvegetated bed:

$$\frac{\tau_o}{\rho \, g \, R_h} = \frac{U^2}{k_{so}^2 \, R_h^{4/3}} \tag{1.23}$$

Table 1.9 Typical geometric vegetation parameters as a function of type diversity (DVWK 1991)

Vegetation type	Development stage	d_p [m]	a_x [m]	a_y [m]
Distributed vegetation				
• reed bed		0.003–0.01	0.01–0.03	0.01–0.03
• shrubs	1 year	0.03	0.25–0.35	0.25–0.35
• willows	more years	0.03–0.06	0.15–0.25	0.15–0.25
Trees				
• birch (Betula alba)	5 years	0.04–0.10	1.0–5.0	1.0–5.0
	>5	0.15–0.50	3.0–10.0	3.0–10.0
	only trunks	0.5–1.0	10.0–20.0	5.0–15.0
Isolated plants or groups of trees				
• bushes	more years	3.5	3.5–10.0	3.0–10.0
• groups of trees	more years	1.0	10.0	10.0

By substituting Eqs. (1.22) and (1.23) into Eq. (1.21), we obtain:

$$\frac{U^2}{k_{s_{eq}}^2 \, R_h^{4/3}} = \frac{U^2}{k_{so}^2 \, R_h^{4/3}} + \frac{U^2}{2\,g} \sum C_D \, \frac{A_{pj}}{A\,L}$$

$$\frac{1}{k_{s_{eq}}^2} = \frac{1}{k_{so}^2} + R_h^{4/3} \frac{1}{2\,g} \sum C_D \, \frac{A_{pj}}{A\,L} = \frac{1}{k_{so}^2} + \frac{1}{k_{s-veg}^2} \tag{1.24}$$

Thus, Eq. (1.24) defines the Strickler coefficient related to vegetation:

$$\frac{1}{k_{s-veg}^2} = R_h^{4/3} \frac{1}{2\,g} \sum C_D \, \frac{A_{pj}}{A\,L} = R_h^{4/3} \frac{1}{2\,g} \sum C_D \, \frac{A_{pj} \, P_e}{A\,L\,P_e}$$

$$= R_h^{1/3} \frac{1}{2\,g} \sum C_D \, \frac{A_{pj}}{L\,P_e} \tag{1.25}$$

In the last term of (1.25), the ratio ($\sum A_{pj}/L\,P_e$) represents the density of the plants. For convenience's sake, this definition usually includes the coefficient C_D which generally assumes values close to unit.

$$\Lambda_v = \sum C_D \, \frac{A_{pj}}{L\,P_e} = C_D \, \frac{h\,d_p}{a_x\,a_y} \tag{1.26}$$

thus defines the density of vegetation. d_p is the average diameter of the plant trunk, and a_x and a_y are the averaged distances between plants in the longitudinal and transverse directions, respectively. Recurring values of these parameters, specially used in river renaturalization projects, are shown in the following table (Table 1.9).

In short, we have (Petryk and Bosmajian 1975; DVWK 1991):

$$k_{s_{eq}} = \frac{k_{so}}{\sqrt{1 + \dfrac{1}{2\,g}\,C_D\,\dfrac{h\,d_p}{a_x\,a_y}k_{so}^2\,R_h^{1/3}}} \tag{1.27}$$

where:

d_p average plant diameter [m];
C_D =1.0–1.5 drag coefficient;
a_x distance between plants in the flow direction;
a_z distance between plants in the transverse flow direction;
R_h hydraulic radius of the cross section;
k_{so} Strickler coefficient of the bed [$m^{1/3}$/s].

Planting shrubby vegetation along watercourse banks has recently become a wide-spread practice. This river restoration technique is included in most river renaturalization projects (Florineth 1982, 1993). The effect on total resistance increase is particularly significant in minor watercourses, where the width can be compared with the water depth. However, the problem must be faced by properly combining the roughness effects of both vegetated and non-vegetated parts of the wetted perimeter, as will be explained below.

1.5   Compound Channels

Very often, natural watercourses have cross sections which greatly change as the water depth increases: They are watercourses endowed with more or less wide floodplain expansion areas. In these cases, it is unrealistic to consider the cross section as compact and directly apply the previous formulae to it. Instead, as a rule, the area is divided by vertical lines into subareas, each then subjected to the uniform flow formula (Fig. 1.11).

Assume that the free surface is horizontal and thus the energy slope i_E is the same for all subareas. We neglect the tangential stresses acting along the vertical separation lines between subareas. The latter simplification involves a margin of error, in that this condition occurs only on the lines normal to isotachs (line connecting the points of the cross section with the same longitudinal velocity); therefore, it is these lines which should be used to subdivide the cross section. If the horizontal width of subareas is much greater than the water depth, any possible error is rather modest.

The total discharge turns out to be the sums of the discharges of each subarea:

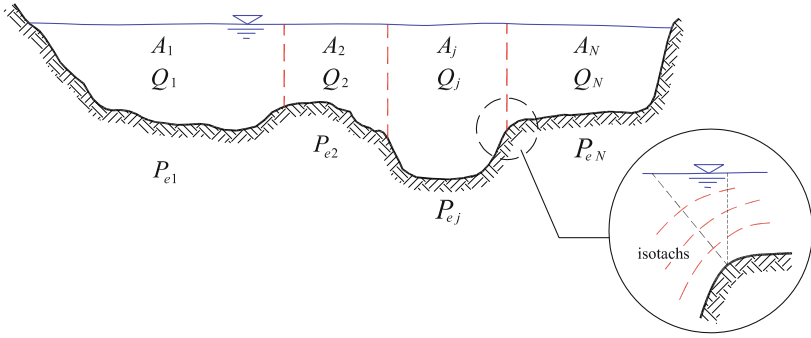$$Q = \sum_{j=1}^{N} Q_j \tag{1.28}$$

Fig. 1.11 Scheme of division into subareas by vertical lines

Referring to global section values is useful, especially in 1D mathematical models, in that it allows to define an equivalent resistance coefficient for the whole section. For instance, the Gauckler-Strickler formula allows to define the following equivalent roughness coefficient:

$$k_{s_{eq}} = \frac{\sum_{j=1}^{N} k_{s_j} A_j^{5/3} \, P_{e\,j}^{-2/3}}{(\sum_{j=1}^{N} A_j)^{5/3}(\sum_{j=1}^{N} P_{e\,j})^{-2/3}} \tag{1.29}$$

Equation (1.29) is based on the hypothesis that the hydraulic radius of the whole section is given by the ratio between the total area and the total wetted perimeter $R_h = A/P_e = \sum_{j=1}^{N} A_j / \sum_{j=1}^{N} P_{e\,j}$ (Lotter 1933).

A slightly different hypothesis about the total hydraulic radius of the whole cross section, $R_h = \left(\sum_{j=1}^{N} A_j^{3/2} P_{e\,j}^{-1/2}\right)^2 / (\sum_{j=1}^{N} A_j)^2$, is on the basis of the formula suggested by Engelund (1964) and Ida (1960), which leads to the following expression of the equivalent roughness coefficient of the whole section:

$$k_{s_{eq}} = \frac{\left(\sum_{j=1}^{N} A_j\right)^{-1/3} \sum_{j=1}^{N} k_{s_j} A_j^{5/3} \, P_{e\,j}^{-2/3}}{\left(\sum_{j=1}^{N} A_j \, P_{e\,j}^{-1/2}\right)^{4/3}} \tag{1.30}$$

In this circumstance also, the kinetic term which appears in the energy balance must be multiplied by the respective *Coriolis momentum coefficient* or *Coriolis correction factor* that, according to Lotter's assumption, is:

$$\alpha_C = \frac{(\sum_{j=1}^{N} A_j)^2 \, \sum_{j=1}^{N} \left(k_{s_j}^3 \, A_j^3 \, P_{e\,j}^{-2}\right)}{\left(\sum_{j=1}^{N} k_{s_j} \, A_j^{5/3} \, P_{e\,j}^{-2/3}\right)^3} \tag{1.31}$$

It goes without saying that the exponents need to be properly modified if a different but monomial formula is used. It has recently been proved that the apparent resistance of watercourses with floodplain expansion is higher than the estimates above would suggest. A reason for this increase in resistance has been identified in the existence of large secondary currents with a vertical axis transferring mass and momentum from the central area (*talweg*) to floodplains and vice versa. These secondary circulations have profound consequences also for the biology and water quality of the river, in that they foster interchange phenomena between talweg and floodplains, as schematized in Fig. 1.12.

Townsend (1968) proposed the following formula (units in MKS) in order to evaluate the dimensionless tangential stress along the separation lines between the main channel and the floodplains:

$$\beta_r = \frac{(\Delta U)^{0.92}}{11.21\, h_{max}\, i_E} \left(\frac{h_g}{h_{max}}\right)^{-1.129} \left(\frac{B_g}{B_c}\right)^{-0.514} \quad [\Delta U] = [\,\mathrm{m/s}\,]; \, [h] = [\,\mathrm{m}\,]$$

(1.32)

where h_g and h_{max} denote the water depth in the floodplains and the talweg, respectively, B_g and B_c are the widths of the floodplains and the talweg, i_E is the energy slope of the channel, and ΔU is the velocity difference between floodplains and talweg.

Roughness increase can be calculated in terms of increase (ΔA) in the liquid cross section A_g due to floodplain expansions, along with a parallel reduction in the liquid section A_c of the talweg. The areas of the floodplains and the talweg which should then be used in calculations result to be, respectively:

$$A'_g = A_g + 2(\Delta A) \quad \text{and} \quad A'_c = A_c - 2(\Delta A)$$

(1.33)

where the area variation (ΔA) is calculated in function of the tangential stress (Eq. 1.32) at the interface between floodplains and talweg:

$$\Delta A = \beta_r h_{max}^2$$

(1.34)

with β_r calculated using expression (1.32). Resistance is then evaluated following the procedure already described with Eqs. (1.28–1.31).

1.6   Channels with Composite Wall Roughness

Similar to the previous problem but referred to watercourses with relatively narrow cross sections is the case when wall roughness significantly varies along the wetted perimeter. This is the case of channels with concrete banks and gravel beds or sand beds, or channels with rocky banks or with natural or planted vegetation, as often adopted in the river restoration projects (Fig. 1.13).
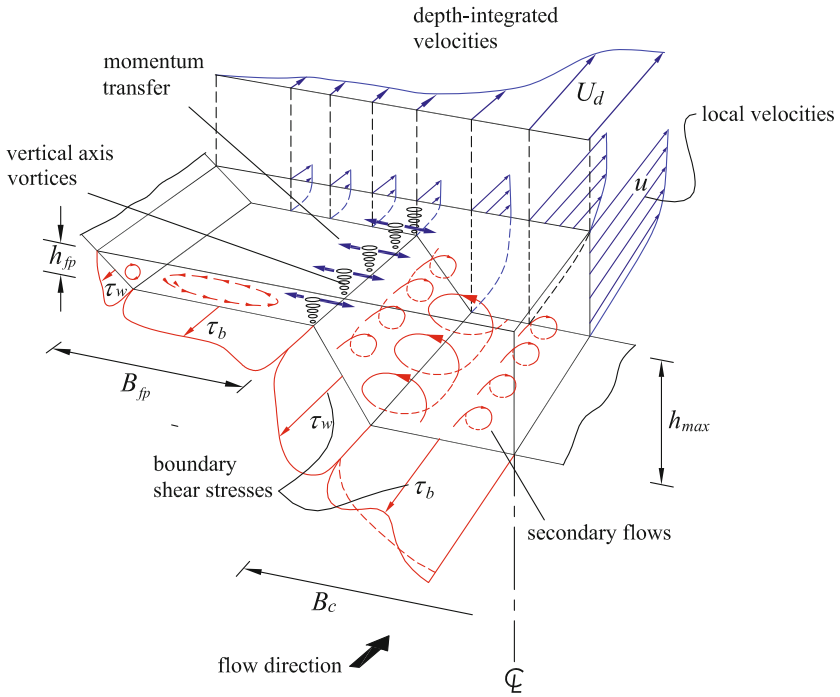
Fig. 1.12   Secondary circulations in channels with floodplain expansion according to Shiono and Knight (1991)
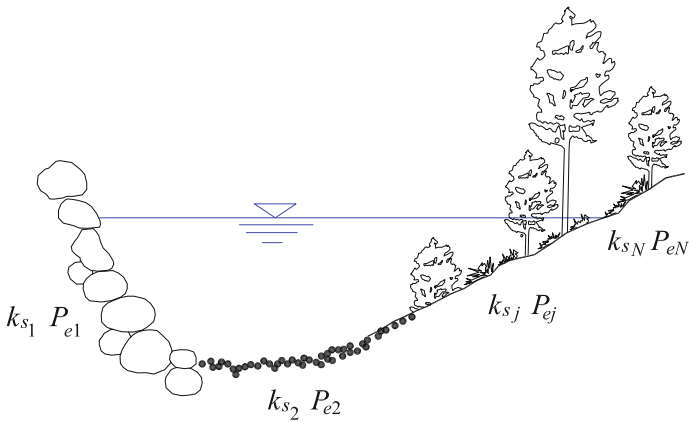

Fig. 1.13   Scheme of a transverse cross section with different roughnesses
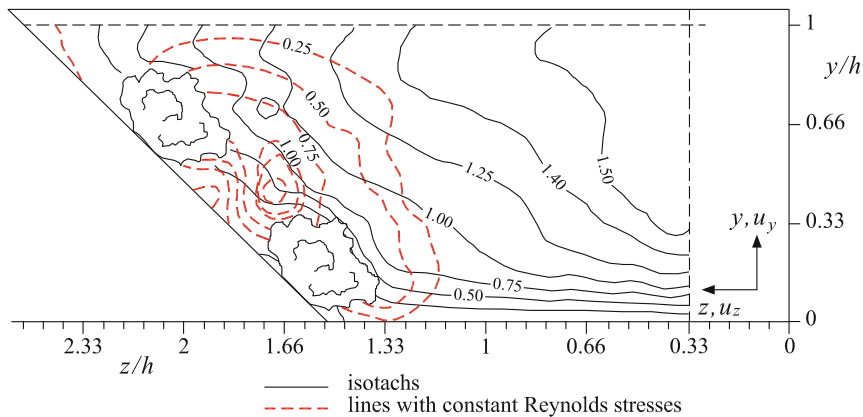
Fig. 1.14 Distribution of isotachs lines, normalized to the average velocity U, (u_x/U), and of the equal Reynolds stress lines, normalized to the average friction velocity $\overline{u_*}$ $(\overline{u_x' u_z'}/\overline{u_*}^2)$, in the presence of thick vegetation on the bank (Righetti and Armanini 1998)

In these circumstances, the velocity distribution can be so significantly influenced by roughness differences that the previously described methods for dividing cross sections by vertical lines can become rather unreliable.

Especially in the presence of dense vegetation on the bank of a relatively narrow channel, the influence of bank roughness can greatly extend inside the central part of the channel, and therefore the tangential stresses on the vertical lines can be compared with those along the walls, which cannot be ignored any longer.

Figure 1.14 illustrates equal velocity lines and equal Reynolds stress lines, obtained in a laboratory channel (Righetti and Armanini 1998). A careful observation of the figure confirms that roughness due to vegetation not only translates the discharge of subareas subtended from banks to zero contribution, but it also allows to reduce the discharge in the central channel. Thus, the omission of the presence of the triangular part created by the bank slope, as suggested by some authors, may be insufficient. There are then several criteria for calculating the equivalent roughness coefficient of these sections. In order to evaluate the equivalent resistance, it is advisable to adopt the Gauckler-Strickler formula since the roughness coefficient of this formula is known to be strongly dependent on the absolute, rather than relative roughness.

1. *Arithmetic mean* In this hypothesis, the equivalent roughness coefficient is assumed to be simply the arithmetic average of the coefficients of the single parts of the wetted perimeter. Quite clearly, such a criterion does not take into account the length of each boundary section whose roughness is referred to, and consequently it can be applied only when these cross sections are the same length:

$$k_{s_{eq}} = \frac{\sum_{j=1}^{N} k_{s_j}}{N} \tag{1.35}$$

2. *Weighted arithmetic mean* The drawback suffered from the previous approach can be overcome if the average is weighted on the single segments of the wetted perimeter:

$$k_{s_{eq}} = \frac{\sum_{j=1}^{N} k_{s_j} \, P_{e\,j}}{\sum_{j=1}^{N} P_{e\,j}} \tag{1.36}$$

As the relation between wetted perimeter and roughness coefficient is not linear, the weighted mean should be adjusted to take nonlinearity into account.

3. *Einstein-Horton's criterion* This criterion considers the above nonlinear feature in equations. The cross section is assumed to be divided into N subareas, each characterized by the same mean velocity U (Fig. 1.15):
The average velocity for a generic *jth* subarea is then evaluated by applying to it the Gauckler-Strickler formula:

$$U = k_{s_j} \, R_{h_j}^{2/3} \, \sqrt{i_E} \tag{1.37}$$

Therefore, since i_E is also constant in the various subareas, we have:

$$\frac{U}{\sqrt{i_E}} = k_{s_j} \, R_{h_j}^{2/3} = const \tag{1.38}$$

In other words,

$$R_{h_j} = \frac{A_j}{P_{e\,j}} = k_{s_j}^{-3/2} \left(\frac{U}{\sqrt{i_E}} \right)^{3/2} \tag{1.39}$$

An equivalent roughness coefficient $k_{s_{eq}}$ can be defined as:

$$U = k_{s_{eq}} \, \sqrt{i_E} \, R_h^{2/3} \tag{1.40}$$

From the previous relations, we obtain:

$$k_{s_{eq}} = \frac{U}{\sqrt{i_E}} \frac{1}{R_h^{2/3}} = \frac{U}{\sqrt{i_E}} \left(\frac{\sum_{j=1}^{N} P_{e\,j}}{\sum_{j=1}^{N} A_j} \right)^{2/3} = \frac{U}{\sqrt{i_E}} \frac{P_e^{2/3}}{\left(\sum_{j=1}^{N} P_{e\,j} \, R_{h_j} \right)^{2/3}} \tag{1.41}$$

By substituting (1.39) into (1.41), we have:

$$k_{s_{eq}} = \frac{U}{\sqrt{i_E}} \frac{P_e^{2/3}}{\left(\sum_{j=1}^{N} P_{e\,j} \, k_{s_j}^{-3/2} \, (\frac{U}{\sqrt{i_E}})^{3/2} \right)^{2/3}} = \frac{P_e^{2/3}}{\left(\sum_{j=1}^{N} P_{e\,j} \, k_{s_j}^{-3/2} \right)^{2/3}} \tag{1.42}$$

This criterion turns out to be precautionary compared to those previously suggested.
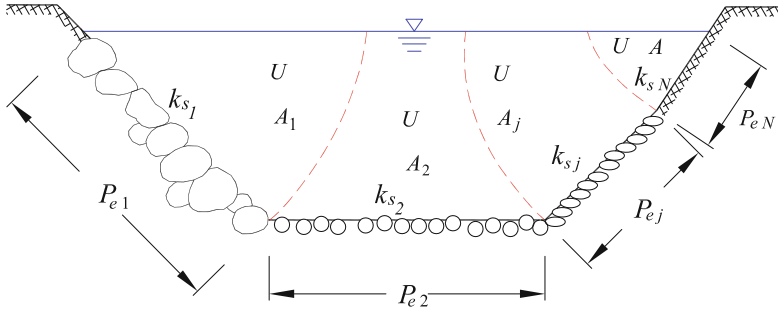
Fig. 1.15 Scheme for Einstein-Horton's criterion of subareas of equal velocity

1.6.1 Shear Stress on Each Portion of the Wetted Perimeter

The average tangential stress exerted on each portion of the wetted perimeter is obtained by applying the uniform flow condition to each subarea:

$$\tau_{oj} \, P_{ej} = \rho \, g A_j \, i_E \tag{1.43}$$

but from (1.39) we have:

$$A_j = P_{ej} \, k_{s_j}^{-3/2} \left(\frac{U}{\sqrt{i_E}} \right)^{3/2} \tag{1.44}$$

After substituting (1.44) into (1.43), we get:

$$\tau_{oj} \, P_{ej} = \rho \, g \, i_E \, P_{ej} \, k_{s_j}^{-3/2} \left(\frac{U}{\sqrt{i_E}} \right)^{3/2} \tag{1.45}$$

Given that from (1.40) it results: $\left(\dfrac{U}{\sqrt{i_E}} \right)^{3/2} = k_{s_{eq}}^{3/2} \, \dfrac{A}{P_e}$, we then obtain:

$$\tau_{oj} = \rho \, g \, i_E \, k_{s_j}^{-3/2} \, k_{s_{eq}}^{3/2} \, \frac{A}{P_e} = \rho \, g \, R_h \, i_E \left(\frac{k_{s_{eq}}}{k_{s_j}} \right)^{3/2} \tag{1.46}$$

and in conclusion,

$$\tau_{oj} = \overline{\tau_o} \left(\frac{k_{s_{eq}}}{k_{s_j}} \right)^{3/2} \tag{1.47}$$

1.6.2 Limits of Einstein-Horton's Criterion

As previously observed, the vegetation effect on banks can be extremely high, especially in minor streams. In this case, the Einstein-Horton's criterion seems to be the right choice for total resistance calculation. Figure 1.16 shows some significant examples after applying such a method. It is evident that the presence of vegetation, even on half the bank, leads to a reduction in discharge up to 60%.

By comparing the previous figures, we can observe that the vegetation effect is much more visible in the narrow channel. The reason is rather obvious: being the vegetation concentrated on banks, the lower the portion of wetted perimeter affected by vegetation, the higher the channel width.

In these cases, however, Einstein's criterion turns out to be too precautionary, as is shown in Fig. 1.17, which shows the results of an accurate investigation conducted with artificial vegetation in a laboratory channel.

Among the different hypotheses considered in Einstein-Horton's criterion, the least acceptable is that one on the same velocity for each subarea referred to each segment of the wetted perimeter with different roughness.

As clearly shown in Fig. 1.14, the average velocity of the vegetated subarea is very low and extremely lower than the average velocity of the whole section. We can deduce that the suggested criterion can be applied only when the different roughnesses are the same size.

Such limits of the Einstein-Horton's criterion can be overcome, at least for nearly trapezoidal section with thick vegetation along banks, by supposing that the cross section can be subdivided into subareas by vertical lines passing through the foot of banks.

The section is then subdivided into three subareas: the central quasi-rectangular part, plus two lateral quasi-triangular subareas, formed by either bank, and by vertical lines passing through their foot (Fig. 1.18).

The central subarea resistance is calculated by applying on the vertical segments a shear stress, which is proportional to the average stress acting on the bank, through an appropriate proportionality coefficient n (Righetti and Armanini 1998). The equivalent roughness coefficient of such a subarea is then calculated by applying Einstein-Horton's method:

$$k_{sc} = \left(\frac{2 + \dfrac{B_c}{h}}{\dfrac{B_c}{h\, k_{sc}^{3/2}} + \left(\dfrac{n}{k_{sl}} \right)^{3/2} + \left(\dfrac{n}{k_{sr}} \right)^{3/2}} \right)^{2/3} \tag{1.48}$$

In (1.48), k_{sc}, k_{sl}, and k_{sr} are, respectively, the equivalent bed roughness coefficients of the central area, and the left and right banks according to Gauckler-Strickler. $A_c \simeq B_c\, h$ is the area of the central subarea and B_c its average width.

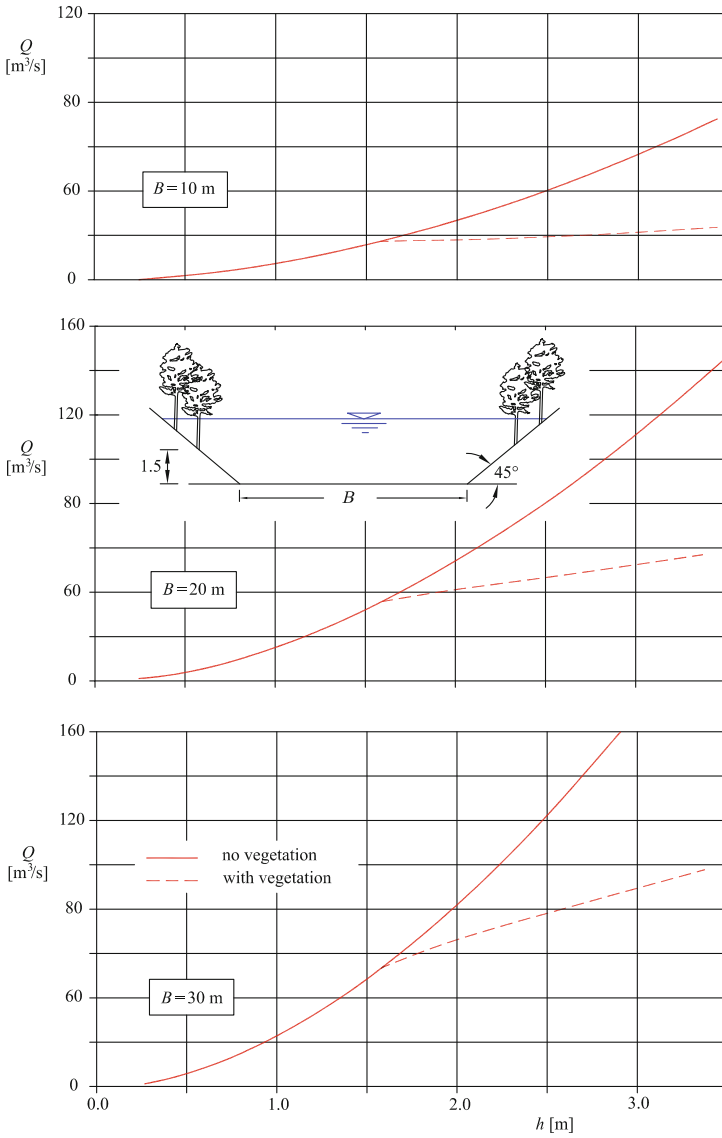Thus, the discharge flowing into the central subarea turns out to be:

Fig. 1.16 Effect of bank vegetation on the rating curve, calculated with Einstein-Horton's criterion

$$Q_c = k_{sc} A_c \left(\frac{A_c}{B_c + 2h} \right)^{2/3} i_E^{1/2}$$

$$= \left(\frac{B_c}{\dfrac{B_c}{h\, k_{sc}^{3/2}} + \left(\dfrac{n}{k_{sl}} \right)^{3/2} + \left(\dfrac{n}{k_{sr}} \right)^{3/2}} \right)^{2/3} h\, B_c\, i_E^{1/2} \qquad (1.49)$$
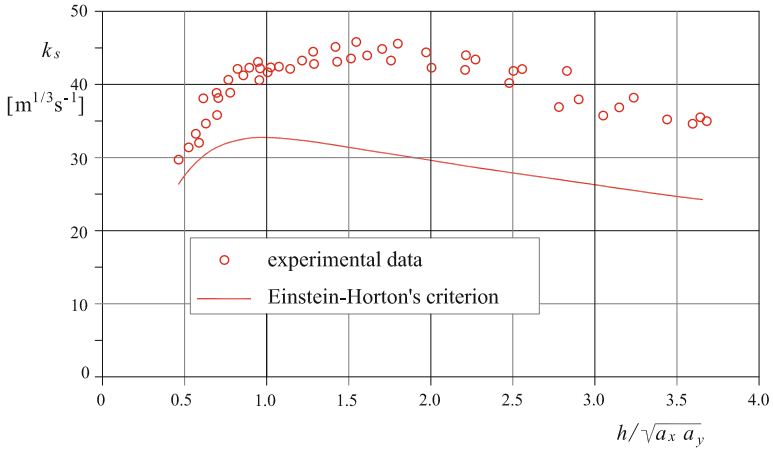
Fig. 1.17 Strickler coefficient in function of the dimensionless water depth scaled by the average distance between plants. Laboratory data obtained by simulating vegetation with cylindrical rods evenly distributed along a 45° inclined slope (Righetti and Armanini 1998)
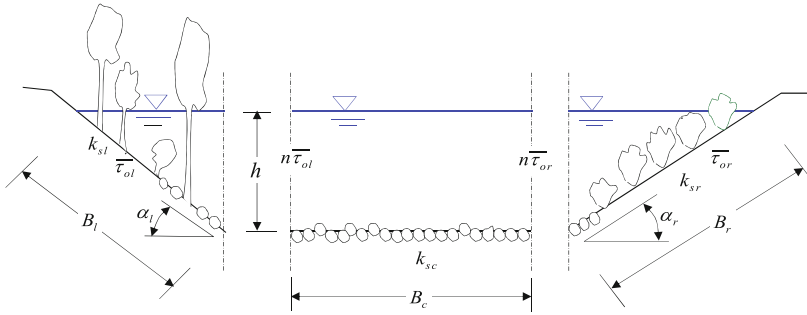

Fig. 1.18 Subarea division scheme for channels with thickly vegetated banks (Righetti and Armanini 1998)

Through each of the lateral subareas, there flows a discharge equal to:

$$Q_j = k_{sj} A_j B_j^{2/3} i_E^{1/2} = k_{sj} \frac{h B_j \cos \alpha_j}{2} B_j^{2/3} i_E^{1/2} \qquad j = 1, 2 \qquad (1.50)$$

where B_j is the length of each bank and A_j is the respective area.

The total equivalent roughness is calculated by adding the three discharges and by applying Lotter's method for vertical subareas (Eq. 1.29):
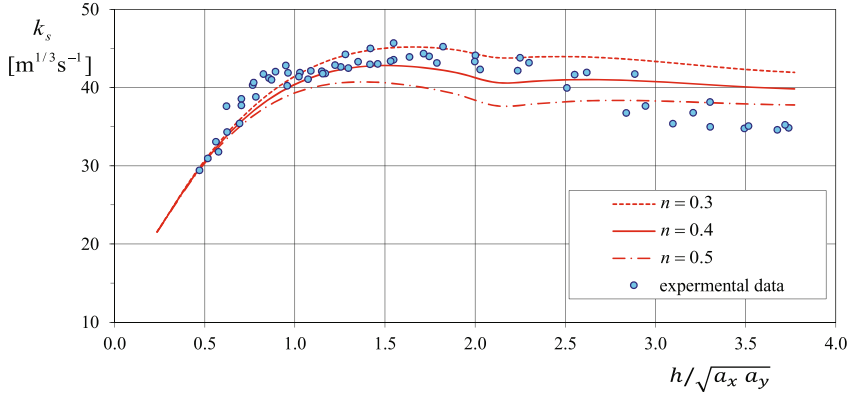
Fig. 1.19 Strickler coefficient in function of the water depth, obtained in laboratory by simulating vegetation with cylindrical rods, evenly distributed on a 45° inclined bank and with a value calculated according to Eq. (1.51) (Righetti and Armanini 1998). a_x and a_y are the averaged distances between plants in the longitudinal and transverse directions, respectively

$$k_{s-eq} = \frac{\left(\dfrac{\dfrac{B_c}{h}}{\dfrac{B_c}{hk_{so}^{3/2}} + \sum_{j=1}^{2}\left(\dfrac{n}{k_{sj}}\right)^{3/2}}\right)^{2/3} + \sum_{j=1}^{2} k_{sj}\dfrac{B_j}{B_c}\left(\dfrac{\cos\alpha_{sj}}{2}\right)^{5/3}}{\dfrac{\left(1 + \sum_{j=1}^{2}\dfrac{B_j}{B_c}\dfrac{\cos\alpha_{sj}}{2}\right)^{5/3}}{\left(1 + \sum_{j=1}^{2}\dfrac{B_j}{B_c}\right)^{2/3}}} \qquad (1.51)$$

If we put $n = 0$ in the previous formulae, the method coincides with the Lotter's Eq. (1.29); if we assume $n = 1$, we hypothesize that bank roughness is totally transferred into the central subarea.

Laboratory measurements (Righetti and Armanini 1998) have shown that n is comprised between 0.3 and 0.5, typically $n = 0.4$ (Fig. 1.19). Moreover, it is also worth observing that if $B_c/h >> (0.4\,k_{so}/k_{sj})^{3/2}$, i.e., if the central subarea is sufficiently wide or the bank is not very rough, the method tends to coincide with Lotter's (Eq. 1.29).

References

J. Bathurst, At-a-site variation and minimum flow resistance for mountain rivers. J. Hydrol. **269**(1), 11–26 (2002)

D.I. Bray, Estimating average velocity in gravel-bed rivers. J. Hydraul. Div. **105**(9), 1103–1122 (1979)

D.I. Bray, Flow resistance in gravel-bed rivers, in *Gravel-Bed Rivers* (1982), pp. 109–133

D.I. Bray, K.S. Davar, Resistance to flow in gravel-bed rivers. Can. J. Civil Eng. **14**(1), 77–86 (1987)

V.T. Chow, *Open Channel Hydraulics* (McGraw-Hill Book Company, Inc, New York, 1959)

C. Colosimo, V.A. Copertino, M. Veltri, Friction factor evaluation in gravel-bed rivers. J. Hydraul. Eng. **114**(8), 861–876 (1988)

DVWK. Hydraulische Berechnung von Fließgewässern. *Wasserwirtschaft, Deutscher Verband für Wasserwirtschaft and Kulturbau, eV DVWK Merkblätter zur Wasserwirtschaft. Bd*, 220 (1991)

F.A. Engelund, *Flow Resistance and Hydraulic Radius* (Technical University of Denmark, Hydraulic Laboratory, 1964)

F. Florineth, Erfahrungen mit ingenieurbiologischen Maßnahmen bei Fließgewässern im Gebirge. *Inst. Für Wassergüte und Landschaftswasserbau, TU Wien, Bd* **3**, 243–263 (1982)

F. Florineth, Ingenieurbiologische Massnahmen an Fliessgewässern. Wildbach-und Lawinenverbauung **57**(123), 83–99 (1993)

W. Graf, H. Cao, L. Suszka. *Hydraulics of Steep, Mobile-Bed Channels*, EV (1987)

W.H. Graf, Flow resistance over a gravel bed: its consequence on initial sediment movement, in *Fluvial Hydraulics of Mountain Regions* (Springer, 1991), pp. 15–32

G.A. Griffiths, Flow resistance in coarse gravel bed rivers. J. Hydraul. Div. **107**(7), 899–918 (1981)

R.D. Hey, Flow resistance in gravel-bed rivers. J. Hydraul. Div. **105**(4), 365–379 (1979)

Y. Ida, Steady flow in wide channel and the effect of shape of its cross section, in *Japanese Trans. Jpn. Soc. Civ. Eng* (1960), pp. 693–2

G.H. Keulegan, *Laws of Turbulent Flow in Open Channels*, vol. 21 (National Bureau of Standards US, 1938)

N. Kouwen, Field estimation of the biomechanical properties of grass. J. Hydraul. Res. **26**(5), 559–568 (1988)

N. Kouwen, T.E. Unny, Flexible roughness in open channels. J. Hydraul. Div. **99**(5), 713–728 (1973)

A.J. Lee, R.I. Ferguson, Velocity and flow resistance in step-pool streams. Geomorphology **46**(1), 59–71 (2002)

J.T. Limerinos, Determination of the Manning coefficient from measured bed roughness in natural channels, in *Water Supply Paper 1898-B U.S. Geological Survey* (1970)

G. Lotter, Considerations on hydraulic design of channels with different roughness of walls, in *Transactions, All-Union Scientific Research Institute of Hydraulic Engineering, Leningrad*, vol. 9 (1933), pp. 238–241

E. Marchi, Il moto uniforme delle correnti liquide nei condotti chiusi e aperti. L'Energia Elettrica **38**(5), 393–413 (1961)

E. Meyer-Peter, R. Müller. Formulas for bedload transport, in *Proceedings of the 2nd Meeting of the International Association for Hydraulic Structures Research*, vol. 133 (IAHS, 1948), pp. 39–64

H. Nakagawa, T. Tsujimoto, Y. Shimizu. Turbulent flow with small relative submergence, in *Fluvial Hydraulics of Mountain Regions* (Springer, 1991), pp. 33–44

V. Nikora, D. Goring, I. McEwan, G. Griffiths, Spatially averaged open-channel flow over rough bed. J. Hydraul. Eng. **127**(2), 123–133 (2001)

S. Petryk, G. Bosmajian, Analysis of flow through vegetation. J. Hydraul. Div. **101**(7), 871–884 (1975)

E.J. Plate, A. Quraishi, Modeling of velocity distributions inside and above tall crops. J. Appl. Meteorol. **4**(3), 400–408 (1965)

B. Przedwojski, R. Błazejewski, K.W. Pilarczyk, et al. *River Training Techniques: Fundamentals, Design and Applications* (AA Balkema, 1995)

M. Righetti, A. Armanini. Flow resistance in compound vegetated channels, in *Proceedings Third International Conference on Hydroscience and Engineering, ICHE* (Cottbus, Berlin, 1998)

K. Shiono, D.W. Knight, Turbulent open-channel flows with variable depth across the channel. J. Fluid Mech. **222**, 617–646 (1991)

A. Strickler, *Beiträge zur Frage der Geschwindigkeitsformel und der Rauhigkeitszahlen für Ströme* (Kanäle und geschlossene Leitungen. Eidg, Amt für Wasserwirtschaft Bern, 1923)

S. Thompson, P. Campbell, Hydraulics of a large channel paved with boulders. J. Hydraul. Res. **17**(4), 341–354 (1979)

D. Townsend, An investigation of turbulence characteristics in a river model of complex cross section. Proc. Inst. Civil Eng. **40**(2), 155–175 (1968)

Chapter 2
Introduction to Sediment Transport

2.1 Introduction

This chapter analyzes watercourses as mobile bed flows, that is, liquid flowing on boundaries that evolve over time under the action of the current.

The river engineering works are almost always made to control morphological processes, either erosion or sedimentation. Also liquid floods due to overflow are often intrinsically due to solid overfeeding. As a matter of fact, dealing with hydrodynamics of natural water streams may sometimes lead to very unfortunate results if we neglect the morphological variations developing simultaneously.

The analysis of these processes will end in Chaps. 7 and 8. But first the following topics need to be addressed in succession:

- *initiation of sediment movement;*
- *evaluation of solid transport rate;*
- *sediment effects on flow resistance;*
- *morphological variations in river courses;*
- *localized effects, like excavations and erosions.*

Although these phenomena are closely interrelated, they will be dealt with separately to make the exposition much clearer.

We will first illustrate how to define the characteristics of the particles that make up a mobile riverbed from the qualitative and quantitative points of view, in particular how to define the particle shape with a reduced number of parameters.

In Sect. 2.3, we will outline some key concepts useful to categorize the solid transport modes, that is to say, we will introduce the concepts of *bedload* and *suspended load*, and in particular the concept of *wash load*. These concepts will then be analyzed in detail in Chaps. 5 and 6, respectively.

Finally, in Sect. 2.5 we will detail the main features of the bed forms observed in river beds: *ripples*, *dunes*, and *antidunes*. This topic will also be discussed later in Chap. 4, devoted to the effect of bed forms on flow resistance.

The aspects related to the so-called *massive sediment transport* (i.e., *debris flows* and *mudflows*) will not be dealt with here.

These types of transport, whose knowledge requires tools other than those used in the study of lowland rivers, concern the mountain streams especially during paroxysmal phenomena of particularly high intensity.

2.2 Characterization of Solid Particles

The sediments that compose the bed of a natural water course are very different in form, composition, and arrangement. They are generally transported where they are by the water flow, but in some cases also deposited on site manually or by geomechanical phenomena. However, the bed composition is continuously changing by erosion and deposition processes.

Typically, the natural river beds are composed of cohesive and loose sediments. Loose sediments are materials that do not show physical–chemical interactions between them. For sake of simplicity, in this book we will refer to loose sediments, without considering, unless otherwise indicated, the effects of the cohesion that usually emerges in the presence of clayey particles.

2.2.1 Sediment Density

By definition, the density of a particle is the ratio between its mass m_s and volume $\forall_s$, e.g.,

$$\rho_s = \frac{m_s}{\forall_s} \tag{2.1}$$

The density of the particle depends on its mineral composition, but the majority of the particles are composed of quartz with a density of nearly 2600–2700 [kg/m^3] or of calcareous material with a density of $\sim$ 2900 [kg/m^3]. In practical calculations, the sediment density is given as a value of 2650 [kg/m^3]. Very often, many sediment transport equations adopt the *relative submerged density* Δ, defined as the ratio of the difference between the material density ρ_s and the water density ρ, divided by the water density:

$$\Delta = \frac{\rho_s - \rho}{\rho} \tag{2.2}$$

which usually takes the value of 1.65.

2.2.2   Geometric Classification

Size, shape, and density are the typical key parameters of a solid particle. In fact, natural particles are never regular in shape, so more than one dimension is required to define them geometrically.

Referring to the textbooks of geotechnics and geomorphology for detail, here it suffices to recall some criteria for defining the representative dimension of a particle, as follows:

- *Triaxial diameter*: $D_t = \dfrac{d_1 + d_2 + d_3}{3}$, where (Fig. 2.1) d_1, d_2, and d_3 are, respectively, the longest, intermediate, and shortest dimension of the particle, measured along three mutually perpendicular axes.
- *Nominal diameter*: it is the diameter of a sphere with equal volume. Although rarely and hardly ever used in practice, this parameter is suitable to define the dimension of particular particles.
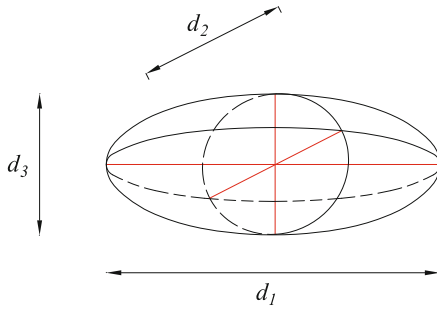

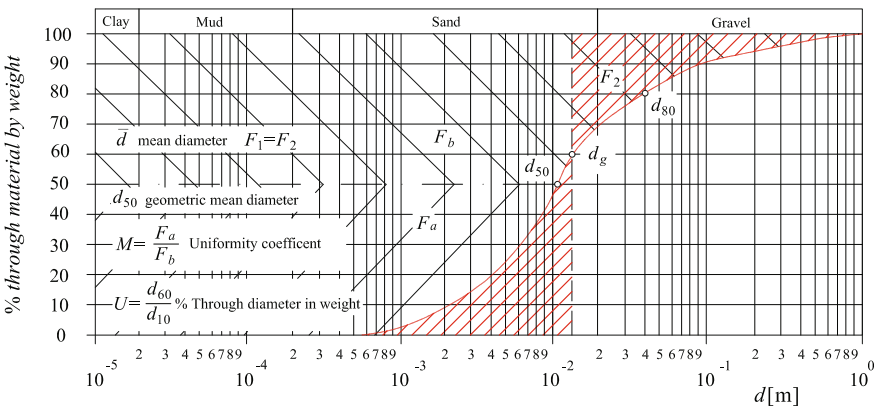**Fig. 2.1** Parameters defining the triaxial diameter

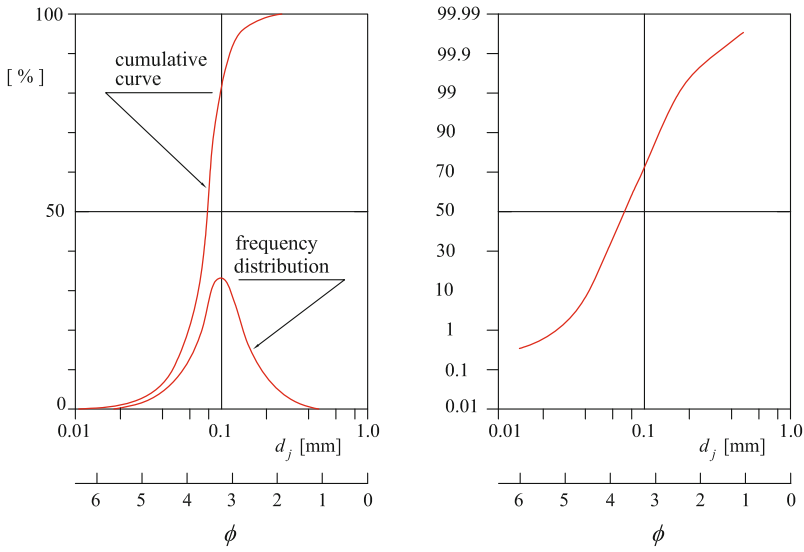**Fig. 2.2** Example of granulometric curve of natural bed material

Fig. 2.3 Cumulative granulometric curve and index ϕ. On the right, the cumulative curve is drawn on a probability scale (concentration of median values and expansion of extreme percentage values)

- *Sieve diameter*: the smallest sieve size through which a particle can pass. In this case, the particle size can be determined by sieving. For practical reasons, such a definition cannot be applied to particles of very small dimensions (less than around 100 μm), or to those with extremely large diameters (more than some centimeters).
  There are several particle size classifications. Probably the most well known are the Udden-Wentworth scale (Wentworth scale) and the British Standard Classification. In the Udden-Wentworth scale, sediments are scaled by grades and class terms as indicated in Table 2.1.

Table 2.1 Solid particle classification by Udden-Wentworth (1922)

Very fine clay	0.24–0.50 μm	Very coarse sand	1–2 mm
Fine clay	0.50–1 μm	Very fine gravel	2–4 mm
Medium clay	1–2 μm	Fine gravel	4–8 mm
Coarse clay	2–4 μm	Coarse grave	8–16 mm
Very fine silt	4–8 μm	Very coarse gravel	16–32 mm
Fine silt	8–16 μm	Small cobbles	32–64 mm
Medium silt	16–31 μm	Medium cobbles	64–128 mm
Coarse silt	31–62 μm	Coarse cobbles	128–256 mm
Very fine sand	62–125 μm	Small boulders	256–512 mm
Fine sand	125–250 μm	Medium boulders	512–1024 mm
Medium sand	250–500 μm	Coarse boulders	1024–2048 mm
Coarse sand	0.5–1.0 mm	Very large boulders	2048–4096 mm

In particular, d_n is the sieve diameter corresponding to $n\%$ finer in the particle size distribution. d_{50} is often called *geometric mean diameter* (or mean value of the grain size distribution) d_g (Fig. 2.2). In the hypothesis, although not always verified, that the grain size distribution follows a lognormal law, the geometric mean diameter and the geometric standard deviation turn out to be:

$$d_g \simeq \sqrt{d_{84.1}\, d_{15.9}} \quad \text{and} \quad \sigma_g = \frac{1}{2}\left(\frac{d_{84.1}}{d_{50}} + \frac{d_{50}}{d_{15.9}}\right) \tag{2.3}$$

Mean diameter, which is obtained by dividing the granulometric curve into N classes. Denoted with d_j and d_{j+1} the diameters defining the jth class and with p_j the percentage of material present in the granulometric class, we have:

$$\bar{d} = \frac{\sum_{j=1}^{N} \frac{1}{2}(d_j + d_{j+1})\, p_j}{\sum_{j=1}^{N} p_j} \tag{2.4}$$

However, the granulometric distribution of streams does not generally follow the Gaussian law, even if in floodplain streams (i.e., far from localized sediment intakes) the grain size distribution downstream tends to be lognormal. In order to express the sediment dimension, the following index ϕ is often used, especially by geomorphologists (Fig. 2.3):

$$\phi = -\log_2 d_{[mm]} = -\frac{\log d}{\log 2} = -\frac{\ln d}{\ln 2} \tag{2.5}$$

- *Sedimentological diameter*: it is the diameter of the sphere with the same density ρ_s and the same fall velocity in still water w_s as the particle in question. This parameter is often used to compare the effects of particles with different density, as happens, for instance, in hydraulic mobile-bed models.
  The fall velocity in still water w_s is the velocity gained by the particle when, letting it fall in still water, it reaches a uniform velocity, that is, when the hydrodynamic resistance is balanced by the submerged weight of the particle:

$$C_D\, \alpha_2\, d^2\, \rho\, \frac{w_s^2}{2} = \alpha_3\, g\, (\rho_s - \rho)\, d^3 \tag{2.6}$$

From this expression it follows:

$$w_s = \sqrt{2\frac{\alpha_3}{\alpha_2\, C_D}} \sqrt{g\, \Delta\, d} \tag{2.7}$$

being $\Delta = (\rho_s - \rho)/\rho$ the reduced relative density of the particles. d is the particle size; α_2 and α_2 are appropriate shape coefficients. In case of the sphere: $\alpha_2 = \pi/4$ and $\alpha_3 = \pi/6$, and thus, $2\alpha_3/\alpha_2 = 4/3$.
C_D is the drag coefficient, a function of the Reynolds number $Re_w = w_s\, d/\nu$ and
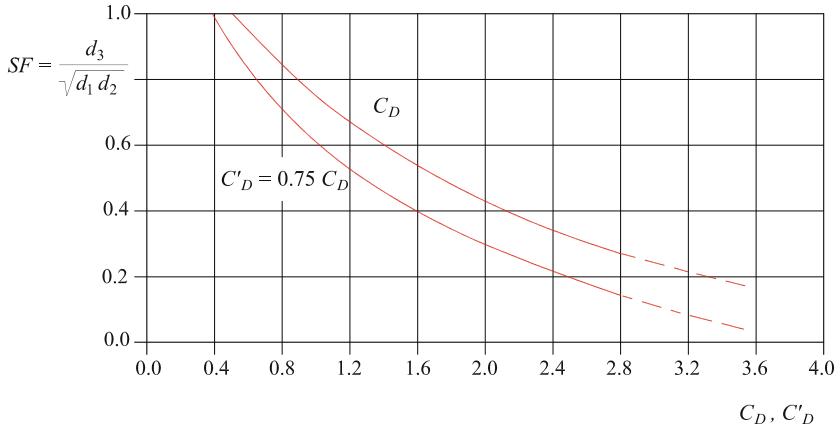
Fig. 2.4 Drag coefficient C_D in function of the shape factor ($Re_w = 45$) (from Helley (1969))

of the particle shape:

$$C_D = f(\frac{w_s d}{\nu}, \, shape)$$ (2.8)

As for a spherical particle falling in a laminar flow regime (Stokes' law), we have $C_D = 24/Re_w$.

In order to characterize the particle shape, various parameters and criteria have been proposed in the literature. Among these, it is worth mentioning the *shape factor*, defined as follows:

$$SF = \frac{d_3}{\sqrt{d_1 d_2}}$$

The shape factor has a remarkable influence on the fall velocity of particles. Figure 2.4 shows this effect for a constant value of the Reynolds number, R_{ew}, referred to the fall velocity in still water (Helley 1969).

Coefficient $C_D' = 0.75 C_D$ represents that in the sphere $\alpha_2/2\alpha_3 = 3/4$.

Natural particles have an average shape factor of around 0.7.

On the other hand, the next figure represents the dependence of the drag coefficient C_D on the Reynolds number for various values of the shape factor. Highly appreciable is the shape factor effect on C_D in coarser materials, whose Reynolds number for the fall velocity is higher (Figs. 2.5 and 2.6).

Other parameters used to characterize the particle shape are *sphericity* and *roundness*.
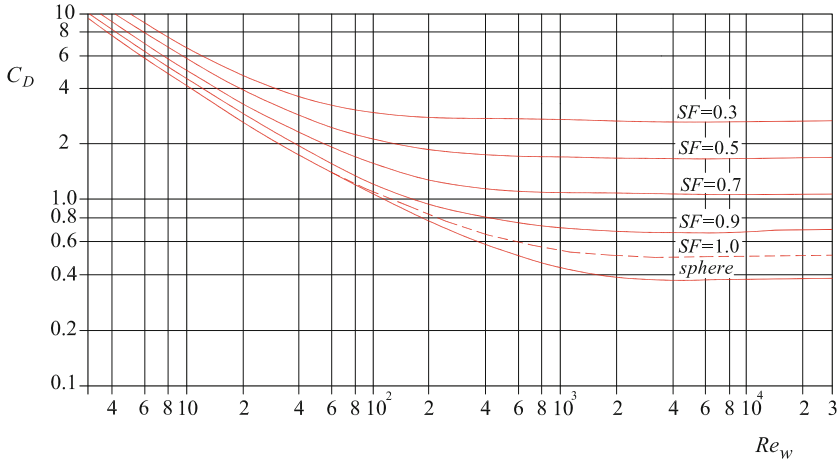
$$sphericity = \frac{S_{sf}}{S_p}$$

Fig. 2.5 Dependence of the hydrodynamic drag coefficient of a particle on the Reynolds number, scaled by various values of the shape factor (from Albertson (1953))

S_{sf} is the surface of the sphere with equal volume. S_p is the particle surface.

$$roundness = \frac{R_p}{R_{cm}}$$

R_p is the average radius of curvature of the particle surface and R_{cm} is the radius of the maximum circle which can be inscribed within the surface of maximum projection of the particle. The cube is very spherical and little round; a cylinder is little spherical and very round.

From Eq. (2.7), we obtain the following definition of the sedimentological diameter d_s:

$$d_s = \frac{1}{2} \frac{w_s^2}{g \, \Delta} \frac{\alpha_2}{\alpha_3} C_D \tag{2.9}$$

2.2.3 Empirical Formulae for the Fall Velocity in Still Water

The method based on the shape factor cannot be easily applied in real conditions since the high geometric variability of natural particles would imply great operational difficulties for defining the shape factor. Alternatively, we can use some empirical relations of fall velocity deduced by experimental observations on natural particles. Some of these empirical relations are shown in Table 2.2, where the fall velocity
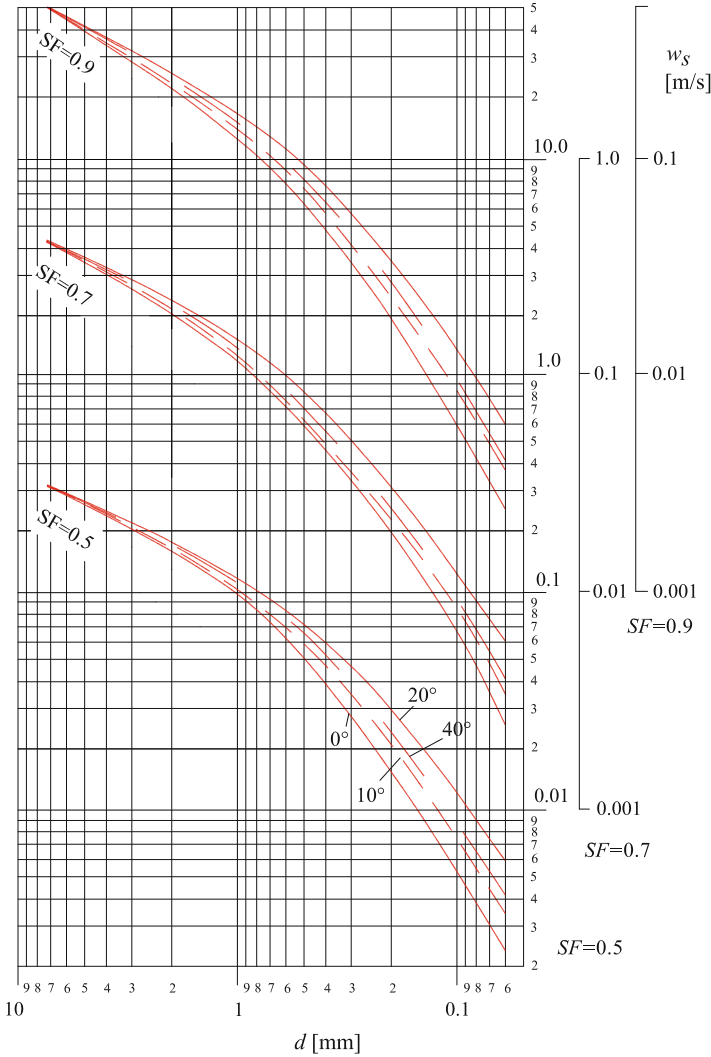
Fig. 2.6 Fall velocity in still water with different shape factor as a function of the sieve diameter and the water temperature (from Colby (1957))

in still water is expressed as the sediment Reynolds number $Re_w = w_s\, d_n/\nu$ concerning the particle dimension d_n in function of the dimensionless particle diameter $D_* = d_n \sqrt[3]{g\,\Delta/\nu^2}$ (Bonnefille 1963).

Table 2.2 Empirical formulae for assessing fall velocity in still water for natural particles, with $D_* = d_n \sqrt[3]{g \Delta / \nu^2}$

Dimensionless fall velocity	Range of validity	Authors
$\dfrac{w_s d_n}{\nu} = \dfrac{D_*^3}{18}$	$D_* < 3.42$; (Stokes' law)	
$\dfrac{w_s d_n}{\nu} = \dfrac{D_*^{2.1}}{6}$	$3.42 < D_* < 21.54$; natural sand	Hallermeier (1981)
$\dfrac{w_s d_n}{\nu} = 1.05 \, D_*^{1.5}$	$D_* > 21.54$; natural sand and gravel	
$\dfrac{w_s d_n}{\nu} = C_1 \, D_*^3 + C_2 \, D_*^{1.5}$	$3.42 < D_* < 21.54$;	
$C_1 = 0.055 \tanh \left(12 \, D_*^{1.77} \, e^{-0.0004 D_*^3} \right)$	Natural sand	Ahrens (2000)
$C_2 = 1.060 \tanh \left(0.016 \, D_*^{1.5} \, e^{-120/D_*^3} \right)$		
$\dfrac{w_s d_n}{\nu} = 1.05 \, D_*^{1.5} \left(1 - e^{-0.08 D_*^{1.2}} \right)$	Natural sand and pebbles	She et al. (2005)
$\dfrac{w_s d_n}{\nu} = 1.05 \, D_*^{1.5} \left(1 - e^{-0.315 D_*^{0.765}} \right)$	Natural sand and pebbles	She et al. (2005)

The last two formulae are practically equivalent

2.3 Sediment Transport Capacity, Solid Discharge, Wash Load, and Bed Material

The sediment *transport capacity* of a stream fluid is the maximum quantity of a particular sediment aggregation transported by the flow in equilibrium condition (e.g., uniform flow condition).

This means that in order to reach the transport capacity a great quantity of such material needs to be available. Otherwise, the flow would carry all the sediments available: in these conditions, the real solid discharge does not coincide with the transport capacity.

Generally in a watercourse, in the presence of variations in hydrodynamic characteristics, the solid discharge tends to the transport capacity. For instance, in the presence of abrupt hydrodynamic variations, we can observe that the coarsest sediments rapidly match the transport capacity, while the finest material is less suitable to quick hydrodynamic variations. Moreover, when the stream velocity increases, the finest bed material may not be enough to satisfy the requirements of the transport capacity: in this case, the corresponding solid discharge can be significantly less than the transport capacity.

The solid discharge of the very fine fraction is thus independent of hydrodynamic conditions. In this case, the solid transport is termed *wash load*, i.e., distinct from the *bed-material load* which instead represents the solid discharge of the material fraction, which is present on the river bed. For the bed material, it then makes sense to speak of transport capacity and solid transport formula, meant as the relation linking the potential solid discharge to the hydrodynamic conditions and characteristics of

particles. The wash load depends, on the contrary, on the quantity of this material coming from upstream.

In a stream, the material transported as bed material is then of the same type as the bed-forming material: it is a material with a continuous exchange between bed and stream. However, it is worth remembering that also in the bed material the grain size distribution of the transported material is generally different from that of the bed-forming material and that a variation in the quantity of the transported material usually implies a variation in the *granulometric curve* of the bed and vice versa.

Generally the *mean diameter of the transported material* is less than the *mean diameter of the bed-forming material*.

2.4 Sediment Transport Mechanisms: Bed Transport and Suspended Transport

The *bed material* of a stream sets into motion when the hydrodynamic forces (*drag* and *lift*) prevail on the forces opposing motion: *weight* and *interparticle friction* (interaction with the surrounding particles). As a matter of fact, it would be more appropriate to refer to moments of forces; however, from the viewpoint of the dimensional analysis it suffices to consider the balance of forces.

Once in motion, the material can continue its flowing according to two basically different modes (Fig. 2.7):

1. *bedload by rolling* or *saltation.* One particle moves by rolling over the other particles, or by alternating small jumps (of the order of the dimension of the particle) slightly lifting from the bed.
2. *suspended load.* From the bed, the particle is lifted up to a height of the order of the water depth, and before returning to the bed it flows along a trajectory, the length of which can be compared to the water depth (and is often many times higher).

With reference to Fig. 2.8, in terms of moments of forces in play, there is motion when the moments of the destabilizing forces (drag **D** and lift **L**) around the pivot point M exceed the moments of the stabilizing forces (submerged weight $\mathbf{G} - \mathbf{B}$).

If the lift is small, ($\mathbf{L} \leq \mathbf{G} - \mathbf{B}$), then it is the hydrodynamic drag to be responsible for the motion and the material tends to flow by *rolling*. Vice versa, if $\mathbf{L} \geq \mathbf{G} - \mathbf{B}$, then the material moves by saltation or in suspension.

The lift **L** is a *conservative force* and depends on the *circulation* around the grain, while the drag is an essentially *dissipative force* due to the stresses on the particles and the flow wake; in a turbulent flow both the lift and the drag continuously change in intensity and, consequently, the turbulent fluctuations produce the suspended load. According to some researchers, the suspended load can occur only if:
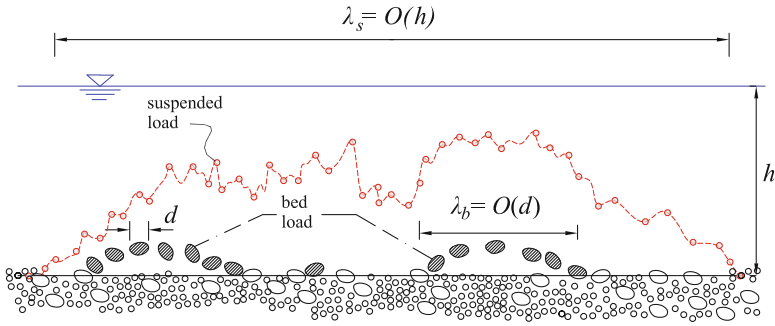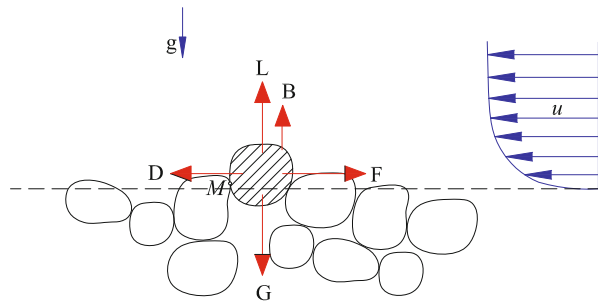
$$w_s < 0.8u_* \tag{2.10}$$

Fig. 2.7 Scheme of bed transport and suspended transport

Fig. 2.8 Scheme of the forces acting on a streambed particle

where w_s is the fall velocity of the particle in still water and $u_* = \sqrt{\tau_0/\rho}$ is the friction velocity of the stream.

2.5   Bed Forms: Ripples, Dunes, and Antidunes

A plane bed, composed of loose particles, run by a water stream, turns out to be unstable. The solid transport, bed or suspended load, induces on the bed surface some organized structures which have relatively regular shapes and depend on the stream regime.

One of the most evident consequences of this phenomenon is the increase in resistance in natural mobile beds as the averaged velocity rises, which is much more remarkable than in fixed beds characterized by the same grain roughness, as well shown in Fig. 2.9.

This increase can be accounted for by the fact that the increasing stream velocity develops the *bed forms* producing an equivalent roughness which then adds to the roughness produced by the single grains.

Fig. 2.9 Trend of the bed
shear stress as a function of
the depth-averaged velocities
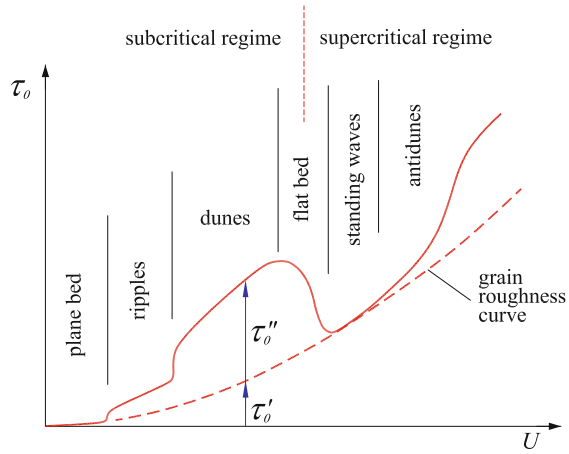
2.5.1 Classification of Bed Forms

Figure 2.10 shows a schematization of the organized bed forms usually taken on by
a natural bed. These are the major bed forms observed both in laboratory (Simons
and Richardson 1966) and in nature.

2.5.1.1 Ripples

The forms observed in conditions near to the incipient motion of fine sand particles
look like small quasi-triangular waves, more or less regular. These waves, known as
ripples, usually develop in the presence of a viscous sub-layer, i.e., when the virtual
thickness of the viscous sub-layer δ' is higher than the grain size:

$$\delta' \simeq \frac{11.6\,\nu}{u_*} \geq d \tag{2.11}$$

Ripples usually have a two-dimensional structure, but three-dimensional ripples
have been observed as well. Their length is generally less than 60 cm and their height
less than 6 cm (Engelund and Fredsøe 1982). However, the ripple length seems to
be independent of the water depth.

In coarse sand beds with average material diameter higher than about 0.5 mm,
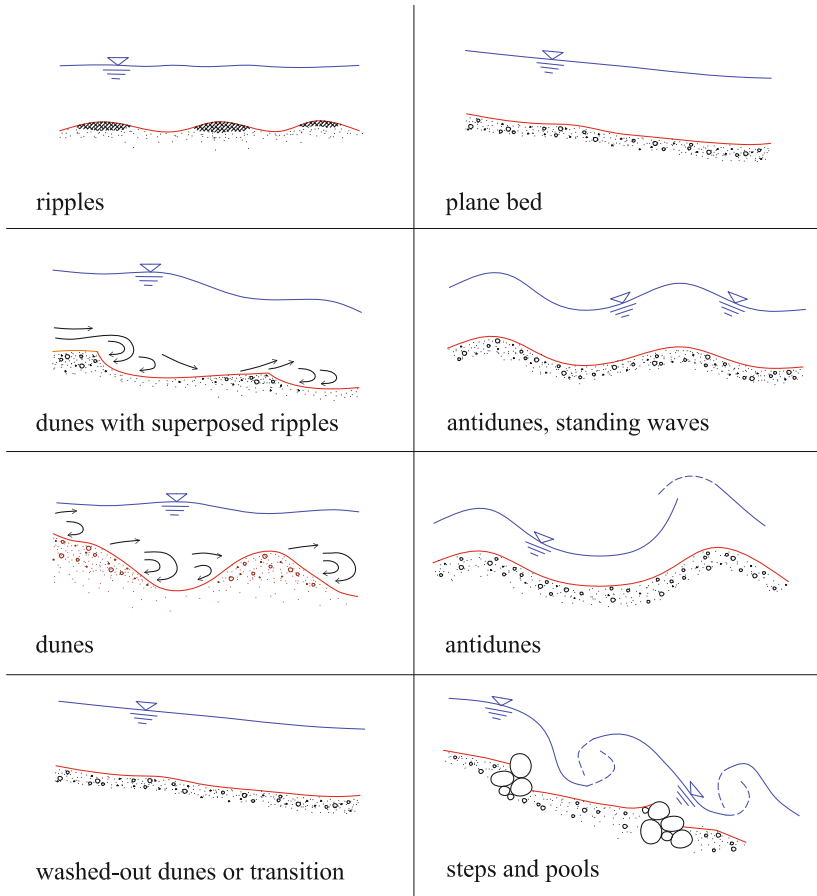ripples do not develop.

Fig. 2.10 Schematic classification of bed forms in function of water stream conditions (Allen 1968)

2.5.1.2   Dunes

In fluvial sand beds, when the bed turns out to be hydraulically rough, bed forms have much more considerable dimensions than ripples, but also triangular-shaped with a gently inclined slope and a steep front. These forms are associated with the Froude number less than unity, that is, *subcritical flows*. These forms are called *dunes*, because of their great similarity to sand desert dunes.

Just in correspondence to the dune ridge, the outer boundary layer tends to separate and to create a wake, characterized by low velocities and highly intense turbulence. The particles are eroded from the dune ridge and start to slide over each other; once they reach the ridge top, the particles tend to drop into the separation area and settle there, thus allowing the dune to migrate downward (Fig. 2.11).

Fig. 2.11 Mechanism of downstream dune migration
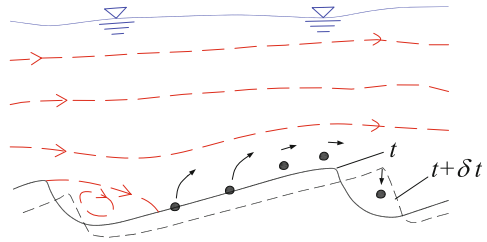
Apparently the dune wavelength ranges from a few to around tens of meters. As a matter of fact, the length scale of dunes basically depends on the water depth. The stream being subcritical, the free surface is slightly affected by bed alterations and, in any case, the changes result to be in phase opposition to bed perturbations.

In coarse-grained beds with an average material diameter higher than about 5–6 mm, dunes do not develop.

In gravel or pebble beds, dunes generally do not form, on the contrary there develop planimetric bed forms like bars, scaled by the section width.

2.5.1.3 Plane Bed

Whenever the stream velocity rises, the dunes first tend to increase in size and, in case of higher velocity, to be washed out. In such conditions, the bed appears to be flat and the global roughness decreases up to the single grain roughness. This occurs when the stream values of the Froude number are near unity.

2.5.1.4 Antidunes

A further increase in stream power leads to the formation of another type of bed forms called *antidunes*. Their shape appears to be more symmetrical than dunes and their trend looks rather sinusoidal. The free surface of the flow is significantly altered in the presence of antidunes and its variations are more accentuated and in phase with the bed perturbations, as easily explained by the hypothesis of constant specific energy. When the Froude number increases, the free surface becomes steeper and steeper until it breaks up. On breaking-up, antidunes tend to elongate, disappear, reshape, and lead to a new breaking-up of the free surface by means of a continuous, definitely non-stationary, and highly dissipative process.

As will be shown later, the name antidune indicates that the dune form tends to move upstream, even if the single particles naturally flow downward.

Fig. 2.12 Scheme of a
step-pool formation
(Egashira and Ashida 1991)
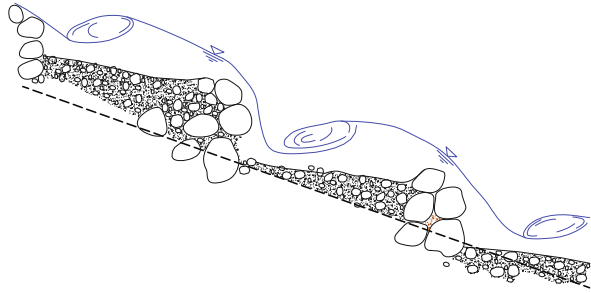
2.5.1.5   Steps and Pools

This type of bed form appears only in torrents with steep slopes ($0.1 > i_b > 0.075$).
It is a bed layout with large steps, with greater boulders forming the downstream
perimeter of the step. Downstream from these boulders, the bed has a leap, while
between the two steps the bed has a lower slope than average (pool). The granulometry
in the pool is on average thinner than the dimension of boulder steps (Whittaker and
Jaeggi 1982) (Fig. 2.12).

References

J.P. Ahrens, A fall-velocity equation. J. Waterw. Port Coast. Ocean Eng. **126**(2), 99–102 (2000)

M.L. Albertson, *Effect of Shape on the Fall Velocity of Gravel Particles* (State University of Iowa, 1953)

J. Allen, *Current Ripples* (1968), pp. 433

R. Bonnefille, Essais de synthèse des lois de début d'entraînement des sédiments sous l'action dun courant en régime continu. Bulletin Centre de Recherhce Chatou **5**, 67–72 (1963)

B. Colby, Some fundamentals of particle size analysis, in *St Antony Falls Hydraulic Laboratory, Minneapolis. Rep*, vol. 12 (1957)

S. Egashira, K. Ashida. Flow resistance and sediment transportation in streams with step-pool bed morphology, in *Fluvial Hydraulics of Mountain Regions* (Springer, 1991), pp. 45–58

F. Engelund, J. Fredsøe, Sediment ripples and dunes. Annu. Rev. Fluid Mech. **14**(1), 13–37 (1982)

R.J. Hallermeier, Terminal settling velocity of commonly occurring sand grains. Sedimentology **28**(6), 859–865 (1981)

E.J. Helley, Field measurement of the initiation of large bed particle motion in Blue Creek near Klamath, California. Technical Report (1969)

K. She, L. Trim, D. Pope, Fall velocities of natural sediment particles: a simple mathematical presentation of the fall velocity law. J. Hydraul. Res. **43**(2), 189–195 (2005)

D.B. Simons, E.V. Richardson, Resistance to flow in alluvial channels. Technical Report (US Govt. Print. Off, 1966)

C.K. Wentworth, A scale of grade and class terms for clastic sediments. J. Geol. **30**(5), 377–392 (1922)

J.G. Whittaker, M.N. Jaeggi, Origin of step-pool systems in mountain streams. J. Hydraul. Div. **108**(6), 758–773 (1982)

Chapter 3
Initiation of Sediment Motion

3.1 Introduction

The incipient motion condition is the hydrodynamic condition, i.e., of velocity and flow depth, whereby the particles lying on a streambed start to move under the action of fluid. But this condition also depends on the particle properties, such as size, density, shape, as well as on the position of each particle with respect to the surrounding particles.

To simplify the analysis, we will initially assume a uniform flow, that is, with water depth and depth-averaged velocity constant over time and in the flow direction. As shown in this chapter, in a turbulent water stream, the action of the water capable of moving the particle is basically determined by turbulence fluctuations and by the degree of particle exposure, conditions which are both randomly distributed. Therefore, although a probabilistic approach would be preferable, we will follow the deterministic theory proposed by Shields in 1936.

Our choice is motivated by theoretical as well as practical reasons: the Shields theory is actually the first rational approach to the problem, and the yielded result is extremely simple and useful for a variety of river engineering problems.

Following Shields's analysis (Sects. 3.1 and 3.2), we will initially make quite restrictive hypotheses, in that we assume homogeneous-sized material and quasi-horizontal and -straight bed, and the water depth much bigger than the grain size (high submergence). In the next sections, these hypotheses will be removed to introduce the effect of the longitudinal slope of the bed on the threshold condition (Sect. 3.3.2), the effect of side slope (Sect. 3.3.3), and the effect of low submergence (Sect. 3.3.4).

We will then address the problem of incipient motion in the presence of non-uniform-sized grains, distinguishing between hiding and armoring (Sects. 3.3.5 and 3.3.6) in Sect. 3.5. Finally, we will introduce some other criteria to define the incipient motion condition.

Under this procedure, we will be able to apply the superposition of the effects to different aspects.

3.2 The Shields Theory

The *threshold motion condition of the particles* (or *incipient motion condition*), which constitute the bed of a water stream, can be determined by imposing the balance between the forces tending to move particles and the forces contrasting their motion.

The approach here considered derives from the classical theory originally proposed by Shields (1936) under the hypothesis of homogeneous, non-cohesive particles resting on a quasi-horizontal and -straight bed.

With reference to Fig. 3.1, each particle is subject to the following forces: the lift force **L** and the hydrodynamic drag force **D** in the vertical and horizontal direction, respectively; **G** and **B** are respectively weight and buoyancy, and **F** is the streamwise component of the friction force. The last represents the resultant of contact actions between the particle in question and the surrounding particles. The friction is assumed to be proportional to the resultant of the normal components of other forces acting on the particle, by means of a proper friction coefficient μ_f which depends on the nature and form of particles. At the beginning of the particle motion, the *coefficient of friction* μ_f equals the value of the tangent of the *friction angle* φ: $\mu_f = \tan \varphi$.

At the very moment of initiation of the particle movement, the hydrodynamic drag force results to be equal and opposite to the friction:

$$\mathbf{D} = -\mathbf{F} \tag{3.1}$$

The forces involved are determined by means of the following relations:

$$\mathbf{D} = \hat{\mathbf{e}}_s \, C_D \, \alpha_2 d^2 \, \rho \frac{u^2}{2} \tag{3.2}$$

$$\mathbf{L} = \hat{\mathbf{e}}_n \, C_L \, \alpha_2 d^2 \, \rho \frac{u^2}{2} \tag{3.3}$$

$$\mathbf{G} - \mathbf{B} = -\hat{\mathbf{e}}_n \, g \, (\rho_s - \rho) \, \alpha_3 d^3 \tag{3.4}$$

where $\alpha_2 d^2$ represents the projected area of the particle, α_2 being an appropriate shape coefficient. Similarly, $\alpha_3 d^3$ is the volume of the particle; α_3 is a shape coefficient

Fig. 3.1 Scheme of the forces acting on a particle on a streambed. Particles are thought to be size-homogeneous and non-cohesive, and the bed is assumed to be quasi-horizontal
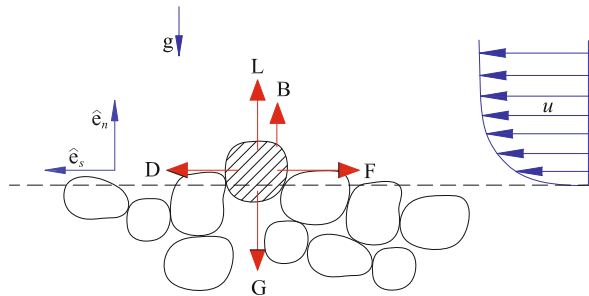
as well. C_D and C_L are, respectively, hydrodynamic drag and lift coefficients. $\hat{\mathbf{e}}_s$ and $\hat{\mathbf{e}}_n$ are the unit vectors (*versors*) in the flow and normal directions, respectively.

The force equilibrium in the flow direction gives:

$$\mathbf{F} = -\hat{\mathbf{e}}_s \tan \varphi \; |\mathbf{G} - \mathbf{B} - \mathbf{L}| \tag{3.5}$$

After replacing the respective expressions, we obtain:

$$C_D \, \alpha_2 d^2 \, \rho \frac{u_d^2}{2} \left(1 + \frac{C_L}{C_D} \tan \varphi\right) = \tan \varphi \, g \, (\rho_s - \rho) \, \alpha_3 d^3 \tag{3.6}$$

The velocity u_d in Eq. (3.6) is the flow velocity at the particle; it can be expressed in function of the friction velocity $u_* = \sqrt{\tau_o/\rho}$, assuming that the local distribution of velocities follows the logarithmic distribution:

$$\frac{u_d}{u_*} = \frac{1}{\kappa} \ln \frac{y}{k_e} + B(\frac{k_e \, u_*}{\nu}) \tag{3.7}$$

k_e is the equivalent bed roughness that can be reasonably assumed as proportional to the particle diameter: $k_e = \alpha_k \, d$. Besides, the reference velocity may be calculated at a distance $y = \alpha_d \, d$, where α_k and α_d are suitable shape coefficients of order of magnitude 1.

Equation (3.7) is written in a general form, valid both for the smooth bed (in this case $B = func(u_* d/\nu)$) and for the hydraulically rough bed ($B = const$) (e.g., Table 1.1 at page 4). We thus obtain:

$$\frac{u_d}{u_*} = f_u(\alpha_k, \alpha_d, \frac{du_*}{\nu}) \tag{3.8}$$

The hydrodynamic drag coefficient C_D depends on the particle shape through an appropriate shape coefficient α_{sf}, and on the local Reynolds number (du_d/ν):

$$C_D = f_D \left(\alpha_{sf}, \frac{d \, u_d}{\nu}\right) \tag{3.9}$$

According to Eq. (3.8), the local velocity u_d can be expressed through the friction velocity u_*, giving for the drag coefficient the following relation:

$$C_D = f_D(\alpha_{sf}, \alpha_k, \alpha_d, \frac{du_*}{\nu}) \tag{3.10}$$

In addition, the ratio C_L/C_D can be assumed as constant with values ranging between 0.8 and 1.3, even if some authors do not consider the lift force by assuming $C_L = 0$.

By replacing Eqs. (3.8) and (3.10) into (3.6), we obtain that at the threshold condition:

$$\frac{u_*^2}{g\dfrac{\rho_s - \rho}{\rho}d} = 2\,\frac{\alpha_3}{\alpha_2}\,\frac{\tan\varphi}{1 + \dfrac{C_L}{C_D}\tan\varphi}\,\frac{1}{f_D f_u^2} \tag{3.11}$$

that is, according to Eqs. (3.8) and (3.10):

$$\frac{u_*^2}{g\dfrac{\rho_s - \rho}{\rho}d} = func\left(\frac{d\,u_*}{\nu}\right) \tag{3.12}$$

In (3.12), the shape coefficients $\alpha_2, \alpha_3, \alpha_f, \alpha_k, \alpha_d$ do not appear, in that they are assumed to be more or less constant for natural particles. For the same reason, we assume constant $\tan\varphi$ and the ratio C_L/C_D.

The parameter on the left of Eq. (3.12) is called the *Shields mobility parameter*, and it is usually denoted with the Greek letter θ, that is:

$$\theta = \frac{u_*^2}{g\dfrac{\rho_s - \rho}{\rho}d} = \frac{u_*^2}{g\,\Delta\,d} \tag{3.13}$$

where $\Delta = (\rho_s - \rho)/\rho$ denotes the *relative density of immersed grains*.

The second dimensionless parameter highlighted by the analysis is the Reynolds grain number:

$$Re_* = \frac{du_*}{\nu} \tag{3.14}$$

The Shields analysis shows, therefore, that at threshold condition the mobility parameter θ takes the critical value of *incipient motion*, which results to be a function of the particle shape and of the Reynolds grain number.

We denote the threshold value of the Shields mobility parameter (*critical Shields mobility parameter*) as $\theta_{co} = u_{*c}^2/(g\,\Delta\,d)$. Since in the next sections we will calculate the critical mobility parameter also in conditions other than those assumed by Shields, the suffix ($_o$) in the above definition refers to the critical mobility parameter calculated in the conditions assumed in the above Shields procedure, i.e., homogeneous material, quasi-horizontal straight bed, and high submergence.

In other words, Eq. (3.12) at the critical incipient motion condition can be more conveniently rewritten as:

$$\theta_{co} = func(Re_*) \tag{3.15}$$

The above relation was experimentally determined by Shields and is shown in Fig. 3.2.

As said above, in Eq. (3.12) we neglected the dependence on the shape, in that we assumed natural particles to have sensibly constant shape factors. However, in case
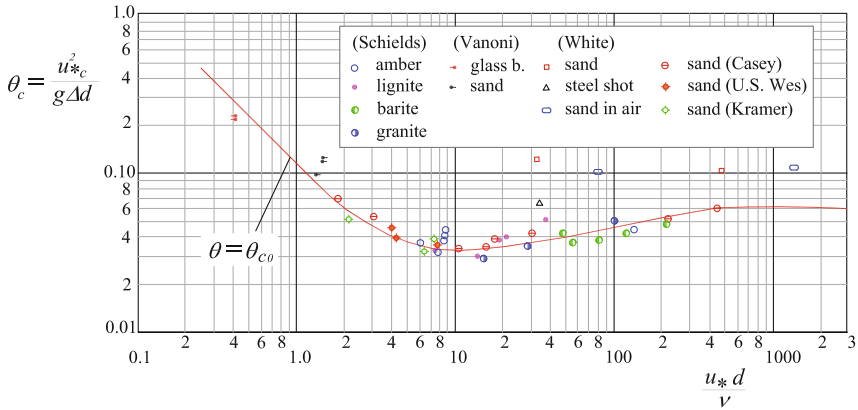
Fig. 3.2 The Shields diagram

(natural or artificial) particles have a particular shape, also this parameter should be properly considered.

The curve in Fig. 3.2 separates the mobility from the immobility area of the particles: for the points lying below the curve ($\theta \leq \theta_{co}$), the flow is not able to move the particles, while the points above the curve represent the conditions of sediment transport.

The curve representing the particle incipient motion ($\theta = \theta_{co}$) can be divided into three parts.

The first part of the curve ($Re_* \leq \sim 2$) is represented by a linear segment in the bi-logarithmic graph; the second part ($\sim 2 \leq Re_* \leq \sim 200$) by a curve with a relative minimum, and the third ($\sim 2 \leq Re_* \leq \sim 200$) by a constant trend.

According to Shields, the first part of the curve (for $Re_* \leq \sim 200$) is described by the following expression:

$$\frac{u_{*c}^2}{g \Delta\, d} = 0.12 \frac{v}{u_{*c}\, d}$$
$$u_{*c}^3 = 0.12 g\, \Delta\, v \tag{3.16}$$

According to Eq. (3.16), the critical particle velocity is independent of the particle diameters, but it depends on the fluid viscosity. This result does not surprise because, even when $Re_* \to 0$, the friction coefficient between grains remains finite and thus the critical velocity remains finite. This implies that, when the Reynolds grain number tends to zero, there may be particle motion only if the particle diameter is sufficiently small. In this case, the bed tends to be covered by a mixture of very fine material, where the single grain loses its individuality. This leads to an essentially viscous flow in this range.

It is useful to remember that Shields did not experiment at $Re_* < 6$, but suggested the hyperbolic trend expressed by Eq. (3.16). Other authors have obtained rather different trends. For example, (Grass 1970) and (White 1970) found that for $Re_* \leq \sim$ 2, the curve is flatter than 45°. It should also be noted that the experiments in this range are very delicate, and often the accuracy of the measurements is not enough to draw any definitive conclusions.

In the third section of the Shields curve, for $Re_* \geq \sim$ 200, the mobility parameter assumes nearly constant values:

$$\theta_{co} = \frac{u_{*c}^2}{g\Delta d} \simeq 0.057 \qquad (3.17)$$

In this case, the mobility condition is independent of the flow viscosity: the regime is therefore that of the turbulent flow on a hydraulically rough wall.

In the middle section, for $\sim 2 \leq Re_* \leq \sim$ 200, the flow condition depends on both grain size and flow viscosity. In this section, the curve presents its minimum $(\theta_c)_{min} \simeq 0.03 \sim 0.04$ at $Re_* = u_* d/\nu \simeq 8 \sim 10$.

3.3   Limits and Extensions of the Shields Theory

The Shields diagram has the peculiarity that the friction velocity appears both in abscissae and ordinates. This may be a limitation, because some applications may require to proceed with an iterative method. This problem can be overcome by replacing the variable Re_* with one that can be obtained by a proper combination between it and the variable θ, so as to eliminate the friction velocity, i.e.,

$$Re_*^2 \; \theta^{-1} = \left(\frac{u_* d}{\nu}\right)^2 \frac{g\Delta d}{u_*^2} = \frac{g\Delta d^3}{\nu^2} \qquad (3.18)$$

The parameter on the right-hand side of Eq. (3.18), raised to the 1/3 power, can be interpreted (Yalin 1977) as a dimensionless particle diameter D_* (Bonnefille 1963) (see Sect. 2.2.3):

$$D_* = d \left(\frac{g\Delta}{\nu^2}\right)^{1/3} \qquad (3.19)$$

The diagram on the incipient motion condition as a function of the dimensionless diameter D_*, reported in Fig. 3.3, is similar to the Shields diagram. The figure also shows the following analytical approximation of the incipient motion condition, proposed by Brownlie (1981):

$$\theta_{co} = 0.22 \, D_*^{-0.9} + 0.06 \, e^{-17.73 \, D_*^{-0.9}} \qquad (3.20)$$
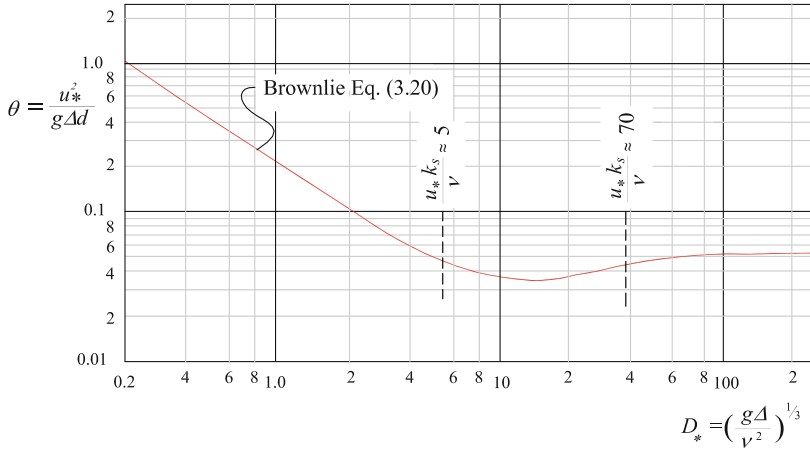
Fig. 3.3 The Shields diagram as a function of the dimensionless diameter (Yalin 1977)

An expression slightly different from the previous one was proposed by Soulsby et al. (1997):

$$\theta_{co} = 0.24\, D_*^{-1} + 0.055 \left(1 - e^{-0.02\, D_*}\right) \tag{3.21}$$

From the figure, we also deduce that in uniform flow a particle with a certain diameter can have one and only one critical condition, corresponding to a specific hydrodynamic condition. Moreover, for natural materials, with immersed relative density $\Delta \simeq 1.67$, the rough bed condition ($D^* \simeq 200 \sim 300$) is reached by particles of dimension equal to $8 \sim 16$ mm, while the smooth bed condition occurs with particles whose size is less than $120\, \mu m$.

3.3.1 Definition of the Incipient Motion Condition

Although the Shields theory is seemingly simple, the practical definition of incipient motion condition in a streambed cannot be taken for granted. Quite evidently, the most exposed grains will tend to be moved as easily as higher is their exposure degree. Some grains move at bed shear stress values significantly lower than those reported in the Shields theory. Even if the concept of critical shear stress, or critical Shields parameter, is deeply rooted in the scientific and technical literature on sediment transport, it is worth underlining that there are some transport theories which disregard these concepts like, for instance, the (Einstein 1950) theory about bedload, which will be detailed in Sect. 5.2.

The incipient motion condition can be experimentally determined by extrapolating the relationship between solid discharge and hydrodynamic conditions toward

zero discharge. Consequently, the incipient motion condition is experimentally determined as that hydrodynamic condition corresponding asymptotically to a nil solid discharge. From the practical point of view, the method appears to be somewhat unreliable and imprecise. Better results can be obtained by correlating the incipient motion condition to some statistical parameters, such as the distribution of lift and drag forces (Graf et al. 1987) and the distribution of the particle exposure.

As a matter of fact, some authors suggest defining the incipient motion condition as that under which a given percentage of the particles per unit of time lifts off from a unit bed surface, e.g., 1% according to Suszka (1991) and 5% according to Tsuchiya (1969).

3.3.2   Effect of the Streamline Bed Slope

Should the bed slope be steep, in order to balance the forces in the direction of motion, also the effect of the weight and buoyance forces need to be introduced (Fig. 3.4).

In this case, the Archimedes force results to be normal to the undisturbed streamlines, and its module ($\mathbf{B} = g\,\rho\alpha_3 d^3\cos\alpha_b$) depends on the longitudinal slope of the bed, where α_b is the bed slope angle.

However, also the hydrodynamic drag is affected by the tangential stresses caused by bed inclination. In this case, it is $\mathbf{D} = C_D\,\alpha_2 d^2\rho u^2/2 - g\,\rho\alpha_3 d^3\sin\alpha_b$; this second term is induced by tangential stresses around the particle, which in the absence of the particle are balanced by the weight of a water volume equal to that of the particle.

The balance of forces in the direction of motion at the incipient motion condition is therefore:

$$\mathbf{D} + \mathbf{G}\sin\alpha_b = \tan\varphi\,|\,\mathbf{G}\cos\alpha_b - \mathbf{L} - \mathbf{B}\,| \tag{3.22}$$

which, after replacing the respective expressions of the different forces, leads to the following relation for the critical mobility parameter θ_{cb} for a sloping bed:
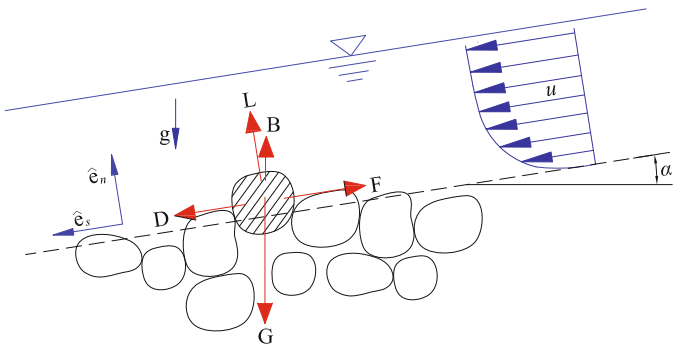

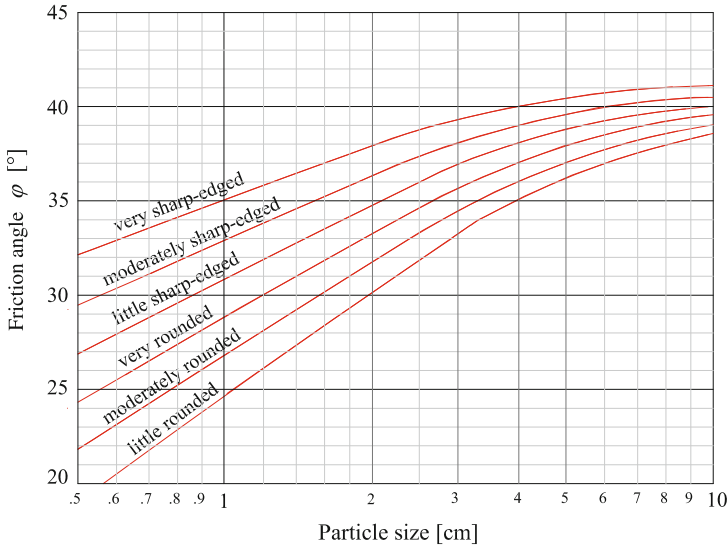**Fig. 3.4** Scheme of the forces acting on a particle on a sloped streambed

Fig. 3.5 Friction angle of different material types according to Lane (1953)

$$\theta_{cb} = \frac{u_{*c}^2}{g\,\Delta\,d} = \theta_{co}\left(\cos\alpha_b - \frac{\sin\alpha_b}{\tan\varphi}\right) \tag{3.23}$$

where α_b is the bed slope, and φ is the friction angle of the bed material (Fig. 3.5). θ_{co} denotes the critical Shields mobility parameter estimated in the hypothesis of quasi-horizontal straight bed, uniform grain size, and high submergence (as in Fig. 3.2 or Fig. 3.3).

In other words, the critical mobility parameter θ_{co} of the Shields diagram needs to be corrected with the factor $(\cos\alpha_b - \sin\alpha_b/\tan\varphi)$ to take the longitudinal bed slope into account (Fig. 3.6).

3.3.3 Effect of Side Slopes

In case of material resting on sloped banks, lift, buoyancy, and weight forces result in a further component also on the plane of the bank.

In this case, the resultant of the forces on the plane of the bank are not aligned with the flow direction. In the incipient motion condition, the balance between forces leads to the following expression (Fig. 3.7):

$$\sqrt{\mathbf{D}^2 + (\mathbf{G} - \mathbf{B})^2 \sin^2\alpha_{sb}} = \tan\varphi\,|(\mathbf{G} - \mathbf{B})\,\cos\alpha_{sb} - \mathbf{L}| \tag{3.24}$$

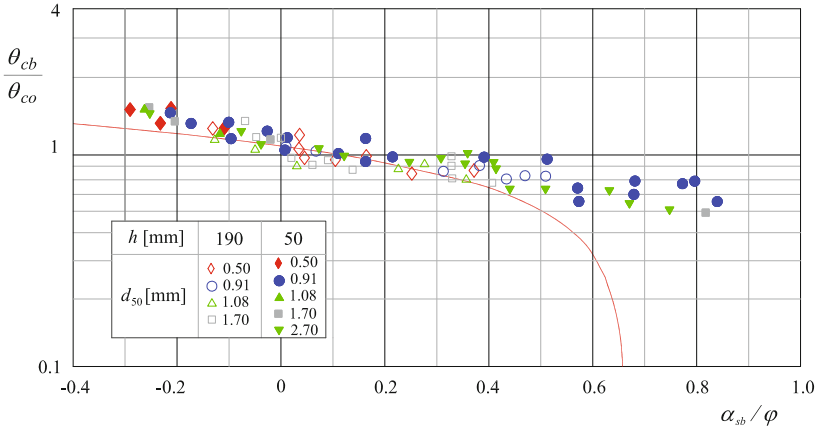α_{sb} is the inclination angle of the bank.

Fig. 3.6 Effect of the longitudinal bed slope on the mobility parameter (Chiew and Parker 1994). θ_{co} denotes the critical Shields mobility parameter estimated in the hypothesis of quasi-horizontal straight bed (original Shields value, Fig. 3.2 or Fig. 3.3)
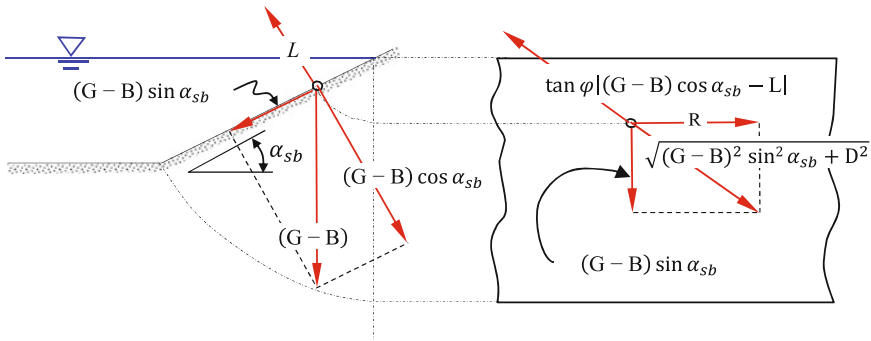

Fig. 3.7 Scheme of the forces acting on a particle on the sloped bank

Equation (3.24) can be solved with regard to the ratio θ_l/θ_o between the critical mobility parameter on the bank θ_{cb} and the critical Shields mobility parameter on a horizontal straight bed θ_{co}.

By substituting the definitions of the different forces (Eqs. 3.2–3.4), we obtain:

$$A_b \left(\frac{\theta_{c\,sb}}{\theta_{co}}\right)^2 - 2\,B_b \left(\frac{\theta_{c\,sb}}{\theta_{co}}\right) - 1 = 0 \tag{3.25}$$

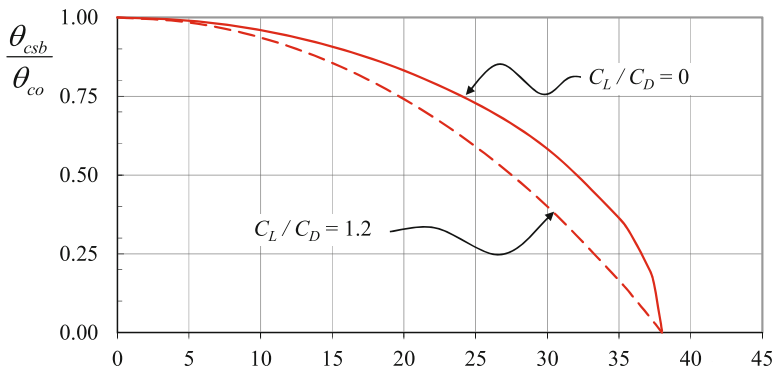where $\theta_{c\,sb}$ is the critical mobility parameter on a side bank, and where:

Fig. 3.8 Effect of the river bank slope on the parameter of critical mobility; for $C_L/C_D = 1.2$ and for $C_L/C_D = 0$ in accordance with Lane (1953). θ_{co} denotes the critical Shields mobility parameter estimated in the hypothesis of quasi-horizontal straight bed

$$A_b = \frac{1 - \dfrac{C_L}{C_D} \tan \varphi}{(1 + \dfrac{C_L}{C_D} \tan \varphi) \left(1 - \dfrac{\sin^2 \alpha_{sb}}{\sin^2 \varphi}\right)} \tag{3.26}$$

$$B_b = \cos \alpha_{sb} \frac{-\dfrac{C_L}{C_D} \tan \varphi}{(1 + \dfrac{C_L}{C_D} \tan \varphi) \left(1 - \dfrac{\sin^2 \alpha_b}{\sin^2 \varphi}\right)} \tag{3.27}$$

and therefore:

$$\frac{\theta_{c\,sb}}{\theta_{co}} = \frac{B_b + \sqrt{B_b^2 + A_b}}{A_b} \tag{3.28}$$

where θ_{co} is the critical Shields mobility parameter estimated in the hypothesis of horizontal bed (original Shields value, Fig. 3.2 or Fig. 3.3).

The solution of Eq. (3.25) is represented in the graph of Fig. 3.8 for $C_L/C_D = 1.2$. Supposing that this ratio is negligible, Lane (1953) obtained the stability condition in an explicit simple form:

$$\frac{u_{*c}^2}{g\,\Delta\,d} = \theta_{co}\sqrt{1 - \frac{\sin^2 \alpha_{sb}}{\sin^2 \varphi}} \tag{3.29}$$

where θ_{co} denotes the critical Shields mobility parameter estimated in the hypothesis of quasi-horizontal straight bed (Fig. 3.2, or Fig. 3.3). Figure 3.8 also illustrates Lane's solution.

Lane's solution is less precautionary since the lift force turns out to be destabilizing at the initial particle motion.

3.3.4   Effect of the Relative Submergence

According to the Shields theory, the relative roughness of the bed is assumed sufficiently small, i.e., so small to admit the presence of a layer of wall turbulence subjected to the logarithmic law (Eq. 3.7). However, the grain size is often the same order of size as the water depth h. This is a typical situation of low relative submergence h/d, as already described in Sect. 1.3.2. In such conditions, there is the formation of a mixing layer near the bed (*macro-roughness layer* according to Nikora et al. (2001)), which is dominated by the wakes created by the roughness elements and is δ_R thick, comparable to the water depth (Fig. 3.9).

In such situations, the grain mobility decreases significantly. Since it is a case of turbulent flow over a rough wall, the critical mobility parameter θ_c is independent of the Reynolds grain number.

The following empirical relation (Armanini 1999) well suits to low submergence conditions:

$$\frac{\theta_{c-ls}}{\cos \alpha_b - \dfrac{\sin \alpha_b}{\tan \phi}} = 0.06 \left(1 + 0.67 \left(\frac{d}{h} \right)^{0.5} \right) \tag{3.30}$$

where α_b is the slope angle of the bed in the streamwise direction (Fig. 3.10).
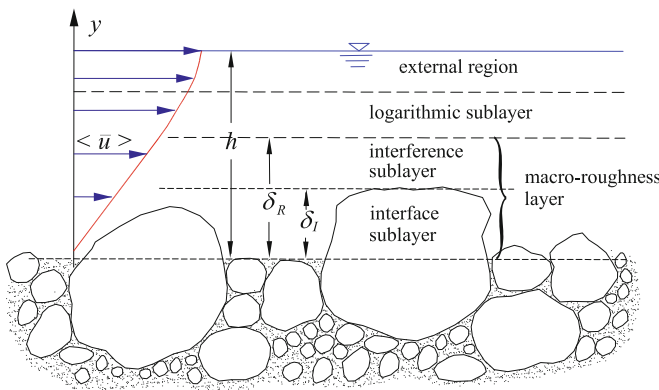

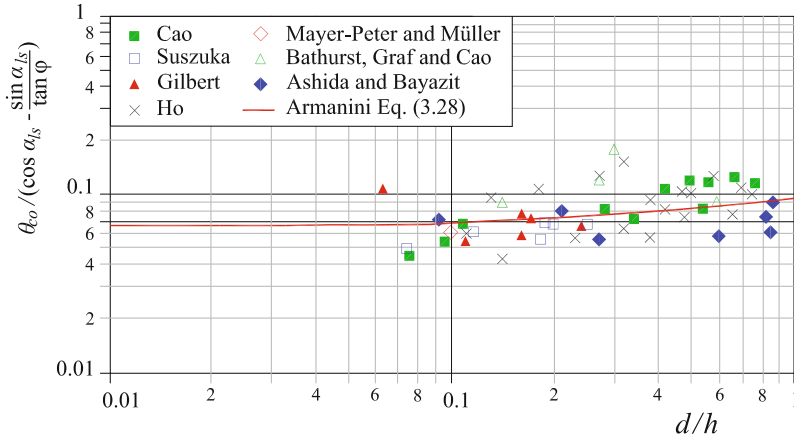**Fig. 3.9**   Wake-dominated mixing layer in the presence of low submergence

Fig. 3.10   Effect of the relative submergence on the incipient motion condition (Armanini 1999)

3.3.5   Effect of Size Heterogeneity of Bed Material

Natural streambeds are hardly composed of homogenous materials. In this case, the incipient motion condition of the single particle is significantly influenced by the non-uniformity of material size. In beds composed by non-homogeneous material, less sized particles are protected by those of higher dimension (*hiding or sheltering effect*), and this reduces their individual mobility. On the other hand, higher-sized particles tend to emerge, and be more exposed than finer particles and be set in motion with smaller shear stresses, thus increasing in mobility (Fig. 3.11).

In order to evaluate the hiding effect, different methods have been suggested. Generally speaking, the critical shear stress concerning each grain size class is assumed to be modified by an appropriate *hiding factor* ξ_j:

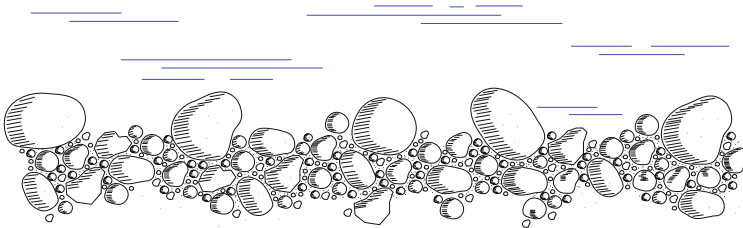$$\theta_{cj} = \theta_{cu}\xi_j \tag{3.31}$$

Fig. 3.11   Hiding effect in beds composed of non-uniform grain size mixtures

where $\theta_{c\,u}$ is the critical mobility parameter related to the representative diameter d_u of the distribution (as a rule, the average geometric diameter $\overline{d}$ or the d_{50} of the grain size distribution).

The hiding factor ξ_j is expressed in function of the ratio between the diameter of the *j-th* fraction d_j and the representative diameter d_u of the distribution (usually the average diameter d of the mixture).[1]

One of the first expressions to calculate the hiding factor was proposed by Egiazaroff (1965) in the following form:

$$\xi_j = \left(\frac{\log_{10} 19}{\log_{10} 19 \frac{d_j}{\overline{d}}} \right)^2 \tag{3.32}$$

Ashida and Michiue (1971) observed that Eq. (3.32) overestimates the mobility of finer particles. Such authors thus confirmed Eq. (3.32) for coarser particles ($d_j \geq 0.4\,\overline{d}$), while they suggested a linear relation for smaller particles ($d_j < 0.4\,\overline{d}$):

$$\xi_j = 0.85 \frac{\overline{d}}{d_j} \qquad \text{for } \frac{d_j}{\overline{d}} < 0.4$$

$$\xi_j = \left(\frac{\log_{10} 19}{\log_{10} 19 \frac{d_j}{\overline{d}}} \right)^2 \quad \text{for } \frac{d_j}{\overline{d}} \geq 0.4 \tag{3.33}$$

There are other expressions for the hiding factor, which have no general validity, since their application has been confined to some specific sediment transport formulae.

More in general, the hiding factor can be expressed by a monomial relation of the type:

$$\xi_j = \left(\frac{d_j}{\overline{d}} \right)^{-n} \tag{3.34}$$

According to Andrews (1983), the exponent is $\simeq 0.6 \leq n \leq \sim 1$ (Fig. 3.12).

On the basis of Eq. (3.34), the incipient motion condition for each grain size class can then be written as follows:

$$\theta_j = \theta_{c\overline{d}}\xi_j$$

$$\frac{u_{*c}^2}{g\,\Delta\,d_j} = \theta_{c\overline{d}} \left(\frac{\overline{d}}{d_j} \right)^n \tag{3.35}$$

---

[1] Alternatively, the mobility of the single grain size class $\theta_{c\,j}$ can be calculated with reference to the expected mobility as if the material were uniform, with the same granulometry as that in question and multiplied by a hiding factor as well. Of course in the presence of rough wall, the two definitions coincide in all grain size classes.
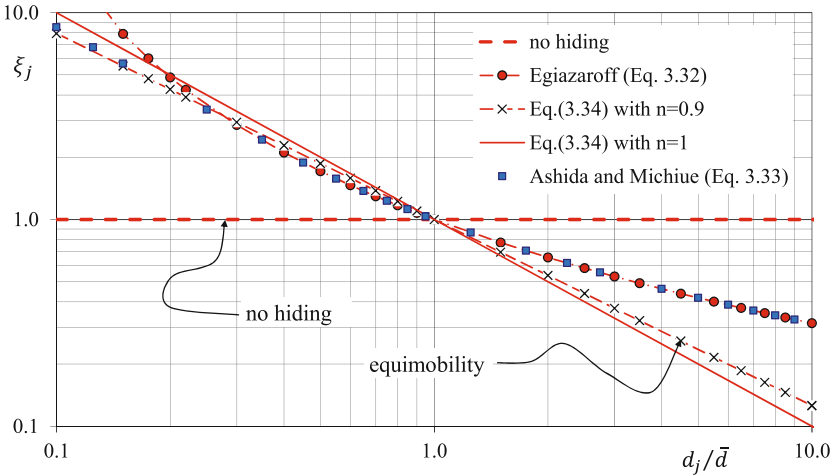
Fig. 3.12 The hiding factor in function of the relative diameter according to Egiazaroff (1965), to Ashida and Michiue (1971), and to the monomial expression (3.34)

where $\theta_{c\bar{d}}$ is the mobility parameter for the average diameter.

The exponent n must be <1. In fact, should n be equal to 1, the incipient motion condition expressed by (3.35) would be independent of the diameter d_j, representative of the single grain size class: that is to say, the mobility condition would be the same for all the grain size fractions. Quite unlikely to occur in a real context, this case is defined as *equimobility* condition. According to Parker et al. (1982), $n \simeq 0.905$ can be assumed for natural grain size mixtures, on average sorted out into gravel and sand beds.

3.3.6   Effect of Bed Armoring

Another phenomenon linked to the non-uniformity of bed material is the *static armoring*.

Static armoring denotes a situation occurring when the solid sediment supply from upstream tends to dissolve and the particles with smaller diameters (i.e., endowed with higher mobility than the critical mobility) are easily washed out by the flow little by little. Thus, the bed surface is enriched with particles of higher diameter (i.e., provided with lower mobility) (Fig. 3.13).

Such a layer, with an average diameter higher than that of the underlying material, is generally from one to three times as thick as the diameter of the greatest particles.

In this case, the incipient motion condition depends on the characteristics of the particles actually present on the surface.

Fig. 3.13 Scheme of static
armoring
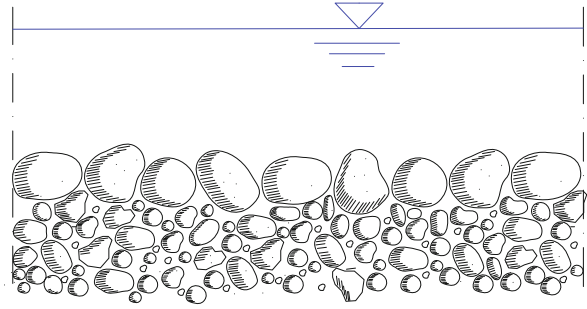
Relying on the protective capacity of the armoring layer can be dangerous in that, when the water discharge exceeds the value which has determined the formation of the armoring layer, the latter can break up thus showing a bed with an average diameter sensibly smaller than that on surface. Sometimes it can even lead to seriously erosive phenomena.

The armoring phenomenon frequently occurs in gravel-bed streams with quite roughly sized bed material (coarse gravel or pebbles) when the solid sediment supply is reduced, especially during the recession limb of the floods.

Very likely, it also takes place in beds composed of even very small-sized material. It is reasonably believed (Armanini 1989) that it, for instance, occurs in the Nile bed, downstream Aswan dam, where the average particle diameter is of the order of some hundreds of micron. In that case, however, the discharge regime strictly follows the dam outflow regime, and the regularity of the maximum discharge creates an armoring layer, composed of sandy material with diameter of the order of the millimeter and thickness of about two or three grains.

It is worth remembering that this type of *static armoring* is basically different from the *dynamic armoring*, in which the average diameter of the transported material is systematically lower than the average diameter of the bed material, as will be better explained in Sec. 5.6.1.

3.4 Effect of the Section Form on the Incipient Motion Condition

In engineering applications of the incipient motion theories, and particularly in assessing the stability of protection with loose material, the mobility parameter needs to be evaluated with regard to the maximum tangential stress acting on the wetted perimeter.

In other words, it should be considered that the shear stress distribution on the bed and banks is not constant, even in uniform flow condition, and that the maximum shear stress is generally higher than the average value calculated as:

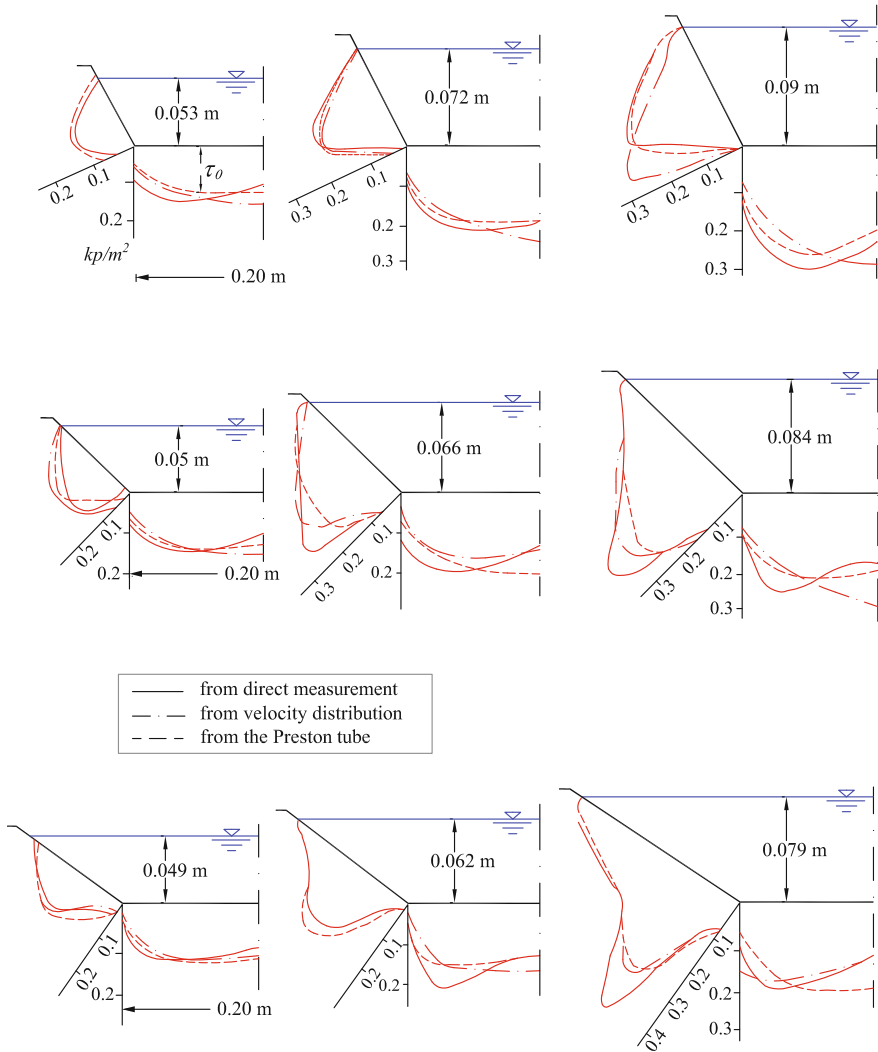$$\overline{\tau_o} = g \, \rho \, R_h \, i_E \tag{3.36}$$

Fig. 3.14 Shear stress distribution on the bed and banks of a laboratory trapezoidal channel with base $B = 20$ cm (Leutheusser 1963)

The ratio between the maximum stress and the average stress basically depends on the section form and on the Reynolds number, even if the dependence on the latter becomes negligible in the presence of sufficiently high values of this parameter ($R_e > 10^4 \sim 10^5$).

Figures 3.14 and 3.15 show the shear stress distributions for differently shaped cross sections.
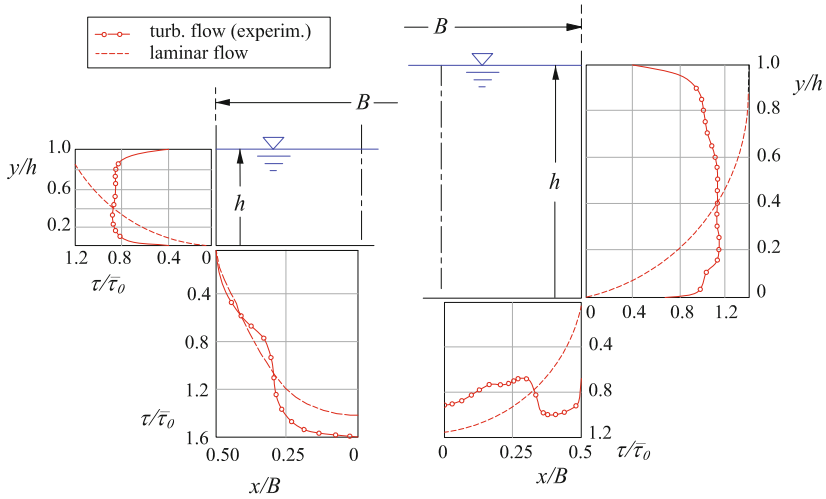
Fig. 3.15 Shear stress distribution on the bed and sidewalls of a rectangular channel (Leutheusser 1963)

3.5   Incipient Motion Condition in Channel Bends

Another case which results in a local increase of the shear stress on the bed, compared to the average value, is near the stream curves. The presence of bends in a stream determines the surface twist and consequently an increased velocity compared to the average values, but it also triggers secondary circular flows inducing tangential stresses along the river banks which are likely to influence the stability of the banks themselves. As a rule, the first effect is highly perceived on the inner bank stability. However, if the streambed is sufficiently mobile, it tends to be attenuated and often overcome by sedimentation phenomena due to the secondary circular flows. In the former case, there is an increase in the maximum shear stress on the bed. In the latter, there is a reduction in the critical mobility parameter and the effect, on the contrary, is more serious on the outer bank since it adds up to the gravity effect.

3.5.1   *Critical Mobility Reduction in Bends Induced by Secondary Circular Flows*

In curved channels, a secondary circular flow generates shear stresses on the bed in the radial direction; these stresses tend to reduce the critical mobility parameter on the outer bank. To evaluate the intensity of this stress, we refer to a curve with a constant radius of curvature in a rectangular channel (Fig. 3.16).

Fig. 3.16 Scheme of secondary circular flows in a curved channel
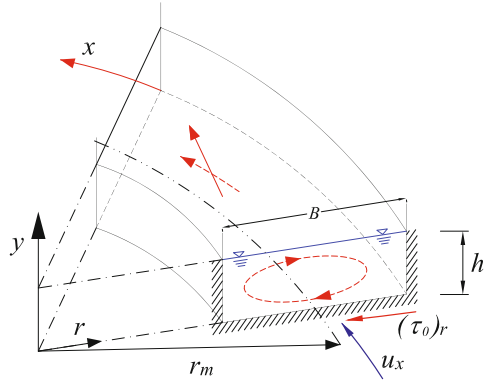
By adopting the simplified approach suggested by Rozovskii (1957), the radial shear stress on the bed can be expressed as follows:

$$\tau_{or} = -2 \left(\frac{n}{\kappa}\right)^2 \frac{1}{(2+n)(3+n)} \rho\, u_{*x}^2 \frac{h}{r_m} = -A_\tau\, \rho\, u_{*x}^2 \frac{h}{r_m} \qquad (3.37)$$

where r_m is the average channel radius of curvature. $n = 7 \sim 11$ is the power law exponent for vertical velocity component distribution ($u_x = u_{*x}\,(n/\kappa)\,(y/h)^{1/n}$) (higher values of n correspond to higher roughness); κ is the von Kármán constant.

In (3.37), we also define:

$$A_\tau = 2 \left(\frac{n}{\kappa}\right)^2 \frac{1}{(2+n)(3+n)} \qquad (3.38)$$

The following table shows the values of coefficient A_τ for some values of the power law exponent n:

n	7	8	9	10	11	12
A_τ	6.48	6.92	7.30	7.63	7.91	8.16

Equation (3.37) can be used to estimate the radial component of the shear stress to the bed which generates along the outer bank in a trapezoidal channel. It is then possible to repeat the analysis carried out for non-cohesive particles on the banks of a rectilinear channel in Sect. 3.3.3.

The stability condition is thus expressed by the following relation (Fig. 3.17):

$$\mathbf{D}^2 + |(\mathbf{G} - \mathbf{B})\,\sin\alpha_{cb} + \mathbf{T_r}\,\cos\alpha_{cb}|^2 \ \leq \tan^2\varphi\,|(\mathbf{G} - \mathbf{B})\cos\alpha_{cb} - \mathbf{P} - \mathbf{T_r}\sin\alpha_{cb}|^2 \qquad (3.39)$$

where α_{cb} is the slope angle of the curved bend, and

$$\mathbf{T}_r = \; . \; \tau_{or} \alpha_2 d^2 = A_\tau \, \rho \, u_{*x}^2 \frac{h}{r_m} \alpha_2 \, d^2 \tag{3.40}$$

represents the force exerted on the grain from the shear stress τ_{or}, as a product of the stress (3.37) and of the projected surface of the particle ($\alpha_2 \, d^2$).

The incipient motion condition is obtained by imposing the equilibrium of the forces in relation (3.39). By properly rearranging it, we get the following expression:

$$A_1 \left(\frac{\theta_{ccb}}{\theta_{co}} \right)^2 - 2 B_1 \left(\frac{\theta_{ccb}}{\theta_{co}} \right) - 1 = 0 \tag{3.41}$$

in which the mobility parameter of the curved bank is dimensionless versus the critical Shields mobility parameter on a quasi-horizontal straight bed θ_{co}. We thus have:

$$\theta_{ccb} = \theta_{co} \left(\frac{B_1 + \sqrt{B_1^2 + A_1}}{A_1} \right) \tag{3.42}$$

where θ_{co} denotes the critical Shields mobility parameter estimated in the hypothesis of quasi-horizontal straight bed (Fig. 3.2 or Fig. 3.3), and

$$A_1 = \frac{1 - \left(\dfrac{C_L}{C_D} \right)^2 \tan^2 \varphi - m^2 \, \tan^2 \varphi \left(1 - \dfrac{\cos^2 \alpha_{cb}}{\sin^2 \varphi} \right) - 2 \, m \, \dfrac{C_L}{C_D} \, \tan^2 \varphi \, \sin \alpha_{cb}}{\left(1 + \dfrac{C_L}{C_D} \, \tan \varphi \right)^2 \left(1 - \dfrac{\sin^2 \alpha_{cb}}{\sin^2 \varphi} \right)} \tag{3.43}$$

$$B_1 = - \cos \alpha_{cb} \, \frac{m \, \dfrac{\sin \alpha_{cb}}{\sin \varphi \; \cos \varphi} + \dfrac{C_L}{C_D} \, \tan \varphi}{\left(1 + \dfrac{C_L}{C_D} \, \tan \varphi \right) \left(1 - \dfrac{\sin^2 \alpha_{cb}}{\sin^2 \varphi} \right)} \tag{3.44}$$

$$m = \frac{h}{r_m} \, A_\tau \frac{\alpha_2}{\alpha_3 \tan \varphi} \left(1 + \frac{C_L}{C_D} \tan \varphi \right) \theta_o \tag{3.45}$$

It is easy to verify that Eq. (3.42) coincides with the corresponding Lane equation (3.29), if we set $r_m \to \infty$ and $C_L = 0$.

The solutions of Eq. (3.42) are given in Fig. 3.18; $\alpha_3 / \alpha_2 = 0.75$ is set as value corresponding to spherical particles. $C_L / C_D = 1.2$ was assumed precautionarily.
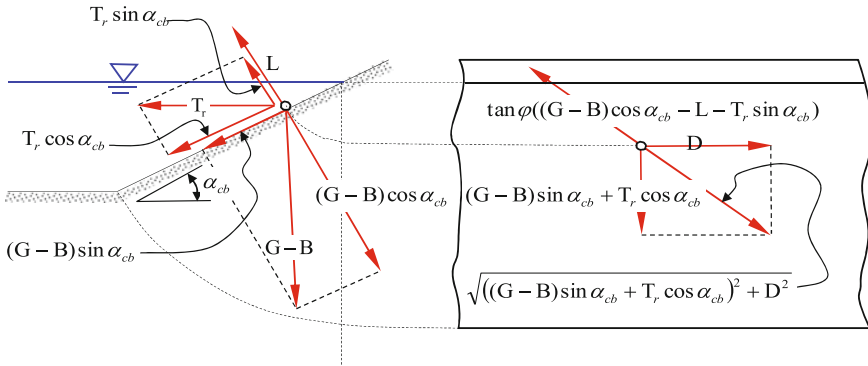
Fig. 3.17 Scheme of the forces acting on a particle resting on the sloped bank of a curved channel
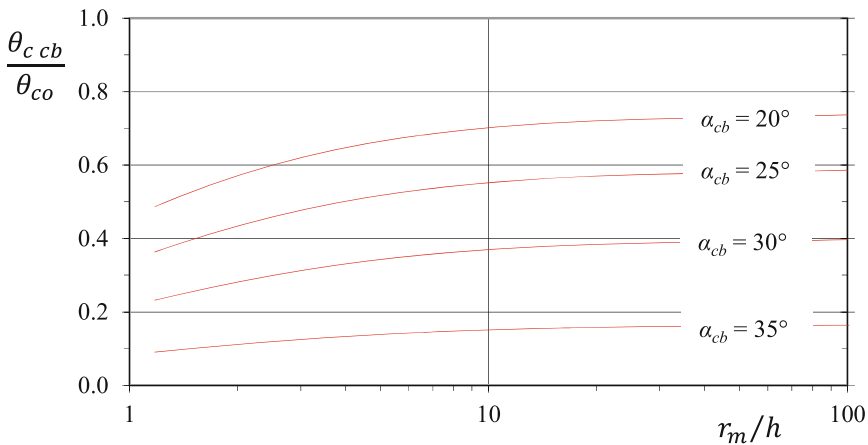

Fig. 3.18 Effect of the stream curvature on the mobility parameter, calculated with Eq. (3.42), with $\alpha_3/\alpha_2 = 0.75$, $\tan \varphi = 0.78$, and $C_L/C_D = 1.2$

3.5.2   Effects on the Inner Bank Due to the Drop of the Free Surface

In the channel bends, there is an elevation of the free surface at the outer bank and a drop at the inner bank due to different components in the flow acceleration. The difference in level between extrados and intrados can be assessed, at first approximation, as:

$$\Delta h \simeq \frac{U^2}{g} \frac{B}{r_m} \tag{3.46}$$

where $U = Q/A$ is the average velocity, B is the section width, and r_m is the average curvature radius (Fig. 3.19).
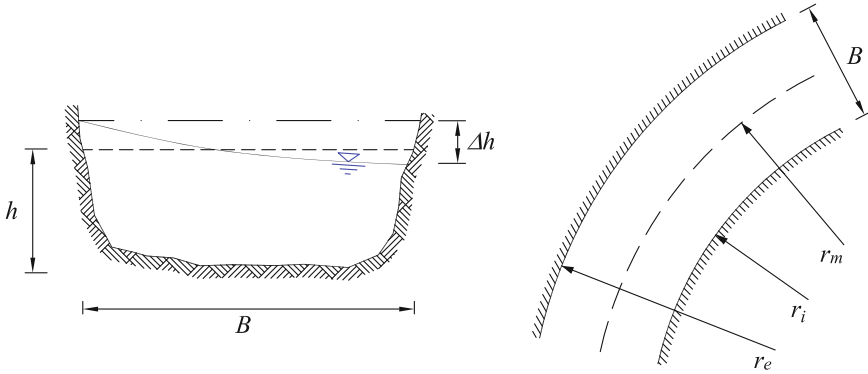
Fig. 3.19 Scheme and symbols of the elevation in channel bends

In case of *subcritical flows* the effect due to the elevation is relatively modest, while in *supercritical flows* this effect is much more remarkable. In this case, the maximum free surface drop at the intrados can be then evaluated, at first approximation, as Ghetti (1984):

$$\Delta h \simeq 2\frac{U^2}{g}\frac{B}{r_m} \tag{3.47}$$

The maximum velocity occurs at the minimum water depth:

$$h_{min} = \bar{h} - \frac{\Delta h}{2} \simeq \bar{h} - \frac{U^2}{g}\frac{B}{r_m} \tag{3.48}$$

The corresponding increase in velocity can be evaluated in the hypothesis of constant specific energy $H = h + U^2/(2g)$ along the radial direction:

$$\bar{h} - \frac{\Delta h}{2} + \frac{(U + \Delta U_{max})^2}{2g} = \bar{h} + \frac{U^2}{2g}$$
$$\Delta U_{max} = \sqrt{U^2 + g\,\Delta h} - U \tag{3.49}$$

The value obtained is then added up to the value of the average velocity:

$$U_{max} = U + \Delta U_{max} = \sqrt{U^2 + g\,\Delta h} \tag{3.50}$$

and from (3.47):

$$U_{max} = U\sqrt{1 + 2\frac{B}{r_m}} \tag{3.51}$$

The corresponding friction velocity can be therefore calculated by means of a uniform formula, like Chézy's formula:

$$(u_*)_{max} = \frac{U_{max}\sqrt{g}}{\chi} \simeq U\sqrt{1 + 2\frac{B}{r_m}}\frac{\sqrt{g}}{\chi} = \overline{(u_*)}\sqrt{1 + 2\frac{B}{r_m}}$$

$$(3.52)$$

The maximum mobility parameter is thus the following:

$$\theta_{max} \simeq \frac{(u_*)^2_{max}}{g\,\Delta\,d} \simeq \overline{\theta}(1 + 2\frac{B}{r_m}) \qquad (3.53)$$

In the previous relations, $\overline{(u_*)}$ and $\overline{\theta}$ have respectively denoted the average friction velocity and average mobility parameter of the section (i.e., the undisturbed).

3.6   Other Criteria for Defining the Incipient Motion Condition

Although the Shields theory—if necessary modified to meet the parameters described in the previous sections—is the rational criterion to determine the incipient motion condition in a stream, in the literature there are other criteria that can be properly traced back to the Shields criterion and often represent the same condition but under more restrictive hypotheses.

A comparison between the different methods can be made by means of the dimensional analysis. In general, we can affirm that the parameters influencing the condition of incipient motion are: depth-average velocity U, water depth h, average particle diameter d, bed shear stress τ_0, water density ρ and particle density ρ_s, water viscosity μ, gravity acceleration g and, if necessary, a significant parameter of the grain size distribution (e.g., its variance σ_g). That is, we have:

$$f(U, h, d, \tau_0, \rho_s, \rho, \mu, g, \sigma_g) = 0 \qquad (3.54)$$

The dimensional analysis allows to reduce relation (3.54) among nine parameters to a relation among the following six dimensionless groups:

$$f\left(\frac{u_*^2}{g\,\Delta\,d}, \frac{\rho u_* d}{\mu}, \frac{h}{d}, \frac{U}{u_*}, \frac{U}{\sqrt{g\,h}}, \sigma_g\right) = 0 \qquad (3.55)$$

where $u_*^2 = \tau_o/\rho$ and $\Delta = (\rho_s - \rho)/\rho$.

The first two groups $\theta = u_*^2/(g\,\Delta\,d)$ and $R_* = \rho u_* d/\mu$ are the two parameters already pointed out in the Shields analysis.

The third parameter is the *relative submergence* (h/d) (the reciprocal of the *relative roughness*), the fourth parameter U/u_* represents the friction coefficient (e.g., $U/u_* = \chi/\sqrt{g}$ according to the Chézy formula), which in uniform flow condition of

rough wall depends on the relative roughness, i.e., on the previous parameter, and as such it can be replaced by it. The fifth group is the Froude number $Fr = U/(\sqrt{g\,h})$.

It is evident that each of these parameters can be combined with the others; the condition searched for can then depend on dimensionless groups, which are combinations of the above-listed groups.

3.6.1 Critical Slope

Among the other criteria for determining the condition of incipient motion in a stream, the *critical slope* is still used today especially in the mountain stream restoration practices.

Should the Reynolds grain number be sufficiently high ($Re_* \geq\sim 200$), then we have:

$$\theta_c = \frac{u_{*c}^2}{g\,\Delta\,d} \simeq 0.057 \tag{3.56}$$

In case of uniform flow, it can be also written:

$$u_{*c}^2 = gR_h i_b \simeq ghi_b \tag{3.57}$$

where i_b denotes the bed slope.

By replacing (3.57) into (3.56), we have:

$$\frac{h\,i_b}{\Delta\,d} \simeq 0.057 \tag{3.58}$$

From which it follows:

$$(i_b)_{cr} = 0.057\Delta\,\frac{d}{h} \tag{3.59}$$

Considering that for the siliceous material $\Delta \simeq 1.65$, Eq. (3.59) becomes:

$$(i_b)_{cr} \simeq 0.09\,\frac{d}{h} \tag{3.60}$$

Equation (3.60) was already suggested by Valentini (1912) on the basis of the data on some streams in Valtellina, Italy.

The channel slope (in uniform motion) can be easily expressed as a combination of the friction coefficient and the Froude number:

$$i_b = \left(\frac{\sqrt{g\,h\,i_b}}{U}\,\frac{U}{\sqrt{g\,h}}\right)^2 = \left(\frac{u_*}{U}\,Fr\right)^2 \tag{3.61}$$

The latter criterion can be used only in condition of uniform flow.

3.6.2 Critical Discharge

A still widespread criterion for establishing the incipient motion condition is the *critical discharge* (Schoklitsch [1962]). Some authors even prefer it, in that the discharge can be measured more easily than the friction velocity (i.e., the bed shear stress). In this case, the parameter denoting the (critical) liquid discharge q_{cr} per unit width properly adimensionalized is used:

$$q_{cr}^* = \frac{q_{cr}}{d\sqrt{g\,d}} \tag{3.62}$$

Experimental observations show that the critical dimensionless discharge basically depends on the bed slope (Fig. 3.20). In case of mountain streams with heterogeneous grain size bed sediment, Bathurst et al. ([1987]) suggested the d_{16} of the surface material as the characteristic diameter, since the smallest fraction tends to be moved first. So the d_{16} of the surface material corresponds to the d_{50} of the substrate material in the presence of *surface-layer armoring*:

$$q_{cr}^* = \frac{q_{cr}}{d_{16}\sqrt{gd_{16}}} = 0.21\,i_b^{-1.12} \tag{3.63}$$

However, this criterion has no general validity. Its limits can be seen by properly manipulating the parameter of Eq. (3.62). This leads to an expression similar to (3.63):

$$q^* = \frac{U\,h}{d\sqrt{g\,d}} = \frac{U\,h}{d\sqrt{g\,d}}\frac{u_*^2}{u_*^2} \simeq \frac{U}{u_*}\frac{u_*^3}{(g\,\Delta\,d)^{1.5}}\Delta^{1.5}i_b^{-1}$$

$$q_{cr}^* = \left(\frac{U}{u_*}\right)_{cr}\theta_c^{1.5}\,\Delta^{1.5}\,(i_b)_{cr}^{-1} \tag{3.64}$$

The ratio U/u_* represents the dimensionless friction coefficient which, on a rough bed, essentially depends on the relative roughness d/h. In its turn, this can be due to the slope i_b in the incipient motion condition (see Eq. 3.59), which explains relation (3.63).

3.6.3 Critical Froude Number and Critical Velocity

Other authors suggest the *critical Froude number* as a key parameter for the incipient motion condition:

$$Fr_{cr} = \frac{U_{cr}}{\sqrt{gh}} == \left(\frac{U}{u_*}\right)\theta_c^{0.5}\sqrt{\Delta}\left(\frac{d}{h}\right)^{0.5} \tag{3.65}$$
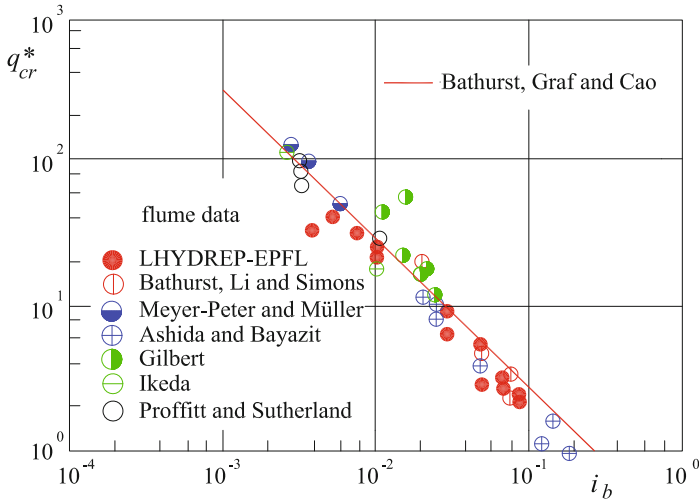
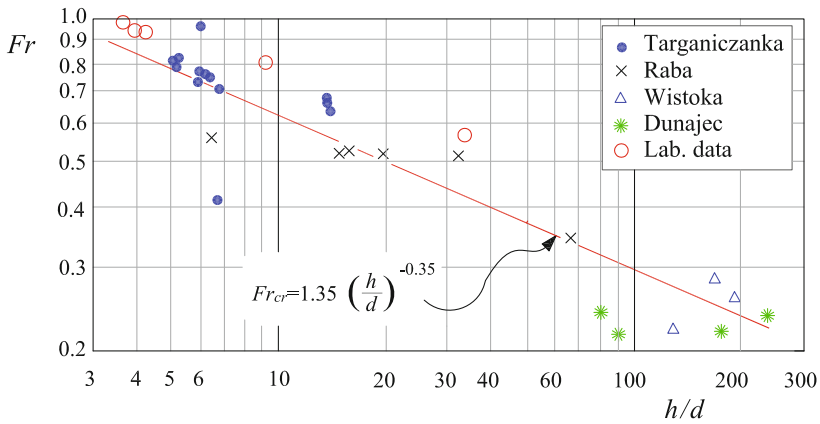**Fig. 3.20** Critical discharge in function of the slope (Tsujimoto 1991)

Fig. 3.21 Critical Froude number in function of the relative submergence according to Bartnik (1991)

As previously said, the first right-hand ratio U/u_{*c} represents the friction coefficient, which depends on the relative roughness. In short, the critical Froude number can be ascribed directly to the relative roughness. On the basis of experimental observations, Bartnik (1991) proposed the following relation (Fig. 3.21):

$$Fr_{cr} = 1.35 \left(\frac{h}{d}\right)^{-0.35} \tag{3.66}$$

This criterion has the same limits as the previous criteria: more precisely, it is based on the hypothesis of stream in uniform flow condition. At present, formulae of this type are not well corroborated by experimental data.

Equation (3.66) shows that the critical velocity depends on the relative roughness d/h. The critical velocity, as criterion for the condition of initial motion, maintains the same limits as non-dimensionless relations.

References

E.D. Andrews, Entrainment of gravel from naturally sorted riverbed material. Geol. Soc. Am. Bull. **94**(10), 1225–1231 (1983)

A. Armanini, Report on the physical model of Esna barrage, in *Internal Report of ELC* (Electro-Consult, Milano, 1989)

A. Armanini. *Principi di idraulica fluviale* (Editoriale Bios, first edition, 1999)

K. Ashida and M. Michiue. Studies on bedload transportation for nonuniform sediment and river bed variation. Disaster Prev. Res. Inst. Annu. **14** (1971)

W. Bartnik. Determination of the critical conditions of incipient notion of bedload in mountain rivers, in *Fluvial hydraulics of mountain regions*, ed. by Armanini and D. Silvio. Lecture Notes on Earth Sciences, vol. 37 (Springer, 1991), pp. 83–88

J. Bathurst, W. Graf, and H. Cao. Bedload discharge equations for steep mountain rivers. in *Sediment Transport in Gravel-Bed Rivers* (8 fig, 5 tab, 55 ref.) (Wiley, New York, 1987), pp. 453-491

R. Bonnefille, Essais de synthèse des lois de début d'entraînement des sédiments sous l'action dun courant en régime continu. Bulletin Centre de Recherhce Chatou **5**, 67–72 (1963)

W.R. Brownlie. Compilation of alluvial channel data: laboratory and field (1981)

Y.M. Chiew, G. Parker, Incipient sediment motion on non-horizontal slopes. J. Hydraul. Res. **32**(5), 649–660 (1994)

I. Egiazaroff, Calculation of nonuniform sediment concentrations. J. Hydraul. Division **91**(4), 225–247 (1965)

H.A. Einstein. *The bedload function for sediment transportation in open channel flows*. vol. 1026 (US Department of Agriculture, 1950)

A. Ghetti. Idraulica (Edizioni Libreria Cortina, Padova, 1984), pp. 566

W. Graf, H. Cao, and L. Suszka. Hydraulics of steep, mobile-bed channels. EV (1987)

A.J. Grass, Initial instability of fine bed sand. J. Hydraul. Div. **96**(3), 619–632 (1970)

E.W. Lane. Progress report on studies on the design of stable channels by the bureau of reclamation (American Society of Civil Engineers, 1953)

H.J. Leutheusser, Turbulent flow in rectangular ducts. J. Hydraul. Div. **89**(3), 1–19 (1963)

V. Nikora, D. Goring, I. McEwan, G. Griffiths, Spatially averaged open-channel flow over rough bed. J. Hydraul. Eng. **127**(2), 123–133 (2001)

G. Parker, P.C. Klingeman, D.G. McLean, Bedload and size distribution in paved gravel-bed streams. J. Hydraul. Div. **108**(4), 544–571 (1982)

I.L. Rozovskii. Flow of water in bends of open channels. (Academy of Sciences of the Ukrainian SSR, 1957)

A. Schoklitsch, *Handbuch des Wasserbaues*, 3rd edn. (Springer, Vienna, 1962)

A. Shields, Anwendung der Aehnlichkeitsmechanik und der Turbulenzforschung auf die Geschiebebewegung (Technical report, Preussischen Versuchsanstalt für Wasserbau, 1936)

R. Soulsby, R. Whitehouse, et al. Threshold of sediment motion in coastal environments. in *Pacific Coasts and Ports' 97: Proceedings of the 13th Australasian Coastal and Ocean Engineering Conference and the 6th Australasian Port and Harbour Conference,* vol. 1 (Centre for Advanced Engineering, University of Canterbury, 1997), p. 145

L. Suszka. Modification of transport rate formula for steep channels. in *Fluvial hydraulics of mountain regions*, ed. by Armanini and D. Silvio. Lecture Notes on Earth Sciences, vol. 37 (Springer, 1991), pp. 59–70

Y. Tsuchiya. Mechanics of the successive saltation of a sand particle on a granular bed in a turbulent stream, vol. 19 (Bull. of Disaster Prevention Research Institute, Kyoto University, 1969)

T. Tsujimoto. Bedload transport in steep channels. in *Fluvial Hydraulics of Mountain Regions*, ed. by Armanini and D. Silvio. Lecture Notes on Earth Sciences, vol. 37 (Springer, 1991), pp. 89–102

C. Valentini, *Sistemazione dei torrenti e dei bacini montani* (Edizioni UTET, Torino, 1912)

S. White, Plane bed thresholds of fine grained sediments. Nature 228, 152–153 (1970)

M. Yalin. *Mechanics of sediment transport*. (Pergamon, 1977)

Chapter 4
Resistance to Flow in Mobile-Bed Channels

4.1 Introduction

As mentioned in Sect. 2.5, the organized bed forms, such as ripples, dunes, and antidunes, developing in a mobile bed induce a flow resistance, which adds to that induced by the roughness reduced by the grains on the bed surface.

From an applicative point of view, the precise calculation of this increase in resistance is crucial. But the problem cannot easily be solved because the bed forms essentially depend on the hydrodynamic regime of the stream (especially on the Froude number) that, in its turn, is dependent on flow resistance. In other words, it is a typical implicit problem to be dealt with.

A widely used approach in this case is based on the idea that the bed stress is partitioned in a shear stress induced by *grain roughness* τ_o', in a stress induced by *bed forms* τ_o'', and in a possible shear stress τ_o''', induced by *interaction among the grains*. Thus, the same partition may be applied to the shear stress distributions, as shown in Fig. 4.1.

Since the stress due to grains interaction can be neglected in the fluvial sediment transport, for the bed shear stress, we can write:

$$\tau_o = \tau_o' + \tau_o'' \tag{4.1}$$

Equation (4.1) can be divided by the water density ρ and expressed in terms of friction velocity:

$$u_*^2 = (u_*')^2 + (u_*'')^2 \tag{4.2}$$

and, because of the uniform flow hypothesis,

$$R_h \, i_E = (R_h \, i_E)' + (R_h \, i_E)'' \tag{4.3}$$

By dividing Eq. (4.2) by U^2, it can be rewritten in function of the friction coefficients, e.g.,
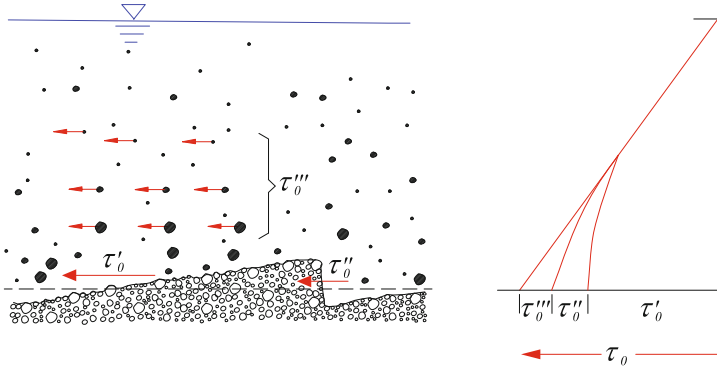
Fig. 4.1 Distribution of different contributions to the tangential shear stress: contribution due to grain roughness τ_o'; contribution due to bed form roughness τ_o''; contribution due to interactions between grains τ_o'''

$$f = f' + f'' \qquad (4.4)$$

or:

$$\frac{1}{\chi^2} = \frac{1}{(\chi')^2} + \frac{1}{(\chi'')^2} \qquad (4.5)$$

where f and χ are the resultant global friction coefficients according to Darcy-Weisbach and Chézy, respectively, and f' and χ' and f'' and χ'' the corresponding equivalent roughness coefficients of grain and bedforms (Sect. 1.2, p. 3).

There are basically three criteria to evaluate the bed-form resistance. The first, proposed by Meyer-Peter and Müller (1948) and revised by Engelund (1964), considers the superimposition in terms of the energy line slope, keeping the value of the hydraulic radius R_h constant in (4.3), that is:

$$i_E = i_E' + i_E'' \qquad (4.6)$$

The second criterion (Einstein 1950) refers to a single value of the energy line slope, while the effects in terms of hydraulic radius or flow depth are summed up, e.g.,

$$h = h' + h'' \qquad \text{and} \qquad R_h = R_h' + R_h'' \qquad (4.7)$$

The last and latest method (Van Rijn 1984) is based on the idea of transforming the flow resistance due to bed forms into an equivalent roughness k_Δ to be summed to the grain roughness k_o, so that the global equivalent roughness k_e results:

$$k_e = k_o + k_\Delta \qquad (4.8)$$

4.2 Einstein's Criterion

Einstein's criterion is based on an experimental graph, which provides the value of the friction velocity u_*'', due to bed forms in function of the water depth *induced by the grain roughness*:

$$\frac{U}{u_*''} = func(\frac{\Delta d_{35}}{h' i_E})\qquad(4.9)$$

The ratio $\Delta d_{35}/(h' i_E) = \Psi_{35}$ represents the Einstein's *flow intensity parameter* expressed as a function of the d_{35}. This parameter is the reciprocal of the Shields mobility parameter θ. The graph is reported in Fig. 4.2.

The graph in Fig. 4.3 represents a modification of Einstein and Barbarossa's original graph (Einstein et al. 1951), proposed by Shen (1962), which contains a second parameter $w_s d_{35}/v$, representing a Reynolds grain number. Shen's graph extends Einstein's method to rivers with a hydrodynamic regime dependent on viscosity.

In order to determine the water depth corresponding to a given discharge and a given bed slope i_b according to Einstein's method, we calculate the value of the *grain hydraulic radius* R_h' and the value of the *grain friction coefficient* (f' or χ'), by using, e.g., in case of Chézy's formula, one of the following expressions:

$$\chi' = 18 \log \frac{12 R_h'}{3 d_{90}} \qquad or: \quad \frac{\chi'}{\sqrt{g}} = 7.66 \left(\frac{R_h'}{d_{65}}\right)^{1/6}\qquad(4.10)$$
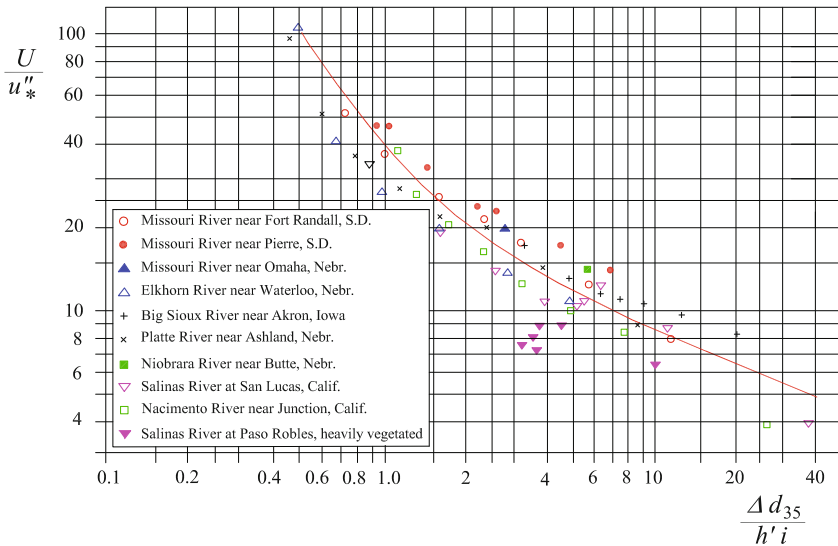

Fig. 4.2 Einstein–Barbarossa's graph (Einstein et al. 1951) for shape drag. Inapplicable in presence of ripples
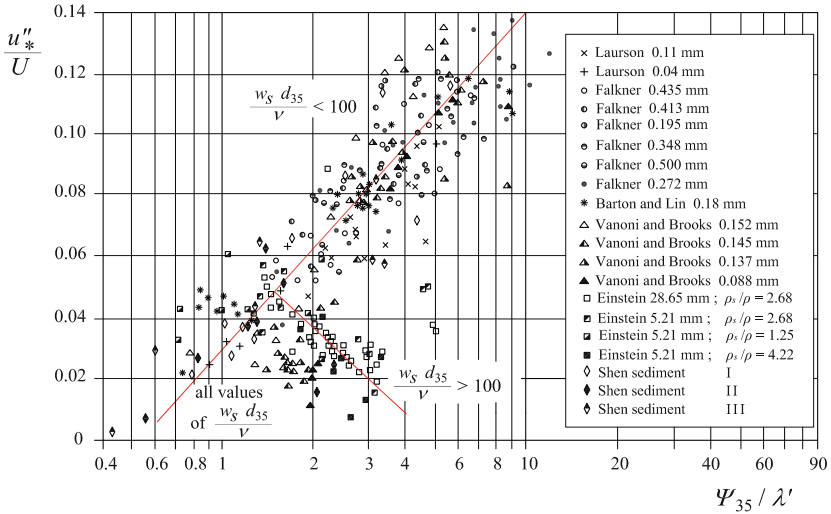
Fig. 4.3 Shen's (1962) graph for bed form resistance. $\Psi_{35} = \Delta d_{35}/R'_h\, i_E$ e $\lambda' = 7.12$ for $(w_s\, d_{35}/v > 100)$ and $\lambda' = \sqrt{w_s\, d_{35}/v}$ for $(1 < w_s\, d_{35}/v < 100)$

along with the corresponding Chézy uniform flow equation:

$$Q = A'\chi'\sqrt{R'_h\, i_b} \tag{4.11}$$

From (4.11) and from either of (4.10), we calculate the hydraulic radius R'_h and then the friction velocity $u'_* = \sqrt{g\, R'_h\, i_b}$ corresponding to the grain roughness.

The value of u''_* is therefore determined by Fig. 4.3, by assuming the value $U = Q/A'$ as first approximation.

The total hydraulic radius is then obtained from the sum of the two contributions:

$$R_h = R'_h + R''_h = \frac{u'^2_*}{g\, i_b} + \frac{u''^2_*}{g\, i_b} \tag{4.12}$$

From u''_*, we thus obtain $\chi'' = \sqrt{g}\, U/u''_*$. From relation (4.5) we have χ, with which we also calculate the velocity U of second approximation, as $U = \chi\sqrt{R_h\, i_b}$.

4.3 Engelund's Criterion

According to Engelund (1966), the energy dissipation due to a single bed form can be calculated as a Borda–Carnot formula for a sudden section enlargement, occurring downstream a bed form (Fig. 4.4):
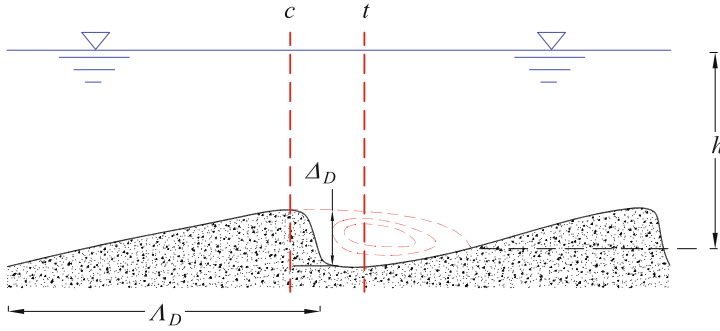
Fig. 4.4 Engelund's scheme for the resistance due to a dune

$$E_c - E_t = \frac{1}{2g} (U_c - U_t)^2 \tag{4.13}$$

where E_c and U_c, and E_t and U_t are the kinetic energy (for unit weight) and the velocity in the crest and the trough of the dune, respectively.

In addition, from the continuity equation, we have:

$$Uh \simeq U_c \left(h - \frac{\Delta_D}{2} \right) = U_t \left(h + \frac{\Delta_D}{2} \right) \tag{4.14}$$

with U and h denoting the average values of water depth and velocity, and with Δ_D the average dune height.

By inserting Eq. (4.14) into Eq. (4.13), we have:

$$E_c - E_t = \frac{1}{2g} U^2 h^2 \left(\frac{\Delta_D}{h^2 - (\Delta_D/2)^2} \right)^2 \simeq \frac{1}{2g} U^2 \left(\frac{\Delta_D}{h} \right)^2 \tag{4.15}$$

More in general, the energy dissipation per unit length due to the dune results as follows:

$$i_E'' = \frac{\Delta E}{\Lambda_D} = \alpha_D \left(\frac{\Delta_D}{h} \right)^2 \frac{1}{\Lambda_D} \frac{U^2}{2g} \tag{4.16}$$

where α_D is a suitable coefficient and Λ_D the average dune length. Considering that:

$$i_E = \frac{\tau_o}{g \rho h} \tag{4.17}$$

according to Eq. (4.1), we have:

$$\frac{\tau_o}{g \rho h} = \frac{\tau_o'}{g \rho h} + \alpha_D \left(\frac{\Delta_D}{h} \right)^2 \frac{1}{\Lambda_D} \frac{U^2}{2g} \tag{4.18}$$

In other words,

$$\tau_o = \tau_o' + \tau_o'' = \tau_o' + \alpha_D \rho \frac{U^2}{2} \left(\frac{\Delta_D}{h}\right)^2 \frac{h}{\Lambda_D} \tag{4.19}$$

Equation (4.19) can be rewritten in function of the Shields mobility parameter, after dividing each of its terms by $g \, \rho \, \Delta \, d$:

$$\frac{\tau_o}{g \, \rho \, \Delta \, d} = \frac{\tau_o'}{g \, \rho \, \Delta \, d} + \frac{\tau_o''}{g \, \rho \, \Delta \, d} \tag{4.20}$$

and

$$\theta = \theta' + \theta'' \tag{4.21}$$

where, according to Eq. (4.19), we put:

$$\theta'' = \frac{\tau_o''}{g \, \rho \, \Delta \, d} = \alpha_D \frac{U^2}{2 \, g \, \Delta \, d} \left(\frac{\Delta_D}{h}\right)^2 \frac{h}{\Lambda_D} = \frac{\alpha_D}{2} \frac{u_*^2}{g \, \Delta \, d} \left(\frac{U}{u_*}\right)^2 \left(\frac{\Delta_D^2}{h \Lambda_D}\right) \tag{4.22}$$

Confining the analysis to those cases whose dependence on the Reynolds grain number can be negligible (thus excluding ripples), the mobility parameter of bed forms θ'' depends then on the total mobility parameter of the stream ($\theta = u_*^2/g \, \Delta \, d$), on the shape geometry and global resistance coefficient.

The bed form geometry essentially depends on the solid discharge, which in its turn mainly depends on the grain mobility parameter, as already observed by Einstein et al. (1951). By introducing such notions into (4.19), the shape mobility parameter proves to depend basically on the total mobility parameter and the grain mobility parameter, that is, $\theta'' = func(\theta, \theta')$. In other words, $\theta = func(\theta')$.

This hypothesis has been empirically confirmed through a series of experiments summarized in Fig. 4.5.

The points in the graph can be fitted by three different relations valid for three bed form types: dunes, flat bed, and antidunes.[1]

$$\begin{array}{lll} \theta' = 0.06 + 0.3\,\theta^{1.5} & \text{for } \theta' \sim < 0.5 & \text{subcritical regime} \\ \theta' = \theta & \text{for } \sim 0.5 < \theta' < \sim 0.75 & \text{transcritical regime} \\ \theta' = 1.8 - \dfrac{1}{\theta^2} & \text{for } \theta' > \sim 0.75 & \text{supercritical regime} \end{array} \tag{4.23}$$

Moreover, Engelund suggests the following expression to calculate the grain resistance:

$$\frac{U}{\sqrt{g \, h \, i_E'}} = \frac{q}{h\sqrt{g \, h \, i_E'}} = 0.06 + 2.5 \ln \frac{h}{2 \, d_{65}} \tag{4.24}$$

where $q = Q/B$ is the discharge per unit width.

---

[1]In a previous work, Engelund suggested for the subcritical regime the following relation $\theta' = 0.06 + 0.4\,\theta^2$ instead of the first of Eq. (4.22).
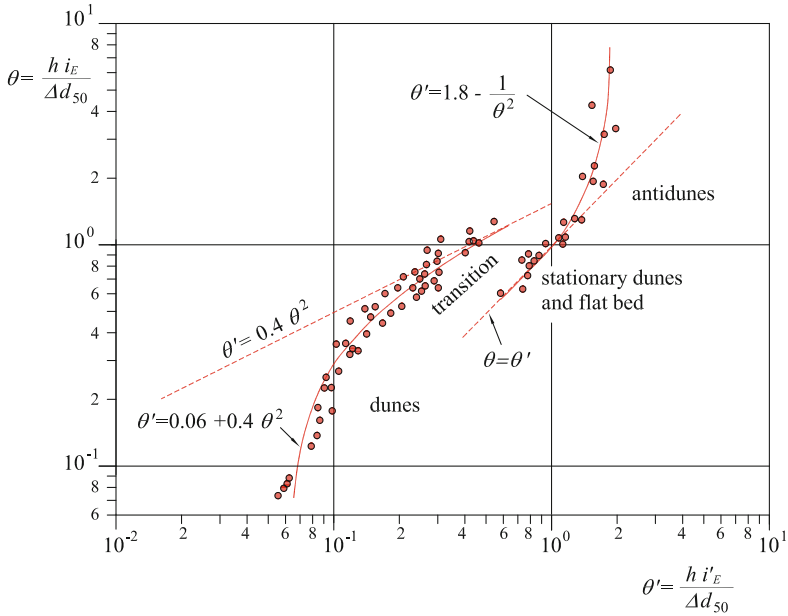
Fig. 4.5 Relation between the total mobility parameter θ and the grain mobility parameter θ', according to Engelund (1965)

Assuming that the discharge per unit width q and the depth h are assigned, the global resistance can thus be calculated with the following procedure:

1. from Eq. (4.24), we first calculate the energy slope due to grain resistance i'_E.
2. then we calculate $\theta' = h\, i'_E/(\Delta\, d_{50})$, with which through the graph (Fig. 4.5) or through one of Eq. (4.23) we calculate the global θ;
3. then we calculate the total energy slope i_E as $i_E = \theta\, \Delta\, d_{50}/h$.

If, instead, we assign the flow rate and the total slope (for example as occurs in uniform motion conditions, in which $i_E = i_b$) and wish to know the flow depth h, we adopt an iterative process:

1. we first calculate the water depth of first approximation $h^{(1)}$ from Eq. (4.24) in which we put $i_E = i_b$;
2. with these values of $i'_E{}^{(1)}$ and $h^{(1)}$, we calculate $\theta' = h^{(1)} i'_E{}^{(1)}/(\Delta\, d_{50})$, which we insert into the graph (Fig. 4.5) or into one of Eq. (4.23) and calculate the global $\theta^{(1)}$ of first attempt;
3. we then calculate the $h^{(2)}$ of second attempt, as $h^{(2)} = \theta^{(1)} \Delta\, d_{50}/i_E$;
4. if necessary, we iterate the process, by inserting $h^{(2)}$ into Eq. (4.24) at point (2).

4.4 Van Rijn's Criterion

Later Van Rijn (1984) proposed a new criterion for evaluating the drag due to dunes and ripples in a more exhaustive manner. Compared to the previous methods, such a criterion has the advantage of being adjusted on an extremely great number of experimental data and, above all, on field rather than laboratory data. This criterion is not applied in supercritical flows, in presence of antidunes.

Van Rijn's criterion is based on the idea that it is possible to sum up the grain roughness, $k_o = 3d_{90}$, and the equivalent roughness induced by the bed forms, k_D, which he assumed to depend on the bed form geometry:

$$k_\Delta = 1.1 \, \Delta_D (1 - e^{-25 \, (\Delta_D/\Lambda_D)}) \tag{4.25}$$

in which δ_D and Λ_D are, respectively, the average height and length of the dunes. The global equivalent roughness is:

$$k_e = 3 \, d_{90} + 1.1 \, \Delta_D (1 - e^{-25 \, (\Delta_D/\Lambda_D)}) \tag{4.26}$$

The dune geometry is given by the flowing expressions:

- *dune height*

$$\frac{\Delta_D}{h} = 0.11 \left(\frac{d_{50}}{h}\right)^{0.3} (25 - T) \left(1 - e^{-0.5\,T}\right) \tag{4.27}$$

- *dune slope*

$$\frac{\Delta_D}{\Lambda_D} = 0.015 \left(\frac{d_{50}}{h}\right)^{0.3} (25 - T) \left(1 - e^{-0.5\,T}\right) \tag{4.28}$$

with:

$$T = \frac{u_*^2 - u_{*c}^2}{u_{*c}^2} \tag{4.29}$$

$$u_* = U \frac{\sqrt{g}}{\chi} \tag{4.30}$$

$$\frac{\chi}{\sqrt{g}} = 5.75 \log \left(12 \frac{R_h}{k_e}\right) \tag{4.31}$$

where T denotes the *transport stage parameter*. The value of u_{*c} is obtained from the Shields diagram, modified in function of the dimensionless particle diameter $D* = d_{50} \left(\Delta g/v^2\right)^{1/3}$, or from Brownlie's formula (Eq. 3.20 at p. 66):

$$\theta_c = 0.22 \, D_*^{-1} + 0.06 \, e^{-17.77 \, D_*^{-1}} \tag{3.20}$$

Note that from the ratio between (4.27) and (4.27), we obtain:

$$\Lambda_D = 7.3 \; h \tag{4.32}$$

The iterative procedure to calculate the global drag according to Van Rijn follows as such:

1. calculate the critical friction velocity u_{*c} in function of the dimensionless particle diameter $d \left(\Delta g / \nu^2 \right)^{1/3}$, e.g., by using Eq. (3.20);
2. calculate the transport stage parameter $T = (u_*^2 - u_{*c}^2)/u_{*c}^2$ of first approximation by using formulas (4.29)–(4.31) and as Chézy coefficient the first approximation value $\chi = 18 \log(12 R_h/(3 \, d_{90}))$ (i.e., by assuming as first approximation the total roughness equal to the grain roughness $k_e \simeq 3 \, d_{90}$);
3. calculate Δ_D and Λ_D by means of formulas (4.27) and (4.28);
4. calculate k_e with (4.26);
5. calculate χ with (4.31);
6. iterate, if required.

References

H. Einstein, N. Barbarossa, A.S. of Civil Engineers, Hydraulics Division, River Channel Roughness (American Society of Civil Engineers, 1951)

H.A. Einstein, The bedload function for sediment transportation in open channel flows. Number 1026 (US Department of Agriculture, 1950)

F. Engelund, A criterion for the occurrence of suspended load. La Houille Blanche **8**(7) (1965)

F. Engelund, Hydraulic resistance of alluvial streams. J. Hydraul. Div. **98**, 315–326 (1966)

F.A. Engelund, *Flow resistance and hydraulic radius* (Technical University of Denmark, Hydraulic Laboratory, 1964)

E. Meyer-Peter, R. Müller, Formulas for bedload transport, in *Proceedings of the 2nd Meeting of the International Association for Hydraulic Structures Research*, IAHS, no. 133 (1948), pp. 39–64

H. Shen, Development of bed roughness in alluvial channels. J. Hydraul. Div. Am. Soc. Civ. Eng. **88**, 45–58 (1962)

L.C. Van Rijn, Sediment transport, Part III: Bed forms and alluvial roughness. J. Hydraul. Eng. **110**(12), 1733–1754 (1984), https://doi.org/10.1061/(ASCE)0733-9429(1984)110:12(1733)

Chapter 5
Bedload Transport

5.1 Introduction

The *bedload transport* in a stream refers to the transport of sediment by *rolling* and *sliding*, sometimes making *short hops* (Einstein 1950). In the former case, the mean lift force acting on particles is generally of the same order as the submerged weight (or even lower); in the latter, the lift force acting on the particle exceeds the submerged weight. In this case, while the particle moves upwards, the lift force tends to decrease as long as the particle begins to fall down and to re-deposit onto the bed after traveling a relatively short distance, i.e. of the same order of magnitude as its diameter.

If, on the contrary, the lift continues to prevail on the gravity forces and the particle hop distance is of the same order as the water depth, the particle moves in *suspension* with mechanisms essentially controlled by turbulence fluctuations. The distinction between suspended load and bedload is not sharp, especially as regards the transport by saltation. For example, according to Kalinske (1942), the transport by saltation that characterizes sediment transport by wind, is negligible in water. Today, however, also the transport by saltation tends to be included in bedload mechanisms (Van Rijn 1984a).

Since the lift force depends on the square of the flow velocity, it is scaled by the friction velocity u_* and, since the submerged gravity force can be expressed through the fall velocity in still water w_s (Sect. 2.2.2 at page 45), the transport mode is dependent on the ratio between fall velocity and friction velocity of the stream:

$$6 \quad > \frac{w_s}{u_*} > 2 \quad \text{bedload transport: rolling}$$
$$2 \quad > \frac{w_s}{u_*} > 0.8 \quad \text{bedload transport: saltation}$$
$$0.8 > \frac{w_s}{u_*} > 0 \quad \text{suspended transport}$$

In order to calculate the bedload rate, a great number of formulae and different theories are available. The existing theories for bedload transport include those based on a Coulomb-like approach which can be referred to the Du Boys (1879) model, probabilistic/stochastic theories among which Einstein's (1950) represents the milestone, particle-based deterministic models, numerical models of particle dynamics, and theories based on the concept of grain interactions.

None of them are, however, considered sufficiently exhaustive of the whole process. For this reason, empirical formulae are still widely used often preferred to rational, but less effective, formulations.

For clarity's sake, in this chapter we will introduce Einstein's theory first, whose exposition helps to better understand some of the physical mechanisms underlying the sediment transport in a stream and especially the bedload, and we will try also to highlight some limits of this theory as well.

In order to overcome some restrictions of Einstein's theory, we will then illustrate a semi-probabilistic approach inspired to the theory.

We will successively present the approach of Du Boys, even if it was developed about 70 years before Einstein's theory. The Du Boys approach is based on some rather simplified physical assumptions, but has the advantage of leading to a very simple mathematical formulation, according to which the solid transport is proportional to the difference between the actual bed shear stress and the critical bed shear stress (the stress in incipient motion condition). Some of the most successful bedload formulae are structured on this assumption, e.g. Meyer-Peter and Müller's formula (1948) and the latest Van Rijn's formulation (1984a) among the others.

Finally, we will tackle some problems related to non-uniformity of particle size (e.g. hiding and armoring).

5.2   Einstein's Bedload Theory

Einstein's theory (1950) represents one of the first attempts to develop a theoretical framework for the bedload on a probabilistic basis. However, this theory has somewhat limiting conceptual assumptions which will be illustrated in the next sections. The final formulation is rather cumbersome and cannot predict the experimental data with sufficient accuracy, especially at high solid flow rates.

Even so, this theory should be described for its rational characteristics and numerous theoretical suggestions. In the following pages, however, we refer to Yalin's version of the theory (Yalin 1977), which appears to be significantly clearer than the original formulation.

Consider a two-dimensional channel flow in steady uniform condition. For simplicity's sake, we made the further hypothesis that the sediment transport consists of a uniform particle, even if in Einstein's original theory, this hypothesis is not considered. We will then extend the results to non-uniform particle size transport.
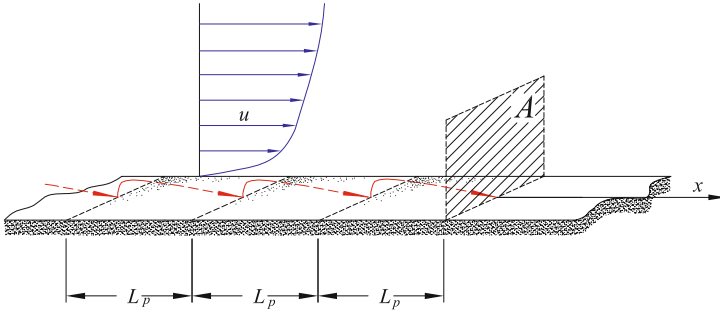
Fig. 5.1 Einstein's layout of average particle jumps (after Yalin 1977)

The particle flow thus occurs when the instantaneous value of the lift force[1] **L** exceeds the submerged weight of the particle $\mathbf{G} - \mathbf{B} = g(\rho_s - \rho)\alpha_3 d^3$; α_3 is, as usual, a suitable shape factor, so that $\alpha_3 d^3$ represents the particle volume:

$$\mathbf{L} \geq \mathbf{G} - \mathbf{B} = g(\rho_s - \rho)\alpha_3 d^3 \tag{5.1}$$

L is subject to turbulence fluctuations and is consequently a random function of time.

Moreover, suppose that particles move with small jumps with an average length equal to L_p, whose value is of the order of magnitude of the particle diameter.

In order to quantify the bedload, Einstein divided the bed surface into strips of unit width and length L_p (Fig. 5.1).

The number of particles constituting every strip is thus:

$$\frac{1}{\alpha_2 d^2} \tag{5.2}$$

where α_2 is a shape factor, such that $\alpha_2 d^2$ is the *projected frontal area* of the particle.

Be now p_n the probability for a single grain to be detached from the bed at least n times in a time T_p, sufficiently long with regard to the duration of the average jump.

Since each detachment corresponds to a jump, p_n also denotes the probability for a particle to make n jumps of length L_p, that is to have covered a distance at least equal to nL_p.

The number of the particles (Fig. 5.2), which in time T_p are detached from each strip and cover at least a distance equal to nL_p, is therefore:

---

[1]In this chapter, we will use the bold notation for some forces, e.g. **B** for the particle buoyancy, **G** for the particle weight, **L** for the hydrodynamic lift acting on the particles. This is a mere choice of notation. Weight and buoyancy are vertical forces, the lift is a force normal to the bed, that in riverbeds, with a moderate inclination, can be considered vertical as well.

In order to avoid additional symbols or any possibile misunderstanding, we will use the bold notation also for the modules of such forces.
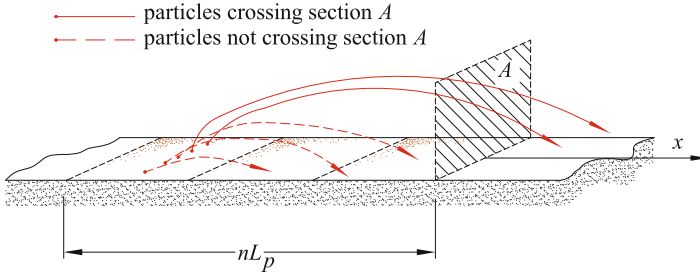
Fig. 5.2 The volume discharge crossing section A is given by all the particles detaching from every strip and able to cover, in a time T_p, a length equal to the distance between the initial point and the section A in question

$$p_n \frac{1}{\alpha_2} \frac{L_p}{d^2} \tag{5.3}$$

The average number of the particles that, leaving from a distance nL_p upstream of the generic vertical section A, cross the section in the unit time is:

$$p_n \frac{L_p}{T_p \, \alpha_2 d^2} \tag{5.4}$$

The total number of the particles crossing area A in an average unit time is thus:

$$\sum_{n=1}^{\infty} p_n \frac{L_p}{T_p \, \alpha_2 d^2} \tag{5.5}$$

The volumetric bedload discharge per unit width q_b can be obtained by multiplying formula (5.5) by the volume of each particle:

$$q_b = \alpha_3 \, d^3 \sum_{n=1}^{\infty} p_n \frac{L_p}{T_p \, \alpha_2 d^2} = \frac{\alpha_3}{\alpha_2} \frac{L_p}{T_p} \, d \sum_{n=1}^{\infty} p_n \tag{5.6}$$

The time T_p, *exchange time of bedload particle* according to Einstein, was assumed as the necessary averaged time for a grain replacement, that is the average time passing between the moment of the particle detachment from a given position and the moment when another particle replaces the vacuum left by the former. According to Einstein this time depends on the properties of the particle and on the step length L_p. However, it is reasonable to assume that the ratio L_p/T_p represents a velocity scale of the phenomenon that Einstein, even if with a different reasoning, assumed to be proportional to particle fall velocity w_s:

$$\frac{L_p}{T_p} = \alpha_6 w_s = \alpha_w \sqrt{g \Delta d} \tag{5.7}$$

Fig. 5.3 Eistein's staircase function of the probability p_n of crossing the vertical section A of a particle leaving from the strip L_p, located at distance nL_p from the section
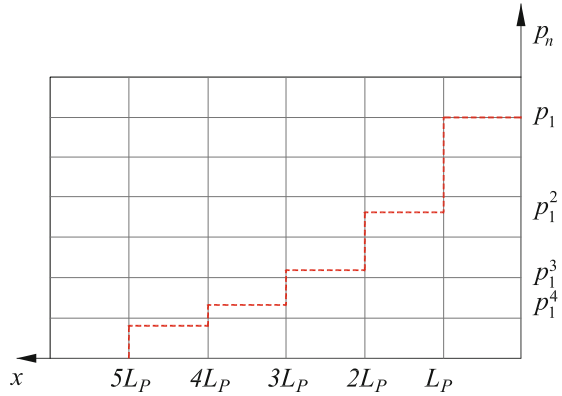
By replacing Eq. (5.7) into Eq. (5.6) it results:

$$q_b = \frac{\alpha_3 \alpha_w}{\alpha_2} \sqrt{g \Delta d}\, d \sum_{n=1}^{\infty} p_n \tag{5.8}$$

A further assumption of Einstein is that each particle jump is independent of the other jumps, that is:

$$p_n = p_1^n \tag{5.9}$$

where p_1 is the probability of a particle being eroded at least once from the bed during T_p (Fig. 5.3).

The sum in Eq. (5.8) results as such:

$$\sum_{i=1}^{\infty} p_i = \sum_{i=1}^{\infty} p_1^i = \frac{p_1}{1 - p_1} \tag{5.10}$$

After substituting (5.10) into (5.8), with some steps we obtain:

$$\frac{q_b}{\sqrt{g \Delta d}\, d} = \frac{\alpha_3 \alpha_w}{\alpha_2} \frac{p_1}{1 - p_1} = \frac{1}{A_*} \frac{p_1}{1 - p_1} \tag{5.11}$$

which includes the different coefficients α in a single coefficient $A_* = \alpha_2/(\alpha_3/\alpha_w)$. The left-hand group of Eq. (5.11) represents the dimensionless solid discharge. In order to denote this parameter, Einstein adopted the symbol Φ.

$$\Phi = \frac{q_b}{\sqrt{g \Delta d}\, d} \tag{5.12}$$

By taking (5.12) into account, Eq. (5.11) can also be rewritten as follows:

$$p_1 = \frac{A_* \, \Phi}{1 + A_* \, \Phi} \tag{5.13}$$

and

$$\Phi = \frac{1}{A_*} \frac{p_1}{1 - p_1} \tag{5.14}$$

where the parameter p_1 is still to be determined.

Determination of the Probability p_1

p_1 represents then the probability for a particle to be eroded at least once in the time T_p. Such a probability can reasonably be dependent on the ratio between the lift force $\mathbf{L}$ and the submerged weight force $(\mathbf{G} - \mathbf{B})$:

$$p_1 = func\left(\frac{\mathbf{L}}{\mathbf{G} - \mathbf{B}}\right) = func\left(\frac{C_L \alpha_2 d^2 \rho \, u^2}{g(\rho_s - \rho) \, \alpha_3 d^3}\right) \tag{5.15}$$

Following the Shields analysis, already described to define the conditions of incipient motion, it is easy to observe that the relationship between brackets is proportional to the mobility parameter:

$$p_1 = func\,(\theta) \tag{5.16}$$

where θ is just the Shields mobility parameter.

The lift force $\mathbf{L}$ depends on the turbulence structure of the flow and assumes random values in time. Einstein assumed that the dimensionless lift force $r = \mathbf{L}/\overline{\mathbf{L}}$ (where $\overline{\mathbf{L}}$ is the time averaged lift), should follow a Gaussian distribution:

$$f(r) = \frac{1}{\sigma \sqrt{2\pi}} e^{-\frac{(r-1)^2}{2\sigma^2}} \tag{5.17}$$

where σ is the variance of the distribution (Fig. 5.4).

Be a the threshold value of r, which causes the particle detachment, we have $a = (\mathbf{G} - \mathbf{B})/\overline{\mathbf{L}}$.
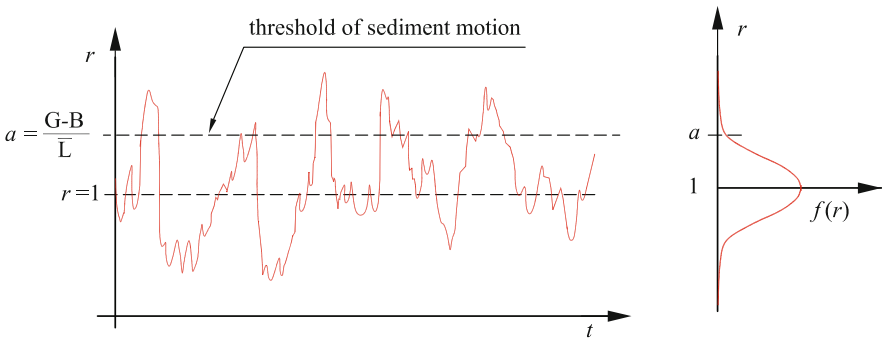

Fig. 5.4 Layout of the time behavior of the lift force

The detachment is possible only if $r > a$. The probability that $r < a$ (probability of non-detachment) then results:

$$P_r = \int_{-\infty}^{a-1} f(r)dr \qquad (5.18)$$

The detachment probability p_1 is therefore equal to $1 - P_r$, that is:

$$p_1 = 1 - P_r = 1 - \int_{-\infty}^{a-1} f(r)dr = 1 - \frac{1}{\sigma\sqrt{2\pi}} \int_{-\infty}^{a-1} e^{-\frac{(r-1)^2}{2\sigma^2}} dr \qquad (5.19)$$

Einstein however changed the lower limit of the integral from $-\infty$ to $-(a+1)$, thus identifying the non-detachment condition as $|\mathbf{L}| < \mathbf{G} - \mathbf{B}$ and not as $\mathbf{L} < \mathbf{G} - \mathbf{B}$, condition that corresponds to $|r| < a$, that is:

for $r > 0$ it results $r < a$ and $r - 1 < a - 1$ (*upper limit*)
for $r < 0$ it results $r > -a$ and $r - 1 > -a - 1 = -(a+1)$ (*lower limit*)

In short, according to Einstein:

$$p_1 = 1 - P_r = 1 - \frac{1}{\sqrt{\pi}} \int_{-\frac{(a+1)}{\sqrt{2}\sigma}}^{\frac{(a-1)}{\sqrt{2}\sigma}} e^{-\left(\frac{r-1}{\sqrt{2}\sigma}\right)^2} d\left(\frac{r-1}{\sqrt{2}\sigma}\right) \qquad (5.20)$$

The detachment threshold value $a = (\mathbf{G} - \mathbf{B})/\mathbf{L}$ can be determined by expressing the forces $\mathbf{G}$, $\mathbf{B}$ and $\mathbf{L}$ in function of the particle and flow characteristics. This analysis has already been made about the Shields theory on the incipient motion (page 61); by repeating the same procedure, the detachment threshold a is found to be inversely proportional to the Shields mobility parameter θ. For this purpose Einstein introduced the parameter $\Psi = g\Delta/u_*^2$ called *flow intensity parameter*, which coincides with the reciprocal of the Shields mobility parameter.

The upper integration limit thus becomes:

$$\frac{(a-1)}{\sqrt{2}\sigma} = B_* \Psi - \frac{1}{\eta_0} \qquad (5.21)$$

where B_* and η_0 are two constants to be determined experimentally.

Similar procedure is adopted for the lower limit of the integral of Eq. (5.20). By replacing Eq. (5.21) into Eq. (5.20) we obtain:

$$p_1 = 1 - \frac{1}{\sqrt{\pi}} \int_{-(B_*\Psi+\frac{1}{\eta_0})}^{B_*\Psi-\frac{1}{\eta_0}} e^{-\xi^2} d\xi \qquad (5.22)$$

where ξ is an integration variable.

As regards the numerical values of the experimental constants, Einstein proposed the following set:

$$A_* = 43.15 \quad ; \quad B_* = 0.143 \quad ; \quad \eta_0 = 0.5 \tag{5.23}$$

which, substituted into (5.22) and (5.14), yields:

$$\Phi = \frac{1}{43.13} \left(\frac{1}{\dfrac{1}{\sqrt{\pi}} \displaystyle\int_{-0.143\,\Psi-2}^{+0.143\,\Psi-2} e^{-\xi^2} d\xi} - 1 \right) \tag{5.24}$$

According to Einstein the sediment bedload does not depend on the roughness induced by bed forms, therefore the u_* to consider in calculating Ψ is only referred to the grain roughness, i.e. a $u_*^{\cdot}$ with the notation given in Sect. 4.1 at page 95. In case of mixtures of non-homogeneous granulometry, it can be calculated in function of d_{65} according to the following expression:

$$\frac{U}{u_*^{\cdot}} = 5.75 \log_{10} \left(12.27 \frac{R_h}{d_{65}} \chi_E \right) \tag{5.25}$$

The parameter χ_E depends on the relative roughness thought as relationship between d_{65} and virtual thickness of the viscose substrate $\delta' = 11.6\nu/u_*$. Its trend is illustrated in the following graph (Fig. 5.5), for the reader's convenience directly in function of the grain Reynolds number $R_{*65} = u_* d_{65}/\nu$.
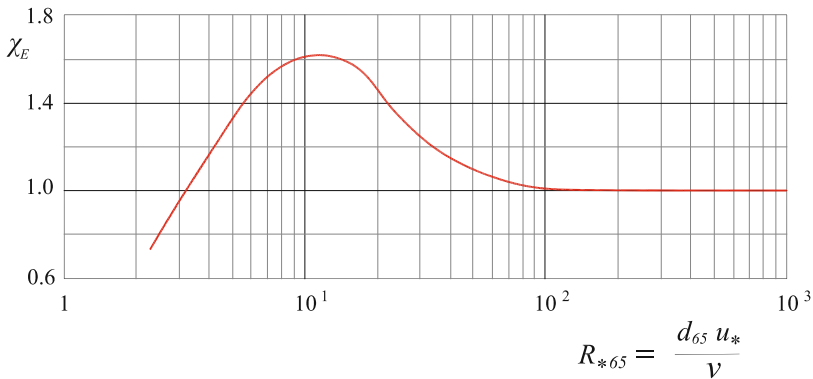
Fig. 5.5 Einstein's correction to the friction factor
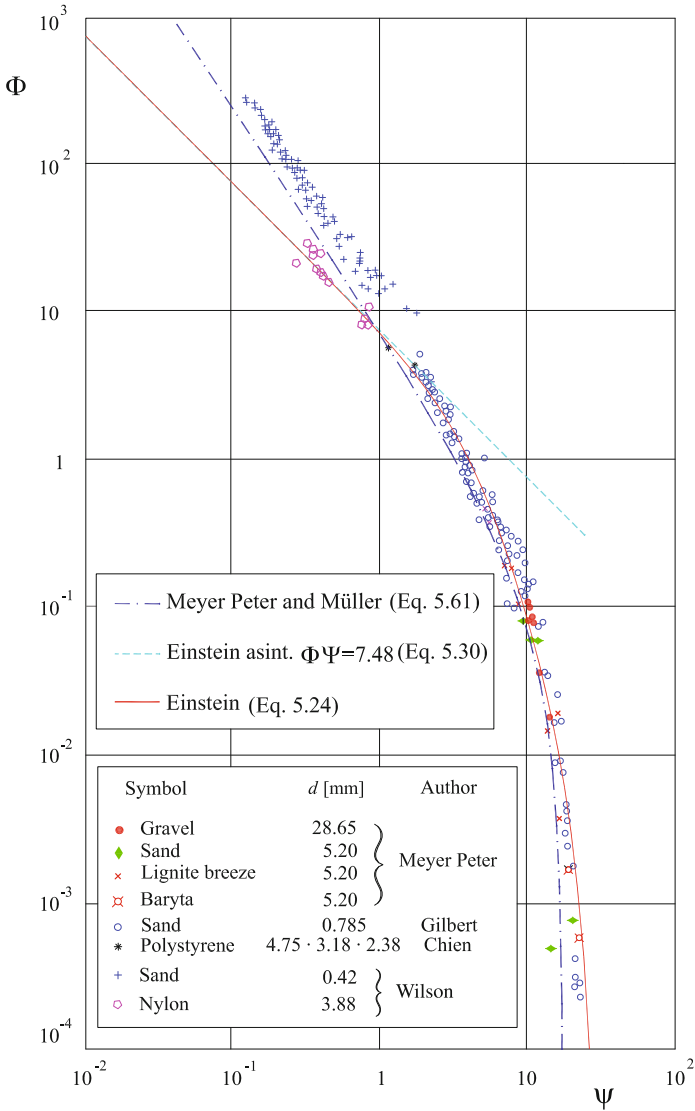
Fig. 5.6 Comparison between Einstein's bedload formula and experimental data (after Yalin 1977)

A good curve approximation of the graph in Fig. 5.5 is represented by the following relation:

$$\chi_E = 1 + 0.921\, e^{-0.027 R_{*65}^{1.275}}\, \ln(0.3028\, R_{*65}) \tag{5.26}$$

5.2.1 Limits of Einstein's Approach

By comparing the predictions of Einstein's theory (Fig. 5.6) and experimental data, Einstein's formula turns out to be in good agreement with them except for the highest values of sediment transport rate.

Several authors have revised Einstein's theory in order to overcome the weakest assumptions of his formulation and obtain a more convincing approach. Especially Yalin (1977) listed the following points of the theory:

- the length of the average jump is treated as proportional to the grain size, but the intuition and some experimental evidences indicate that this length also depends on the flow intensity;
- also the period T_p should depend on turbulence intensity, i.e. on u_*, and not only on the settling velocity w_s.
- the hypothesis that $p_n = p_1^n$, i.e. the hypothesis that the events (particle hops) are independent of each other, seems acceptable only if the jumps are infrequent, in other words only for low sediment transport;
- the change of the lower integration limit of the probability integral of Eq. (5.20) introduced by Einstein is rather doubtful.

Among the previous items, the most limiting assumptions are probably the first two. The two inconsistencies could be solved by observing that the ratio L_p/T_p is the scale velocity of the phenomenon, which reasonably depends not only on the fall velocity, as virtually Einstein assumed, but also on the flow intensity, i.e.

$$\frac{L_p}{T_p} \propto \sqrt{g\,\Delta\,d}\,\Phi^n \tag{5.27}$$

where the exponent n, by comparison with the experimental data, results to be equal to 0.5. By introducing only this change and with a suitable revision of constants, Einstein's formula well matches the experimental data (Armanini et al. 2015). The resulting equation is:

$$\Phi = \frac{\Psi^{1/2}}{A_{*1}}\left[\left(\frac{1}{\sqrt{\pi}}\int_{-\left(B_{*1}\Psi+\frac{1}{\eta_0}\right)}^{B_{*1}\Psi-\frac{1}{\eta_0}} e^{-\xi^2}d\xi\right)^{-1} - 1\right] \tag{5.28}$$

and the constant $\eta_0 = 0.5;\quad A_{*1} = 15;\quad B_{*1} = 0.214$.

5.2.2 Einstein's Equation for $q_b \to \infty$

In conditions of high mobility, there is $\theta \to \infty$ ($\Psi \to 0$). In this case, the sediment transport is particularly intense ($\phi \gg 1$). For low Ψ values the integral at the second member of (5.22) can be expanded in Taylor's series (Yalin 1977):

$$\int\limits_{-0.143\,\Psi-2}^{+0.143\,\Psi-2} e^{-\xi^2}\,d\xi = I(\Psi) \simeq I(\Psi = 0) + \left(\frac{\partial I}{\partial \Psi}\right)_{\Psi=0}\Psi + \mathcal{O}(\Psi^2)$$

$$\simeq B_* \left(e^{-(\frac{1}{\eta_0})^2} + e^{-(\frac{1}{\eta_0})^2}\right)\Psi = 2\,B_*\,\Psi\,e^{-(\frac{1}{\eta_0})^2}$$

which replaced into (5.24) yields:

$$\frac{A_*\Phi}{1 + A_*\Phi} = 1 - \frac{2}{\sqrt{\pi}}\,e^{-(\frac{1}{\eta_0})^2}\,B_*\Psi \tag{5.29}$$

Considering that in this case $A_*\,\Phi \gg 1$, after some manipulations from (5.29) we have

$$\Phi\,\Psi = 7.84 \tag{5.30}$$

according to which the relationship between Φ and Ψ is hyperbolic, as also appears from Fig. 5.6.

5.2.3 Einstein's Equation for $q_b \to 0$

Einstein's theory is based on the assumption that the probability distribution for the particle detachment is Gaussian type. In other words, there is no lower limit for the particle motion. This hypothesis overtly contrasts with Shields's theory of the incipient motion, which rather implies a threshold shear stress value for the particle entrainment. In the next sections, we will describe some bedload transport theories and formulae which consider, on the contrary, the threshold shear stress value. Under low mobility close to the incipient motion, Einstein's expression (5.22) virtually lacks precision. However, it is worth pointing out that in these conditions the sediment discharge is so low that such approximations seem to have negligible practical consequences. When the sediment discharge tends to zero, that is in dimensionless terms $\Phi \to 0$ and $A_*\Phi \ll 1$, the term on the right of the expression (5.13) becomes:

$$\frac{A_*\,\Phi}{1 + A_*\,\Phi} \to A_*\,\Phi \tag{5.31}$$

The parameter Ψ gets bigger and the integral of the second member of (5.22) can be approximated with an expression of the type:

$$\frac{2}{\sqrt{\pi}}\int_0^{B_*\,\Psi-1/\eta_o} e^{-x^2}\,dx \simeq 1 - \frac{1}{(1 + a_1\,(B_*\,\Psi - 1/\eta_o))^k} \tag{5.32}$$

with $k \gg 1$. In these conditions the sediment transport formula can be represented with a hyperbolic relationship whose exponential k is much higher than 1:

$$\Phi \simeq const \frac{1}{\Psi^k} \tag{5.33}$$

The use of monomial expressions without a threshold value for very low solid discharges has some undoubted advantages in mathematical elaborations, even in numerical models, so some researchers prefer them to formulations implying a threshold shear stress value and dealt with in the next paragraphs.

5.2.4   Effect of Material Non-uniformity

From the very beginning of his theory Einstein assumed that the particle size was not uniform. Such hypothesis can be easily introduced at this point of the argument.

To this end, it is worth subdividing the particle size curve of the *bed material* into N classes of percentage β_j, each characterized by the mean diameter d_j (Fig. 5.7). It clearly follows $\sum_{j=1}^{N} \beta_j = 1$.

Einstein's theory can then be iterated for each particle size class, starting from the specific surface area covered with particles belonging to the same class inside the strip L_{pj}:

$$A_j = \beta_j \; L_{pj} \; 1 \tag{5.34}$$

Table 5.1 illustrates how to reach the conclusion without iterating the steps previously indicated.
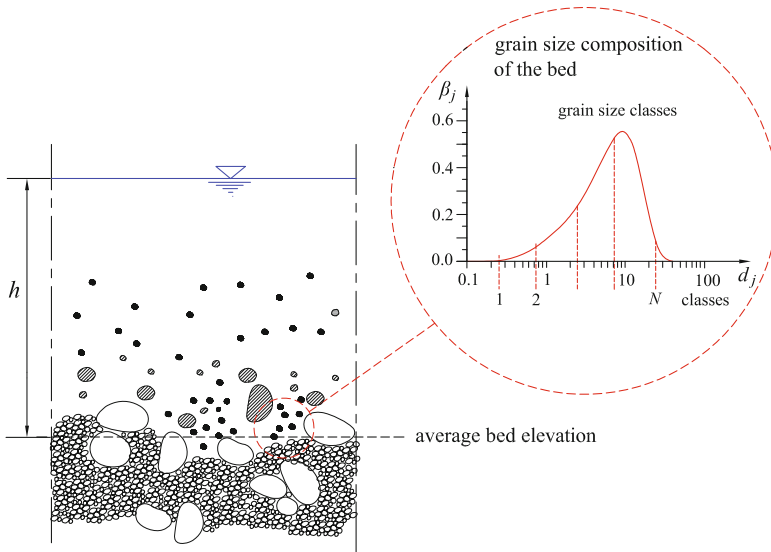
Fig. 5.7   Sediment transport layout of non-uniform grain size mixtures

Table 5.1 Conceptual scheme of Einstein's theory: comparison between uniform particle size material and non-uniform particle size mixtures

	Uniform particle size	Non-uniform particle size for every single class
Number of grains per surface unit	$\dfrac{L_p}{\alpha_2 d^2}$	$\beta_j \dfrac{L_{pj}}{\alpha_2 d_j^2}$
Number of grains separating in time T_p and covering distance nL_p	$p_n \dfrac{L_p}{\alpha_2 d^2}$	$p_n\,\beta_j \dfrac{L_{pj}}{\alpha_2 d_j^2}$
Idem per unit time	$p_n \dfrac{L_p}{T_p}\dfrac{1}{\alpha_2 d^2}$	$(p_n)_j \beta_j \left(\dfrac{L_p}{T_p}\right)_j \dfrac{1}{\alpha_2 d_j^2}$
Solid discharge for single size class crossing the generic section	$\displaystyle\sum_{n=1}^{\infty} p_n \dfrac{L_p}{T_p}\dfrac{\alpha_3 d^3}{\alpha_2 d^2}$	$\displaystyle\sum_{n=1}^{\infty} (p_n)_j \beta_j \left(\dfrac{L_p}{T_p}\right)_j \dfrac{\alpha_3\, d_j^3}{\alpha_2 d_j^2}$
Idem	$q_b = \dfrac{p_1}{1-p_1}\dfrac{1}{A_*} d\sqrt{g\Delta d}$	$q_{bj} = \left(\dfrac{p_1}{1-p_1}\right)_j \beta_j \dfrac{1}{A_*} d_j\sqrt{g\Delta d_j}$

If the solid discharge per unit of width related to the j-th grain size class is denoted with q_{bj}, it follows:

$$\Phi_j = \frac{q_{bj}}{d_j\,\sqrt{g\Delta d_j}} = \beta_j \frac{1}{A_*}\left(\frac{p_1}{1-p_1}\right)_j \tag{5.35}$$

We can generally write:

$$q_{bj} = \beta_j\, q_{bj}^* \tag{5.36}$$

where q_{bj}^* is the *transport capacity* related to particle size d_j, that is the solid discharge assessed as if, in the same hydrodynamic conditions, the bed material had a uniform grain size with the diameter equal to the j-th class.

As already observed with the incipient motion, the presence of particles with different diameter involves a hiding effect, which has repercussions on the erosion probability p_1 that, consequently, needs to be properly modified.

The procedure introduced by Einstein to consider the mutual interaction between classes is somewhat more complex than that described in Sect. 3.3.5 at page 74, where we introduced the hiding effects on the incipient motion of a particle. Here we will present a synthesis of the consequences of Einstein's method.

In brief, Einstein proposed to modify the *flow intensity parameter* with three different coefficients:

$$\Psi_j^* = \Psi_j\, \xi_{Ej} Y_E \left(\frac{\log_{10} 10.6}{\log_{10} 10.6\dfrac{X_E}{d_{65}}}\right)^2 \tag{5.37}$$
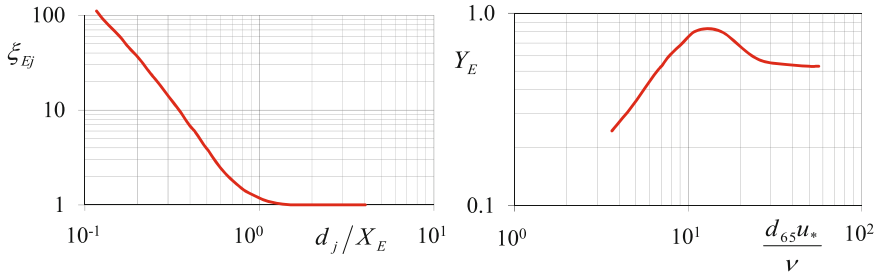
Fig. 5.8 Hiding functions according to Einstein

where the hiding coefficient ξ_{Ej} is a function of the ratio d_j/X_E as depicted in the graph a) of Fig. 5.8.

The parameter Y_E takes into account the effect of material non-uniformity on the lift force and is a function of the ratio d_{65}/δ' between the grain roughness d_{65} and the potential thickness of the *viscous sublayer* $\delta' = 11.6\nu/u_*'$, even if in Fig. 5.8b, for the reader's convenience, the parameter Y_E is directly expressed in function of the grain Reynolds number u_*d_{65}/ν.

The parameter X_E considers the influence of the material non-homogeneity on the equivalent roughness and is expressed by the following relations:

$$X_E = 0.77\frac{d_{65}}{\chi_E} \text{ for } \frac{d_{65}\,u_*}{\nu} > 20.9\chi_E \text{ and } X_E = 1.39\delta' \text{ for} \frac{d_{65}\,u_*}{\nu} < 20.9\chi_E$$
(5.38)

where d_{65}/χ_E represents the equivalent roughness. The factor $\chi_E = func(d_{65}\,u_*/\nu)$ has already been defined in Fig. 5.5, and is well approximated by Eq. (5.26).

In short,

$$\frac{q_{bj}}{\sqrt{d\,\Delta\,d_j}\,d_j} = \beta_j\,\frac{1}{43.13}\left(\frac{1}{\dfrac{1}{\sqrt{\pi}}\displaystyle\int_{-0.143\,\Psi_j^*-2}^{+0.143\,\Psi_j^*-2} e^{-x^2}dx} - 1\right)$$
(5.39)

where Ψ_j^* is calculated with expression (5.37) to consider the different effects of the particle size range.

5.3 Ballistic Approach

Starting from Einstein's framework but rejecting the least convincing hypotheses, we can obtain a semi-probabilistic model that may offer also an easier final formulation. The model, called *ballistic model* (Armanini et al. 2015), is based on the observation that in a stationary condition the solid discharge is due to all the grains crossing, in a unit time, the generic cross section of a channel (*A* in Fig. 5.9). The infinitesimal contribution to the bedload dq_s of the infinitesimal strip dx per unit width, located in the generic position x upstream of the section A, is given only by the particles that, once detached from the bed, are able to jump from x to the section A, i.e. the particle with a probability P_j of having a range longer than x. That is:

$$dq_s = u_s \alpha_2 d^2 \frac{dx}{\alpha_2 d^2} P_j P_0 \tag{5.40}$$

where u_s is the longitudinal component of the particle velocity when it crosses the section A; $\alpha_2 d^2$ is the projected frontal area of the particle, and the ratio $dx/\alpha_2 d^2$ expresses the number of particles contained in the surface element dx of unit width. P_0 is the particle detachment probability.

Note that in Eq. (5.40) the two probabilities P_0 and P_j are supposed to be independent. In addition, we assume that both have a gamma distribution, that is:

$$P_j = P\left(\frac{l_d}{\overline{l_d}} > \frac{x}{\overline{l_d}}\right) = \int_{x/\overline{l_d}}^{\infty} \xi e^{-\xi} \, d\xi = \left(1 + \frac{x}{\overline{l_d}}\right) e^{-x/\overline{l_d}}, \tag{5.41}$$

and

$$P_0 = \int_{\eta_{*lim}}^{\infty} \zeta e^{-\zeta} d\zeta = (1 + \eta_{*lim}) e^{-\eta_{*lim}}, \tag{5.42}$$

where x is between 0 and ∞. l_d is the effective distance jumped by the particle (*particle range*), $\overline{l_d}$ is the average jump of particles contributing to the bedload. ξ and ζ are two variables of integration.
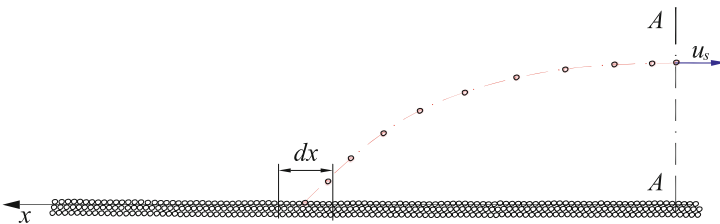

Fig. 5.9 The infinitesimal solid discharge dq_s consists of all the grains contained in strip dx with a certain probability of crossing the reference vertical section A

η_{*lim} represents the average value of the ratio between the lift force and the submerged weight, at which the particle detachment occurs. According to Einstein (1950), η_{*lim} is proportional to the *flow intensity parameter* $\Psi = g\,\Delta\,d/u_*^2$, that is, $\eta_{*lim} = B_{*A}\Psi - 1/\eta_{0A}$, with B_{*A} and η_{0A} being two parameters to be determined by experiment. Hence:

$$P_0 = \int_{B_{*A}\Psi - 1/\eta_{0A}}^{\infty} \zeta e^{-\zeta} d\zeta = (1 + B_{*A}\Psi - 1/\eta_{0A})e^{-B_{*A}\Psi + 1/\eta_{0A}} \qquad (5.43)$$

Finally, it is assumed that u_s (Eq. 5.40) depends on the shear velocity and on the mobility parameter, that is:

$$u_s = A_u \frac{u_*}{\Psi^n} = A_u \frac{\sqrt{g\Delta d}}{\Psi^{n+1/2}} \qquad (5.44)$$

where A_u is an experimental constant. By substituting all the relative expressions into Eq. (5.40), we obtain:

$$dq_s = \frac{\sqrt{g\,\Delta\,d}\,2A_u}{\Psi^{n+1/2}} \left(1 + \frac{x}{l_d}\right) e^{-x/\overline{l_d}} \frac{\overline{l_d}}{d}(1 + B_{*A}\Psi - 1/\eta_{*A})e^{-B_{*A}\Psi + 1/\eta_{0A}} \;, \quad (5.45)$$

which, integrated in x between 0 and ∞, gives:

$$\frac{q_s}{d\sqrt{g\,\Delta\,d}} = \frac{2A_u}{\Psi^{n+1/2}} \frac{\overline{l_d}}{d}(1 + B_{*A}\Psi - 1/\eta_{*A})e^{-B_{*A}\Psi + 1/\eta_{0A}} \qquad (5.46)$$

The left hand ratio of Eq. (5.46) represents the dimensionless sediment transport rate Φ.

Finally the average particle jump is expressed through a hyperbolic function of the flow intensity parameter Ψ:

$$\frac{\overline{l_d}}{d} = \frac{100}{1 + 4\Psi} \qquad (5.47)$$

Notice that at high values of sediment transport rate ($\Psi < \sim 10^{-2}$), the average particle jump tends to be 100 times the particle diameter, as suggested by Einstein. As the grain mobility decreases - thus increasing Ψ - the relative particle range, as expected, decreases with hyperbolic trend.

By substituting Eq. (5.47) into Eq. (5.40), we obtain:

$$\Phi = \frac{200A_u}{\Psi^{n+1/2}(1 + 4\Psi)}(1 + B_{*A}\Psi - 1/\eta_{0A})\,e^{-B_{*A}\Psi + 1/\eta_{0A}} \qquad (5.48)$$

On the basis of a comparison with a large number of experimental data, the following set of constants for their model can be assumed $A_u = 0.3$; $B_{*A} = 0.25$;
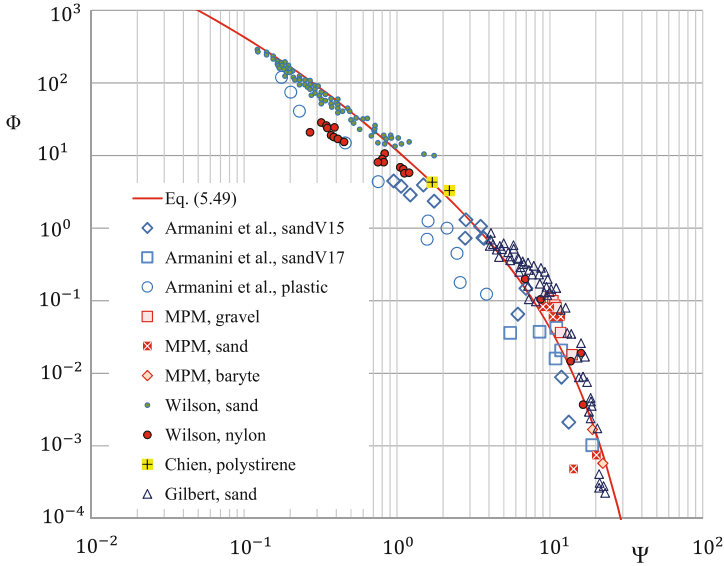
Fig. 5.10 Comparison between experimental data and results of Eq. (5.49)

$\eta_{0A} = 0.0.$[2] The final form of the formula is therefore:

$$\Phi = 60\frac{1 + 0.25\Psi}{\Psi\,(1 + 4\Psi)}\mathrm{e}^{-0.25\Psi} \tag{5.49}$$

Figure 5.10 shows a comparison between the prediction of the ballistic model (Eq. 5.49) and some experimental data.

Note that in Fig. 5.10 the experimental data that mostly deviate from Eq. 5.49 are those relating to light materials, which could reflect the presence of a non-negligible component of suspended load.

5.4   Sediment Transport Formulae Implying a Critical Threshold for the Incipient Motion

Einstein's theory is based on the particle detachment probability ranging from 1 to 0: for this reason no threshold is introduced to define the absolute absence of transport. Most of bedload transport formulae that have preceded or followed Einstein's theory are based, on the contrary, on the concept of the critical value of incipient motion

---

[2]In their original paper Armanini et al. (2015) suggested the following values of the constants $A_u = 0.25$; $B_{*A} = 0.25$; $\eta_{0A} = 0.5$, but a more careful analysis of the data has given the above set of constants.

introduced in Chap. 3. Many of these formulae are purely empirical, i.e. deduced from a series of experimental observations carried out in a laboratory or in the field.

The most commonly used formulae will be illustrated below in a dimensionless form, more specifically they will be described by using Einstein's dimensionless variables, rather than by means of the original variables suggested by different authors.

5.4.1 Du Boys Bedload Approach

The formula of Du Boys dating back to 1879 was widely used in the past, especially in the European countries, but rarely today. However, it has a remarkable historical importance, in that it is considered the first rational approach of the solid bedload transport and used as a reference for many later formulae (Graf 1984).

Du Boys assumes that the bedload transport occurs in stratified layers, each ε thick, put in motion by the bed shear stress due to the water motion: $\tau_o = g \, \rho \, h \, i_b$ where i_b denotes the bed slope.

The top layer sets the next in motion by exerting a friction stress, which is proportional to the weight of the layer itself, through a friction coefficient μ_f, and balances the tangential stress τ_o exercised by the water on it:

$$\tau_o = \mu_f \, \varepsilon \, g \, (\rho_s - \rho) \tag{5.50}$$

In addition, Du Boys assumed that the stress τ_o (*active stress*) is transmitted unaltered from the top layer to the subsequent layers, neglecting, in fact, the possible contribution of the longitudinal component of the weight of solid material and that of water.

Since the weight of the overlying material increases in the following layers, the friction stress between layers increases as well, and consequently the velocity of the underlying layers gets slower and slower. Du Boys hypothesized that the velocity of layers decreases linearly up to be annulled when the stress between layers reaches the critical threshold condition. If we assume all the layers as equal in thickness ε, v_s is the difference in velocity between two successive layers.

Layer 1 is the top layer. Be the layer number n the first immobile layer, i.e. above which the friction stress equals the critical value. $n - 1$ are then the layers in motion (Fig. 5.11).

From the momentum balance, applied to the control volume consisting of the n layers considered, the active tangential stress τ_o, which acts on the top layer, in uniform motion is balanced by the passive shear stress acting on the interface between the layer n and the underlying layer. Such a stress is assumed to be Coulomb-type, that is proportional to the submerged weight of the superimposed solid material $n \, \varepsilon \, g \, (\rho_s - \rho)$, by means of the friction coefficient μ_f:

$$\tau_o = \mu_f \, n \, \varepsilon \, g \, (\rho_s - \rho) \tag{5.51}$$
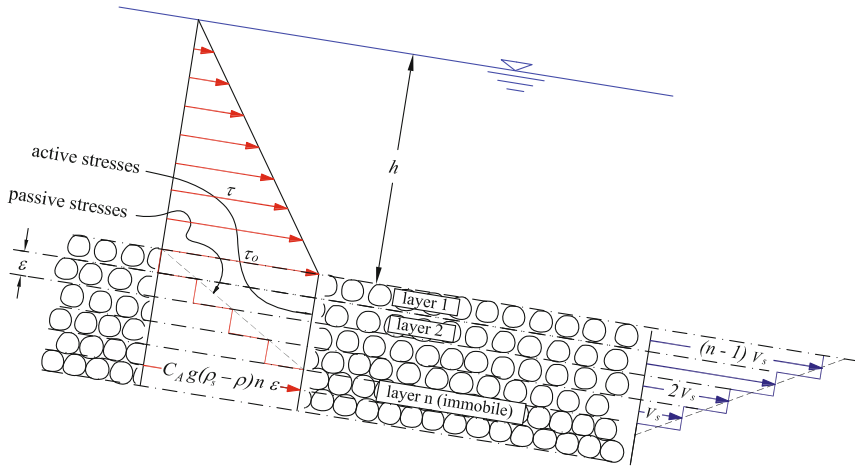
Fig. 5.11 Du Boys layout for the bedload transport. On the left are the distributions of active and passive stresses; on the right is the trend of the particle velocity

Note that in critical condition of incipient motion, that is when $\tau_o = \tau_c$, we have that $n = 1$; in this condition Eq. (5.51) becomes:

$$\tau_c = \mu_f \, \varepsilon \, g \, (\rho_s - \rho) \tag{5.52}$$

and therefore from the ratio between Eqs. (5.51) and (5.52) we have:

$$n = \frac{\tau_o}{\tau_c} \tag{5.53}$$

Since velocity has been supposed to vary linearly, the average velocity of the solid phase is $1/2 \, (n-1)v_s$, while the depth of the bedload layer is $n \, \varepsilon$, thus the solid discharge results:

$$q_b = \frac{(n-1)}{2} \, v_s n\varepsilon \tag{5.54}$$

By replacing the previous relation into Eq. (5.53), we have:

$$q_b = \left(\frac{\varepsilon \, v_s}{2 \, \tau_c^2}\right) \tau_o \, (\tau_o - \tau_c) \tag{5.55}$$

According to Du Boys, the parameter $\varepsilon \, v_s/(2 \, \tau_c^2)$ basically depends on the particle diameter, while Schoklitsch (1914) suggested:

$$\frac{\varepsilon \, v_s}{2 \, \tau_c^2} = 0.54 \frac{1}{g \, (\rho_s - \rho)} \tag{5.56}$$

The above relations are evidently metric: in fact, forces are measured in [kp], lengths in [m].

Finally, dividing both sides of Eq. (5.55) by $d\sqrt{g\Delta d}$, we obtain:

$$\frac{q_s}{d\sqrt{g\Delta d}} = \frac{\varepsilon}{d}\frac{v_s}{\sqrt{g\Delta d}}\frac{\tau_o}{\rho\,g\Delta d}\left(\frac{\tau_o}{\rho\,g\Delta d} - \frac{\tau_c}{\rho\,g\Delta d}\right)\left(\frac{\rho\,g\Delta d}{\tau_c}\right)^2 \tag{5.57}$$

In (5.57) we can assume that $\varepsilon \propto d$ and $vs \propto u_*$, from which you have:

$$\Phi \propto \theta^{1.5}(\theta - \theta_c) \tag{5.58}$$

in which we have assumed a rough wall, that is $\theta_c = cost$. Equation (5.58) may be generalized in the following form:

$$\Phi \propto \theta^{\alpha}(\theta - \theta_c)^{\beta} \tag{5.59}$$

where α and β are two suitable coefficients to be determined by experiments.

5.4.2   *Meyer-Peter and Müller Formula*

Still today Meyer-Peter and Müller's (1948) formula is very widespread. The formula was obtained from a great number of experimental tests carried out in the hydraulics laboratory of the Polytechnic of Zürich (*Eidgenössische Technische Hochschule*), thereby it is also called *ETH* or *Swiss formula*. Also this formula was originally given in metric form:

$$0.4\frac{g_s^{2/3}}{d} = \frac{g^{2/3}\,i_b}{d} - 17 \tag{5.60}$$

where g and g_s are the weight transport rates per unit width $[kps^{-1}m^{-1}]$ of water and solid sediment respectively.

Successive experiments have allowed to generalize the formula and rewrite it preferably in function of Einstein's dimensionless solid discharge and the Shields mobility parameter:

$$\Phi = 8(\theta^{\cdot} - \theta_c)^{1.5} \tag{5.61}$$

where $\theta^{\cdot} = (u_*^{\cdot})^2/(g\,\Delta\,d)$ is the mobility parameter whose assessment only refers to the grain resistance, that is, neglecting any contribution to resistance due to bed forms. Referring only to the grain resistance has the advantage that the knowledge of neither bed form types nor their resistance is required in applications. In fact, some authors (e.g. Einstein 1950) believe that the bedload transport is not substantially influenced by bed forms. However, since in the literature and in many applications the reference to the global resistance is found very frequently, the formula can then

be adjusted in this respect by introducing the ratio between the respective roughness coefficients:

$$\theta^{`} = \left(\frac{k_s^{`}}{k_s}\right)^{-1.5} \frac{u_*^2}{g\,\Delta\,d} \tag{5.62}$$

where $k_s^{`}$ represents the Strickler coefficient for grain roughness and k_s denotes the global one. Notice that Meyer-Peter and Müller's formula coincides with the general Eq. (5.59) if we set $\alpha = 0$ and $\beta = 1.5$.

In its original form Meyer-Peter and Müller's formula sets $\theta_c = 0.047$. The formula was calibrated for materials with quite rough diameter ($0.4 \sim 29\,\text{mm}$) in a laboratory channel and is suggested for gravel-bed streams with slopes up to 2%. For steeper slopes the formula underestimates the sediment discharge (Smart 1984).

5.4.3 Smart and Jäggi Formula

Smart and Jäggi's (1983) formula represents the extension of Meyer-Peter and Müller's to channels with steep slope ($3\,\% < i_b < 20\,\%$). The formula was obtained in the E.T.H. laboratory in Zürich by using the same type of material as Meyer-Peter and Müller did.

$$\Phi = 4\left(\frac{d_{90}}{d_{30}}\right)^{0.2} i_b^{0.6}\ \theta^{0.5}(\theta - \theta_c)\left(\frac{U}{u_*}\right) \tag{5.63}$$

in the formula the ratio $(d_{90}/d_{30})^{0.2}$ can be replaced by the number 1.05, a value of first approximation which takes into account the dependence on the non-uniformity of natural material. The authors suggest $\theta_c = 0.05$. Moreover, it should be noted that this formula employs the total value of the Shields parameter θ, i.e. inclusive of form resistance that in this case can be antidunes, instead of $\theta^{`}$ as in Meyer-Peter and Müller's formula.

5.4.4 Van Rijn Bedload Formula

Van Rijn (1984a) and (1984b) suggested two empirical formulae, one for the suspended load transport and the other for the bedload transport. The Van Rijn bedload formula was achieved at the Hydraulic Laboratory in Delft and was calibrated by analyzing a great quantity of experimental data:

$$\frac{q_b}{d\sqrt{g\,\Delta\,d}} = 0.053\left[\frac{\theta^{`} - \theta_c}{\theta_c}\right]^{2.1} D_*^{-0.3} \tag{5.64}$$

Table 5.2 Formulae for bedload transport, structurally similar to the Du Boys formula and more commonly used in the literature

Authors	Formula	Range of validity
Meyer-Peter and Müller (1948)	$\Phi = 8(\theta^{\grave{}} - \theta_c)^{1.5}$	$i_b \le 0.02$
Shields (1936)	$\Phi = 10\,(\theta - \theta_c)\theta^{1.5}\dfrac{\rho}{\rho_s}\dfrac{U}{u_*}$	
Ashida and Michiue (1971)	$\Phi = 17\,(\theta^{\grave{}})^{1.5}(1 - \dfrac{\theta_c}{\theta})(1 - \sqrt{\dfrac{\theta_c}{\theta}})$	$0.3\,\text{mm} \le d_{50} \le 7\,\text{mm}$
Suszka and Graf (1978)	$\Phi = 10.4\,\theta^{1.5}(1 - \dfrac{0.045}{\theta})^{2.5}$	for $\Phi \le 10^{-2}$
	$\Phi = 10.4\,\theta^{2.5}$	for $\Phi > 10^{-2}$
Smart and Jaeggi (1983)	$\Phi = 4\left(\dfrac{d_{90}}{d_{30}}\right)^{0.2} i_b^{0.6}\theta^{0.5}(\theta - \theta_c)\left(\dfrac{u}{u_*}\right)$	$0.03 \le i_b \le 0.20$

where $\theta^{\grave{}} = (u_*^{\grave{}})^2/(g\,\Delta\,d)$ represents the mobility parameter calculated only on the grain resistance:

$$u_*^{\grave{}} = U\,\frac{1}{5.75\log\left(\dfrac{12\,R_h}{3\,d_{90}}\right)} \tag{5.65}$$

Such a distinction becomes crucial when the ratio $T = (\theta^{\grave{}} - \theta_c)/\theta_c$ (*transport stage parameter*) is higher than 25. R_h is the hydraulic radius. $D_* = d_{50}(g\Delta/\nu^2)^{1/3}$ is the dimensionless particle diameter (Sect. 3.1 at page 59).

Van Rijn's bedload formula was calibrated for particle diameters ranging between 200 μm and 2 mm.

5.4.5   *Other Formulae Structurally Similar to the Du Boys Formula*

Other formulae, similar in structure to the Du Boys formula, are given in Table 5.2.

5.5   **Bedload Formulae Explicitly Depending on the Liquid Discharge or on the Stream Velocity**

Some of the bedload formulae were originally written in function of the flow velocity; only later they were rewritten in function of the mobility parameter and of the critical mobility parameter. Some formulae, however, have been written intentionally in function of flow velocity and velocity in critical conditions, possibly made

dimensionless. Such formulae could also be rewritten in function of the mobility parameter. It is however preferable to give at least one of these expressions in the original form for its historical importance.

In this expression the sediment discharge is directly dependent on the liquid discharge and the critical liquid discharge (of incipient motion), already defined in Sect. 3.6.2. According to the proponent authors, these expressions have the advantage of depending on easily measurable parameters both in the field and in laboratory; more specifically, they do not require defining the critical velocity, a parameter hardly measurable in some cases.

5.5.1 Schoklitsch's Formula

The formula proposed by Schoklitsch (1914) was based on measurements in gravel-bed streams. Also this formula is here rewritten in dimensionless form:

$$\Phi = \frac{2.5}{\Delta + 1} i_b^{1.5} \frac{q - q_c}{d \sqrt{g \Delta d}} \tag{5.66}$$

According to Takahashi (1987) this formula works if $0.05 < i_b < 0.09$; beyond this interval it underestimates the discharge.

5.6 Sediment Transport of Non-uniform Size Mixtures

From Meyer-Peter and Müller's formula (Eq. 5.61):

$$\Phi = \frac{q_b}{d \sqrt{g \, \Delta \, d}} = 8 \left(\frac{(u_*^{\backprime})^2}{g \Delta d} - \theta_c \right)^{1.5}$$

derives the following expression for the solid discharge:

$$q_b = 8 \sqrt{g \Delta d} \, d \left(\frac{(u_*^{\backprime})^2}{g \, \Delta \, d} - \theta_c \right)^{1.5} = 8 \sqrt{g \, \Delta} \left(\frac{(u_*^{\backprime})^2}{g \, \Delta} - d \, \theta_c \right)^{1.5} \tag{5.67}$$

In high mobility conditions, i.e. when for $\theta \gg \theta_c$, the second term in the parenthesis can be neglected compared to the first; thus we have:

$$q_b \simeq 8 \sqrt{g \, \Delta} \left(\frac{(u_*^{\backprime})^2}{g \, \Delta} \right)^{1.5} \tag{5.68}$$
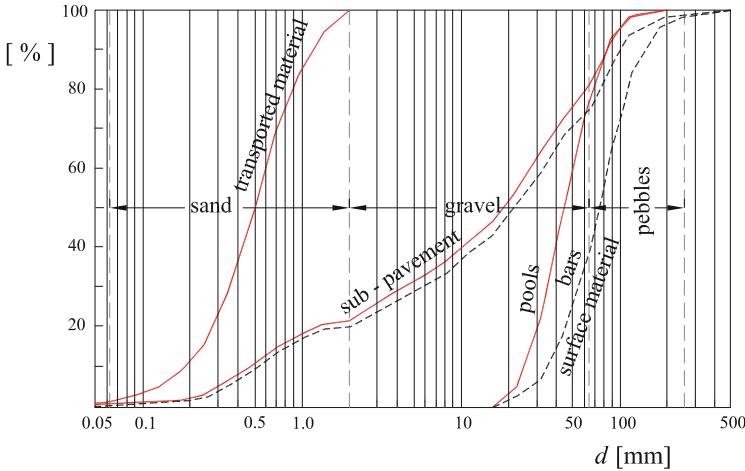
Fig. 5.12 Grain size distributions of transported, surface and sublayer (sub-pavement) materials observed in the stream Harris Creek in the presence of bars (Church et al. 1991)

According to Eq. (5.68) the sediment transport rate is independent of the particle diameter, in other words there would be *equimobility* conditions.

However, the equimobility condition hardly occurs in nature since a sufficiently large particle size fraction close to the critical mobility is very likely to be present, even if in very modest amounts. During the erosion process and bed motion, a grain size sorting naturally occurs: the finest grain sizes are easily removed, so that larger sized material tends to concentrate on the bed surface and creates a phenomenon named *dynamic armoring*, no matter how small the percentage of fractions with larger diameter (Fig. 5.12). This phenomenon will be described in Sect. 5.6.1 at page 137.

However, in applying the formulae to mixtures of non-uniform particle sizes, it is also necessary to consider the *hiding effect* already described in Sect. 3.3.5 at page 74 with regard to the conditions of incipient motion.

Also in the presence of grain movement, higher-sized particles protect the smaller-sized ones which consequently reduce their individual mobility and show a greater mobility than in case of uniform grain size.

The hiding effect can be considered in sediment transport formulae, by multiplying either the stress of particles of every class or the critical shear stress (provided it is in the formula) by an adequate hiding factor.

The first method is used in formulae neglecting the critical condition. In this case the mobility parameter of each grain size class is written as follows (Church et al. 1991):

$$\theta_j = \frac{u_*^2}{g \, \Delta \, d_j} G_j \tag{5.69}$$

where G_j is an adequate hiding coefficient, function of the ratio $(\bar{d}/d_j)$ between the diameter d_j of the single class and the average diameter $\bar{d}$ of the mixture.[3]

The latter criterion is applied to Du Boys-like formulae which explicitly contain the critical mobility parameter. For instance, with reference to Meyer-Peter and Müller's formula, the sediment discharge related to the single grain size class (Eqs. 5.36 and 5.67) is written as follows:

$$q_{bj} = 8 d_j \sqrt{g \, \Delta \, d_j} \; \beta_j \; \left(\theta_j - \xi_j \theta_{c\bar{d}}\right)^{1.5} \tag{5.70}$$

where ξ_j is the hiding coefficient related to the single grain size class, which is function of the ratio $(\bar{d}/d_j)$. $\theta_{c\bar{d}}$ is the critical mobility parameter related to the mean diameter.

According to other authors, this case can use as well the Shields mobility parameter of each grain size class, calculated as if the material had a uniform diameter equal to the grain size of the class in question.

In particular, Meyer-Peter and Müller's formula is usually combined with Egiazaroff's (1965) hiding coefficient, already introduced in Sect. 3.32 at page 75:

$$\xi_j = \left(\frac{\log_{10} 19}{\log_{10} 19 \dfrac{d_j}{\bar{d}}}\right)^2 \tag{5.71}$$

Generally speaking, it is also possible to use the monomial expression (3.34) (on page 76):

$$\xi_j = \left(\frac{d_j}{\bar{d}}\right)^{-n} \tag{5.72}$$

In this case, according to Meyer-Peter and Müller' formula (Eq. 5.70) the sediment discharge related to the single grain size class becomes:

$$\frac{q_{bj}}{d_j \sqrt{g \, \Delta \, d_j}} = 8 \, \beta_j \left(\frac{u_*^2}{g \, \Delta \, d_j} - \theta_{c\bar{d}} \left(\frac{\bar{d}}{d_j}\right)^n\right)^{1.5} \tag{5.73}$$

Clearly if we set $n = 1$, we obtain the same sediment discharge for all the grain size classes. The situation is similar to the equimobility described above in Sect. 3.3.5 at page 74, a very unlikely situation, as previously said. The exponent n is generally lower than the unity. A reliable value for n is $\simeq 0.9$.

Similar procedure is carried out for the other sediment transport formulae.

---

[3]In this case it is worth remembering that hiding factors suggested in the literature are applied after making the sediment discharge dimensionless with regard to the friction velocity, so that in the resulting parameter $\Phi/\theta^{1.5}$ the particle diameter does not appear explicitly.

5.6.1   Dynamic Armoring

It is worth pointing out that there is a difference between the grain size distribution of the bed and the distribution of the transported material.

With reference to Fig. 5.13, on the top left-hand graph the continuous line represents a possible grain size distribution of material on the bed ($\beta_j = func(d_j)$).

Consider a formula for the transport capacity for each grain size fraction, that is the sediment transport formula in function of the diameter, represented by the dotted curve in the same graph. This relation is a monotonically decreasing function of the diameter of type:

$$q_{bj}^* \propto \left(\frac{d_j}{\bar{d}} \right)^{-m} \tag{5.74}$$

with $m \simeq 0.1 \sim 0.4$ (Lanzoni and Tubino 1999).

According to Einstein (Eq. 5.36), the sediment discharge of every single grain size class is given by multiplying the transport capacity q_{bj}^* by the percentage β_j of the grain size of class on the bed.

$$q_{bj} = \beta_j \, q_{bj}^* \tag{5.75}$$
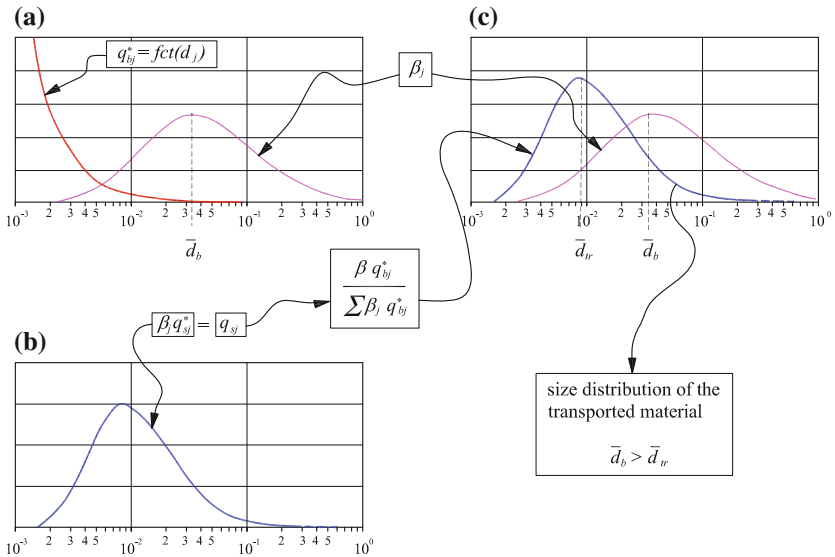
Fig. 5.13 Layout illustrating the existence of the dynamic armoring. **a** β_j represents the grain size distribution of the surface layer; $q_{bj}^* = func(d_j)$ the transport capacity related to the generic diameter d_j (Eq. 5.74); **b** $\beta_j \, q_{bj}^* = q_{sj}$ represents distribution of the transported material; **c** the curve of Graph (**b**), rescaled with regard to the total sediment discharge $\sum_{j=1}^{N} \beta_j \, q_{bj}^*$ represents the grain size distribution of the transported material. d_{tr} is the mean diameter of the transported material and d_b is the mean diameter of the bed material

The curve corresponding to this product is represented in the graph of Fig. 5.13, on the lower left-hand side.

It is worth observing that, as the grain size distribution tends to be null at the extremes of the interval, also the curve representing the product of the two functions will tend to null at the extremes.

Properly normalized, this curve represents then the grain size distribution α_j of the transported material (dotted line in graph on the right-hand side in Fig. 5.13):

$$\alpha_j = \frac{\beta_j q_{bj}^*}{\sum_{j=1}^{N} \beta_j q_{bj}^*} \tag{5.76}$$

In the same graph also the grain size distribution of the bed material β_j is reported by comparison.

The sediment discharge function (e.g. Eq. 5.74) being decreasing at grain size increasing, the distribution of the transported material results to have the barycenter towards left (the thinnest diameters) and to be steeper than the grain size distribution β_j. The mean diameter of the transported material $\overline{d}_{tr}$ is then thinner than that of the bed material $\overline{d}_b$. This effect is known as *dynamic armoring*, in that it concerns material in motion and is different from the static armoring which, on the other hand, regards the immobile material.

References

A. Armanini, V. Cavedon, M. Righetti, A probabilistic-deterministic approach for the prediction of the sediment transport rate. Adv. Water Resour. **81**, 10–18 (2015), https://doi.org/10.1016/j.advwatres.2014.09.008

K. Ashida, M. Michiue, Sediment transport rate and bed transportation. The Disaster Prevention Laboratory of the Kyoto University, Annual Report, 14, 1971

M. Church, J. Wolcott, W. Fletcher, A test of equal mobility in fluvial sediment transport: behavior of the sand fraction. Water Resour. Res. **27**(11), 2941–2951 (1991)

M. Du Boys, Études du régime du Rhône et de l'action exercée par les eaux sur un lit á fond de graviers indéfiniement affouillable. Annals des Pontes et Chaussées, Série **5**(18), 141–195 (1879)

I. Egiazaroff, Calculation of nonuniform sediment concentrations. J. Hydraul. Div. **91**(4), 225–247 (1965)

H.A. Einstein, The bedload function for sediment transportation in open channel flows, no. 1026. US Department of Agriculture (1950)

W.H. Graf, *Hydraulics of Sediment Transport* (Water Resources Publication, 1984)

A.A. Kalinske, Criteria for determining sand-transport by surface-creep and saltation. Eos Trans. Am. Geophy. Union **23**(2), 639–643 (1942)

S. Lanzoni, M. Tubino, Grain sorting and bar instability. J. Fluid Mech. **393**, 149–174 (1999)

E. Meyer-Peter, R. Müller, Formulas for bedload transport, in *Proceedings of the 2nd Meeting of the International Association for Hydraulic Structures Research*, no. 133 (IAHS, 1948), pp. 39–64

A. Schoklitsch, *Über Schleppkraft und Geschiebebewegung*, ed. by W. Engelmann (1914)

A. Shields, *Anwendung der Aehnlichkeitsmechanik und der Turbulenzforschung auf die Geschiebebewegung* (Technical report, Preussischen Versuchsanstalt für Wasserbau, 1936)

G.M. Smart, Sediment transport formula for steep channels. J. Hydraul. Eng. **110**(3), 267–276 (1984)

G.M. Smart, M. Jaeggi, Sediment transport on steep slopes, in *Alternierende Kiesbänke, Mitteilung der Versuchsanstalt für Wasserbau, Hydrologie und Glaziologie*, no. 64 (1983)

L. Suszka, W. Graf, Sediment transport in steep channels at unsteady flow, in *Proceedings of 22nd IAHR Congress* (1978), pp. 166–170

T. Takahashi, High velocity flow in steep erodible channels, in *Proceedings 22th IAHR Congress* (1987), pp. 42–53

L.C. Van Rijn, Sediment transport, part I: bedload transport. J. Hydraul. Eng. **110**(10), 1431–1456 (1984a)

L.C. Van Rijn, Sediment transport, part II: suspended load transport. J. Hydraul. Eng. **110**(11), 1613–1641 (1984b)

M. Yalin. *Mechanics of Sediment Transport* (Pergamon, 1977)

Chapter 6
Suspended Transport and Total Transport

6.1 Introduction

As previously stated (Sects. 2.4 and 5.1), sediments are transported by suspension when the fluctuating lift force prevails over the gravity force in the balance of the forces acting on the particles, and the trajectories covered by the particles are at least of the same size order as the water depth.

However, the distinction between bedload and suspended load is not straightforward, in that it is associated to the lift forces subject to turbulent fluctuations. As the lift forces are scaled by the friction velocity u_*, we can assume that particles with a certain diameter and density are characterized by a critical friction velocity value which causes them to be on average transported in suspension.

In dimensionless terms, i.e., looking at the relationship between submerged weight and hydrodynamic lift, we can define a significant mobility parameter value for the suspended transport, e.g., the initiation of the suspended load can be represented on the Shields diagram (Figs. 3.2 or 3.1).

According to Bagnold (1966), the particle is transported by suspension when its terminal fall velocity w_s is lower than the local turbulence intensity. Since this latter is scaled by the friction velocity, the parameter indicative of the initiation of suspension is a mobility index expressed in function of the fall velocity: $(\theta_c)_{ss} = w_s^2/(g \Delta d_{50})$. Similar observations led Engelund and Fredsøe (1976) to the conclusion that the initiation of suspension occurs for $(\theta_c)_{ss} = 0.0625 \, w_s^2/(g \Delta d_{50})$.

Figure 6.1, suggested by Van Rijn (1984b), shows these criteria graphically. Unlike the critical threshold of the initial motion, the initiation of the suspended transport is more difficult to define and more susceptible to the subjective interpretations of the authors who proposed it.

According to Van Rijn (1984b), the threshold of suspended load can conveniently be made dependent on the dimensional diameter (Sect. 3.1) $D_* = d(g \Delta/\nu^2)^{1/3}$ for values lower than 40–100; while it is independent of it at higher values. In this case, the threshold value ranges from 0.15 to 0.25 (according to Van Rijn) to 1.2 (according to Bagnold).
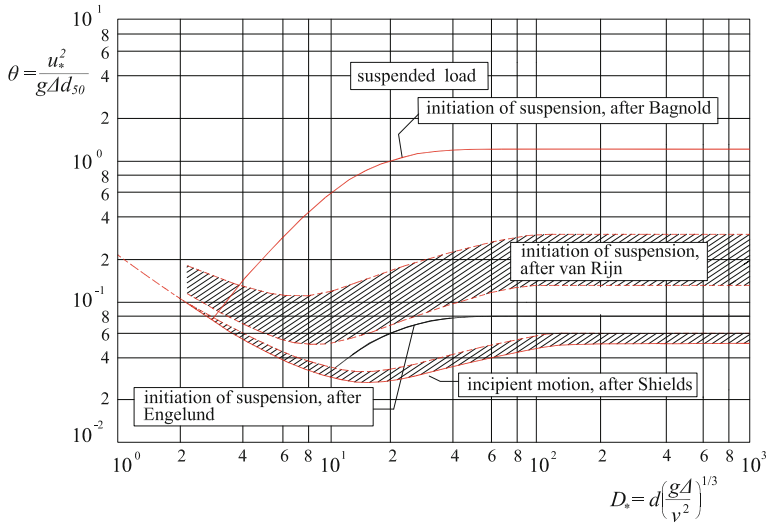
Fig. 6.1 Initial conditions for suspended transport suggested by Van Rijn (1984b)

In the generally acceptable hypothesis that the particle concentration is sufficiently small, the suspended transport can be studied with the same criteria as those adopted for studying the diffusion of a scalar in turbulent flows.

6.2 Flow Equations

With reference to an infinitesimal control volume $\forall$, the instantaneous volume concentration of solid material $\widetilde{c}$ is defined as follows:

$$\widetilde{c} = \frac{\forall_s}{\forall} = \frac{\forall_s}{\forall_s + \forall_w} \tag{6.1}$$

where $\forall_s$ and $\forall_w$ are, respectively, the volumes of the solid and liquid phases, and $\forall = \forall_s + \forall_w$. In a natural watercourse, it is usually $0 \le \widetilde{c} \ll 1$.

The continuity equation of the solid phase for a Cartesian reference frame can be written as follows:

$$\frac{\partial}{\partial t}(\rho_s\,\widetilde{c}) + \frac{\partial}{\partial x_i}\,(\rho_s\,\widetilde{c}(\widetilde{u}_s)_i) = 0 \tag{6.2}$$

where $(\widetilde{u}_s)_i$ are the Eulerian components of the velocity vector of the solid phase. In case of sedimentable particles, it is generally acknowledged that the vector difference between the liquid phase velocity $\widetilde{\mathbf{u}}$ and the solid phase velocity $\widetilde{\mathbf{u}}_s$ is given by the terminal fall velocity vector $\mathbf{w_s}$ of the particle itself:

$$(\widetilde{u}_s)_i = \widetilde{u}_i + (w_s)_i \tag{6.3}$$

If then, we assume a system in a horizontal plane (x, z) and the vertical axis y as positive along the upward vertical, we have:

$$(\widetilde{u}_s)_x = \widetilde{u}_x \quad ; \quad (\widetilde{u}_s)_y = \widetilde{u}_y - w_s \quad ; \quad (\widetilde{u}_s)_z = \widetilde{u}_z \tag{6.4}$$

Moreover, if we consider that the particle density ρ_s is constant, we obtain:

$$\frac{\partial \widetilde{c}}{\partial t} + \frac{\partial}{\partial x}\widetilde{u}_x\widetilde{c} + \frac{\partial}{\partial y}\widetilde{u}_y\widetilde{c} - \frac{\partial}{\partial y}w_s\widetilde{c} + \frac{\partial}{\partial z}\widetilde{u}_z\widetilde{c} = 0 \tag{6.5}$$

where ($\widetilde{}$) denotes the instantaneous values of the above variables.

Should the flow be turbulent, the Reynolds decomposition can be applied to instantaneous values of velocity and solid concentration:

$$\widetilde{u}_i = u_i + u_i' \quad \text{and} \quad \widetilde{c} = c + c' \tag{6.6}$$

where $u_i = \lim\limits_{T\to\infty} \dfrac{1}{T} \displaystyle\int_{t-T/2}^{t+T/2} \widetilde{u}_i(\tau, \mathbf{x})\, d\tau$ and $c = \lim\limits_{T\to\infty} \dfrac{1}{T} \displaystyle\int_{t-T/2}^{t+T/2} \widetilde{c}(\tau, \mathbf{x})\, d\tau$ represent the time average values, and u' and c' the fluctuating components of velocity and concentration in the hypothesis of statistically stationary turbulence. We then obtain:

$$\frac{\partial u_i}{\partial t} = 0 \quad ; \quad \overline{u'}_i = \lim\limits_{T\to\infty} \frac{1}{T} \int_{t-T/2}^{t+T/2} u_i'(\tau, \mathbf{x})\, d\tau = 0$$

$$\frac{\partial c}{\partial t} = 0 \quad ; \quad \overline{c'} = \lim\limits_{T\to\infty} \frac{1}{T} \int_{t-T/2}^{t+T/2} c'(\tau, \mathbf{x})\, d\tau = 0 \tag{6.7}$$

The above hypothesis of statistically stationary turbulence cannot be applied to natural streams, where it is advisable to choose an integration interval T much longer than the average period of vortices containing the turbulent energy. In this case, we may well assume $\dfrac{\partial u_i}{\partial t} \neq 0$ and $\dfrac{\partial c}{\partial t} \neq 0$.

After introducing Eq. (6.6) into (6.5) and averaging the equation over the time T, we obtain:

$$\frac{\partial c}{\partial t} + \frac{\partial u_x\, c}{\partial x} + \frac{\partial}{\partial x}\overline{u_x'c'} + \frac{\partial u_y\, c}{\partial y} - \frac{\partial w_s\, c}{\partial y} + \frac{\partial}{\partial y}\overline{u_y'c'} + \frac{\partial u_z\, c}{\partial z} + \frac{\partial}{\partial z}\overline{u_z'c'} = 0 \tag{6.8}$$

If we make the hypothesis that the flow is quasi-unidirectional in x (e.g., channel flow), we can assume that:

$$u_z \simeq 0 \quad , \quad u_y \simeq 0 \quad \text{and} \quad \frac{\partial}{\partial z} \simeq 0 \tag{6.9}$$

Equation (6.8) reduces to the following:

$$\frac{\partial c}{\partial t} + \frac{\partial u_x\, c}{\partial x} - \frac{\partial w_s\, c}{\partial y} = -\frac{\partial}{\partial x}\overline{u'_x c'} - \frac{\partial}{\partial y}\overline{u'_y c'} \tag{6.10}$$

The terms on the left of Eq. (6.10) represent the convective transport of the solid phase, the terms on the right represent the turbulent diffusion of the same phase. In the quasi-two-dimensional flows, the diffusive term in the flow direction can be neglected with respect to the convective term in the same direction, i.e., $\partial(u_x\, c)/\partial x \gg \partial\overline{u'_x c'}/\partial x$. Thus, we obtain:

$$\frac{\partial c}{\partial t} + \frac{\partial u_x\, c}{\partial x} = \frac{\partial}{\partial y}(w_s\, c - \overline{u'_y c'}) \tag{6.11}$$

Similarly to the Reynolds stress tensor, the diffusive term can be expressed by means of the diffusive Boussinesq model (Rouse 1937):

$$-\overline{u'_y c'} = \varepsilon_s \frac{\partial c}{\partial y} \tag{6.12}$$

With a good approximation, we can assume that the turbulent diffusion coefficient of the solid phase ε_s is proportional to the turbulent diffusion coefficient of the momentum ε, defined as $\varepsilon = -\overline{u'_x u'_y}/(\partial u_x/\partial y)$:

$$\varepsilon_s = \beta_\varepsilon\, \varepsilon \tag{6.13}$$

where β_ε is a suitable coefficient of order 1.

The continuity equation finally assumes the following form:

$$\frac{\partial c}{\partial t} + \frac{\partial u_x\, c}{\partial x} = \frac{\partial}{\partial y}(w_s\, c + \beta_\varepsilon\varepsilon\frac{\partial c}{\partial y}) \tag{6.14}$$

The term between brackets represents the vertical net flow: $w_s\, c$ denotes the downward flow due to the particle tendency to sediment, while $\beta_\varepsilon\varepsilon(\partial c/\partial y)$ represents the upward flow due to the turbulent diffusion.

6.3 Distribution of Suspended Concentrations in Equilibrium Channels

Equation (6.14) can be integrated in the hypothesis of stationary uniform channel flow. In this case, the two terms in the first member vanish and the equation becomes:

$$w_s\, c + \beta_\varepsilon \varepsilon \frac{\partial c}{\partial y} = cost \tag{6.15}$$

The constant can be calculated by considering that it represents the vertical net flux of the solid phase and that this flux at the free surface must be zero. In other words:

$$w_s\, c + \beta_\varepsilon \varepsilon \frac{\partial c}{\partial y} = 0 \tag{6.16}$$

In order to integrate (6.15), it is necessary to assign an appropriate expression to the turbulent diffusion coefficient. In general, we can write:

$$\varepsilon = u_* h\, f\!\left(\frac{y}{h}\right) \tag{6.17}$$

where $f(y/h)$ is a function to be defined, denoting the dimensionless vertical distribution of the turbulent diffusion coefficient. By inserting (6.17) into (6.16), after a few steps, we obtain:

$$c + \beta_\varepsilon \frac{u_*}{w_s}\, f(\eta) \frac{dc}{d\eta} = 0 \tag{6.18}$$

where $\eta = y/h$.

6.3.1 The Rouse Solution

In 1937, Rouse proposed a solution of Eq. (6.18) by neglecting the average viscous shear stress, thus assuming $\tau_{yx} \simeq -\overline{u'_x u'_y}$, so that the momentum diffusion coefficient results:

$$\varepsilon = \frac{-\overline{u'_x u'_y}}{\dfrac{du_x}{dy}} = \frac{\dfrac{\tau_{yx}}{\rho}}{\dfrac{du_x}{dy}} \tag{6.19}$$

In a uniform channel flow, the shear stress distribution is of a triangular type with the bed value τ_o, that is:

$$\frac{\tau_{yx}}{\tau_o} = \frac{h - y}{h} \tag{6.20}$$

Moreover, by assuming a logarithmic velocity distribution:

$$\frac{u_x}{u_*} = \frac{1}{\kappa} \ln \frac{y}{y_o} \tag{6.21}$$

and by taking the derivative:

$$\frac{du_x}{dy} = \frac{u_*}{\kappa y} \tag{6.22}$$

Regarding the constant y_0, in a hydraulically rough bed, experimentally, it has been found that (Jansen et al. 1979):

$$y_o \simeq \frac{k}{33} \tag{6.23}$$

where k [L] is the roughness of the bed.

After substituting (6.20) and (6.22) into (6.19), we obtain a parabolic distribution of the turbulent diffusion coefficient:

$$\varepsilon = \frac{\tau_o}{\rho} \frac{h - y}{h} \frac{\kappa y}{u_*} = \kappa u_* h \frac{y}{h} \left(1 - \frac{y}{h}\right) \tag{6.24}$$

in which $\kappa \simeq 0.4$ is the von Kármán constant. In other words, $f(\eta) = \kappa\eta(1 - \eta)$ (Fig. 6.2), which replaced into (6.18) yields:

$$c + \beta_\varepsilon \frac{u_*}{w_s} \kappa \eta(1 - \eta)\frac{dc}{d\eta} = 0 \tag{6.25}$$

By separating the variables of (6.25), we obtain:

$$\frac{dc}{c} = -\frac{w_s}{\beta_\varepsilon u_* \kappa} \frac{d\eta}{\eta(1 - \eta)} \tag{6.26}$$

The solution of which is:

$$\ln \frac{c}{c_a} = \ln \left(\frac{\eta}{1 - \eta} \frac{1 - \eta_a}{\eta_a}\right)^Z \tag{6.27}$$

where $Z = w_s/\beta_\varepsilon u_* \kappa$.

Since, if $\eta \to 0$, the concentration $c \to \infty$, the boundary condition was not set on the bed, but at a reference distance a from it where the suspended transport supposedly initiates. Within the layer a, the transport is assumed to occur as bedload. Equation (6.27) can, therefore, be rewritten in the following form:

$$\frac{c}{c_a} = \left(\frac{\eta}{1 - \eta} \frac{1 - \eta_a}{\eta_a}\right)^Z \tag{6.28}$$

Rouse proposed to assume $\beta_\varepsilon \simeq 1$. Moreover, he suggested to set $\eta_a = 0.05$. Rouse's law has been verified experimentally by various scholars, e.g., Vanoni (1946) first among others (Fig. 6.3).

6.3.2 The Lane Solution

It is also worth mentioning how Lane and Kalinske (1941) solved Eq. (6.18) in case of constant distribution of the dimensionless turbulent diffusion coefficient $f(\eta)$:

$$\beta_\varepsilon \varepsilon = \frac{u_* h}{15} \tag{6.29}$$

Figure 6.2 shows a comparison between the diffusion coefficient calculated according to Eq. (6.29) and the parabolic distribution proposed by Rouse (Eq. 6.24). Equation (6.29), inserted into (6.18), yields:

$$c + \frac{u_*}{15\, w_s} \frac{dc}{d\eta} = 0 \tag{6.30}$$

The solution of (6.30) is:

$$\ln \frac{c}{c_a} = -15 \frac{w_s}{u_*} (\eta - \eta_a) = -15 \frac{w_s}{u_*} \frac{y-a}{h} \tag{6.31}$$

Equation (6.31) can then be rewritten in the following form (Lane's solution):

$$c = c_a\, e^{-15\, \frac{w_s}{u_*} \frac{y-a}{h}} \tag{6.32}$$

Fig. 6.2 Distribution of the turbulent diffusion coefficient according to Rouse (Eq. 6.24) and to Lane (Eq. 6.29) described below
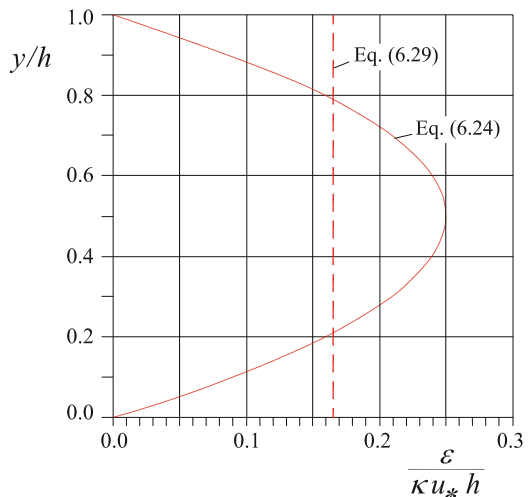
According to Lane's solution, on the free surface ($y = h$), the concentration is different from 0:

$$c(h) = c_a\, e^{-15\,\dfrac{w_s}{u_*}\dfrac{h-a}{h}} \tag{6.33}$$

This result contrasts with the necessity to set the surface concentration equal to zero, since there is no flux of sediments across the free surface. Such a drawback is not present in Rouse's solution (Eq. 6.28).

6.3.3 The Reference Concentration c_a

We still have to specify the concentration value c_a at the reference height $y = a$ (*bedload layer thickness* or *saltation layer thickness*). As previously observed, in the presence of mobile bed, it is rather difficult to give an exact definition of bed level. Even more uncertain is then how to establish the reference height a as suitable for setting the boundary conditions for suspended transport, while defining the parameters for quantifying the suspended solid discharge is clearly fundamental. The solution to this problem has been suggested by various theories which practically depend on the same definition of the layer a. Fairly widespread are those by Brown (1950), Engelund and Fredsøe (1976), and more recently Van Rijn (1984b).

According to Einstein, the reference concentration c_a is the solid phase concentration in the bedload layer, in which the solid transport occurs almost exclusively as bedload, i.e., through the mechanisms of saltation or rolling dealt with in Sect. 5.2. According to Einstein, the thickness of this layer is proportional to the average height of the particle jumps and is assumed to be around twice the diameter of the largest particles (Fig. 6.4):

$$a \propto \delta_b \simeq 2\,d_{90}$$

The sediment concentration distribution in the bedload layer is supposed to be uniform and, in any case, equivalent to the reference concentration c_a of the suspended solid transport. That is, we have:

$$q_b = c_b u_b \delta_b = A\, c_a\, u_a\, a \tag{6.34}$$

where q_b is the bedload per unit width, u_b is the average longitudinal velocity component of the bedload in the saltation layer and u_a the average value in the presence of bed forms; A is an appropriate proportionality coefficient.

On the assumption that $u_b \propto u_a \propto u_*$, Einstein reached the following expression:

$$c_a = \frac{1}{11.6}\frac{q_b}{a\, u_*} \tag{6.35}$$
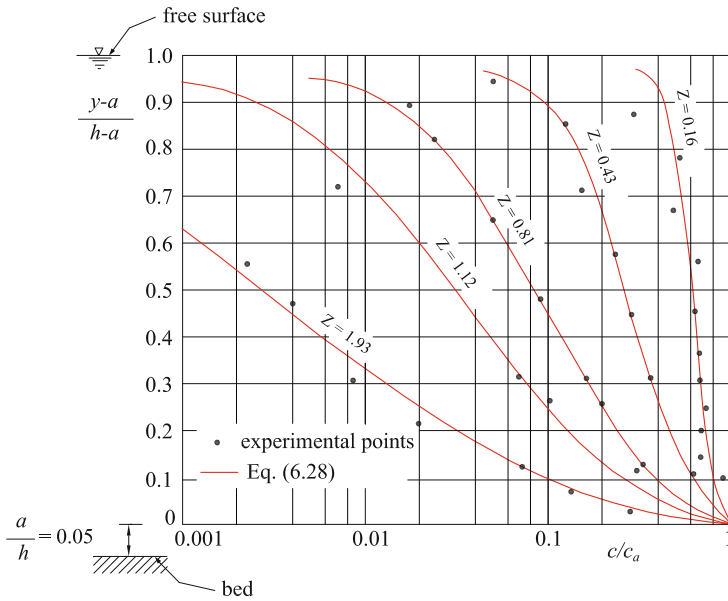
Fig. 6.3 Distribution of suspended particle concentration (A.S.C.E. Vanoni (1946))
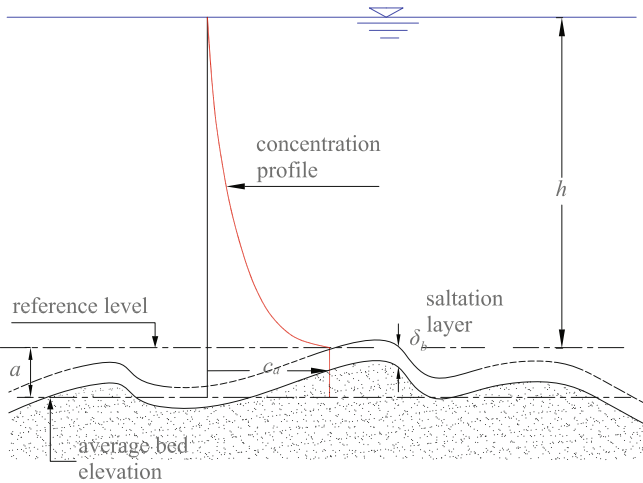
Fig. 6.4 Distribution of the concentration. δ_b denotes the average height of particle jumps (Van Rijn 1984b)

The Engelund and Hansen (1967) scheme, later modified by Engelund and Fredsøe (1976), refers to Bagnold's sediment transport theory (Bagnold 1956). Like Rouse, Engelund and Hansen assumed the reference level a as proportional to the water depth ($a = 0.05\,h$). The concentration c_a is essentially dependent on the Shields mobility parameter:

Fig. 6.5 Concentration c_a in function of the Shields mobility parameter according to Engelund and Hansen (1967)
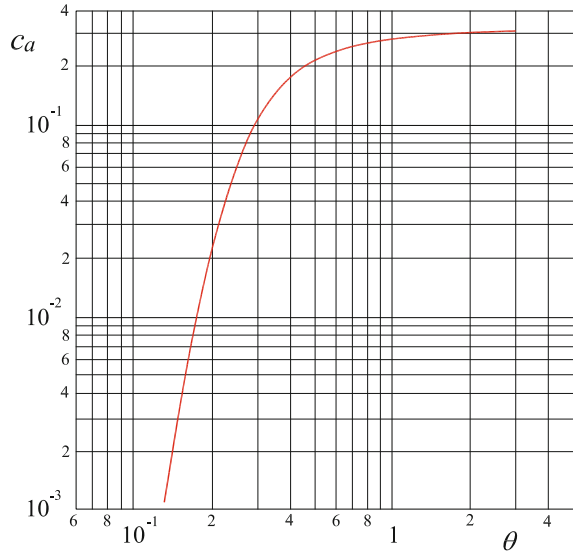
$$\theta = \frac{u_*^2}{g\,\Delta\,d}$$

The relation between c_a and θ is graphically shown in the next Fig. 6.5. It should be noted that the bed concentration tends to an asymptotic value equal to around 0.32.

More recently, Van Rijn (1984a, b) developed an analytical expression, based both on the grain mobility parameter $\theta`$ and on the dimensionless grain size $D_* = d_{50}\left(\Delta\,g/\nu^2\right)^{1/3}$:

$$c_a = 0.015\frac{d_{50}}{a}\left(\frac{\theta` - \theta_c}{\theta_c}\right)^{1.5} D_*^{-0.3} \qquad (6.36)$$

in which the author proposes to assume $a = 0.015\,h$ in case of plane bed and $a = 0.5\,H_{dune}$ in the presence of bed forms (dunes). θ_c and $\theta`$ are, respectively, the critical mobility parameter and the mobility parameter referred to the grain roughness.

The expression is valid for $0.1 < d_{50} < 0.5$ [mm]. Notice that Van Rijn's supposed $\beta \neq 1$, as it will be explained in Sect. 6.4.

6.4 Suspended Load

Since the vertical velocity distribution and the vertical concentration distribution are known, the suspended solid discharge can be calculated by integrating the product of these two distributions on the water depth. The suspended sediment discharge per

unit width q_{ss} is then:

$$q_{ss} = \int_a^h c\,u\,dy \tag{6.37}$$

Inserting (6.21) and (6.28) into (6.37), we obtain:

$$q_{ss} = \frac{u_* c_a}{\kappa}\left(\frac{a}{h-a}\right)^{-\frac{w_s}{u_* \kappa}}\int_a^h \left(\frac{h-y}{y}\right)^{-\frac{w_s}{u_* \kappa}}\ln\frac{y}{y_0}\,dy \tag{6.38}$$

where y_o depends on the roughness of the bed (Eq. 6.23).

There is no knowledge of a closed-form expression for the integral in Eq. (6.38). It can be calculated by a series expansion of the functions to integrate, or it can be calculated numerically. c_a is, on the other hand, given by (6.35) or by (6.36).

Van Rijn (1984b) suggested the following exemplified expression of Eq. (6.38):

$$q_{ss} = F\,U\,h\,c_a \tag{6.39}$$

where:

$$F = \frac{\left(\frac{a}{h}\right)^{Z'} - \left(\frac{a}{h}\right)^{1.2}}{\left(1-\frac{a}{h}\right)^{Z'}(1.2-Z')} \tag{6.40}$$

and

$$Z' = \frac{w_s}{\beta_\varepsilon\,u_*\,\kappa} + 2.5\left(\frac{w_s}{u_*}\right)^{0.8}\left(\frac{c_a}{C_*}\right)^{0.4} \tag{6.41}$$

Figure 6.6 shows the behavior of the function F versus the exponent Z' for different value of the relative thickness of the bedload layer a/h.

The coefficient β_ε can be calculated with the following expression:

$$\beta_\varepsilon = 1 + 2\left(\frac{w_s}{u_*}\right)^2, \qquad \text{for} \qquad \frac{w_s}{u_*} < 1 \tag{6.42}$$

The parameter Z' is the same as defined in Sect. 6.3.1 on p. 150, modified to consider some secondary effects neglected in the Rouse theory. C_* represents the maximum volumetric concentration at the bed, i.e., the *random packing concentration*, which, according to the author, can be assumed to be equal to 0.65 for natural particles. According to Van Rijn (1984b), Eq. (6.39) along with (6.40) approximate the original relation (6.38) with a precision higher than 75% for $0.3 \leq Z' \leq 3$ and $0.01 \leq a/h \leq 0.1$.
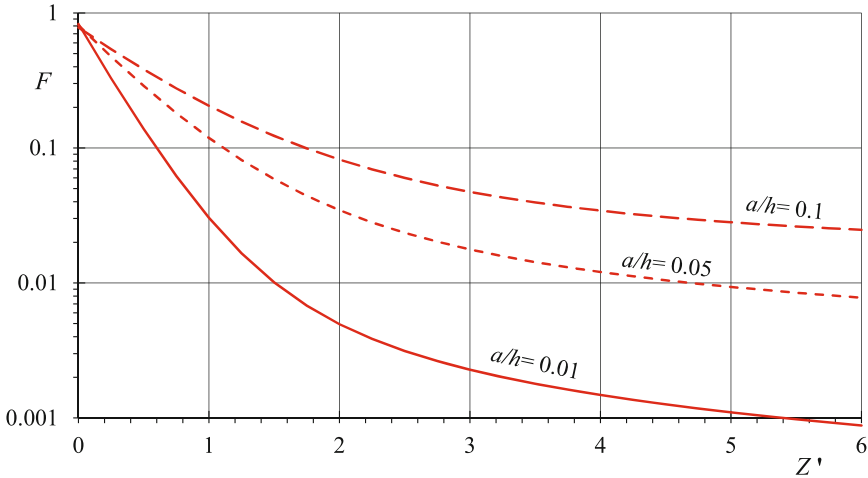
Fig. 6.6 F factor of suspended load (Eq. 6.40) in function of the exponent Z', parameterized with respect to ratio a/h, according to Van Rijn (1984b)

6.5 Total Solid Discharge

Several transport formulae mentioned in the previous chapter are explicitly referred to the bedload transport. In other formulae, the particle diameter interval may lead to the conclusion that they may be valid only for the bedload. In many other cases, formulae were calibrated specifically for the total transport.

For some formulae, it is expressly said that the total sediment transport rate q_s is given by the sum of the bed sediment discharge q_b and the suspended sediment discharge q_{ss}:

$$q_s = q_b + q_{ss} \tag{6.43}$$

This is the case of Einstein's and Van Rijn's formulae, both already mentioned in the previous chapter (Eq. 5.24) and (Eq. 5.64).

As already said, the relation between bed and suspended sediment discharges essentially depends on the relation between the friction velocity u_* and the fall velocity in still water w_s.

According to Van Rijn (1984b), in Eq. (6.43), the bed sediment discharge can be assessed with an expression which is quite analogous to (6.34) on p. 152, where the bed concentration c_a is calculated with the previous Eq. (6.36):

$$q_b = c_a \, \delta_b \, u_b = c_a \, a \, u_a \tag{6.44}$$

where u_a is the effective velocity of the bedload particles.

By using Eqs. (6.39) and (6.40), we obtain the ratio between the suspended load and the total sediment transport:
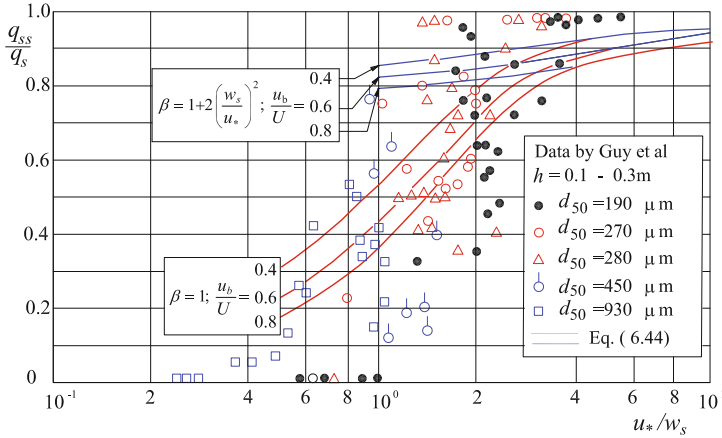
Fig. 6.7 Behavior of the ratio between suspended load q_{ss} and total load q_s in function of ratio u_*/w_s between shear velocity and particle fall velocity, according to Van Rijn (1984b)

$$\frac{q_{ss}}{q_s} = \frac{q_{ss}}{q_b + q_{ss}} = \frac{F\dfrac{U}{u_a}\dfrac{h}{a}}{1 + F\dfrac{U}{u_a}\dfrac{h}{a}} \tag{6.45}$$

According to Van Rijn (1984b), the ratio u_a/U varies from about 0.4 to 0.8. The former limit concerns the large, steep bed forms in the subcritical regime, while the latter is relevant to flat beds and supercritical regime (Fig. 6.6).

Figure 6.7, reused by Van Rijn (1984b), shows such a dependence, parameterized with respect to the ratio u_b/U between bed layer and average velocities. The figure compares the prediction of Eq. 6.45 against experimental data provided by Guy et al. (1966). The ratio u_b/U varies from 0.4 for beds with dunes to 0.8 for plane beds (*transcritical regime*).

6.5.1   Monomial Formulae

Einstein's bedload formula clearly shows how it may be approximated, within a certain mobility parameter range, with an adequate monomial formula of the type:

$$\Phi = \alpha_\Phi \theta^n \tag{6.46}$$

Among the numerous formulae of the type (6.46) suggested in the literature, it is worth remembering:

- Einstein and Brown (1950)

$$\Phi = \left(\sqrt{\frac{2}{3} + \frac{36\,\nu^2}{g\,\Delta d^3}} - \sqrt{\frac{36\,\nu^2}{g\,\Delta d^3}} \right) 40\,\theta^3 \qquad (6.47)$$

- Engelund and Hansen (1967)

$$\Phi = 0.084\,\theta^{2.5} \qquad (6.48)$$

This formula gives good results if applied in water streams with beds consisted of fine sand ($d > 0.190\,\mathrm{mm}$), by utilizing d_{50} as the characteristic material diameter.

As previously said, the parameter diversity in these formulae, and especially the difference between the values assumed by the exponent, is not surprising at all. The latter tends to assume very high values near the conditions of incipient motion ($n = 17.7$ according to Parker (1990)), while it tends to the exponent $n = 1.5$ of Meyer-Peter and Müller's formula when the mobility parameter is much higher than the critical value. Other formulae for sediment transport are given in Table 6.1.

Table 6.1 Some formulae of sediment transport frequently used in the literature

Authors	Formula	Range of validity
Ashida and Michiue (1971)	$\Phi = 17\,(\theta')^{1.5} \left(1 - \frac{\theta_c}{\theta}\right)\left(1 - \sqrt{\frac{\theta_c}{\theta}}\right)$	
Brown (1950)	$\dfrac{43.13\,\Phi}{1 + 43.13\,\Phi} = 1 - \dfrac{1}{\sqrt{\pi}} \displaystyle\int_{-0.143\,\Psi - 2}^{+0.143\,\Psi - 2} e^{-\xi^2}\,d\xi$	$\Psi = 1/\theta$; bedload
Einstein and Brown (1950)	$\Phi = 40\,\theta^3 \left(\sqrt{\dfrac{2}{3} + \dfrac{36\,\nu^2}{g\,\Delta d^3}} - \sqrt{\dfrac{36\,\nu^2}{g\,\Delta d^3}} \right)$	
Engelund and Hansen (1967)	$\Phi = 0.084\,\theta^{2.5}$	$d_{50} \geq 190\ ^-\mathrm{m}$
Graf and Suszka (1987)	$\Phi = 10.4\,\theta^{1.5} \left(1 - \dfrac{0.045}{\theta}\right)^{2.5}$ $\Phi = 10.4\,\theta^{2.5}$	for $\Phi \leq 10^{-2}$ for $\Phi > 10^{-2}$
Meyer-Peter and Müller (1948)	$\Phi = 8\,(\theta' - \theta_c)^{1.5}$	$i_f \leq 0.02$; prevailing bedload transport
Parker (1990)	$G = \xi_0^{14.2}$ $G = e^{\left(14.2(\xi_0 - 1) - 9.28(\xi_0 - 1)^2\right)}$ $G = 5474 \left(1 - \dfrac{0.853}{\xi_0}\right)^{4.5}$ with: $\Phi = G(\xi_o)\,0.00218\,\theta^{1.5}$ and $\xi_0 = \dfrac{\theta}{0.0386}$	for $\xi_0 < 1$ for $1 \leq \xi_0 \leq 1.59$ for $\xi_0 > 1.59$
Shields (1936)	$\Phi = 10\,(\theta - \theta_c)\theta^{1.5}\,\dfrac{\rho}{\rho_s}\,\dfrac{U}{u_*}$	
Smart and Jaeggi (1983)	$\Phi = 4 \left(\dfrac{d_{90}}{d_{30}}\right)^{0.2} i_f^{0.6}\,\theta^{0.5}(\theta - \theta_c)\left(\dfrac{u}{u_*}\right)$	$0.03 \leq i_f \leq 0.20$

References

K. Ashida, M. Michiue, Studies on bedload transportation for nonuniform sediment and river bed variation. Disaster Prev. Res Inst. Annu. **14** (1971)

R. Bagnold, *An Approach to the Sediment Transport Problem General Physics Geological Survey* (Prof. paper, 1966)

R.A. Bagnold, The flow of cohesionless grains in fluids. Trans. Royal Soc. Lond. ser. A: Math. Phy. Eng. Sci. **249**(964), 235–297 (1956)

C.B. Brown, Sediment transportation. Eng. Hydraul. **12** (1950)

H.A. Einstein. *The Bedload Function for Sediment Transportation in Open Channel Flows*, Vol. 1026 (US Department of Agriculture, 1950)

F. Engelund, J. Fredsøe, A sediment transport model for straight alluvial channels. Nord. Hydrol. **7**(5), 293–306 (1976)

F. Engelund, E. Hansen, A monograph on sediment transport in alluvial streams. Monogr. Den. Tech. Univ. Hydraul. Lab. **62** (1967)

W.H. Graf, L. Suszka, Sediment transport in steep channels. J. Hydrosci. Hydraul. Eng. 11–26 (1987)

H.P. Guy, D.B. Simons, E.V. Richardson, *Summary of Alluvial Channel Data from Flume Experiments* (Technical Report 462-I, 1956-61, 1966)

P. Jansen, L. Van Bendegom, J. Van den Berg, M. De Vries A. Zanen. *Principles of River Engineering: The Non-Tidal Alluvial River* (Pitman London, 1979)

E. Lane, A. Kalinske, Engineering calculations of suspended sediment. Trans. AGU **22**, 603–607 (1941)

E. Meyer-Peter, R. Müller, Formulas for bedload transport, in *Proceedings of the 2nd Meeting of the International Association for Hydraulic Structures Research IAHS*, Vol. 133 (1948), pp. 39–64

G. Parker, Surface-based bedload transport relation for gravel rivers. J. Hydraul. Res. **28**(4), 417–436 (1990)

H. Rouse, Modern conceptions of the mechanics of fluid turbulence. Trans. ASCE **102**, 463–543 (1937)

A. Shields, *Anwendung der Aehnlichkeitsmechanik und der Turbulenzforschung auf die Geschiebebewegung* (Technical report, Preussischen Versuchsanstalt für Wasserbau, 1936)

G.M. Smart, M. Jaeggi, Sediment transport on steep slopes. *Alternierende Kiesbänke, Mitteilung der Versuchsanstalt für Wasserbau, Hydrologie und Glaziologie*, (N 64, 1983)

L.C. Van Rijn, Sediment transport part I: bedload transport. J. Hydraul. Eng. **110**(10), 1431–1456 (1984a)

L.C. Van Rijn, Sediment transport, part II: suspended load transport. J. Hydraul. Eng. **110**(11), 1613–1641 (1984b)

V.A. Vanoni, Transportation of suspended sediment by water. Trans. Am. Soc. Civ. Eng. **111**(1), 67–102 (1946)

Chapter 7
Mathematical Models of Riverbed Evolution

7.1 Introduction

Mobile-bed mathematical models are powerful complex tools, suitable to analyze the condition of a river under some hydrological and geometrical assumptions and to simulate their spatial and temporal evolution. More generally, these models are suitable to predict the evolution of riverbeds and are also necessary to predict the evolution in space and time of the modifications induced by interventions of river engineering and river restoration.

Nowadays, mathematical models are tools indispensable for designing river works. Particularly, in a first step, it is convenient to use simplified solutions, while complete mathematical models become fundamental in the phase of efficiency verification of the designed works.

In general, the mathematical models of riverbed evolution consist of a system of differential equations in the time-space domain, initial and boundary conditions, a discretization scheme and a numerical scheme for solving discretized equations.

The category of river numerical models is very broad, mainly depending on the equations that they are intended to solve. In this chapter, we will make special reference to models integrated on the water depth or on the cross section, in which the longitudinal scale is predominant with respect to the transverse or normal scale, according to the shallow water hypothesis.

In short, we will treat only 1D models, which support the hypothesis of the hydrostatic distribution of pressures along the vertical direction. In these mobile-bed models, the bed elevation is a dependent variable of the problem. The analysis will be confined to river models, in which the average concentration of the sediments, C, is much less than unit. The features of the 2D depth-integrated models with the same characteristics can be easily obtained from the 1D models.

From Sects. 7.2 and 7.3 we will derive the equations of mass and momentum conservation of the liquid phase and the sediments, in a two-phase approach. However, since in the fluvial environment the depth-average sediment concentration is very

small, the momentum conservation equations for the liquid phase coincide with that for the total mixture (*isokinetic models*).

We will, then, clarify also the question of the closure relations, which represents another important issue of river models. The resulting system of equations will be analyzed with the method of characteristics (Sect. 7.4), focusing the issues related to the assignment of boundary conditions. We will then analyze some stationary solutions (Sect. 7.5), which involve widening and narrowing of the cross section.

In Sect. 7.6 we will describe some simplified solutions, namely the so-called *kinematic model* and *parabolic model*, which can be useful for the design phase of the first approximations of some river works.

In the next section we will illustrate two specific problems of river modeling which, however, are assuming greater space especially in the commercial codes: more precisely, the *adaptive models* (Sect. 7.7) - which hypothesize that local solid discharge (and/or concentration) is always equal to the equilibrium solid discharge (*transport capacity*) - and the *non-uniform size models* (Sect. 7.8) - which will be used to simulate the time and space evolution of the particle size distribution.

7.2   Mass Conservation Equations

The morphological evolution of an erodible bed channel can be conveniently described by adopting a two-phase approach, that is, treating separately the liquid and solid phases. The liquid phase generally consists of water, a Newtonian fluid governed by the Navier–Stokes equations, while the solid phase, composed of the sediment, can be treated as a *granular fluid*, the rheology of which is rather complex (Campbell 1990; Drew 1983) and will not be addressed in this chapter.

In this context, we just say that the (Eulerian) velocity of the granular phase $\overrightarrow{\mathbf{u}}_s$ is represented by the average of the velocities of the individual particles $(\overrightarrow{\mathbf{u}}_p)_k$ contained inside an *infinitesimal* control volume $dx_1\,dx_2\,dx_3$, namely (Fig. 7.1):

$$u_{si} = \frac{\sum_{k=1}^{n_p}(u_{pi})_k}{n_p} \qquad\qquad (i = 1, 3) \qquad\qquad (7.1)$$

where n_p is the number of particles inside the control volume.

The volume concentration c of granular phase is defined as the volume $\forall_s$ of all solid particles contained in the control volume, divided by the total volume:

$$c = \frac{n_p \forall_p}{dx_1\,dx_2\,dx_3} = \frac{\forall_s}{dx_1\,dx_2\,dx_3} \qquad\qquad (7.2)$$

where $\forall_p$ is the volume of the single particle.

These definitions are problematic when the volume of a particle is of the same order as the control volume. The problem is still unresolved, but for simplicity,

Fig. 7.1 Granular flow notation
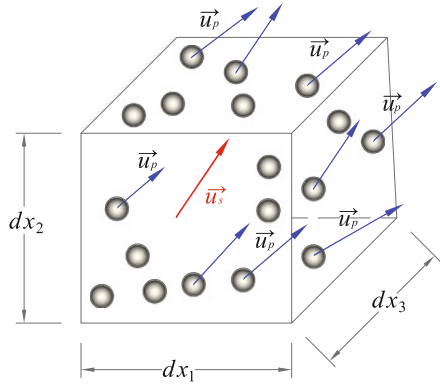
we adopt this approach, assuming that $c = func(t, \mathbf{x})$ and $(u_s)_i = func(t, \mathbf{x})$ are continuous functions of space and time within the flow field.

The conservation equation of the mass of each phase with respect to a finite control volume $\forall_c$ is:

$$0 = \frac{\partial}{\partial t} \int_{\forall_c} \rho_\beta \, c_\beta \, d\forall + \oint_{\Sigma_c} \rho_\beta \, c_\beta \, (\overrightarrow{\mathbf{u}}_\beta \cdot d\overrightarrow{\mathbf{A}}) \tag{7.3}$$

where β represents both the liquid and granular phases. ρ_β, c_β, and $\overrightarrow{\mathbf{u}}_\beta$ are the material density, the concentration, and the velocity of the generic phase, respectively. It is worth noting that if c is the volume concentration of the solid phase, $(1 - c)$ is the concentration of the liquid phase, as a consequence of the incompressibility of both materials (solid and liquid).

7.2.1 Equation of Conservation of Solid Mass

Let us consider a quasi-rectangular channel of width B (Fig. 7.2), in which the control volume is composed of two cross sections at an infinitesimal distance dx, the free surface and a suitable portion of the bed. We first apply the mass conservation equation to the solid phase, e.g., $\beta = s$ in Eq. (7.3), which becomes:

$$\frac{\partial}{\partial t} \left(C A + B C^* z_b \right) + \frac{\partial Q_s}{\partial x} = 0 \tag{7.4}$$

where A is the area of the cross section and $C = (\int_h c \, dz)/h$ the depth-averaged concentration (c is the local concentration and z is normal to the bed). C^* represents the concentration of the material on the bed (*random packing concentration*), complement to one of the bed material porosity p, that is, $(C^* = 1 - p)$. z_b is the bed elevation.
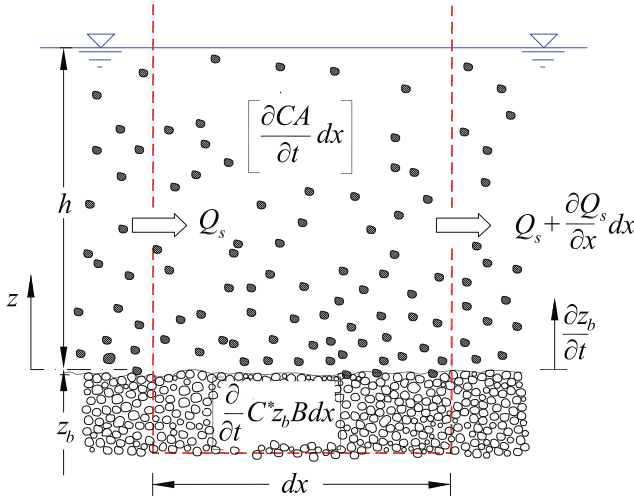
Fig. 7.2 Mass balance of the solid phase

$Q_s = \int_h c\, u_s\, dz$ is the discharge of the solid phase, where u_s is the longitudinal component of the local velocity of the solid phase.

Notice that, according to the shallow water assumption, in Eq. (7.4), we neglected the possible diffusive fluxes across the cross sections.

By inserting an adequate correction coefficient for the concentration, the sediment concentration can be expressed in function of the solid discharge:

$$C A = C B h = \frac{Q_s}{\alpha_{cu} U_s} \tag{7.5}$$

where $C = (\int_h c\, dz)$ and $U_s = (\int_h u_s\, dz)/h$ are the depth-average solid concentration and velocity, respectively. $\alpha_{cu} = (\int_h c\, u_s\, dz)/(C\ h\ U_s)$ is the correction coefficient for the concentration; $U_s = (\int_h u_s\, dz)/h$. Thus, Eq. (7.4) becomes:

$$\frac{\partial}{\partial t}\left(\frac{Q_s}{\alpha_{cu}U_s} + B\,C^*\,z_b\right) + \frac{\partial Q_s}{\partial x} = 0 \tag{7.6}$$

The first term inside the parenthesis refers to the variation of sediment mass inside the flow, and the second term denotes it inside the bed. The third term is the net sediment flux through the cross sections.

7.2.1.1 The Exner Equation

Often in Eq. (7.4), the term CA is considered negligible with respect to $B\,C^*z_b$, since $C = \mathcal{O}(10^{-3})$ and $C^* = \mathcal{O}(1)$. In addition, if we assume the bed width constant, according to the hypothesis of large quasi-rectangular cross sections, we reach the following simplified expression of the sediment mass balance, known as the Exner equation (Exner 1925):

$$\frac{\partial q_s}{\partial x} = -C^* \frac{\partial z_b}{\partial t} \tag{7.7}$$

where $q_s = Q_s/B$ is the solid discharge per unit width. The term C^*, denoting the complement to one of the material porosity, is often incorporated into the solid discharge, so it does not always appear in the Exner equation. From a physical point of view, the Exner equation can be easily interpreted, in that when $\partial q_s/\partial x > 0$ (*the solid discharge increases to the detriment of the bed sediment*), the bed is being eroded ($\partial z_b/\partial t < 0$).

When $\partial q_s/\partial x < 0$, the bed is in deposit ($\partial z_b/\partial t > 0$) (*the solid discharge decreases by increasing the volume of sediment deposited*).

The Exner equation makes it possible to understand how a bed perturbation moves downstream or upstream depending on the fact that the flow is, respectively, subcritical ($F_r <\sim 0.9$) or supercritical ($F_r >\sim 1.1$).

Should the flow be subcritical, the bed rise leads to a lowering of the free surface, even if rather limited, in phase opposition with the bed (Fig. 7.3a). On the upstream slope of the dune, the water depth tends to decrease in the flow direction ($\partial h/\partial x < 0$), and consequently, the velocity tends to increase; the solid discharge increases as well ($\partial q_s/\partial x > 0$). Thus, on the basis of the Exner Eq. (7.7), it follows that ($\partial z_b/\partial x < 0$), that is, the upstream slope of the dune is subject to erosion.

Just the reverse occurs on the downstream slope of the dune: the water depth h increases in the flow direction ($\partial h/\partial x > 0$), with consequent decrease in velocity and in solid discharge ($\partial q_s/\partial x < 0$). Therefore, there is a sediment deposition in the downstream slope of ($\partial z_b/\partial x > 0$). The result is that the dune shape migrates downward.

Just the reverse is observed in supercritical flows, as schematized in Fig. 7.3b.

In conditions of near-critical flows ($\sim 0.9 < F_r <\sim 1.1$), the observations made so far can fail by defect, in that they also require assessing any change in the hydrodynamic conditions induced by morphological variations.

7.2.2 Mass Conservation of the Liquid Phase

With the same procedure as described in Sect. 7.2.1, we obtain the equation of mass conservation of the liquid phase. It is sufficient to replace the concentrations of the
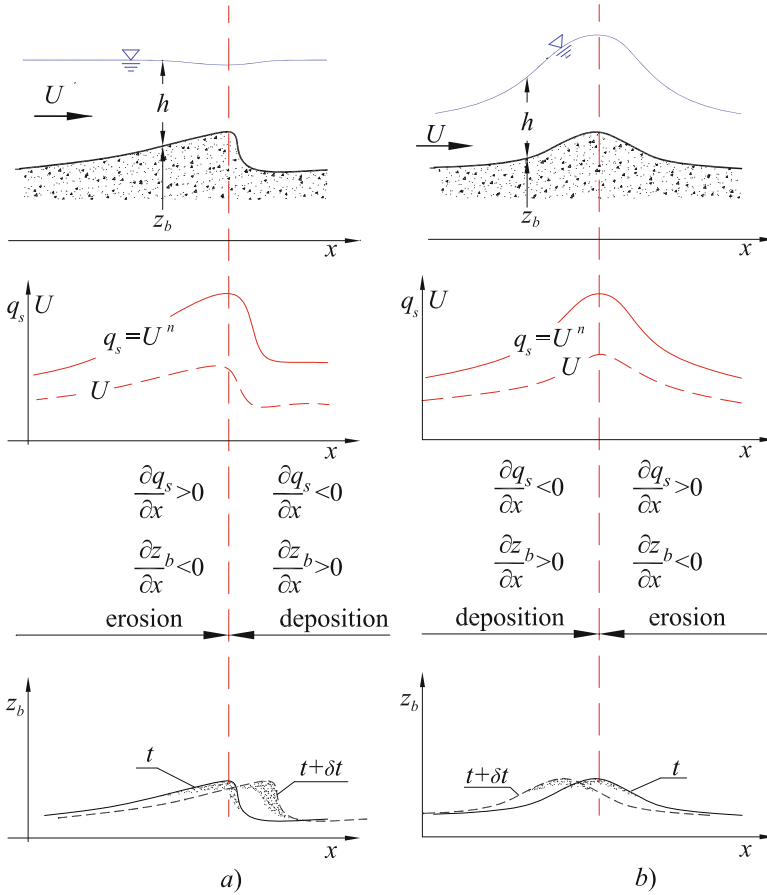
Fig. 7.3 Layout of the propagation of a bed perturbation **a** in a subcritical channel flow: $F_r <\sim 0.9$; **b** in a supercritical channel flow: $F_r >\sim 1.1$ with $n \simeq 3 \sim 5$

solid phase C and C^* with those of the liquid phase $(1-C)$ and $(1-C^*)$, respectively, and the solid discharge Q_s with the liquid discharge Q into Eq. (7.4):

$$\frac{\partial}{\partial t}\left((1-C)A + B(1-C^*)z_b\right) + \frac{\partial Q}{\partial x} = 0 \tag{7.8}$$

The physical meaning of Eq. (7.8) is analogous to that of Eq. (7.4). The first term (after the parenthesis) denotes the liquid volume variation inside the flow, and the second term the liquid volume variation inside the bed. The third term refers to the net volume flux through the two cross sections.

7.2.3   Total Mass Conservation

If we add term by term the mass conservation equations of the two phases (Eqs. 7.4 and 7.8), we obtain:

$$\frac{\partial}{\partial t}\,(A + Bz_b) + \frac{\partial}{\partial x}\,(Q_s + Q) = 0 \tag{7.9}$$

Since in fluvial environments the liquid discharge is generally much bigger than the solid one, that is, $Q >> Q_s$, Eq. (7.9) becomes:

$$\frac{\partial}{\partial t}\,(A + Bz_b) + \frac{\partial Q}{\partial x} = 0 \tag{7.10}$$

7.3   Momentum Conservation Equations

The application of the Reynolds theorem to the momentum conservation of the generic phase β with respect to a finite control volume $\forall_c$ gives:

$$\overrightarrow{F_{e\beta}} = \frac{\partial}{\partial t}\int_{\forall_c}\rho_\beta\,c_\beta\,\overrightarrow{u}_\beta\,d\forall + \oint_{\Sigma_c}\rho_\beta\,c_\beta\,\overrightarrow{u}_\beta(\overrightarrow{u}_\beta\cdot d\overrightarrow{A}) \tag{7.11}$$

where β may be either the liquid or the solid phase.

The left term is the resultant of the external forces acting on the phase β, such as **weight force** and **surface forces** acting on the control surface. This term also includes the **interphase forces** exerted on the phase β by the other phase.

The first term on the right represents the **variation in time of momentum** of the phase β within the control volume, and the second term on the right is the **net flux of momentum** of the phase β through the control surface Σ_c.

We apply Eq. (7.11) to the same control volume as above, in the longitudinal flow direction.

Note that in this case, we placed the lower limit of the control volume on the bed surface, since there is no momentum variation within the bed and since we have assumed that the contribution of the masses flowing through the bed surface to the momentum balance in the longitudinal direction is null, given that the longitudinal velocity components of both phases are zero.

7.3.1   Momentum Conservation Equation of the Liquid Phase

With reference to Fig. 7.4, the **external forces** in the longitudinal direction are:

- the *longitudinal component* of the *resultant of hydrostatic pressure S_x* on the cross sections of the flow;
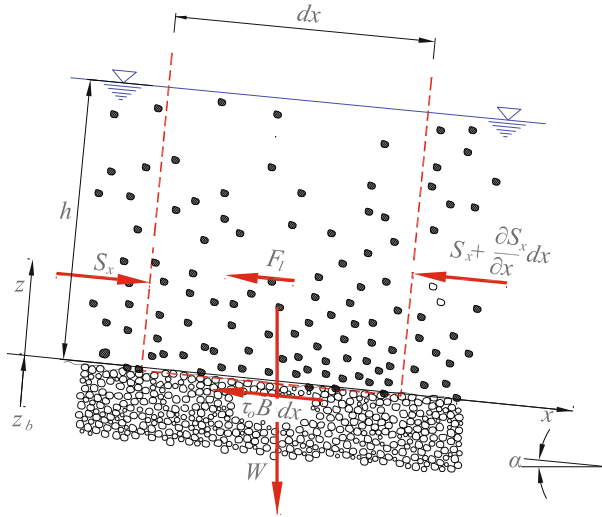
Fig. 7.4 External forces acting on the liquid phase. S_x is the longitudinal component of hydrostatic pressure forces, W the weight force, F_l the interphase force, $\tau_o\, B\, dx$ the shear stress forces on the bed

- the *longitudinal component of the weight* of the liquid phase, e.g.,

$$W_x = -\rho(1 - C)\, g\, B\, h \frac{\partial z_b}{\partial x}\, dx \qquad ; \tag{7.12}$$

- the resultant of the *shear stresses on the bed*: $\tau_o\, B\, dx$;
- the component of the resultant of *interphase forces*. In this case, it is the resultant of the forces exerted on the liquid phase by the solid phase F_l in the longitudinal direction. Typically, this force can be decomposed in a drag, due to the difference between the velocities of the two phases, and in a buoyancy force, independent of the velocity difference between the two phases.

The **time variation of momentum** of the liquid phase within the control volume is:

$$\frac{\partial}{\partial t}\,(\rho(1 - C\alpha_{cu})U B h)\, dx \tag{7.13}$$

where $\alpha_{cu} = (\int_h c\, u_s\, dz)/(C\, h\, U_s)$ is the correction coefficient for the concentration.

The **net flux of momentum** of the liquid phase through the control surface is:

$$\frac{\partial}{\partial x}\,\left(\rho(\beta_2 - \beta_{c2}\, C\,)\, U^2 B\, h\right)\, dx \tag{7.14}$$

where $\beta_2 = (\int_h u^2 dz)/(h\,U^2)$ and $\beta_{c2} = (\int_h c\,u^2 dz)/(C\,h\,U^2)$ are two *correction coefficients* for momentum.

We remind that, since the longitudinal velocity on the bed is assumed to be zero (Newtonian fluid), there is no longitudinal momentum entrainment from the bed surface. Finally, we obtain:

$$\frac{\partial}{\partial t}\rho(1 - \alpha_{uc}C)UA + \frac{\partial}{\partial x}\left(\rho\beta_2(1 - \frac{\beta_{c2}}{\beta_2}\,C\,)\,U^2 A\right)$$
$$+\frac{\partial S_x}{\partial x} + \rho(1 - C)\,g\,A\,\frac{\partial z_b}{\partial x} = -\tau_o\,B + F_l \qquad (7.15)$$

where the last term on the right represents the depth-integrated forces exerted by the solid phase on the liquid phase.

7.3.2 Momentum Conservation of the Solid Phase

The momentum equation of the solid phase is formally similar to the previous Eq. (7.15):

$$\frac{\partial}{\partial t}\rho_s\alpha_{uc}\,CU_sA + \frac{\partial}{\partial x}\left(\rho\beta_{c2}\,CU_s^2A\right) + \frac{\partial S_x}{\partial x} + \rho_s\,CgA\frac{\partial z_b}{\partial x}$$
$$= -\tau_{os}\,B - F_l \qquad (7.16)$$

The meaning of the different terms is similar to the corresponding terms of liquid momentum equation (7.15). In particular, S_{sx} represents the longitudinal gradient of the solid pressure due to the interparticle interaction, which is very infrequent with a small concentration as in this case. $-F_l$ represents the forces per unit length exerted by the water on the particles (e.g., drag and buoyancy forces) in the longitudinal direction, which on the basis of reciprocity principles is the contrary of the forces exerted by the solid phase on water F_l.

7.3.3 Momentum Conservation of the Mixture

By adding Eqs. (7.15) and (7.16) term by term, we obtain the total momentum equation. Since all the terms of the Eq. (7.16) are proportional to the average concentration C that in the fluvial environment is always much less than one, in the resultant equation all these terms can be neglected, and the interphase forces cancel each other. So that the total momentum conservation equation results as:

$$\frac{\partial UA}{\partial t} + \frac{\partial}{\partial x} \left(\beta_2 A U^2 \right) + \frac{\partial S_x/\rho}{\partial x} + g A \frac{\partial z_b}{\partial x} = -\frac{\tau_o}{\rho} B \qquad (7.17)$$

According to the shallow water hypothesis (hydrostatic pressure distribution) and since we assumed that the bed slope is sufficiently small to consider the pressure distribution hydrostatic indifferently along the normal or vertical direction, we have:

$$\frac{\partial S_x}{\partial x} = \frac{\partial}{\partial x} \left(\frac{1}{2} \rho g B h^2 \right) = \rho g B h \frac{\partial h}{\partial x} \qquad (7.18)$$

and again according to the shallow water hypotheses (i.e., the bed shear stress in unsteady and non-uniform flow is the same as in steady uniform condition under the same hydrodynamic condition):

$$\frac{\tau_o}{\rho} = g R_h i_E \qquad (7.19)$$

where R_h is the hydraulic radius of the cross section, and i_E is the slope of the energy line, that is, the energy dissipated per unit weight and length.

Finally, we obtain:

$$\frac{\partial UA}{\partial t} + \frac{\partial}{\partial x} \left(\beta_2 A U^2 \right) + Bhg \frac{\partial}{\partial x} (h + z_b) = -g A i_E \qquad (7.20)$$

7.4   Water-Sediment Coupling

Combining Eqs. (7.4), (7.10), and (7.17), we obtain the system of equations governing the flow and the bed evolution:

$$\begin{cases} \dfrac{\partial A}{\partial t} + \dfrac{\partial UA}{\partial x} + B \dfrac{\partial z_b}{\partial t} = 0 \\[2mm] \dfrac{\partial UA}{\partial t} + \dfrac{\partial}{\partial x} \left(\beta_2 U^2 A \right) + g A \dfrac{\partial}{\partial x} (h + z_b) = -g A i_E \\[2mm] \dfrac{\partial CA}{\partial t} + \dfrac{\partial Q_s}{\partial x} + B C^* \dfrac{\partial z_b}{\partial t} = 0 \end{cases} \qquad (7.21)$$

The first two equations of the system coincide with the Saint-Venant equations of the fixed-bed case, with the only exception of the new term $B(\partial z_b/\partial t)$ in the first equation of the system.

By considering that the area A can be expressed in function of the water depth, the system (7.21) contains the following dependent variables:

$$Q_s ; \quad C ; \quad U ; \quad h ; \quad z_b ; \quad i_E.$$

Since the system (7.21) is composed of three equations only, its solution requires three other equations (*closure relations*) in addition to the initial and boundary conditions. The closure equations are usually based on local equilibrium hypotheses:

1. the slope of energy line is calculated with a uniform flow formula, that is, as if the flow were locally uniform under the same hydrodynamic conditions: same velocity and same depth. For instance, by adopting the Chézy formula, it is:

$$i_E = \frac{U^2}{\chi^2 R_h} = \frac{Q^2}{A^2 \chi^2 R_h}$$

2. the solid discharge is evaluated as if the sediment transport were locally in equilibrium, that is, as if locally the flow were steady and uniform, therefore by means of an appropriate sediment transport formula:

$$Q_s = f_s(Q, h, B, \chi, d, \dots)$$

At this stage, it is worth making a further simplifying hypothesis by assuming that the sediment size distribution is uniform or that it may be represented with a proper equivalent diameter d. We will show later how such hypothesis may be removed;

3. the same approximation (local equilibrium) can be made for the sediment concentration C:

$$C = f_c(Q, h, B, \chi, d, \dots)$$

Moreover, it is worth expressing the concentration in function of the solid discharge (Eq. 7.5), although, as already stated, the term referring to the break concentration—the first term of the third equation of the system—can be neglected, as will be generally assumed below without loss of generality.

Should the variables U and h be continuous, that is, without hydraulic jumps in the examined stretch of the channel, we obtain a hyperbolic system of partial differential equations, which was studied with the method of characteristics by Korteweg and de Vries (1965).

In the further hypothesis of wide rectangular channel, the equations of the system (7.21) can be rewritten per unit width. Moreover, we can observe that the solid discharge per unit width $q_s = Q_s/B$ essentially depends on two dependent variables of the system: velocity and water depth, i.e., $q_s = func(U, h)$. Thus, we have:

$$\frac{\partial q_s}{\partial x} = \frac{\partial q_s}{\partial U}\frac{\partial U}{\partial x} + \frac{\partial q_s}{\partial h}\frac{\partial h}{\partial x}$$

In addition, for simplicity, we will set $\beta_2 = 1$ in the second equation of the system. We thus obtain the following system of equations, here given in the matrix form:

$$\frac{\partial \mathbf{U}}{\partial \mathbf{t}} + \mathbf{A_U}\frac{\partial \mathbf{U}}{\partial \mathbf{x}} + \mathbf{S_U} = 0 \tag{7.22}$$

where:

$$
\mathbf{U} = \begin{bmatrix} h \\ U \\ z_b \end{bmatrix} \qquad
\mathbf{A_U} = \begin{bmatrix} U & h & 0 \\ g & U & g \\ \dfrac{1}{C^*}\dfrac{\partial q_s}{\partial h} & \dfrac{1}{C^*}\dfrac{\partial q_s}{\partial U} & 0 \end{bmatrix} \qquad
\mathbf{S_U} = \begin{bmatrix} 0 \\ g\,i_E \\ 0 \end{bmatrix} \quad (7.23)
$$

are, respectively, the vector of the dependent variables, the matrix of coefficients, and the vector of known terms. The eigenvalues $(\lambda_1, \lambda_2, \lambda_3)$ of the matrix $\mathbf{A_U}$ are obtained by solving the following equation:

$$
\det(\mathbf{A_U} - \lambda \mathbf{I}) = 0 \tag{7.24}
$$

where $\mathbf{I}$ is the *identity matrix* (or *unit matrix* or *elementary matrix*). This is a square matrix, in which all the elements of the principal diagonal are one and all non-diagonal terms are zero. Equation (7.24) leads to the following *characteristic polynomial equation*:

$$
p(\lambda) = -\lambda^3 + 2U\lambda^2 + \left(gh - U^2 + gh\frac{1}{C^*h}\frac{\partial q_s}{\partial U} \right)\lambda
$$
$$
- gh\,U\left(\frac{1}{C^*h}\frac{\partial q_s}{\partial U} - \frac{1}{C^*U}\frac{\partial q_s}{\partial h} \right) = 0 \tag{7.25}
$$

By dividing Eq. (7.25) by $(gh)^{1.5}$, we turn it into dimensionless:

$$
\widetilde{\lambda}^3 - 2\widetilde{\lambda}^2 F_r + \widetilde{\lambda}\left(F_r^2 - 1 - A_\lambda \right) + F_r(A_\lambda - B_\lambda) = 0 \tag{7.26}
$$

where:

$$
\widetilde{\lambda} = \lambda/\sqrt{gh} \qquad\qquad F_r = U/\sqrt{gh}
$$
$$
A_\lambda = \frac{1}{C^*h}\frac{\partial q_s}{\partial U} = \frac{1}{C^*}\frac{U}{q}\frac{\partial q_s}{\partial U} \qquad B_\lambda = \frac{1}{C^*U}\frac{\partial q_s}{\partial h} = \frac{1}{C^*}\frac{h}{q}\frac{\partial q_s}{\partial h}
$$

with $q = U\,h$.

The eigenvalues λ_i also represent the directions of the characteristic lines. The characteristic lines are the lines of equation $\lambda_i = dx/dt$ with $(i = 1, 3)$, along which discontinuities (the infinitesimal perturbations of the system variables) can propagate.

Figure 7.5 shows the dimensionless characteristics of the system in function of the Froude number in the hypothesis, suggested for analytical simplicity, that the solid discharge q_s can be expressed as a power of the water depth and of the velocity: $(q_s = a_s\,U^m\,h^n)$. The curves are parameterized by the ratio q_s/q, which represents the solid *transport concentration*. We can observe that when the transport concentration decreases, the characteristic curves of the mobile-bed system tend to fail in those of the fixed-bed system $(\lambda_{1,2} = U \pm \sqrt{gh})$.
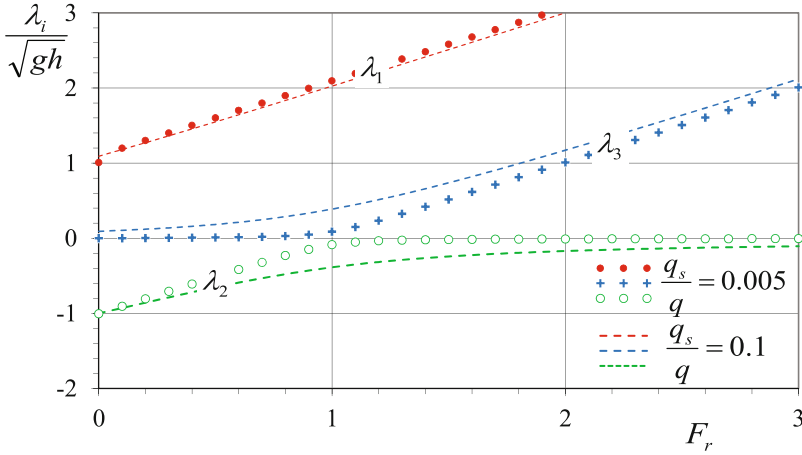
Fig. 7.5 Dimensionless characteristics of system (7.22) in function of the Froude number, for different parameter values q_s/q, assuming for the sediment transport the following power formula $q_s/q = a_s U^2 h^{-1}$

Here, we propose an explicit form of the solution of Eq. (7.25) which approximates very well the exact solution and which, with respect to the de Vries solution, is also suitable for the trans-critical condition ($F_r = 1$) and for relatively elevated transport concentration:

$$\tilde{\lambda}_1 = \frac{1}{2}\left(F_r + 1 + \sqrt{(F_r + 1)^2 + 2(A_\lambda + F_r B_\lambda)}\ \right)$$

$$\tilde{\lambda}_2 = \frac{1}{2}\left(F_r - 1 + \sqrt{(F_r - 1)^2 - 2(A_\lambda - F_r B_\lambda)}\ \right) \qquad (7.27)$$

$$\tilde{\lambda}_3 = \frac{1}{2}\left(F_r - 1 - \sqrt{(F_r - 1)^2 + \frac{4F_r}{F_r + 1}(A_\lambda - B_\lambda)}\ \right)$$

where $\tilde{\lambda}_i = \lambda_i/\sqrt{gh}$ ($i = 1, 2, 3$) are the characteristics written in dimensionless form.

Indeed, when the Froude number is sufficiently different from 1 and the ratio q_s/q (transport concentration) and consequently the depth-averaged concentration C are much lower than 1, the characteristics can be approximated with the following expressions, as suggested by de Vries (1965):

$$
\begin{array}{cc}
F_r < 1 & F_r > 1 \\
\lambda_1 = U + \sqrt{g\,h} + O(C) & \lambda_1 = U + \sqrt{g\,h} + O(C) \\[2mm]
\lambda_2 = U - \sqrt{g\,h} + O(C) & \lambda_2 = \dfrac{U}{1 - F_r^2}\,(A_\lambda - B_\lambda) \\[2mm]
\lambda_3 = \dfrac{U}{1 - F_r^2}\,(A_\lambda - B_\lambda) & \lambda_3 = U - \sqrt{g\,h} + O(C)
\end{array}
\tag{7.28}
$$

This solution fails at $F_r = 1$, where it yields ($\lambda_2 \to 0$ and $\lambda_3 \to \infty$) and ($\lambda_2 \to \infty$ and $\lambda_3 \to 0$), respectively. If the solid concentration is not very high, we can assume:

$$
\lambda_3 \ll \lambda_1, \lambda_2 \ \text{ for } \ F_r <\sim 0.85
$$
$$
\lambda_2 \ll \lambda_1, \lambda_3 \ \text{ for } \ F_r >\sim 1.15
$$

Such expressions confirm that the small bed perturbations migrate down- or upstream depending on the flow regime (subcritical or supercritical, respectively), as seen in the previous sections.

7.4.1 System in Normal Form

As said in Sect. 7.2.1.1, by neglecting the storage term ($\partial(Ch)/\partial t$) in the equation of sediment mass conservation and the bed variation term ($\partial z_b/\partial t$) in the total mass conservation equation, the system (7.22) takes on a particularly simple form, as the matrix of the terms of temporal variation is unitary (main diagonal terms are one and off-diagonal terms zero), and consequently, the system can be rewritten in function of the variables $\mathbf{U}$, in the following form:

$$
\mathbf{T}\left(\frac{\partial \mathbf{U}}{\partial t} + \Lambda\,\frac{\partial \mathbf{U}}{\partial x} \right) + \mathbf{T}\,\mathbf{S_U} = 0
\tag{7.29}
$$

where Λ is a diagonal matrix whose elements are the eigenvalues of the original system:

$$
\Lambda = \begin{bmatrix} \lambda_1 & 0 & 0 \\ 0 & \lambda_2 & 0 \\ 0 & 0 & \lambda_3 \end{bmatrix}
\tag{7.30}
$$

The system (7.29) is said to be written in *canonical form*. The new matrix $\mathbf{T}$ has been shown (Toro 2013) to be the matrix of the right eigenvectors, deriving from the original matrix $\mathbf{A_U}$, by means of the following transformation:

$$
\mathbf{T}\,(\mathbf{A_U} - \Lambda \mathbf{I}) = 0
\tag{7.31}
$$

where **I** is the *identity matrix.* In the observed case, after a series of steps, we have:

$$\mathbf{T} = \begin{bmatrix} \lambda_1 + UB_\lambda \; \lambda_1 \dfrac{\lambda_1 - U}{g} \; \lambda_1 - U \\[2ex] \lambda_2 + UB_\lambda \; \lambda_2 \dfrac{\lambda_2 - U}{g} \; \lambda_2 - U \\[2ex] \lambda_3 + UB_\lambda \; \lambda_3 \dfrac{\lambda_3 - U}{g} \; \lambda_3 - U \end{bmatrix} \tag{7.32}$$

Thus, the system becomes:

$$(\lambda_k + UB_\lambda) \frac{D}{D_k t} h + \lambda_k \frac{\lambda_k - U}{g} \frac{D}{D_k t} U + (\lambda_k - U) \frac{D}{D_k t} z_b = b'_k$$

with :

$$\frac{D}{D_k t} = \frac{\partial}{\partial t} + \lambda_k \frac{\partial}{\partial x} \qquad\qquad k = 1, 2, 3 \tag{7.33}$$

Quite interesting is the form assumed by the system (7.33) when the eigenvalues are approximated according to de Vries's scheme (7.28):

$$F_r < 0.8 \begin{cases} \lambda_1 \simeq U + \sqrt{g\,h} \\[1ex] \lambda_2 \simeq U - \sqrt{g\,h} \\[1ex] \lambda_3 \simeq \dfrac{U}{1 - F_r^2} (A_\lambda - B_\lambda) \end{cases} \qquad F_r > 1.2 \begin{cases} \lambda_1 \simeq U + \sqrt{g\,h} \\[1ex] \lambda_2 \simeq \dfrac{U}{1 - F_r^2} (A_\lambda - B_\lambda) \\[1ex] \lambda_3 \simeq U - \sqrt{g\,h} \end{cases} \tag{7.34}$$

Consider the first case on mild streams ($F_r < 0.8$) (Fig. 7.6).

Along the characteristic λ_1, of equation ($\dfrac{dx}{dt} \simeq U + \sqrt{g\,h}$), we have:

$$\left((U + \sqrt{g\,h}) + UB_\lambda \right) \left(\frac{\partial h}{\partial t} + (U + \sqrt{g\,h}) \frac{\partial h}{\partial x} \right)$$

$$+ (U + \sqrt{g\,h}) \frac{\sqrt{g\,h}}{g} \left(\frac{\partial U}{\partial t} + (U + \sqrt{g\,h}) \frac{\partial U}{\partial x} \right)$$

$$+ \left(\sqrt{g\,h} \right) \left(\frac{\partial z_b}{\partial t} + (U + \sqrt{g\,h}) \frac{\partial z_b}{\partial x} \right) = b'_1 \tag{7.35}$$

Along the characteristic λ_2, of equation ($\dfrac{dx}{dt} \simeq U - \sqrt{g\,h}$), we have:

$$\left((U - \sqrt{g\,h}) + UB_\lambda \right) \left(\frac{\partial h}{\partial t} + (U - \sqrt{g\,h}) \frac{\partial h}{\partial x} \right)$$

$$+ (U - \sqrt{g\,h}) \frac{-\sqrt{g\,h}}{g} \left(\frac{\partial U}{\partial t} + (U - \sqrt{g\,h}) \frac{\partial U}{\partial x} \right)$$

$$-\left(\sqrt{g\,h}\right)\left(\frac{\partial z_b}{\partial t} + (U - \sqrt{g\,h})\frac{\partial z_b}{\partial x}\right) = b_2' \qquad (7.36)$$

Along the characteristic λ_3, of equation $\left(\dfrac{dx}{dt} \simeq \dfrac{U}{1 - F_r^2}\,(A_\lambda - B_\lambda)\right)$, we have:

$$\left(\frac{U\,(A_\lambda - B_\lambda)}{1 - F_r^2}\right)\left(\frac{\partial h}{\partial t} + \left(\frac{U\,(A_\lambda - B_\lambda)}{1 - F_r^2}\right)\frac{\partial h}{\partial x}\right)$$
$$+\frac{U\,(A_\lambda - B_\lambda)}{g(1 - F_r^2)}\left(\frac{U\,(A_\lambda - B_\lambda)}{1 - F_r^2} - U\right)\left(\frac{\partial U}{\partial t} + \frac{U\,(A_\lambda - B_\lambda)}{1 - F_r^2}\,\frac{\partial U}{\partial x}\right)$$
$$+\left(\frac{U\,(A_\lambda - B_\lambda)}{1 - F_r^2} - U\right)\left(\frac{\partial z_b}{\partial t} + \left(\frac{U\,(A_\lambda - B_\lambda)}{1 - F_r^2}\right)\frac{\partial z_b}{\partial x}\right) = b_3' \quad (7.37)$$

If in Eqs. (7.35), (7.36), and (7.37) we neglect the terms of order of concentration $C = \mathcal{O}(10^{-3})$ with respect to those of higher order, as well as the term $(\partial z_b/\partial t)$ with respect to $h\,(\partial U/\partial x)$ following the Exner Eq. (7.7), the system (7.35–7.37) becomes:

$$\text{along } \lambda_1 \quad \left(\frac{\partial}{\partial t} + (U + \sqrt{g\,h})\frac{\partial}{\partial x}\right)\left(U + 2\sqrt{g\,h}\right) = i_E - \frac{\partial z_b}{\partial x}$$
$$\text{along } \lambda_2 \quad \left(\frac{\partial}{\partial t} + (U - \sqrt{g\,h})\frac{\partial}{\partial x}\right)\left(U - 2\sqrt{g\,h}\right) = i_E - \frac{\partial z_b}{\partial x}$$
$$\text{along } \lambda_3 \quad \frac{\partial z_b}{\partial t} + \frac{U}{1 - F_r^2}(A_\lambda - B_\lambda)\frac{\partial z_b}{\partial x} = 0 \qquad (7.38)$$

In this uncoupled model, the first two characteristic lines $\lambda_{1,2} \simeq U \pm \sqrt{g\,h}$ coincide with those in the fixed-bed case, thus driving the perturbations of the hydrodynamic variables dU and dh. The corresponding bed perturbation associated with them is of a lower order.

Vice versa, the third characteristic $\lambda_3 \simeq U/(1 - F_r^2)(A_\lambda - B_\lambda)$ seems to drive the bed perturbation dz_b, while the free surface variation dh associated with it results to be lower. The same behavior is maintained by supercritical flows with $F_r > 1.2$ (Fig. 7.7).

7.4.2 Boundary Conditions

In order to choose the right boundary conditions, the problem should be well posed at boundaries. If the problem is properly set, the boundary conditions can be determined by the characteristics entering the calculation domain.

By solving the characteristic polynomial Eq. (7.25) (see also Fig. 7.5), two of the three characteristics appear to be always positive and one negative: two entering from
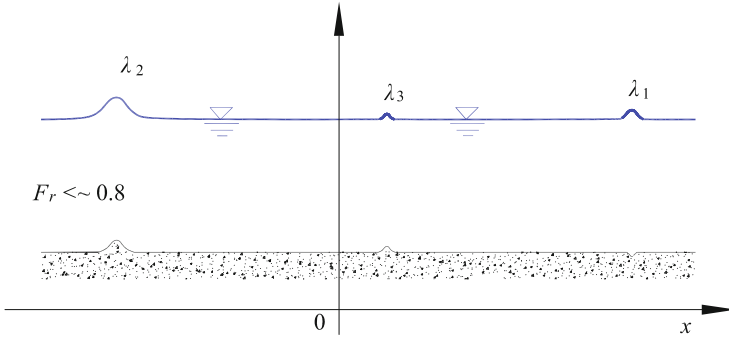
Fig. 7.6 Layout of the three perturbation waves and their respective lengths for relatively slow streams, $F_r <\sim 0.8$, according to Eqs. (7.35), (7.36), and (7.37) (Rosatti et al. 2004)
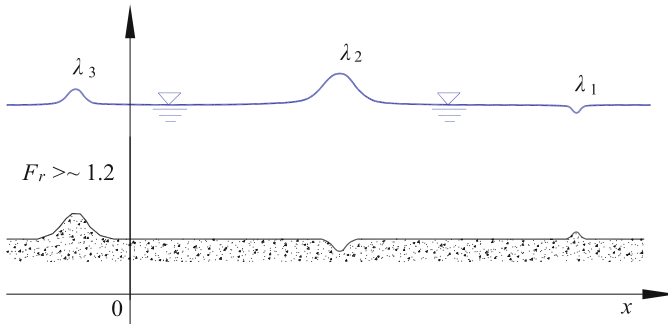
Fig. 7.7 Layout of the three perturbation waves and their respective lengths for relatively fast streams, $F_r >\sim 1.2$, according to Eqs. (7.35), (7.36), and (7.37) (Rosatti et al. 2004)

upstream cross section, one entering from downstream cross section. Therefore, two conditions are then set upstream, one downstream (Fig. 7.8).

In principle, these conditions can be given on any dependent variable (U, h, z_b) or on any of their combinations. However, such a system considers some conditions as more appropriate than others (Sieben 1997). Intuitively, this conclusion can be drawn from the inferences about the simplified compatibility Eqs. (7.38). The most appropriate conditions are summarized in the following table proposed by Sieben (1997).

The table shows that the downstream condition is suggested on the water depth h or on the velocity U in *subcritical* or *trans-critical regime*, and on the bed elevation z_b in *supercritical conditions*. Regarding upstream conditions with low Froude numbers, the conditions are better on the velocity and on bed elevation, while the velocity and water depth should be given in *supercritical* or *trans-critical* conditions.

Very often, however, the variable combinations are preferred: for instance, the free surface elevation $z_b + h$, or the liquid discharge $q = U/h$, or the solid discharge $q_s = func(U, h)$.

Assigning the free surface elevation downstream gives good results in both sub-critical and supercritical regimes, in that substantially the water depth is imposed in
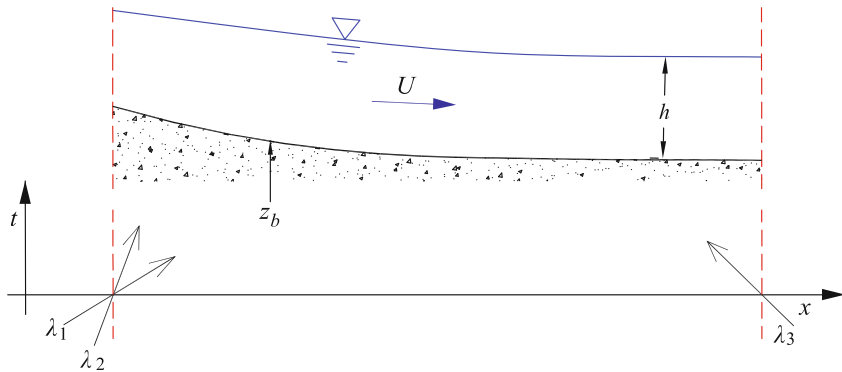
Fig. 7.8 Layout of the characteristics entering upstream and downstream

Upstream conditions	Downstream conditions		
	h	U	z_b
	$F_r < 1.2$	$F_r < 1.2$	$F_r > 1.2$
U, z_b	$F_r < 0.8$		
$F_r < 0.8$			
h, z_b			
h, U		$0.8 < F_r < 1.2$	$F_r > 1.2$
$F_r > 0.8$			

the former case, while this imposition especially influences the bed elevation in the latter. Similarly, the assignment of the liquid and solid discharges upstream allows the velocity U and the bed elevation z_b to be imposed in subcritical flows, and it is the same as imposing h and U in trans-critical and supercritical regimes.

7.5 Stationary Solutions: Section Enlargements and Contractions

The analysis of the system (7.21) shows that the asymptotic stationary solution in a prismatic channel coincides with the uniform flow profile. In stationary condition, in fact, all the time derivatives of the system (7.21) vanish, so the two mass conservation equations reduce to:

$$\frac{\partial UA}{\partial x} = 0 \tag{7.39}$$

$$\frac{\partial Q_s}{\partial x} = 0 \tag{7.40}$$

For solid discharge, we may assume, in all generality, the following relationship, represented by a two-sided relation between the dimensionless sediment transport rate $\Phi = Q_s/(Bd\sqrt{g\,\Delta\,d})$ and the mobility parameter $\theta = \tau_o/(\rho g \Delta\,d)$:

$$Q_s = Bd\sqrt{g\,\Delta\,d}\,F_\theta \tag{7.41}$$

where $F_\theta = func\,(\tau_o/(\rho g \Delta\,d))$ is a general function representing any type of bed-load formula, so that Eqs. (7.39) and (7.40) become:

$$U\,h\frac{\partial B}{\partial x} + B\frac{\partial Uh}{\partial x} = 0 \tag{7.42}$$

$$\frac{Q_s}{B}\frac{\partial B}{\partial x} + Bd\sqrt{g\,\Delta\,d}\frac{\partial F_\theta}{\partial \theta}\frac{\partial \theta}{\partial x} = 0 \tag{7.43}$$

If we assume a quasi-rectangular prismatic channel ($B = const$), the above equations become, respectively:

$$U\frac{\partial h}{\partial x} + h\frac{\partial U}{\partial x} = 0 \tag{7.44}$$

$$\frac{\partial F_\theta}{\partial \theta}\frac{\partial \theta}{\partial x} = 0 \tag{7.45}$$

With reference to a generic uniform flow formula, like the Gauckler-Strickler one (e.g., Eqs. (1.9) and (1.10), at page 14), where the bed roughness is represented by a characteristic grain size d and the friction coefficient is inversely proportional to $d^{1/6}$, we have:

$$U = K_f\left(\frac{h}{d}\right)^{1/6}\sqrt{g\,R_h\,i_E} = K_f\left(\frac{h}{d}\right)^{1/6}\left(\frac{\tau_o}{\rho}\right)^{1/2} \tag{7.46}$$

By inserting into the definition of the mobility parameter θ the above equation, we have:

$$\theta = \frac{1}{K_f^2}\frac{U^2}{g\,\Delta\,d}\left(\frac{d}{h}\right)^{1/3} \tag{7.47}$$

Equation (7.47) can be generalized as:

$$\theta = \frac{1}{K_f^2}\frac{U^2}{g\,\Delta\,d}\left(\frac{d}{h}\right)^{1/m} \tag{7.48}$$

with $m > 1$ (see Table 1.6 at page 13). By differentiating Eq. (7.48) with respect to U and h, we obtain:

$$\frac{\partial \theta}{\partial U} = 2\frac{\theta}{U}\quad\text{and}\quad\frac{\partial \theta}{\partial h} = -\frac{1}{m}\frac{\theta}{h} \tag{7.49}$$

So that we obtain:

$$\frac{\partial\theta}{\partial x} = \frac{\partial\theta}{\partial U}\frac{\partial U}{\partial x} + \frac{\partial\theta}{\partial h}\frac{\partial h}{\partial x} = 2\frac{\theta}{U}\frac{\partial U}{\partial x} - \frac{1}{m}\frac{\theta}{h}\frac{\partial h}{\partial x} \tag{7.50}$$

and, because of (7.44), we may conclude that:

$$\frac{\partial\theta}{\partial x} = \frac{\theta}{U}\frac{\partial U}{\partial x}\left(1 + \frac{1}{2\,m}\right) \tag{7.51}$$

which, inserted into Eq. (7.45), gives:

$$\frac{\partial F_\theta}{\partial\theta}\frac{\theta}{U}\frac{\partial U}{\partial x}\left(1 + \frac{1}{2\,m}\right) = 0 \tag{7.52}$$

and

$$\frac{\partial Q_s/B}{\partial x} = 2d\sqrt{g\,\Delta\,d}\,\theta\frac{\partial F_\theta}{\partial\theta}\frac{\theta}{U}\left(1 + \frac{1}{2\,m}\right)\frac{\partial U}{\partial x} = 0 \tag{7.53}$$

Since $\partial F_\theta/\partial\theta \neq 0$, otherwise there is no sediment transport, the only possibility is:

$$\frac{\partial U}{\partial x} = 0 \tag{7.54}$$

that is, the only possible solution of steady flow in a prismatic mobile-bed channel is the uniform flow.

This conclusion is valid for any sediment transport formula and for any uniform flow formula, in which the flow rate is inversely proportional to the flow depth. Since a different situation in case of natural grain roughness is not realistic, the conclusion can be taken to be valid in general.

Different solutions are possible only in non-prismatic channels (section enlargements or contractions). It is worth keeping in mind that in a mobile-bed channel, the *water surface profiles of gradually varied flows*, which lead to the profile classification M and S, cannot be applied.

However, the results of this theory can be utilized for short periods and modest distances. In these conditions, the bed is considered as fixed and the terms of time variation in the equation of water continuity and momentum as negligible. These considerations can be applied, for instance, to analyze situations concerning channel width variations. Simplified balances must be done with great care. As a matter of fact, if the time interval is long enough, the altimetric variations of the bed can decisively influence the behavior of the free surface.

In order to investigate the stationary solution of a long contraction, consider a channel with a large rectangular section as schematized in Fig. 7.9 composed of two stretches of different width. Let B_1 be the width of a rectangular channel upstream of the contraction and B_2 the width of the downstream section (e.g., $B_2 < B_1$). Assume that the channel is fed by liquid and solid discharges constant in time, denoted with Q

and Q_s, respectively, and that the channel is sufficiently long. In stationary condition ($\partial/\partial t = 0$), the flow is uniform upstream and downstream of the transit to the restricted section.

In this case, the conservation of the liquid and solid masses can be imposed near the width variation by assuming a power expression of the type $Q_s = c_s BU^n$ for the solid discharge, where c_s is a suitable parameter not depending on U and h:

$$Q = h_1 B_1 U_1 = h_2 B_2 U_2$$
$$Q_s = c_s B_1 U_1^n = c_s B_2 U_2^n$$

from which we obtain:

$$h_2 = h_1 \left(\frac{B_1}{B_2}\right)^{(1-1/n)} = h_1 R^{(n-1)/n} \tag{7.55}$$

$$U_2 = U_1 R^{1/n} \tag{7.56}$$

with $R = B_1/B_2$ (contraction ratio).

The asymptotic solution tends to a situation, in which the uniform flow establishes upstream and downstream of the contraction but there is discontinuity between the free and bed surfaces near the contraction with:

$$\Delta z_b + h_1 = h_2 + \Delta h \tag{7.57}$$

The value of these discontinuities can be calculated with the momentum balance applied to the control volume of Fig. 7.9:
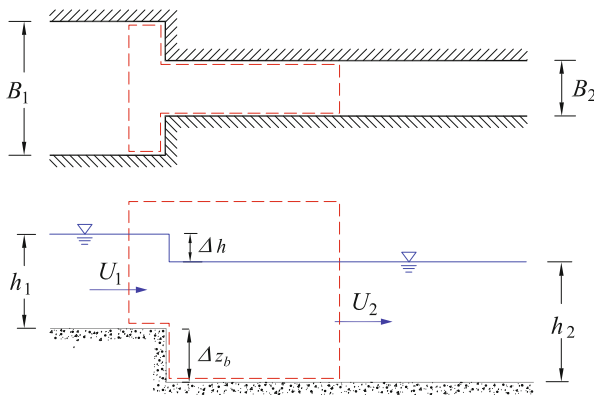
Fig. 7.9 Layout of a section contraction in a rectangular mobile-bed channel. The dotted red lines represent boundary of the control volume

Fig. 7.10 Variation in bed and free surface near a section contraction in a rectangular mobile-bed channel
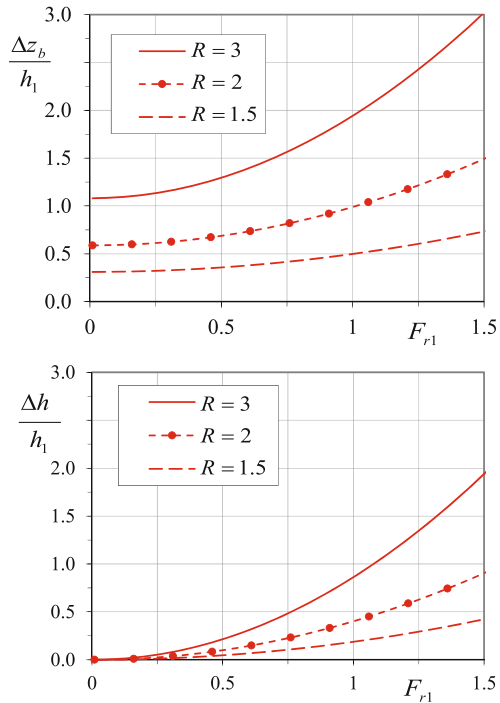
$$B_2 \, \rho \, g \left[\frac{1}{2} h_1^2 + \Delta z_b \left(\frac{h_2 + h_1 + \Delta z_b}{2} - \frac{\Delta z_b}{2} \right) - \frac{h_2^2}{2} \right] = \rho \, B_2 \, h_2 \, U_2 \, (U_2 - U_1)$$

(7.58)

By inserting (7.55) and (7.56) into (7.58), we obtain:

$$\frac{\Delta z_b}{h_1} = R^{1-1/n} - 1 + 2 \, F_{r1}^2 \, R \frac{R^{1/n} - 1}{R^{1-1/n} + 1}$$

(7.59)

where $F_{r1} = U_1 / \sqrt{g \, h_1}$ is the Froude number of the upstream reach. By inserting Eq. (7.59) into (7.57), we obtain also the variation of the free surface level (Fig. 7.10):

$$\frac{\Delta h}{h_1} = 2 \, F_{r1}^2 \, R \frac{R^{1/n} - 1}{R^{1-1/n} + 1}$$

(7.60)

In general, Δz_b results to be bigger than Δh.

Within the limits of the one-dimensional approach, the resulting relations are also suitable to section enlargements. In this case, of course, the variations change sign. In general, the most critical hypothesis of this approach concerns the force against the wall of the transition section. Moreover, independently of the Froude number, we observe erosion and free surface lowering in contractions, but elevation of bed and free surface in enlargements.

If the problem had been faced with a fixed-bed scheme in a mild slope channel, there would have been an upstream backwater profile. On the contrary, the asymptotic solution of the mobile-bed approach does not involve any gradually varied free surface profile, but only a succession of two profiles of uniform flow with discontinuity on the bed and on the free surface through the width change. In practice, however, flood events often have an insufficient duration to the achievement of an equilibrium profile of the bed. An additional phenomenon which tends to further complicate the situation is the non-uniformity of the material, in that the grain size sorting and armoring can further slow down the adjustment process of the bed.

Moreover, it is worth considering also the effect of the secondary circulations, occurring in proximity of width variations, responsible for the formation of bars and pools which, unlike one-dimensional schemes, cause local erosion or deposit values significantly different from the average values.

7.6   Simplified Models

The time variation terms of the first two equations of the system (7.21) can be neglected in first approximation compared to the respective terms of spatial variation:

$$\frac{\partial U}{\partial t} \ll g \frac{\partial h}{\partial x} \qquad \text{and} \qquad \frac{\partial h}{\partial t} \ll U \frac{\partial h}{\partial x} \tag{7.61}$$

Besides, for the reasons repeatedly expressed so far, in the third equation of the same system, the time variation term of the concentration inside the volume control, $\partial(CA)/\partial t$, can be neglected as well. In other words, we adopt a decoupled scheme. Moreover, we can assume that the solid discharge only depends on the velocity, that is:

$$\frac{\partial q_s}{\partial x} \simeq \frac{dq_s}{dU} \frac{\partial U}{\partial x} \tag{7.62}$$

Should there be no discontinuity in variables U, h, and z_b, we have:

$$\begin{cases} h \dfrac{\partial U}{\partial x} + U \dfrac{\partial h}{\partial x} = 0 \\[2mm] U \dfrac{\partial U}{\partial x} + g \dfrac{\partial h}{\partial x} + g \dfrac{\partial z_b}{\partial x} = -g\, i_E \\[2mm] \dfrac{dq_s}{dU} \dfrac{\partial U}{\partial x} + C_* \dfrac{\partial z_b}{\partial t} = 0 \end{cases} \tag{7.63}$$

After explicating $\partial U/\partial x$ from the first equation of the system and after substituting it into the two other equations of (7.63), we obtain:

$$\begin{cases} \left(-\dfrac{U^2}{g\,h} + 1\right)\dfrac{\partial h}{\partial x} + \dfrac{\partial z_b}{\partial x} = -i_E \\[3mm] \dfrac{dq_s}{dU}\left(-\dfrac{U}{h}\right)\dfrac{\partial h}{\partial x} = -C_*\,\dfrac{\partial z_b}{\partial t} \end{cases} \tag{7.64}$$

We will apply the simplified system (7.64) to two particular solutions: the *simple wave model* and the *parabolic model*.

7.6.1   The Simple Wave Model

Following Vreugdenhil and Vries (1973), we obtain a solution in the simple wave form of the system; we neglect the term i_E in the first equation of the system (7.64), and thus, we retrieve:

$$\frac{\partial h}{\partial x} = -\frac{1}{1 - \dfrac{U^2}{g\,h}}\frac{\partial z_b}{\partial x} \tag{7.65}$$

which, substituted into (7.64), yields:

$$\frac{\partial z_b}{\partial x}\left(\frac{dq_s}{dU}\frac{U}{h}\frac{1}{(1 - \dfrac{U^2}{g\,h})}\right) = -C_*\frac{\partial z_b}{\partial t} \tag{7.66}$$

Equation (7.66) can be written as:

$$\frac{\partial z_b}{\partial t} + c_Z\frac{\partial z_b}{\partial x} = 0 \tag{7.67}$$

Equation (7.67) represents the equation of a simple wave moving with celerity:

$$c_Z = \frac{dq_s}{dU}\frac{1}{C_*}\frac{U}{h}\frac{1}{(1 - F_r^2)} \tag{7.68}$$

where we set $F_r = U/\sqrt{g\,h}$. Equation (7.68) coincides with λ_3, already calculated by de Vries with the method of characteristics (Eq. 7.38 on page 181).

Having neglected the resistance term, the possibility of applying this procedure is limited only to small distances and short time intervals.

7.6.2 The Parabolic Model

The equation system is still (7.63). But here, we hypothesize that the flow can be considered as locally uniform, which is less restrictive than the hypothesis on the simple wave model. We thus obtain:

$$i_E = i_f = -\frac{\partial z_b}{\partial x} \tag{7.69}$$

The first term of Eq. (7.69) can be expressed with a uniform flow formula (e.g., Chézy's), in which the water depth can be written in function of the solid discharge per unit width and of the velocity ($h = q/U$):

$$-\frac{\partial z_b}{\partial x} = \frac{U^2}{\chi^2 h} = \frac{U^3}{\chi^2 q} \tag{7.70}$$

Equation (7.70) is then differentiated with respect to the variable x:

$$\frac{\partial}{\partial x}\frac{\partial z_b}{\partial x} = -3\frac{U^2}{\chi^2 q}\frac{\partial U}{\partial x} \tag{7.71}$$

The expression of $\partial U/\partial x$ derived from the above equation is inserted into the second equation of the system (7.64), thus obtaining:

$$\frac{dq_s}{dU}\left(-\frac{\chi^2 q}{3C_* U^2}\right)\frac{\partial}{\partial x}\frac{\partial z_b}{\partial x} = -\frac{\partial z_b}{\partial t} \tag{7.72}$$

Equation (7.72) is usually written as:

$$\frac{\partial z_b}{\partial t} - \kappa_Z\frac{\partial^2 z_b}{\partial x^2} = 0 \qquad \text{with :} \qquad \kappa_Z = \frac{\chi^2 q}{3C_* U^2}\frac{dq_s}{dU} \tag{7.73}$$

which represents the *parabolic model*. This model gives reliable results only for elevated values of x and t. In other words, according to Vreugdenhil and Vries (1973), the model is applied for $x > 3\ h/i$. Since no time differentiations have been done in deriving the model, all parameters can be made dependent on time. In particular, the time dependence of the discharge ($q = q(t)$, the flood hydrograph) can be inserted in the diffusion coefficient $\kappa_Z(t)$.

7.6.2.1 Application

The solution of the parabolic model was employed by de Vries (1965) to define the morphological scale of rivers.
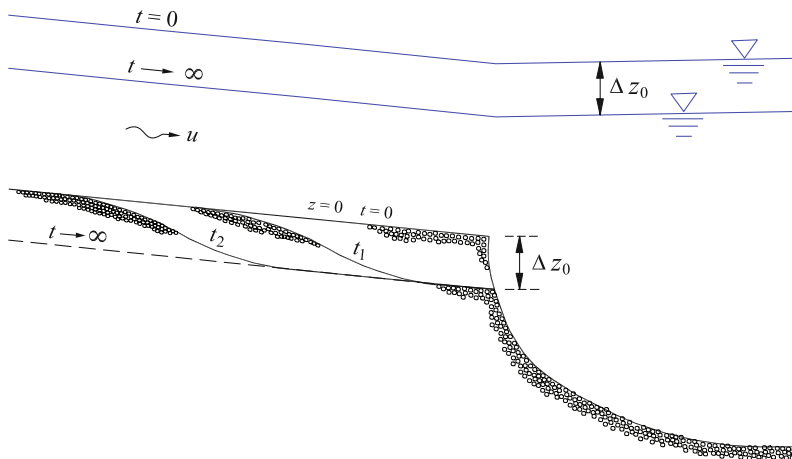
Fig. 7.11 Layout of the morphological scale of a stream

Consider a stream flowing into a reservoir and suppose it initially in equilibrium (uniform flow with constant liquid and solid discharges) (Fig. 7.11).

Suppose to lower the free surface of the reservoir by a quantity Δz_o; the same variation is imposed on the bed surface of the outflow section ($x = 0$). Since the liquid and solid discharges are kept constant, the whole bed will tend asymptotically to lower by the same quantity Δz_o and become parallel to the initial position.

If the problem is dealt with a parabolic model, we can obtain the spatial and temporal evolution of the bed lowering Δz_b:

$$\Delta z_b(x, t) = \Delta z_o \left(1 - \frac{2}{\sqrt{\pi}} \int_0^Y e^{-\xi^2} \, d\xi \right) \tag{7.74}$$

with:

$$Y = \frac{x}{2\sqrt{\int_0^t \kappa_Z(t) \, dt}} \tag{7.75}$$

For example, we can calculate how long a reduction of the level Δz_o in the outflow section takes to produce a lowering which is equal to half the initial one, in a section at the distance L_m from the outflow. That is:

$$\Delta z_b(L_m, T_{0.5}) = \frac{1}{2} \Delta z_o$$

With a few simple steps, we obtain the time $T_{0.5}$:

$$T_{0.5} = \frac{L_m^2}{Y_m} \qquad T \text{ [years]}$$

with:

$$Y_m = \int_0^{1\, year} k(t)\ dt \simeq \frac{1}{3}\frac{b}{i}\int_0^{1\, year} q_s(t)\ dt \qquad (7.76)$$

where q_s represents the solid discharge proportional to the velocity by means of a power law exponent b: $q_s = a\ U^b$.

7.6.3 Complete Hyperbolic Model

In addition, we can obtain a complete hyperbolic model by combining the hypothesis of the two models previously described:

$$\frac{\partial z_b}{\partial t} - \kappa_Z \frac{\partial^2 z_b}{\partial x^2} - \frac{\kappa_Z}{c_Z}\frac{\partial^2 z_b}{\partial t\ \partial x} = 0. \qquad (7.77)$$

with the same meaning of symbols.

7.7 Adaptive Models

In some cases, especially in the processes dominated by suspended load where the transported material is very fine, it is advisable to leave out the hypothesis that the solid discharge Q_s coincides with the transport capacity Q_s^*, whereby transport capacity is meant the solid discharge in equilibrium with the local hydrodynamic conditions (uniform flow with no erosion or deposition). The actual transport rate could be either higher or lower than the transport capacity, depending on the upstream condition. In this case, the solid discharge becomes a dependent variable problem, depending not only on the local hydrodynamic conditions but also on the initial and boundary conditions. In other words, the solid discharge is then dependent on the transport capacity by means of a differential equation. By approximately integrating the two-dimensional differential equations for the suspended sediment transport (Eq. 6.14), we can show (Armanini and Silvio 1982) that the solid discharge Q_s can be linked to the transport capacity Q_s^*, by means of a first-order *reaction equation*:

$$Q_s = Q_s^* - L^*\frac{\partial Q_s}{\partial x} - \tau^*\frac{\partial Q_s}{\partial t} \qquad (7.78)$$

The transport capacity is a function of the characteristics of the sediment and the local hydrodynamic conditions: $Q_s^* = func(U, h, B, d, \dots)$. It is a relation provided
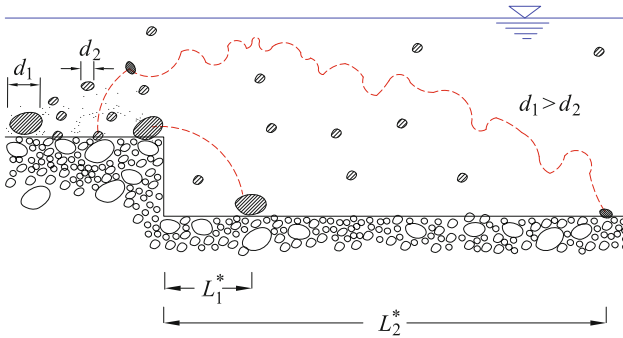
Fig. 7.12 Adaptation length

by a proper formula for the sediment transport. L^* represents the *characteristic length* of the adaptation process.

Figure 7.12 shows how the finer particles fail to adapt immediately to changes of the hydrodynamic conditions that occur along the flow. The adaptation length represents the distance necessary for the transport to adapt to the new hydrodynamic conditions: the coarser particles will tend to adjust more rapidly than those with finer diameter.

Analogous reasoning can be made for the *time variations* of the solid discharge. The reaction tends to be more or less delayed based on whether particles are light or not, respectively. The *adaptation time* τ_* represents the *characteristic time* of the process.

Rational expressions for adaptation length and time were obtained by an approximated integration of Eq. (6.14) (Galappatti 1983). A simplified expression, in explicit form, was proposed by Armanini and Silvio (1988):

$$\frac{L^* \, w_s}{h \, U} = \frac{a}{h} + \left(1 - \frac{a}{h}\right) \exp\left(-1.5 \, \left(\frac{a}{h}\right)^{-1/6} \frac{w_s}{u_*}\right) \tag{7.79}$$

where w_s is the particle fall velocity; h is the water depth; a is the thickness of the bedload layer. In (7.79), we can set $a = 0.05 \, h$ (Fig. 7.13).

In a first approximation, we can assume that the adaptation time is directly proportional to the L^* and inversely to the depth-average velocity U, e.g.,

$$\tau^* = \alpha_\tau \frac{L^*}{U} \tag{7.80}$$

where $\alpha_\tau = \mathcal{O}(1)$.

From Eqs. (7.78) and (7.80), we can see that when $L^* \to 0$ (and therefore, $\tau^* \to 0$), the solid discharge tends to the transport capacity: $Q_s \to Q_s^*$, which usually occurs in the bedload transport. Vice versa, when $L^* \to \infty$, since $Q_s \neq 0$, from (7.78), we have that $\partial Q_s / \partial x \to 0$, that is, the solid discharge remains constant: this is the case of
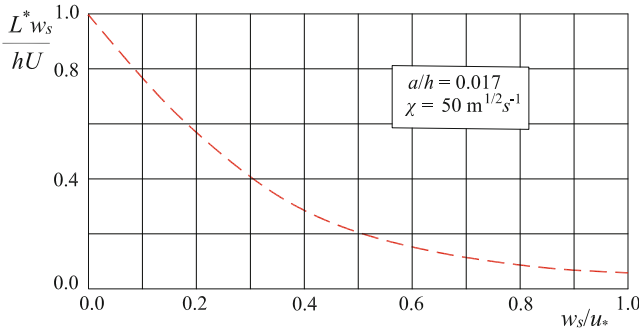
Fig. 7.13 Adaptation length according to Armanini and Silvio (1988)
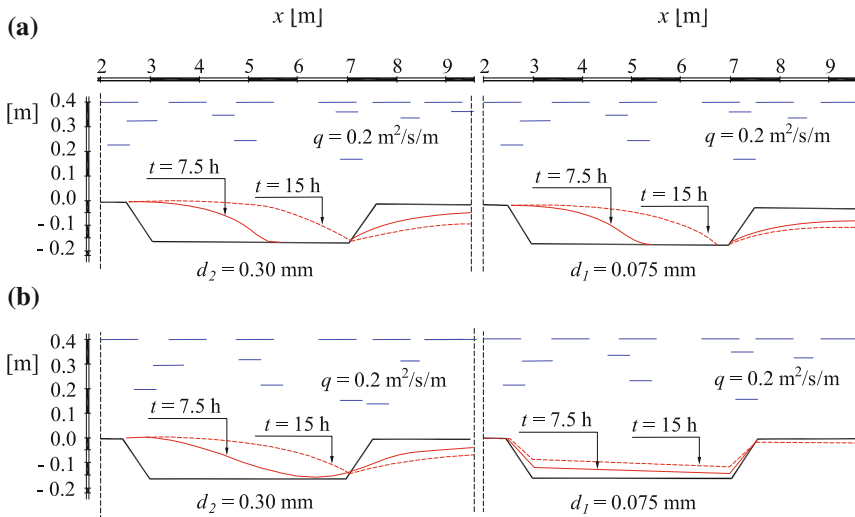
Fig. 7.14 Filling process of a trench for various particle sizes according to Armanini and Silvio (1988): **a** immediate adaptation conditions ($L^* = 0$); **b** accounting for the adaptive hypothesis

wash load, in which the solid discharge is constant and independent of hydrodynamic conditions.

Equation (7.78) together with the equations of system (7.21) forms a system of partial differential equations in the dependent variables U, Q_s, h, and z_b, which still requires two closure relations, one for i_E and the other for Q_s^*. The system can be solved numerically.

Figure 7.14 shows the simulation of the filling process of a trench dug across a wide rectangular channel. The simulation was made by assuming a uniform-sized material according to two particle size hypotheses: coarse material with a 0.300 mm diameter, or fine material with a diameter $d = 0.075$ mm. The channel is fed with constant solid and liquid discharges up to the complete filling of the trench.

Figure 7.14a illustrates the results of the simulation performed under the hypothesis of immediate adaptation, that is, with $L^* = \tau^* = 0$. Figure 7.14b shows the results of the simulation carried out by taking the adaptation process into account, where the adaptation length and time were calculated with Eqs. (7.79) and (7.80).

The figure shows that the two simulations with the coarse material ($L^*/h \simeq 0$) are basically the same: the filling process occurs by forming a *delta* which migrates downstream, while the downstream edge of the trench in the meantime is subject to erosion and the trench elongates downstream.

Different results occur with the fine material. In the adaptation hypothesis, the filling process (Fig. 7.14b; graph on the right) occurs quite uniformly on the whole length of the trench, whose bed thus appears to fill up nearly horizontally. In case of immediate adaptation (Fig. 7.14b; graph on the left), instead, the filling process of the fine material virtually occurs the same way as with the coarse material by the delta formation.

7.8 Non-uniform Sediment Models

In the previous chapters, we have often underlined how insufficient it may be to consider the transported sediment as made up of uniform particle sizes. In order to overcome this simplification, it is advisable to subdivide the grain size curve of the bed material (which is different than the size distribution of the transported material) in a discrete number N of classes and write the conservation equations for the solid mass of each class:

$$\frac{\partial}{\partial t} \int_{\forall_c} \rho_s\, c_j\, d\forall + \oint_{\Sigma_c} \rho_s\, c_j\, (\overrightarrow{u}_{sj} \cdot d\overrightarrow{A}) = 0 \qquad (7.81)$$

With reference to the control volume and parameters given in Fig. 7.15, Eq. (7.81) becomes:

$$\frac{\partial h\, C_j}{\partial t} + \frac{\partial q_{sj}}{\partial x} + C^* \beta_j\, \frac{\partial z_b}{\partial t} = 0 \qquad (7.82)$$

The term $C^* \beta_j\, \partial z_b/\partial t$ of Eq. (7.82) represents the net flux per unit width through the bed surface of the j-th class, written in agreement with Einstein's hypothesis, under which this flux is just proportional to the percentage β_j of the class on the bed.

q_{sj} and C_j are, respectively, the solid discharge and the concentration of the j-th class. These two variables can be related to the transport capacity of the class, always on the basis of Einstein's hypothesis:

$$q_{sj} = \beta_j\, q_{sj}^* \quad\text{and}\quad C_j = \frac{q_{sj}}{\alpha_{cu} U h} = \beta_j\, \frac{q_{sj}^*}{\alpha_{cu} U h} \qquad (7.83)$$
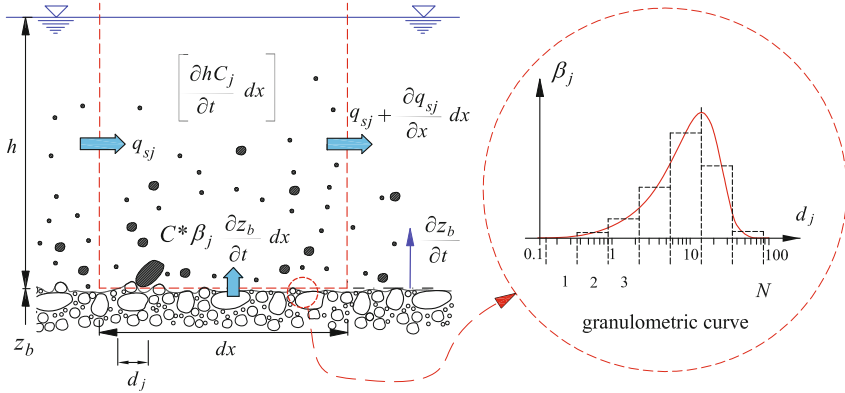
Fig. 7.15 Layout of the mass balance for the j-th particle size class sediments referring to the control volume indicated by the dotted red line

where $q_{sj}^* = func(U, h, d_j, \rho, \rho_s, ...)$ is the *transport capacity* of the single class, that is, the solid discharge which would form if the material were of uniform size with diameter d_j, hydrodynamic conditions being equal, and possibly including the hiding factor. Such an expression corresponds to one of the solid transport formulae previously described, properly adjusted to consider the hiding factor (Sect. 5.6, page 137).

By inserting Eq. (7.83) into Eq. (7.82), we obtain:

$$\frac{\partial}{\partial t}\left(\beta_j \frac{q_{sj}^*}{\alpha_{cu}U}\right) + \frac{\partial}{\partial x}\left(\beta_j q_{sj}^*\right) + C^* \beta_j \frac{\partial z_b}{\partial t} = 0 \tag{7.84}$$

Equation (7.84) is valid for both the suspended and bedloads.

Thus, we obtain so many differential equations as many grain size classes considered which, together with the conservation equations for momentum, for total solid mass, and for water mass (system 7.21), form a system of $N + 3$ hyperbolic equations that can be solved with proper numerical methods.

It is worth observing that the system will be properly set after correctly assigning the closure relations (a uniform flow formula for the bed shear stress and a suitable sediment transport formula for the transport capacity), and the initial and the boundary conditions. No other assumption is required, in principle.

However, most, or maybe all, of the applications in the literature enlarge the control volume of the mass balance of each size fraction by including a further layer, set below the surface, called *mixing layer* or *active layer*, introduced by Hirano (1971) (Fig. 7.16).

More precisely, Hirano's model hypothesizes that there is a finite thickness layer, δ, in which all classes mix instantaneously. The mixing layer is introduced to mediate the bed surface irregularities and the particle size mixing induced by the bed form migration.
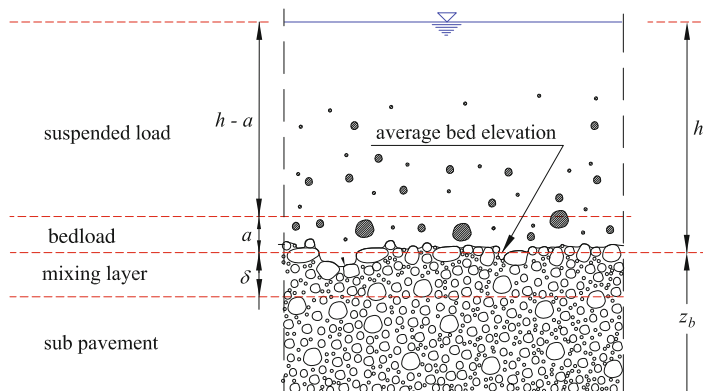
Fig. 7.16 Layout of the mixing layer and (bed and suspended) transport layers (Armanini and Silvio 1989)

The extension of the control volume to this layer involves the addition of a further term in the equation to represent the mass variations of each class in the layer itself. The continuity equation (7.82) of the single size class is then rewritten as:

$$\frac{\partial}{\partial t}\left(C_j\,h + C^*\,\beta_j\,\delta\right) + \frac{\partial q_{sj}}{\partial x} + C^*\,\beta_j^*\,\frac{\partial}{\partial t}(z_b - \delta) = 0 \qquad (7.85)$$

Compared to Eqs. (7.82), (7.85) adds the second term and modifies the last. The second term ($C^*\,\beta_j\,\delta$) represents the variation in the j-th class material in the mixing layer. The last term represents the net flux entraining from the lower surface of the new control volume, that is, at the level ($z_b - \delta$). In this term, then, β_j^* is equal to β_j in deposit processes, while in erosion processes, β_j^* is set as equal to the material percentage, $(\beta_j)_{subpv}$, of the j-th class below the mixing layer (*sub-pavement*), a percentage which must be, however, known (as boundary condition), i.e., $\beta_j^* = (\beta_j)_{subpv}$.

The thickness δ of the mixing layer is the most uncertain parameter of this approach, while its dimension is of utmost importance for the time evolution of the bed and its composition. The mentioned models usually assume ($\delta \simeq 2 \sim 3\,d_{90}$) in plane beds, while they assume ($\delta = 0.5\,\Delta_D$) in duned beds, where Δ_D is the average height of the bed forms.

Hirano's formulation has some intrinsic limits later focused by different authors: first among the others, the arbitrariness of the layer thickness (Armanini 1995; Ribberink 1987; Di Silvio 1992).

The complete equation system governing the phenomenon and written per unit width appears as follows:

$$
\begin{cases}
\dfrac{\partial h}{\partial t} + \dfrac{\partial}{\partial x}(hU) + \dfrac{\partial z_b}{\partial t} = 0 \\[2ex]
\dfrac{\partial}{\partial t}(Uh) + \dfrac{\partial}{\partial x}(hU^2) + gh\dfrac{\partial h}{\partial x} + gh\dfrac{\partial z_b}{\partial x} = -\dfrac{\tau_o}{\rho} \\[2ex]
\dfrac{\partial}{\partial t}\left(\displaystyle\sum_{j=1}^{N} \beta_j \dfrac{q_{sj}^*}{\alpha_{cu}U}\right) + \dfrac{\partial}{\partial x}\left(\displaystyle\sum_{j=1}^{N} \beta_j q_{sj}^*\right) + C^* \dfrac{\partial z_b}{\partial t} = 0 \\[2ex]
\dfrac{\partial}{\partial t}\left(\beta_j \dfrac{q_{sj}^*}{\alpha_{cu}U} + C^* \beta_j \delta\right) + \dfrac{\partial}{\partial x}\left(\beta_j q_{sj}^*\right) + C^* \beta_j^* \dfrac{\partial}{\partial t}(z_b - \delta) = 0 \\[2ex]
\qquad\qquad\qquad \text{for} \qquad (j = 1, \ldots, N)
\end{cases}
\tag{7.86}
$$

in which the total solid discharge and total sediment concentration were calculated by means of the hypotheses (7.83):

$$
q_s = \sum_{j=1}^{N} q_{sj} = \sum_{j=1}^{N} \beta_j q_{sj}^* \quad \text{and} \quad C = \sum_{j=1}^{N} C_j = \sum_{j=1}^{N} \frac{q_{sj}}{\alpha_c U h} = \beta_j \frac{q_{sj}^*}{\alpha_c U h} \tag{7.87}
$$

The first equation of the system (7.86) represents the conservation of the total volume (liquid and solid), the second equation the momentum balance of the mixture, the third equation the conservation of the total solid volume, and the following N equations represent the mass conservation of each size class. It is also worth noting that the third equation is the sum of the N successive equations (if $\beta_j^* = \beta_j$, in deposit processes) and that the equation $\sum_{j=1}^{N} \beta_j = 1$ could be written in place of the third equation.

In the system (7.86), the bed shear stress $\tau_o/\rho = func(U, e_s, h, \ldots)$ can be expressed by means of a suitable uniform flow formula, while $q_{sj}^* = func(U, h, w_{sj}, \ldots)$ can be expressed by means of an adequate solid transport formula.

The solution to the system is a remarkably complex operation, in that it is a system of partial differential equations, in which the hydrodynamic equations and the sediment transport equations cannot always be decoupled. The system is usually solved with the finite difference or the finite volume method. In some cases, the decoupling between hydrodynamics and solid transport can be justified; sometimes, it is even possible to calculate the hydrodynamic conditions as a succession of permanent flow profiles. The decision whether to adopt or not these simplifications depends on the type of problem to be solved.

Alternatively, the N equations of mass conservation of each size class can be replaced by the conservation equations of the moments of the particle size distribution β_j (*method of moments of the distribution*) (Armanini 1989, 2002).

If we limit this approach to the first-order moment equation, and consider the superior order moments as invariable, we obtain a system of four differential equations, whose first three coincide with the first three of the system (7.86), while the fourth represents the spatial and temporal variation of the average diameter (Armanini 2002). The resulting four system characteristics are shown in Fig. 7.17.
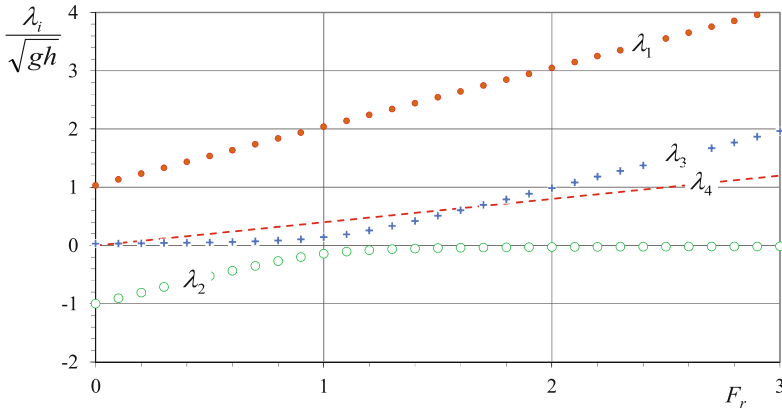
Fig. 7.17 Behavior of the characteristics in non-uniform sediment models. Equations were written with the method of moments. The characteristic λ_4 can be seen as referred to the average diameter of the particle size distribution β_j of the bed material. The average transport concentration is here extremely high $q_s/q = 0.01$ (Armanini 2002)

The first three characteristics (λ_1, λ_2, λ_3) correspond to those of the system with homogeneous material (Eq. 7.27, on page 177). The fourth is specific to the process of grain size selection. It can be associated with a particle size variation (also induced by a variation in the water depth and velocity) which, however, always migrates downward with the same transport velocity as the solid particles.

In conclusion, we can observe that:

- for sufficiently low concentration, the trend of the first three characteristics follows that of the characteristics of the homogeneously sized mobile-bed channels. The characteristics of the two cases coincide when the moment of the second order of the particle size distribution vanishes;
- the fourth characteristic is always positive;
- the celerity of this characteristic essentially depends on the transport velocity of the solid material and to some extent also on the mixing layer thickness;
- the fourth characteristic is the same order as the characteristics of the hydrodynamic part; in other words, the grain size sorting effects can be studied also without considering the variation in the bed elevation.

7.8.1 Physical Meaning of the Mixing Layer

As previously said, the hypotheses on the mixing layer are not convincing: The determination of its thickness seems to be rather arbitrary; the immediate mixing between size classes and the intrinsic layout hypothesis about a discontinuity of
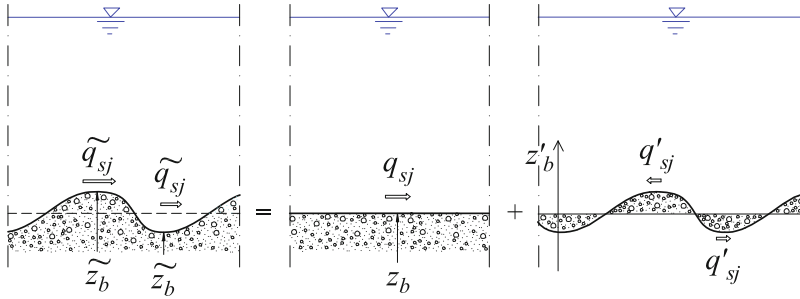
Fig. 7.18 Layout of different variable decompositions in the average and fluctuating components (Armanini 1995)

the grain size distribution between the mixing layer and the underlying bed (*sub-pavement*) are still dubious ideas.

A more convincing explanation of the process can be obtained (Armanini 1995) by considering the instantaneous mass balance of the single class j in the control volume indicated in Fig. 7.16:

$$\frac{\partial \widetilde{C_j}\,\widetilde{h}}{\partial t} + \frac{\partial \widetilde{q_{sj}}}{\partial x} + C^* \widetilde{\beta}_j \frac{\partial \widetilde{z_b}}{\partial t} = 0 \tag{7.88}$$

in which the mark ($\widetilde{}$) was introduced to indicate instantaneous values or values integrated on a period (e.g., on the time macro-scale of turbulence) much shorter than the timescale of the morphological variations.

All the variables in Eq. (7.88) (solid discharge $\widetilde{q}_{sj}$, bed surface composition $\widetilde{\beta}_j$, bed elevation $\widetilde{z}_b$, etc.) are instantaneous quantities subject to disordered fluctuations induced by the bed surface fluctuation, due to macro-vortices and especially to the migration of bed forms.

With reference to Fig. 7.18, we can divide these instantaneous variables into *average* and *fluctuating* components. In order to take into account the non-stationarity at large timescale, for instance, the non-stationarity due to erosion and deposition processes during a flood passage, it is advisable to refer to *ensemble averages*, that is, to the arithmetic means on a great number of realizations, just as the case of turbulence in non-stationary processes at large timescale. Below, the unmarked symbols will be referred to ensemble average values, while the fluctuating components (with respect to this average) will be denoted with the symbol prime ($'$).

$$
\begin{aligned}
\widetilde{\beta}_j(t, x) &= \beta_j + \beta'_j \\
\widetilde{q}_{sj}(t, x) &= q_{sj} + q'_{sj} \\
\widetilde{C}_j(t, x) &= C_j + C'_j \\
\widetilde{z}_b(t, x) &= z_b + z'_b
\end{aligned}
\tag{7.89}
$$

in which the averages of the fluctuating components are equal to zero.

By inserting the variable decompositions (7.89) into Eq. (7.88) and after averaging the obtained equation on a great number of realizations, we have:

$$\frac{\partial C_j h}{\partial t} + \frac{\partial q_{sj}}{\partial x} = C^* \left(-(\beta_0)_j \frac{\partial z_b}{\partial t} - \overline{(\beta_0)'_j \frac{\partial z'_b}{\partial t}} \right) \tag{7.90}$$

The last term in Eq. (7.90) represents the average of the products of the fluctuating components of the size composition of the class j-th and of the displacement velocity of the bed surface $(\partial z_b/\partial t)$. This term is generally different from zero and its definition represents a typical closure problem. One possible solution is to express this term with a Boussinesq diffusive model.

$$\overline{(\beta_0)'_j \frac{\partial z'_b}{\partial t}} = \varepsilon_z \left(\frac{\partial \beta_j}{\partial y} \right)_{y=z_b} \tag{7.91}$$

where ε_z is a suitable diffusion coefficient and y is the vertical axis $(y \le z_b)$ positive downward. β_j, the percentage of the class j-th on the bed, is here function of the vertical coordinate y: $\beta_j = \beta_j(x, y, t)$, while $(\beta_0)_j = \beta_j(x, y = z_b, t)$ is its average value on the surface $(y = z_b)$.

By integrating Eq. (7.91) on a finite thickness δ, we obtain an equation similar to Hirano's, but with the addition of the diffusive term.

Equation (7.91) shows that the mixing process on the bed is a continuous, non-instantaneous fluctuating process which cannot be confined to a finite thickness layer as, on the contrary, is assumed in the mixing layer process. Such an observation shows the limits of Hirano's mixing layer theory, especially for the arbitrariness about the layer thickness which, as a matter of fact, results to be function of the spatial and temporal integration phase of the mathematical model employed.

Hirano's mixing layer equation, moreover, lacks in diffusive terms and thus cannot describe the particle size selection processes below this layer. Such processes are, in some cases, very important.

The models based on the mixing layer are, however, the only complete tools today available to describe morphological and granulometric evolution processes in streams. The observations made so far lead to the conclusion that in field applications, the mixing layer thickness must be significantly higher than that indicated by the relations previously provided for to evaluate the thickness.

7.8.2   Non-uniform Sediment Adaptive Models

The adaptive scheme, introduced in Sect. 7.7, can be always included in non-uniform sediment models.

The non-immediate adaptation scheme assumes a certain importance in presence of spatial or temporal variations of hydrodynamic properties of the stream in presence of suspended load. What is required is to modify the closure relations (Eq. 7.83) on page 199, by substituting them with so many differential relations similar to Eq. (7.78) on page 194; e.g.,

$$q_{sj} = \beta_j \, q_{sj}^* - L_j^* \frac{\partial q_{sj}}{\partial x} - \tau_j^* \frac{\partial q_{sj}}{\partial t} \tag{7.92}$$

and similarly for the concentrations, for which we can set:

$$C_j \simeq \frac{q_{sj}}{\alpha_{cu} U h} \tag{7.93}$$

where L_j^* and τ_j^* are the *adaptation length* and *adaptation time* which can be calculated with Eqs. (7.79) and (7.80), respectively. Thus, the resulting equation system is as follows:

$$
\begin{cases}
\dfrac{\partial h}{\partial t} + \dfrac{\partial U h}{\partial x} + \dfrac{\partial z_b}{\partial t} = 0 \\[2mm]
\dfrac{\partial U}{\partial t} + U \dfrac{\partial U}{\partial x} + g \dfrac{\partial h}{\partial x} + g \dfrac{\partial z_b}{\partial x} = -g \, i_E \\[2mm]
\dfrac{\partial}{\partial t} (\sum_{j=1}^{N} \dfrac{q_{sj}}{\alpha_{cu} \, U}) + \dfrac{\partial}{\partial x} (\sum_{j=1}^{N} q_{sj}) + C^* \dfrac{\partial z_b}{\partial t} = 0 \\[2mm]
\dfrac{\partial}{\partial t} \left(\dfrac{q_{sj}}{\alpha_{cu} \, U} + C^* \beta_j \delta \right) + \dfrac{\partial}{\partial x} q_{sj} + C^* \beta_j^* \dfrac{\partial}{\partial t} (z_b - \delta) \; (j = 1, \dots, N) \\[2mm]
q_{sj} = \beta_j \, q_{sj}^* - L_j^* \dfrac{\partial q_{sj}}{\partial x} - \tau_j^* \dfrac{\partial q_{sj}}{\partial t} \qquad\qquad (j = 1, \dots, N)
\end{cases}
\tag{7.94}
$$

in which $q_{sj}^* = func(U, h, d_j, \rho, \rho_s, ...)$ is the transport capacity of the single size class, including any hiding effect, and thus, in principle, function of the complete particle size distribution curve ($\beta_j, \, j = 1, N$) of the bed material.

7.8.3   Two-Dimensional Depth-Integrated Models

The approach adopted to derive the one-dimensional depth-integrated models can be easily applied to two-dimensional depth-integrated models. In this case, in addition to the conservation equations of the total (liquid + solid) mass (Eq. 7.95) and of solid mass (Eq. 7.96), it is necessary to write the momentum balance equations, respectively, in the two horizontal directions x_1 and x_2 (Eqs. 7.97 and 7.98):

$$\frac{\partial}{\partial t} (h + z_b) + \frac{\partial h U_1}{\partial x_1} + \frac{\partial h U_2}{\partial x_2} = 0 \tag{7.95}$$

$$\frac{\partial}{\partial t} (Ch + C_* \, z_b) + \frac{\partial (q_s)_1}{\partial x_1} + \frac{\partial (q_s)_2}{\partial x_2} = 0 \tag{7.96}$$

$$\frac{\partial hU_1}{\partial t} + \frac{\partial hU_1U_1}{\partial x} + \frac{\partial hU_1U_2}{\partial x_2} + g\frac{\partial h + z_b}{\partial x_1} = -\frac{\tau_{o1}}{\rho} \qquad (7.97)$$

$$\frac{\partial hU_2}{\partial t} + \frac{\partial hU_1U_2}{\partial x_1} + \frac{\partial hU_2U_2}{\partial x_2} + g\frac{\partial h + z_b}{\partial x_2} = -\frac{\tau_{o2}}{\rho} \qquad (7.98)$$

$(q_s)_1 = \int_h cu_1 dy$ and $(q_s)_2 = \int_h cu_2 dy$ represent the sediment fluxes in the directions x_1 and x_2, respectively, where y is the vertical direction, and c is the local value of the solid concentration.

U_1 and U_2 are the depth-integrated velocities, and τ_{o1} and τ_{o2} the bed shear stress components in the horizontal directions x_1 and x_2. C is the depth-averaged solid concentration.

The system (7.95–7.98) contains only the horizontal components of the velocity (U_1 and U_2), that is, it does not contain the vertical velocity components and, as such, it cannot simulate the secondary circulations with horizontal axis, which instead are also composed of the vertical component of the velocity vector.

In river environment, however, the secondary circulations are extremely important, as they are responsible, for example, of bar formation and local scours.

One of the most important consequences of the secondary circulations is represented by a different orientation of the bed shear stress with respect to the orientation of the streamline of the depth-average velocity. In particular in the presence of a curvature of the streamline, the secondary circulations induce a component of the bed shear stress τ_{on} in direction normal to the streamline of the depth-averaged velocity vector, which in turn determines a normal component of the solid discharge. This situation is sketched in Fig. 7.19.

In two-dimensional depth-integrated models (2DH models), this effect can be simulated by adding a normal component of the bed shear stress as a function of the curvature of the streamline.

The normal component of the bed shear stress can be calculated in different ways (Odgaard 1989). An expression suitable for this purpose has already been introduced in Sect. 3.5.1 at page 81, by adopting a simplified approach suggested by Rozovskii (1957):

$$\tau_{on} = 2\left(\frac{n}{\kappa}\right)^2 \frac{1}{(2+n)(3+n)}\rho\,u_{*x}^2\frac{h}{r_m} = A_\tau\,\rho\,u_{*x}^2\frac{h}{r_m} \qquad (7.99)$$

where r_m is the radius of curvature of the streamline of the depth-averaged velocity. n is the power law exponent for the vertical distribution of velocity ($u_i = u_{*i}\,(n/\kappa)\,(z/h)^{1/n}$); it assumes values ranging between 7 and 11 depending on the roughness of the bed, higher values of n correspond to higher roughness. $\kappa = 0.41$ is the von Kármán constant.

The parameter A_τ depends on n and κ according to the following expression:

$$A_\tau = 2\left(\frac{n}{\kappa}\right)^2 \frac{1}{(2+n)(3+n)} \qquad (7.100)$$

Fig. 7.19 The normal component of the bed shear stress in a curve streamline
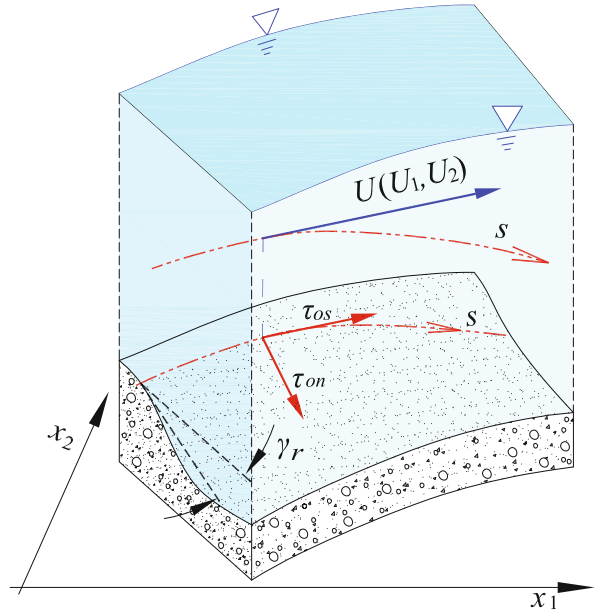
The next table shows the values of coefficient A_τ for some values of the power law exponent n:

n	7	8	9	10	11	12
A_τ	6.48	6.92	7.30	7.63	7.91	8.16

The radius of curvature r_m of the streamline can be expressed in function of the components of the depth-averaged velocity vector, U_1 and U_2, and their gradients:

$$r_l = \frac{\left(U_1^2 + U_2^2\right)^{3/2}}{U_1^2 \dfrac{\partial U_2}{\partial x_1} - U_2^2 \dfrac{\partial U_1}{\partial x_2} - U_1 U_2 \dfrac{\partial U_2}{\partial x_2} + U_1 U_2 \dfrac{\partial U_1}{\partial x_1}} \qquad (7.101)$$

The sign of the above expression is taken as positive if the rotation of the particle is clockwise, negative when it is counterclockwise.

In order to properly simulate the effect of the secondary circulation, it is necessary (Parker 1984) to include a parameter that explicitly takes into account the slope of the bed in the expression of the solid flow rate (Fig. 7.19):

$$(q_b)_s = \frac{q_b}{\sqrt{1 + \left(\dfrac{\alpha_r}{\sqrt{\theta}} \dfrac{\partial z_b}{\partial n}\right)^2}} \qquad \text{and} \qquad (q_b)_n = q_b\, h \frac{\alpha_r}{\sqrt{\theta}} \frac{\partial z_b}{\partial n} \qquad (7.102)$$

where α_r is a suitable parameter of order unity.

$$\frac{\partial h}{\partial n} = \text{sign}\left(\frac{1}{r_l}\right)\left(\frac{\partial z_b}{\partial x_1}\sin\beta_o - \frac{\partial z_b}{\partial x_2}\cos\beta_o\right) \qquad (7.103)$$

and β_o is the sloping angle of the bed. As a consequence, the solid flow rate does not follow the direction of the bed shear stress.

7.8.4   Two-Dimensional Models in a Vertical Plane

The depth-integrated models, under shallow water assumptions, are not suitable to simulate the diffusive effects due to turbulence, in particular when the suspended load is important. In this case, we have to resort to complete three-dimensional models. These models are rather complex, because they also have to include suitable sophisticated turbulence closure models, capable to correctly simulate the water-particle interactions.

In some applications, however, it is possible to make use of simplified two-dimensional models in the vertical plane.

In this case, it is useful to include the possible effect of particle size sorting. For this purpose, the scheme for simulating the morphological processes by taking into account the non-uniformity of the particle size can be also extended to two-dimensional models in the vertical plane, especially for the suspended sediment transport. It needs to numerically integrate the conservation equation for the solid volume, expressed in concentration terms, i.e., Eq. (6.14) on page 147, rewritten for the volume concentration of the generic j-th class:

$$\frac{\partial c_j}{\partial t} + \frac{\partial u_x c_j}{\partial x} = \frac{\partial}{\partial y}(w_{sj}c_j + \beta_\varepsilon\varepsilon\frac{\partial c_j}{\partial y}) \qquad (j = 1, N) \qquad (7.104)$$

In this case, the effect of particle size interaction between classes is introduced in the boundary condition. The downward flux (deposit) for the single class can be set as equal to $w_{sj}c_j$ (Fig. 7.20), while the upward flux (erosion) can be assumed to be proportional to the concentration β_j of the bed class, that is, equal to $\beta_j\varepsilon\partial c_j/\partial y$.

The net flux at the level $(y = a)$ is:

$$\left(w_{sj}c_j + \beta_j\varepsilon\frac{\partial c_j}{\partial y}\right)_{y=a} \qquad (7.105)$$

As a boundary condition on the lower boundary $(y=a)$, we can hypothesize that the bed concentration value is locally the same as in the equilibrium condition:

$$(c_j)_{y=a} = c_{aj}^* \qquad (7.106)$$

Fig. 7.20 Bed boundary conditions for two- or three-dimensional schemes of non-uniform sediment models (Armanini and Silvio 1989)
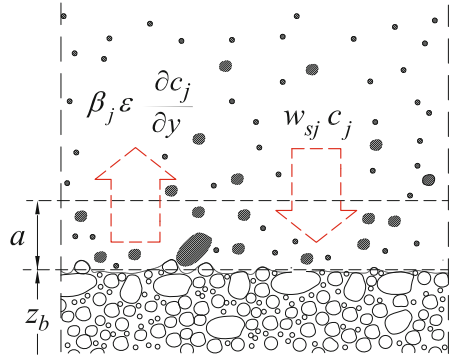
or, alternatively, that the erosive flux (upward) assumes the same value as in equilibrium condition; in this case, we have:

$$\left(\varepsilon \frac{\partial c_j}{\partial y}\right)_{y=a} = -w_{sj} c_{aj}^* \tag{7.107}$$

where c_{aj}^* represents the equilibrium concentration at the reference level ($y = a$) for every j-th class. It is a function of the local hydrodynamic variables, which can be calculated with the methods explained in Sect. 6.3.3 on page 152.

Equation (7.104), written for each grain size class, must be coupled with a mass balance equation for every class in the mixing layer δ, similar to the last N equations of the system (7.86), in which the net flux on the upper boundary of the mixing layer is represented by (7.105):

$$\frac{\partial}{\partial t}\left(C^* \beta_j \delta\right) + C^* \beta_j^* \frac{\partial}{\partial t}\left(z_b - \delta\right) = \left(w_{sj} c_j + \beta_j \varepsilon \frac{\partial c_j}{\partial y}\right)_{y=a} \tag{7.108}$$

In (7.108), β_j^* is equal to β_j in the deposition stages, while during the erosion stages, β_j^* is set as equal to the percentage $(\beta_j)_{subpv}$ of the j-th size class of the material below the mixing layer (*sub-pavement*) $\beta_j^* = (\beta_j)_{subpv}$, a percentage that, however, must be known *a priori*.

References

A. Armanini, Variation of bed and transport mean diameter in non-equilibrium conditions. *Fluvial hydraulics of mountain regions. Lecture Notes on Earth Sciences*, vol. 34. pp. 459–468, 1989

A. Armanini, Non-uniform sediment transport: dynamics of the active layer. J. Hydraul. Res. **33**(5), 611–622 (1995)

A. Armanini, Hydraulics of the natural systems: general lecture on theme A, in *Proceedings of the Congress XXVII Italian Congress of Hydraulics and Hydraulic Constructions*, volume 5. Local Organizing Committee of the XXVII Italian Congress, Ed. Bios Cosenza Italy, 2002

A. Armanini, G. Di Silvio, Sudden morphological modifications along mountain river simulated by mathematical model, in *3rd Congress of the APD of IAHR, Bandung, Indonesia*, 1982

A. Armanini, G. Di Silvio, A one-dimensional model for the transport of a sediment mixture in non-equilibrium conditions. J. Hydraul. Res. **26**(3), 275–292 (1988)

A. Armanini, G. Di Silvio, On the coexistence of bedload and suspended transport for a uniform grainsize material, in *Proceedings of the Symposium on Sediment Transport Modeling- New Orleans* (ASCE, 1989), pp. 581–587

C.S. Campbell, Rapid granular flows. Ann. Rev. Fluid Mech. **22**(1), 57–90 (1990)

M. de Vries, *Consideration about non-steady bedload transport in open channels, paper presented at 11th congress* (Int. Assoc. of Hydraul. Res, St. Petersburg, Russia, 1965)

G. Di Silvio, Sediment exchange between stream and bottom: a four layer model. Mitteilungen der Versuchsanstalt für Wasserbau, Hydrologie und Glaziologie an der Eidgenössischen Technischen Hochschule Zürich **117**, 163–191 (1992)

D.A. Drew, Mathematical modelling of two-phase flow. Ann. Rev. Fluid Mech. **15**, 261–291 (1983)

F.M. Exner, Über die Wechselwirkung zwischen Wasser und Geschiebe in Flüssen. Akad. der Wiss in Wien, Math-Naturwissenschafliche Klasse, Sitzungsberichte, Abt IIa, **134**, 165–203 (1925)

R. Galappatti, A depth integrated model for suspended transport. Technical Report common in HDR 7, Delft University of Technology, 1983

M. Hirano, River-bed degradation with armoring, in *Proceedings of the Japan Society of Civil Engineers*, vol. 1971 (Japan Society of Civil Engineers, 1971), pp. 55–65

A.J. Odgaard, River-meander model. I: development. J. Hydraul. Eng. **115**(11), 1433–1450 (1989)

G. Parker, Discussion of: lateral bedload transport on side slopes, by S. Ikeda (november, 1982). J. Hydraul. Eng. **110**(2), 197–199 (1984)

J.S. Ribberink, *Mathematical Modelling of One-dimensional Morphological Changes in Rivers with Non-uniform Sediment* (Delft University of Technology, Faculty of Civil Engineering, 1987)

G. Rosatti, L. Fraccarollo, A. Armanini, Behaviour of small perturbations in 1d mobile-bed models. River Flow, 67–73 (2004)

I.L. Rozovskii, *Flow of Water in Bends of Open Channels* (Academy of Sciences of the Ukrainian SSR, 1957)

J. Sieben, *Modelling of Hydraulics and Morphology in Mountain Rivers* (Delft University of Technology, TU Delft, 1997)

E.F. Toro, *Riemann Solvers and Numerical Methods for Fluid Dynamics: a Practical Introduction* (Springer Science & Business Media, 2013)

C. Vreugdenhil, M. De Vries, Analytical approaches to non-steady bedload transport. Res. Rep. (S 78) (1973)

Chapter 8
Local Scours

8.1 Introduction

The suspended sediment and bedload transport in a turbulent channel flow are basically governed by the turbulence generated by the bed (*wall turbulence*). However, there are situations where the bed experiences the effects of free turbulence phenomena, such as boundary layer separation and secondary circulations induced by hydraulic structures inserted in the channel. These secondary vortices interact with the bed and lead to local scour phenomena, which in their turn reinforce and heighten the original secondary circulations which generated them. These phenomena that typically appear near some hydraulic structures cannot be easily systematized since their explanation requires a complete three-dimensional approach. However, their main characteristics can be quantified by means of empirical formulae, which are also useful for dimensioning the relevant hydraulic works. The main parameters responsible for localized scours can also be conveniently identified through the dimensional analysis which is not only particularly useful to understand whether all the variables of the phenomena have been included in the empirical formulae, but also suitable for designing the works and verifying their stability. In order to get a general framework for local scours, we should first consider a width contraction due to hydraulic structures inserted into the river. To this end, the case of a local width contraction in an erodible-bed stream, seen from a one-dimensional perspective of a mobile-bed channel, may be of help.

8.2 Contraction Scour: A One-Dimensional Analysis

Consider a large quasi-rectangular channel of width B_o, in which a contraction of width, B_r, is inserted, as shown in Fig. 8.1.

Under constant liquid and solid discharges, the asymptotic solution ($\partial/\partial t = 0$) leads to uniform flow conditions upstream and downstream of the restriction with
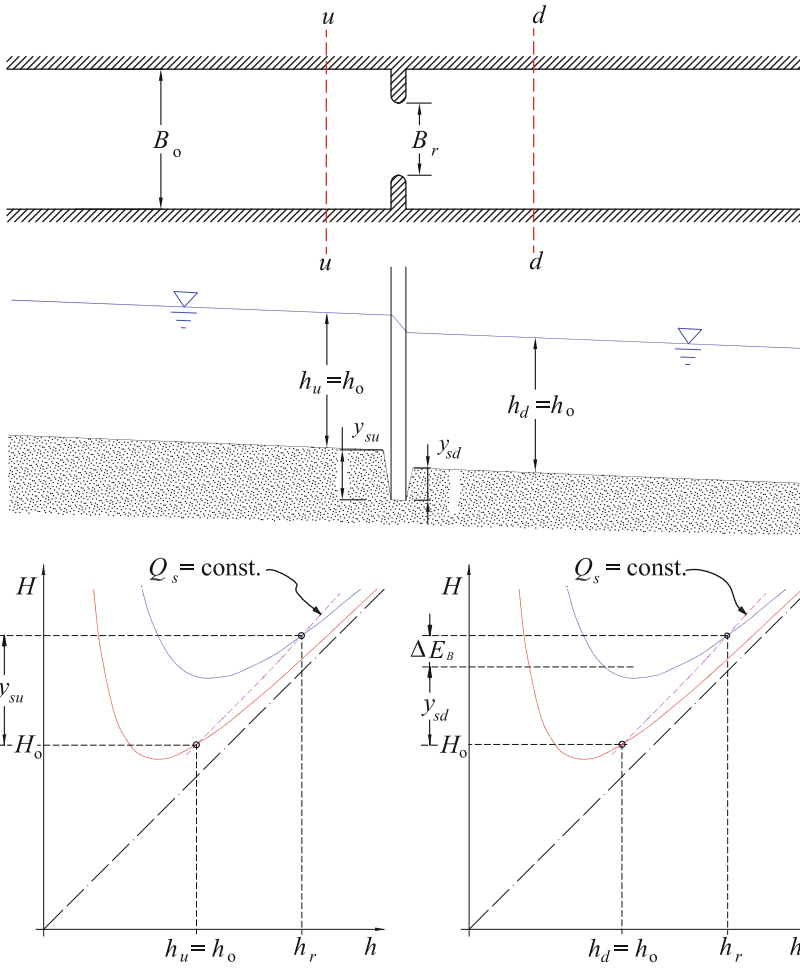
Fig. 8.1 Layout and notation of scour at width contraction

constant flow depth h_o and depth average velocity U_o, as explained in Sect. 7.5 (page 148), while across the contraction a local excavation takes place, as illustrated in Fig. 8.1. Be $h_u = h_o$ and $h_d = h_o$ the water depths upstream and downstream of the contraction, after the two- and three-dimensional effects have been exhausted, and be h_r the water depth inside the contraction.

Through the width variation, the conservation of the solid and liquid volume rates can be imposed. If, for simplicity, we assume a power law formula to express the sediment transport rate, e.g., $Q_s = c_s B U^m h^{-n}$ with $c_s, m = 3 \sim 5$ and $n = 0 \sim 0.5$ as suitable parameters independent of the velocity and the depth, we have:

$$Q = h_o B_o U_o = h_r B_r U_r \tag{8.1}$$

$$Q_s = c_s B_o U_o^m h_o^{-n} = c_s B_r U_r^m h_r^{-n} \tag{8.2}$$

which yield:

$$U_r = U_o \frac{h_o}{h_r} \frac{B_o}{B_r} = U_o R \frac{h_o}{h_r} \tag{8.3}$$

$$h_r = h_o \left(\frac{B_o}{B_r}\right)^{(-1/n)} \left(\frac{U_r}{U_o}\right)^{(-m/n)} = h_o R^{(-1/n)} \left(\frac{U_r}{U_o}\right)^{(-m/n)} \tag{8.4}$$

with $R = B_o/B_r$, the width contraction ratio.

Combining Eqs. (8.3) and (8.4), it follows:

$$U_r = U_o R^{\left(\frac{1+n}{m+n}\right)} \tag{8.5}$$

$$h_r = h_o R^{\left(\frac{m-1}{m+n}\right)} \tag{8.6}$$

With the above-mentioned values of the exponents of the transport law (e.g., $m = 3 \sim 5$ and $n = 0 \sim 0.5$), we, respectively, obtain:

$$U_r = U_o R^{(0.43 \sim 0.20)} \tag{8.7}$$

$$h_r = h_o R^{(0.57 \sim 0.80)} \tag{8.8}$$

If we hypothesize that downstream of the contraction a localized energy loss, ΔE_d (per unit weight), occurs as a consequence of a sudden enlargement, the energy balance gives:

$$H_d = H_r - y_{sd} - \Delta E_d \tag{8.9}$$

$$H_u = H_r - y_{su} \tag{8.10}$$

where H_u, H_d, H_r denote the specific energy $H = h + U^2/(2g)$ upstream, downstream, and inside the contraction, respectively, while y_{sd} denotes the variation of the bed elevation between the downstream reach and the contraction, and y_{su} the difference in bed elevation between the upstream reach and the contraction. Given that in the steady condition $H_u = H_d$, by comparing (8.9) and (8.10) we have:

$$y_{su} = y_{sd} + \Delta E_d \tag{8.11}$$

By replacing (8.5) and (8.6) into (8.10), we have:

$$\frac{y_{su}}{h_o} = R^{\left(\frac{m-1}{m+n}\right)} - 1 + \frac{F_{ro}^2}{2} \left(R^{2\left(\frac{1+n}{m+n}\right)} - 1\right) \tag{8.12}$$

that is,

$$\frac{y_{su}}{h_o} = R^{(0.80\sim0.57)} - 1 + \frac{F_{ro}^2}{2}\left(R^{(0.40\sim0.86)} - 1\right) \tag{8.13}$$

$F_{ro} = U_o/\sqrt{gh_o}$ is the Froude number of the undisturbed flow. The third right-hand term in Eq. (8.13) containing this parameter is negligible when the flow is moderately mild ($Fro \ll 1$). However, generally, y_{su} turns out to have an absolute value higher than, or at most equivalent to the difference between the water depths in the restriction and in the undisturbed section ($\Delta h = h_r - h_o$).

8.2.1 Two- and Three-Dimensional Effects

The application of the one-dimensional theory generally leads to underestimate the maximum scour depth at width contractions. This underestimation can first be justified by the fact that the velocity in the contraction is non-uniformly distributed along the width, especially in the large cross section (small depth/width ratios). As a matter of fact, the velocity of the contraction close to the lateral walls is generally higher than the average velocity assumed in the one-dimensional approach. Moreover, the spatial acceleration close to the contraction is also the cause for the vortex stretching experienced by the secondary circulations in the transverse plane (Fig. 8.2).

The vorticity strengthening leads to an increase in the transverse bed shear stress, which induces a local scour near the constriction head. Under these conditions, the local scour tends to increase and modify the bed channel, as well as reinforces and stabilizes the secondary circulation, until the local equilibrium is achieved between the entrainment force induced by the bed shear stress and the gravity force, which tends to bring the grains back onto the scour bed.
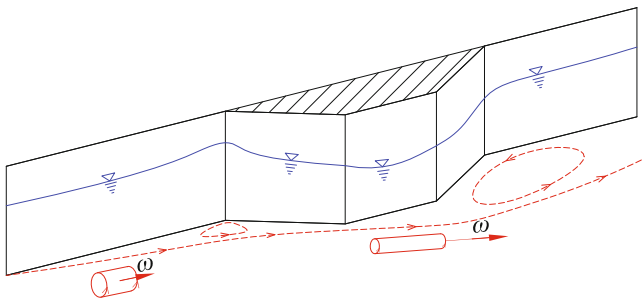
Fig. 8.2 Layout of vortex stretching close to a localized section constriction

8.2.2 Clear-Water Scours and Live-Bed Scours

The one-dimensional balance previously shown has also the limit to adopt a power law monomial formula for the sediment transport rate. This type of formulation is generally acceptable in conditions of high mobility. However, a larger validity estimation of these phenomena can be obtained by adopting a binomial formula that includes the Shields critical mobility parameter θ_c, like the Meyer-Peter and Müller formula (Eq. (5.61) at page 112):

$$Q_s = 8\,Bd\sqrt{g\,\Delta d}\,(\theta_o - \theta_c)^{3/2} \tag{8.14}$$

In this case, instead of (8.6) we obtain the following relation between the depth h_r in the constriction and the undisturbed flow depth h_o:

$$h_r = h_o \frac{R^{4/7}}{\left(1 - \dfrac{\theta_c}{\theta_o}(1 - R^{-2/3})\right)^{3/7}} \tag{8.15}$$

where θ_o denotes the mobility parameter of the undisturbed flow. With a procedure analogous to that of Sect. 8.2 (page 173), we finally obtain:

$$\begin{aligned}
\frac{y_{sm}}{h_o} = {} & \frac{R^{4/7}}{\left(1 - \dfrac{\theta_c}{\theta_o}(1 - R^{-2/3})\right)^{3/7}} - 1 \\
& + \frac{F_{ro}^2}{2}\left(R^{6/7}\left(1 - \frac{\theta_c}{\theta_o}(1 - R^{-2/3})\right)^{6/7} - 1\right)
\end{aligned} \tag{8.16}$$

A similar result was achieved by Laursen (1962) on the basis of a previous work of Straub (1940). Moreover, it is worth observing that in the restricted section an erosion can also occur even if the mobility in the upstream section is lower than the critical one ($\theta_o \leq \theta_c$). The erosion proceeds until the incipient motion condition is achieved inside the constriction. The prediction of the maximum excavation carried out with the 1D theory given by Eq. (8.16) must, however, be completed by adding the effect of the secondary circulations. The excavation process that occurs when the mobility parameter of the undisturbed flow is less than the critical one is identified as clear-water scour. If this is the case, by neglecting the kinematic effects (the third term of Eq. (8.16)), e.g., if $F_{ro} << 1$, the equation becomes:

$$\frac{y_{sm}}{h_o} = R^{6/7}\left(\frac{\theta_o}{\theta_c}\right)^{3/7} - 1 \tag{8.17}$$

We easily realize that the scour extent in this condition can be higher than that occurring when, other parameters being equal, the mobility of the upstream flow
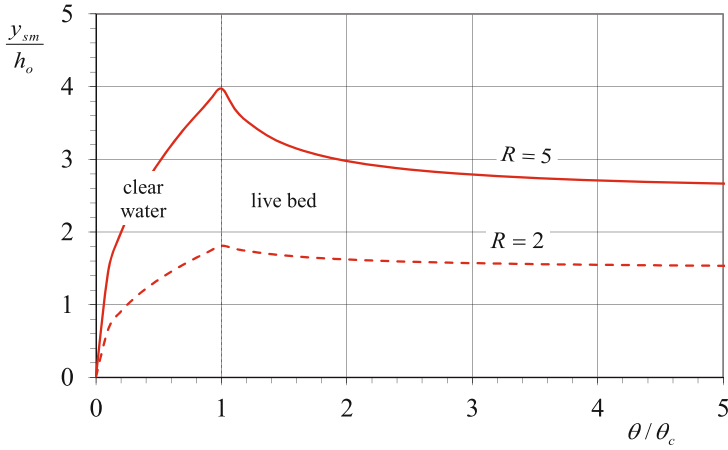
Fig. 8.3 Maximum scour value normalized to the undisturbed water depth h_o in function of the ratio between mobility and critical parameters of the undisturbed flow, for different values of the width contraction ratio R, according to the one-dimensional theory
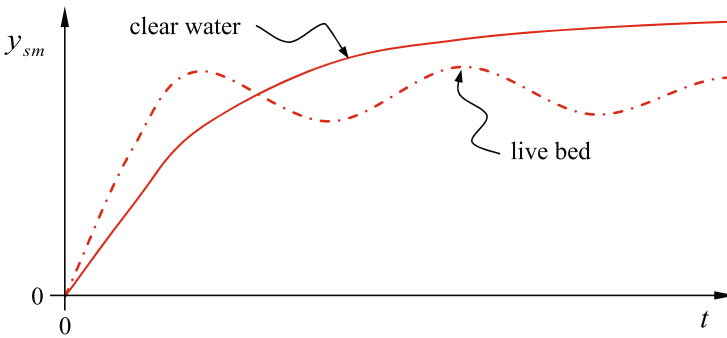
Fig. 8.4 Typical time development of a local scour in clear-water and live-bed conditions

exceeds the critical mobility because, in the latter condition, the solid material carried from upstream by the incoming flow feeds the excavation and reduces its maximum value (*live-bed scour*) (Fig. 8.3).

The scour development is observed to have a gradual, quite monotonous trend in clear-water conditions, while it can show an oscillatory behavior in *live-bed* conditions (Fig. 8.4).

Table 8.1 Types of abutments in Hoffmans' formula (Eq. 8.18) (Hoffmans and Verheij 1997)

Types of artefacts	Acronym	b/l	α	K_b
Circular pier	CP			1.5
Semicircular pier	SCP	<3		1.5
Semicircular end	SCE1	<3		1.5
	SCE2	3−5		2.25
	SCE3	>5		3.0
Vertical wall abutment	VWA			3.0
Streamlined wing-wall abutment	WWS1	0.2	45°	0.75
	WWS2	0.2	35−45°	1.25
Blunt wing-wall abutment	WWB1	0.5−1.5	30°	1.5
	WWB2	1.5−2.5	30°	2.0
Triangular abutment	TS		45°	1.0
Spill-through abutment (1.5:1)	ST1	0.2		0.75
Spill-through abutment (1:1)	ST2	0.2		1.0
Spill-through abutment (1:1)	ST2	0.5−1.5		1.5

8.2.3 Empirical Formulae for the Maximum Scour Depth at Section Contractions

The maximum scour depth also depends on the shape of the structure forming the constriction, usually a bridge abutment or some other artifacts, or provisional works built during the construction phase of complex hydraulic structures.

The effect of secondary circulations on the maximum scour depth can be hardly deduced analytically, so we need to adopt empirical approaches. In the literature, there are different empirical formulae to quantify the maximum erosion near a constriction: many also have a non-dimensionally correct structure and therefore are valid only under specific conditions, insomuch that they do not take some generally important parameters into consideration.

Among them, Hoffmans' formula (Hoffmans and Verheij 1997) seems to be structured in a rather complete manner:

$$\frac{y_{sm}}{h_o} = R^{2/3} - 1 + K_b \frac{(B_o - B_r)}{h_o} \tanh \frac{h_o}{B_o - B_r} \quad \text{for} \quad U_o > U_{cr} \qquad (8.18)$$

VWA: Vertical wall abutment

SCE: Semi-circular end abutment

VW: Wing-wall abutment,
Streamlined

VW: Wing-wall abutment,

TS: Triangular-shaped abutment

ST: Spill-through abutment
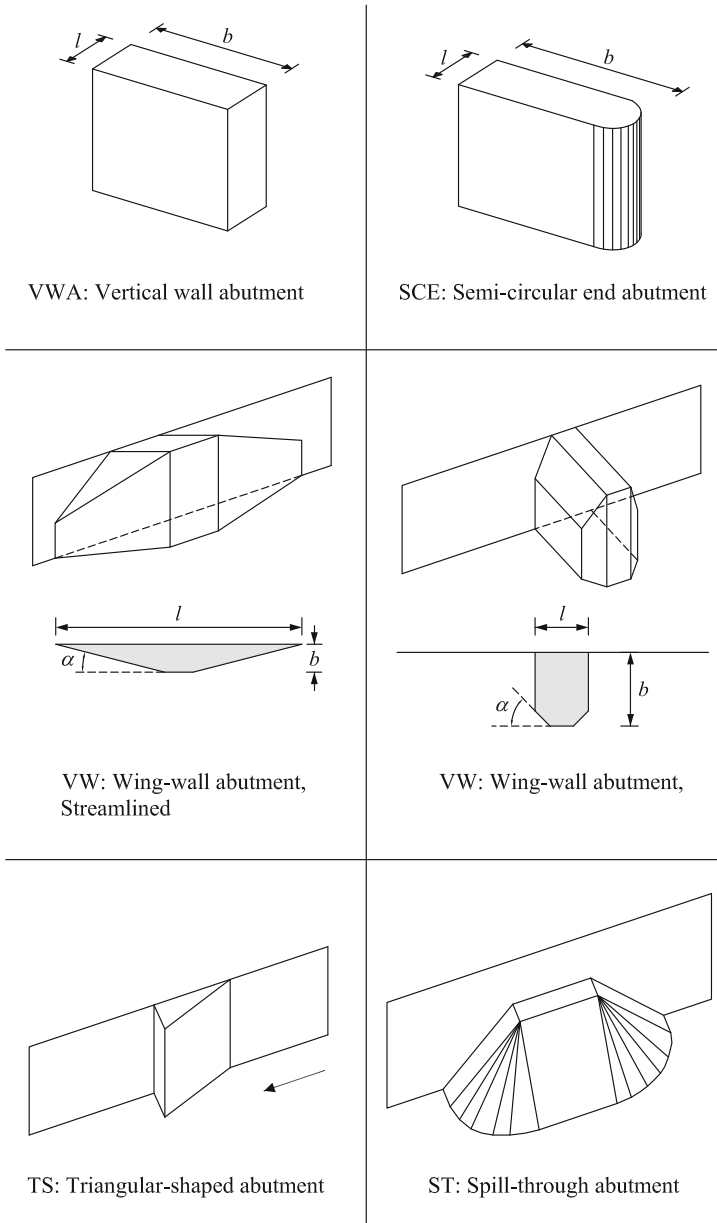
Fig. 8.5 Types of abutments in Hoffmans' formula (Eq. 8.18) (Hoffmans and Verheij 1997)

where y_{sm} is the maximum scour depth and K_b is a coefficient which basically depends on the form of the abutment (Table 8.1). Equation (8.18) is valid in live-bed conditions ($U_o > U_{cr}$). Quite interestingly, the first two terms in (8.18) coincide with the scour in the one-dimensional approach (Eq. 8.13) by assigning the value 0.667 to the exponent and neglecting the kinematic effect of the flow ($F_r \ll 1$); the third term of Eq. (8.18) represents the secondary effects. The formula is valid for quite long restrictions. For relatively high depths ($h_o > B_o - B_r$), the formula is reduced to:

$$\frac{y_{sm}}{h_o} \simeq K_b \frac{(B_o - B_r)}{h_o} \tag{8.19}$$

while for low depths we have:

$$\frac{y_{sm}}{h_o} \simeq K_b \tag{8.20}$$

Table 8.1 shows the values of the form coefficient K_b. The acronyms correspond to the types described in Fig. 8.5.

8.2.4 Particle Size Effect

The observations so far show that the influence of particle size on the maximum scour depth is not significant, unless in the case of the flow velocity close to that of incipient motion, as also appears from Eq. (8.17) by using Meyer-Peter and Müller's formula. According to Melville (1992) and Graf and Altinakar (1998), the particle size effect becomes important when the ratio b/d_{50} between the contraction width b and the material d_{50} exceeds 50, that is:

$$y_{sm} \simeq 2b \quad \text{for} \quad b/d_{50} > 50 \tag{8.21}$$

8.3 Scour at Bridge Piers

The bridge pier placed in a stream can be seen as a width reduction in the middle of the flow, rather than on lateral walls. Thus, the approach to this problem will be closely analogous to that adopted for the section contraction. The scour at bridge piers is a topic of great importance, widely and deeply analyzed, even with sophisticated mathematical models, nonetheless the approach based on empirical formulations turns out to be still the most diffused and reliable. The scour starts laterally to the pier, in the region of maximum longitudinal acceleration, to migrate to the front and rear of the pier. Particularly interesting is the fact that as the local scour develops, the secondary vortices strengthen at both lateral sides of the pier, thus creating a single
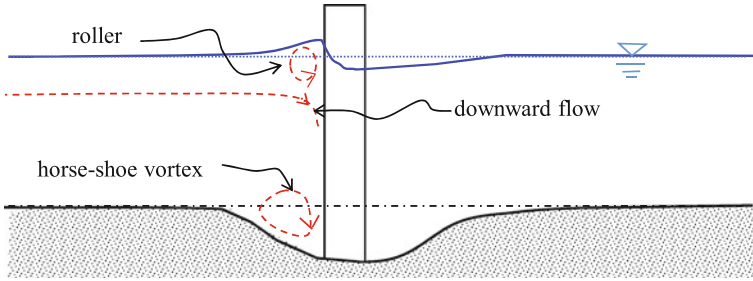
Fig. 8.6 Layout of a longitudinal scour profile localized near a bridge pier
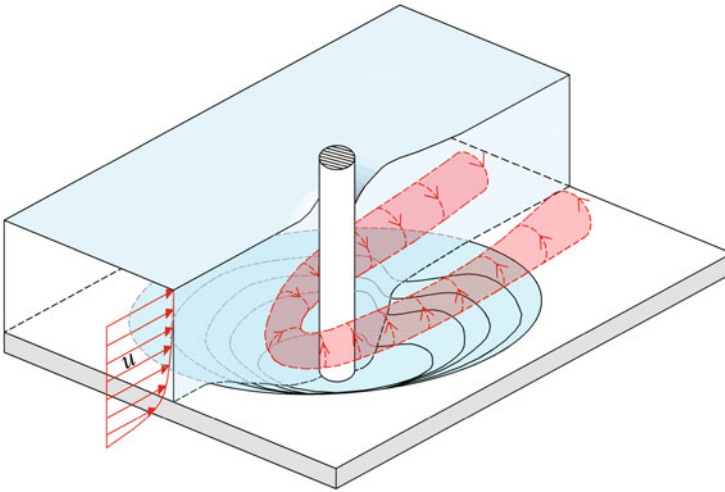
Fig. 8.7 Layout of the horseshoe vortex near the localized scour of a bridge pier

horseshoe vortex (Chabert and Engeldinger 1956; Raudkivi and Sutherland 1981) (Figs. 8.6 and 8.7).

The wake vortices downstream of the pier also contribute to the scour; they are due to the separation of the boundary layer whose characteristics are often typical of the von Kármán shedding with Strouhal numbers $S_t = f_S D_p / U_o \simeq 0.19 \sim 0.21$ for circular-shaped piers, where S_f is the vortex frequency.

8.3.1 Maximum Scour at Bridge Piers

In bridge piers, the effects of the flow contraction, analyzed with the one-dimensional theory, can often be neglected, in that the pier width is modest compared to the stream width. However, in the literature this effect is sometimes neglected even if, strictly

speaking, it should not be; so this aspect needs to be considered before applying formulae that do not take this effect into account.

The different effects and parameters, which contribute to determine the maximum scour depth, can be assessed by the dimensional analysis. Generally speaking, the parameters influencing the maximum scour entity y_{sm} at a bridge pier are: the undisturbed flow velocity U_o, the water depth h_o, the undisturbed bed width B_o, the bed shear stress τ_o, the water density ρ, the bed-material density ρ_s, the water viscosity μ, the gravity acceleration g, the longitudinal dimension of the pier D_p, or the diameter in circular piers, the pier shape which can be expressed by means of a proper shape factor Sf_p, the mean bed-material diameter d and, if necessary, a significant parameter of the particle size distribution (for instance, its relative variance σ_g). In other words, we have:

$$f_1(y_{sm}, U_o, h_o, B_o, \tau_o, \rho_s, \rho, \mu, g, D_p, Sf_p, d, \sigma_g) = 0 \qquad (8.22)$$

The dimensional analysis makes it possible to reduce the thirteen parameters which appear in the previous relation into the following ten dimensionless groups:

$$\frac{y_{sm}}{D_p} = f_2 \left(\frac{u_*^2}{g\,\Delta\,d}, \; \frac{\rho u_* d}{\mu}, \; \frac{B_o}{D_p}, \; \frac{h_o}{D_p}, \; \frac{d}{D_p}, \; \frac{U_o}{u_*}, \; \frac{U_o}{\sqrt{g\,h_o}}, \; Sf_p, \; \sigma_g \right) \qquad (8.23)$$

where we set $u_*^2 = \tau_o/\rho$ and $\Delta = (\rho_s - \rho)/\rho$.

The left-hand group represents the maximum scour non-dimensionalized with respect to the pier width. This parameter, being apparently the most significant, is usually chosen to non-dimensionalize the maximum scour and replaces the flow depth used in the one-dimensional approach.

The first two groups on the right-hand side of the equals sign, $\left(\theta = u_*^2/(g\,\Delta\,d)\right)$ and $(R_* = \rho u_* d/\mu)$, are respectively the flow mobility parameter and the grain Reynolds number, two parameters already highlighted by the Shields analysis on incipient motion. They especially influence the incoming undisturbed flow, in the sense that they determine the undisturbed sediment transport rate and bed forms.

The third parameter (B_o/D_p) is the relative pier width, already focused by the one-dimensional theory of contractions: such a parameter is especially significant when one or more piers produce a considerable reduction in the flow width.

The fourth parameter (h_o/D_p) represents the encumbrance of the pier with regard to the water depth, while (d/D_p) denotes the grain size compared to the pier dimension. The ratio between these two parameters (h_o/d) represents the relative grain submergence, the last being a crucial element in itself in case of low submergence and deeply affecting the following sixth parameter. The sixth parameter represents the friction coefficient (e.g., $U/u_* = \chi/\sqrt{g}$ according to Chézy's formula) which usually depends on the relative roughness (e.g., the ratio h_o/d between the previous two parameters) and on the mobility parameter in case of roughness due to bed forms and grain Reynolds number; both dimensionless groups can then replace this parameter.

The seventh group is the Froude number of the undisturbed flow ($F_{ro} = U_o/\sqrt{gh_o}$), a parameter mainly affecting the morphodynamic conditions of the undisturbed flow. Obviously, should the parameter be rather high, it can influence especially the scour in front of the pier, since this parameter is a decisive factor for the growth of the free surface on the pier front.

The eighth and the ninth parameters denote the pier form and the particle size gradation of the bed material, respectively.

Quite clearly, these parameters can each be combined with the others, and therefore, the maximum scour depth can be expressed in function of dimensionless groups which are combinations of those previously mentioned.[1] The problem can be approached with the scheme used for width contractions, that is, by considering the scour as a combination of one- (Eq. 8.16) and two- or three-dimensional effects:

$$
\frac{y_{sm}}{D_p} = \frac{h_o}{D_p}\left[\frac{R^{4/7}}{\left(1 - \frac{\theta_c}{\theta_o}(1 - R^{-2/3})\right)^{3/7}} - 1\right.
$$
$$
\left. + \frac{F_{ro}^2}{2}\left(R^{6/7}\left(1 - \frac{\theta_c}{\theta_o}(1 - R^{-2/3})\right)^{6/7} - 1\right)\right]
$$
$$
+ K_{Fr}(F_{ro})K_h(\frac{h_o}{D_p})K_d(\frac{d}{D_p})K_{Sf}(Sf_p)K_\sigma(\sigma_g) \qquad (8.27)
$$

where $K_{Fr}(F_{ro})$, $K_h(h_o/D_p)$, $K_d(d/D_p)$, $K_{Sf}(Sf_p)$, $K_\sigma(\sigma_g)$ denote the two- or three- dimensional effects which are induced by the parameters indicated between brackets. This simplified approach makes it possible to separate the effects of the

---

[1]In the literature, especially that developed at the University of Auckland (Raudkivi and Ettema 1977; Raudkivi and Sutherland 1981; Melville 1992) but also by Graf and Altinakar (1998), the flow velocity is not directly included among the parameters which determine the maximum scour depth. In fact, the parameters identified by these authors are:

$$
f_3(y_{sm}, h_o, u_*(\text{or } \tau_o), \rho_s, \rho, \nu, g, D_p, Sf_p, d, \sigma_g) = 0 \qquad (8.24)
$$
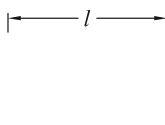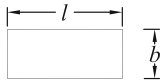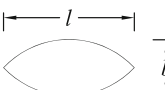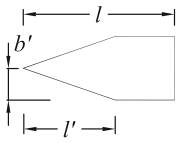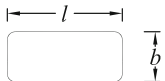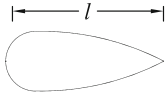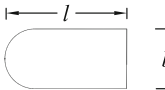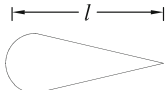
The dimensional analysis allows Eq. (8.24) with eleven parameters to move to the relation with the following seven dimensionless groups:

$$
f_4\left(\frac{y_{sm}}{D_p}, \frac{u_*^2}{g\Delta d}, \frac{u_* d}{\nu}, \frac{h_o}{D_p}, \frac{d}{D_p}, \frac{\rho_s - \rho}{\rho}, Sf_p, \sigma_g\right) = 0 \qquad (8.25)
$$

Here, we consider the hypothesis of the uniform flow upstream of the pier, and thus, we assume that the ratio (U/u_*) is assigned a priori and is equal to the dimensionless friction coefficient, for instance, $(U = u_*\chi/\sqrt{g})$, being $\chi = func(\theta, d/h_o, R_*)$ the Chézy friction coefficient. The Froude number, instead, appears in Eq. (8.23) and is replaced by a combination of other parameters to obtain the reduced relative density of the material or vice versa, e.g.,

$$
\Delta\frac{u_*^2}{g\Delta d}\frac{d}{h_o}\left(\frac{U}{u_*}\right)^2 = \frac{U^2}{gh} = F_r^2 \qquad (8.26)
$$

.

Table 8.2 Shape coefficients for different pier types

$D_P = b$	$b:l$	K_{Sf}	$D_P = b$	$b:l$	$b':l'$	K_{Sf}
circle (D_P)		1.22		1:2		0.83
				1:3		0.80
				1:5		0.61
rectangle	1:1	1.22				
	1:3	1.08	wedge (b', l')	1:03	1:2	0.76
	1:5	0.99		1:03	1:4	0.65
lens	1:2	0.80				
	1:3	0.70	teardrop (rounded)	1:3.5		0.80
rounded-end rectangle	1:4	0.76				
round-nose	1:3	0.90	teardrop	1:5		0.86

single parameters. In most applications, such effects are prevailing over the contraction effects. Therefore, the 1D effects are either neglected or, if minor, included in K parameters concerning the two- or three-dimensional effects. In other words, the maximum scour depth is frequently expressed as follows:

$$\frac{y_{sm}}{h_o} = K_{Sf} K_\theta K_{Fr} K_h K_d K_\sigma \tag{8.28}$$

In the next subsections, we are going to examine the influence on the maximum scour of some of the most important parameters involved in the previous relations.

8.3.1.1   Effects Due to the Pier Form

Most laboratory tests concern the scours at cylindrical piers with circular cross sections. If we then assume this pier type as reference, the values related to differently shaped piers can be obtained by multiplying the maximum scour depth of the circular pier by a shape factor (K_{Sf}), whose values for different pier shapes are given in Table 8.2.

For example, quite understandably, a square-section pier will create a recirculating area lateral to the pier, larger than the square side, thus causing a deeper scour than

that produced by a circular pier with a diameter equal to the square side. Another
parameter affecting the scour is the pier alignment. In case of obliquely aligned piers,
the pier width is represented by its projection normal to the flow direction. An elongate
pier nonaligned with the flow causes an encumbrance significantly higher than that
produced by an aligned pier. The effects are, however, much more complicated than
it appears at first sight, especially in the presence of marked pier asymmetries in
the direction of flow. Studies on this effect were made by Tison (1940) and later by
Laursen and Toch (1956), who produced an experimental graph widely mentioned
and completely convincing. We suggest Froehlich's (1988) relation, valid for angles
30°:

$$K_\alpha = \left(\cos \alpha + \frac{l}{b} \sin \alpha \right)^{0.62} \tag{8.29}$$

The parameter K_α is a factor which multiplies the K_{Sf} in order to consider the effect
of the pier nonalignment to the flow.

8.3.1.2   Influence of the Flow Mobility Parameter

In general, the direct dependence of the maximum scour depth on the flow mobility
parameter alone is not frequently focused in the literature. However, the distinc-
tion between clear-water and live-bed scour conditions, pointed out in the previous
section, is of paramount importance. The previous considerations (Sect. 8.2.2) are
also worth for the scour around bridge piers.

In case of a clear-water scour near a pier, the longitudinal vortex stretching leads
to a lateral scour which soon moves to the upward pier. In that region, the scour is
reinforced with the downward flow along the upstream face of the pier. The scour then
migrates downward (Graf and Altinakar 1998). In equilibrium condition, along the
scour sides there occurs a balance between the gravity force which moves particles
toward the scour bed and the shear stress which, induced by the secondary vortex,
pushes them in the opposite direction. The scour slope at the upper pier is steeper
than the lower slope: therefore, the scour appears to be elongated downwards.

Breusers et al. (1977) observed, and later Raudkivi and Ettema (1977) confirmed
after an accurate survey, that:

- for ($\theta_o/\theta_c \leq 0.5$), there is virtually no scour;
- for ($0.5 \leq \theta_o/\theta_c \leq 1$ (*clear-water scour condition*), the scour depth was observed
  to extend when the ratio (θ_o/θ_c) increases until the maximum value at ($\theta_o/\theta_c \simeq 1$);
- for ($\theta_o > \theta_c$) (*live-bed*, that is *sediment transport fed from upstream*), a balance
  occurs between the incoming load and the sediment load flowing inside the scour.
  The maximum scour depth stops increasing with (θ_o/θ_c). The maximum scour
  depth fluctuates with time and is, on the average, $10-30\%$ lower than the mean
  scour determined in clear-water conditions, the other parameters being equal (Shen
  et al. 1969).
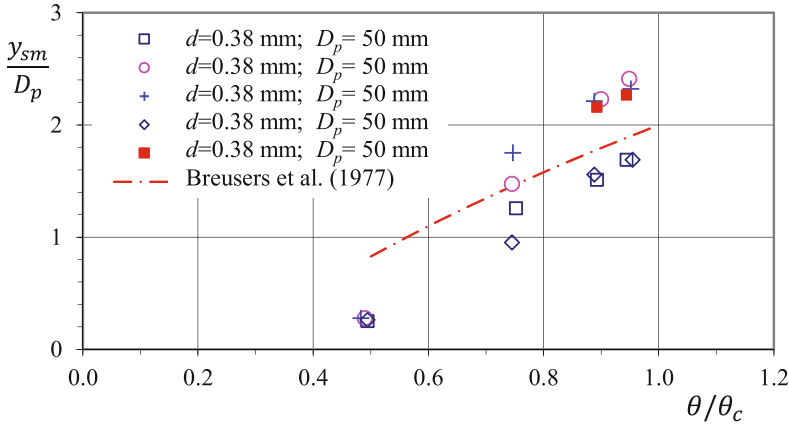
Fig. 8.8 Behavior of the maximum scour with the mobility parameter (Raudkivi and Ettema 1977) and comparison with the formula (8.30) of Breusers et al. (1977)

The dependence of the maximum scour depth on the mobility parameter has never been quantified precisely; it is mostly perceived in the interval ($0.5 \leq \theta_o/\theta_c \leq 1$). According to Breusers et al. (1977), the dimensionless maximum scour is linearly proportional to the mobility parameter which, however, includes also the dependence on the ratio (h_o/D_p):

$$\frac{y_{sm}}{D_p} = 2K_{Sf}\left(2\frac{\theta_o}{\theta_c} - 1\right)\tanh\frac{h_o}{D_p} \tag{8.30}$$

Figure 8.8 illustrates some experimental laboratory results obtained by Raudkivi and Ettema (1977). The same figure also shows the comparison with the formula (8.30) of Breusers et al. (1977) that sets ($K_{Sf} = 1$) since the piers are circular.

This relation appears to underestimate the scour in some cases and, as a matter of fact, in a more recent work, among whose authors is Breusers himself (Breusers 1965), the formula is no more mentioned. And indeed, with regard to applications, it is advisable to refer to the maximum scour depth in conditions of incipient motion ($\theta_o/\theta_c \simeq 1$) in the undisturbed section, expressed as follows:

$$\frac{y_{sm}}{D_p} \simeq 2.45 \tag{8.31}$$

This result is, however, influenced also by the sediment particle size distribution, as will be explained in the next Sect. 8.3.1.5. The maximum scour depth occurs when in the incoming flow the velocity is close to the incipient motion velocity, provided there are no bed forms (*ripples*). In this case, the maximum depth is given by Eq. (8.31). The relative maximum scour depth reduces until it reaches the minimum value for ($\theta_o/\theta_c \simeq 2.2 \sim 2.6$), and then it increases again when the undisturbed
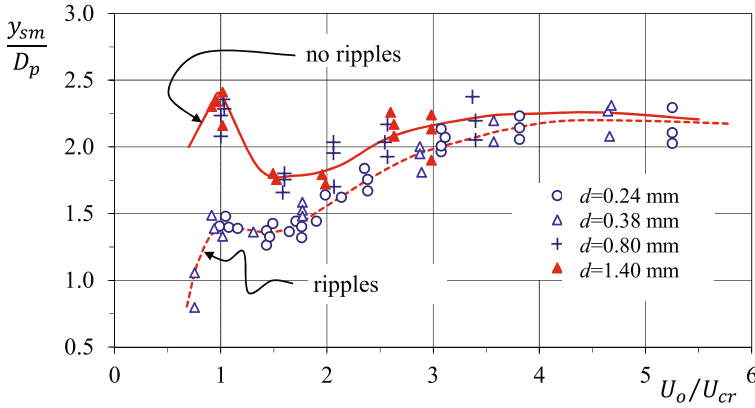
Fig. 8.9 Maximum scour depth at a circular pier when the relative velocity varies with high relative submergence values. Laboratory data by Chee (1982) (revised by Breusers and Raudkivi (1991), page 77)

velocity rises. The curve expressing the relative maximum depth in function of the velocity related to the incipient motion velocity shows two peaks, as illustrated by Fig. 8.9, parameterized to the velocity and not to the mobility parameter (consider $\theta_o/\theta_c \propto (U_o/U_{cr})^2$).

The figure also shows the behavior in the presence of ripples in the incoming flow. The relative scour is significantly lower. The double peak remains but the former, corresponding to the condition of incipient motion, results extremely lower than the latter. This can be accounted for by the fact that near the latter peak the flow is at near-critical conditions ($F_r \simeq 1$) and therefore with no bed forms.

8.3.1.3   Influence of the Froude Number

Some empirical formulae link the maximum scour depth directly to the Froude number of the flow, e.g., the following formula from Colorado State University (Johnson 1992):

$$\frac{y_{sm}}{D_p} = 2 F_r^{0.43} \left(\frac{h_o}{D_p}\right)^{0.65} \tag{8.32}$$

It should be pointed out that the effects of the Froude number cannot be always separated by those of the mobility parameter. Indeed, if the tests do not use material with different density, the two effects cannot be separated, as easily verified with the undisturbed flow (near-uniform flow):

$$F_r^2 = \frac{U^2}{gh} = \frac{U^2}{u_*^2} \frac{u_*^2}{g \Delta d} \Delta \frac{d}{h_o} = \frac{\chi^2}{g} \theta \Delta \frac{d}{h_o} \tag{8.33}$$
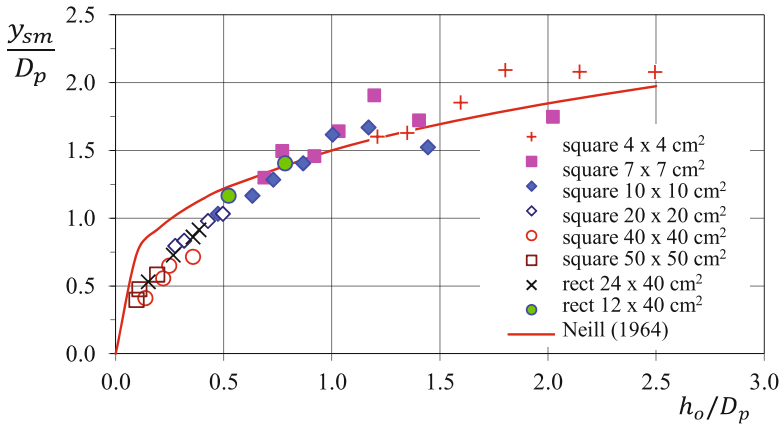
Fig. 8.10 Behavior of the maximum scour with the water depth of undisturbed flow (Basak et al. 1977) and comparison with Neill (1964) formula

We can see that with constant material density Δ, the Froude number F_r and the mobility parameter θ only differ by the effect of the relative roughness d/h that intuitively has scarce influence on the localized scour.

Therefore, Eq. (8.32) and other similar formulae containing the parameter F_r are, more than often, simple expressions equivalent to those with the mobility parameter previously mentioned, e.g., Eq. (8.30). Unlike the latter, which leads to underestimate the scour depth, Eq. (8.32) tends, on the contrary, to overestimate a scour.

8.3.1.4   Influence of the Flow Depth

As already said, the scour near a pier is basically governed by secondary circulations and especially by the horseshoe vortex (Raudkivi and Ettema 1977) in asymptotic conditions with constant solid and liquid discharges; the influence of water depth is thus important only if it is relatively small.

Figure 8.10 illustrates some results on the influence of the relative flow depth (non-dimensionalized by the pier size) obtained by Basak et al. (1977) for $(\theta_o/\theta_c > 1)$, showing that when (h_o/D_p) increases, the relative maximum scour (y_{sm}/D_p) tends to the asymptotic value 2.1.

In case of circular piers, the Bonasoundas (1973) experiments show a slightly lower asymptotic value, equal to 1.75. According to Neill (1964) for a circular pier, we have:

$$\frac{y_{sm}}{D_p} = 1.5 \left(\frac{h_o}{D_p} \right)^{0.3} \tag{8.34}$$
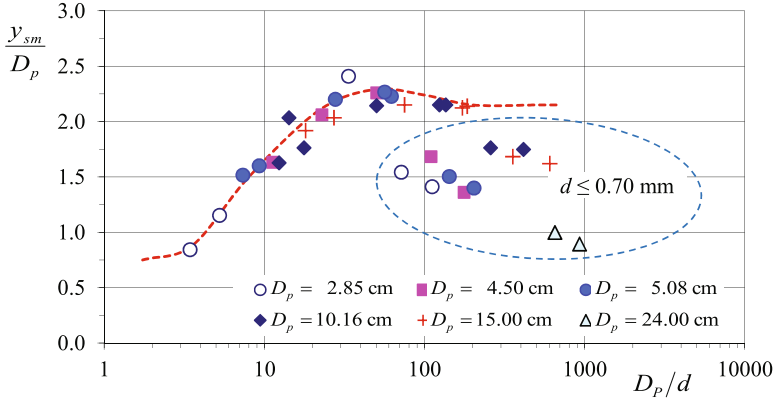
Fig. 8.11 Variation of the maximum scour with the material diameter for $\theta_o/\theta_c = 0.90$ (Raudkivi and Ettema 1977)

A similar relation was suggested by Breusers et al. (1977):

$$\frac{y_{sm}}{D_p} = 1.35 \left(\frac{h_o}{D_p} \right)^{0.3}$$

$$(8.35)$$

In case of the dune regime in the incoming flow (live-bed condition), the scour calculated by means of (8.34) should, according to the authors, be increased by a factor equal to $0.5 H_{Dune}$.

The fact that both the flow velocity and the material diameter are not present in Eq. (8.34) may suggest that it can be applied only in the presence of sediment transport in the undisturbed flow.

8.3.1.5   Particle Size Influence

The effect of the material size on the maximum scour was also studied by Raudkivi and Ettema (1977). Figures 8.11 and 8.12 show the values of the relative maximum scour in equilibrium conditions in function of the relative particle-grain size, d, non-dimensionalized by the pier diameter D_p for $\theta_o/\theta_c = 0.90$ and $\theta_o/\theta_c = 0.95$, respectively.

The first distinction concerns the presence or absence of *ripples* ($d \leq 0.70$ mm), which significantly reduces the scour depth. In case of *absence of ripples*, the scour peak occurs in the interval $130 \geq D_p/d \geq 30$ where we obtain $y_{sm}/D_p \simeq 2.45$.

If the sediment size is large enough compared to the pier diameter ($D_p/d \leq 30$), the maximum scour systematically decreases at decreasing particle size.

Moreover, the two figures confirm that the maximum scour occurs at conditions very close to the incipient motion in the incoming flow.
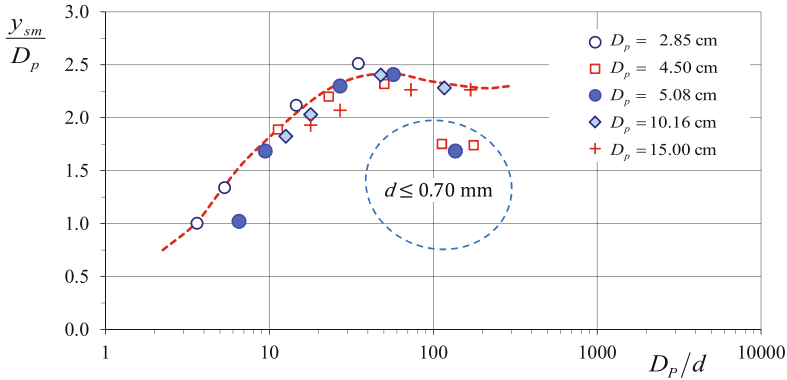
Fig. 8.12 Variation of the maximum scour with the material diameter for $\theta_o/\theta_c = 0.95$ (Raudkivi and Ettema 1977)

The particle sorting is proved to be an extremely decisive parameter especially when the bed tends to get armored. The local armoring can even represent a system for reducing the erosion depth. Such an effect was studied by Raudkivi and Ettema (1977) in slightly lower conditions than those of the incipient motion in the incoming flow. The next figure shows the survey results, expressed in function of the parameter K_σ, a multiplier of the other effects according to Eq. (8.28). The parameter K_σ in the figure is thus defined as:

$$\frac{y_{sm}(\sigma_g)}{D_p} = K_\sigma \frac{y_{sm}(\sigma_g = 1)}{D_p} \tag{8.36}$$

where $y_{sm}(\sigma_g = 1)$ denotes the scour with uniform material and particle-grain size equal to the d_{50} of the mixture.

Also in this case, two performances can be seen with or without the development of ripples ($d_{50} \leq 0.7$ mm). For the material mobility corresponding to d_{50} very close to the critical mobility ($1 > \theta_o/\theta_c \geq 0.8$), in the presence of ripples for the uniform material ($d_{50} \leq 0.7$ mm), the maximum scour occurs with non-uniform materials characterized by particle size curves whose standard deviations σ_g range between 1.5 and 2. In this case, the non-uniformity of the material can suppress the ripples in the upstream section, without any visible armoring effects in the scour (Fig. 8.13).

If the undisturbed flow mobility θ_o is lower than the critical one ($\theta_o < 0.8\,\theta_c$), the bed upstream the pier remains flat and the effect of the sediment non-uniformity, compared to the homogeneous material, tends to form an armoring effect in the scour which reduces its depth: the parameter K_σ tends to decrease monotonically when the sediment non-uniformity increases (standard deviation σ_g of the particle size curve), whether or not the ripples occur in the undisturbed section. When the standard deviation increases, the coefficient K_σ tends to values of around 0.15.
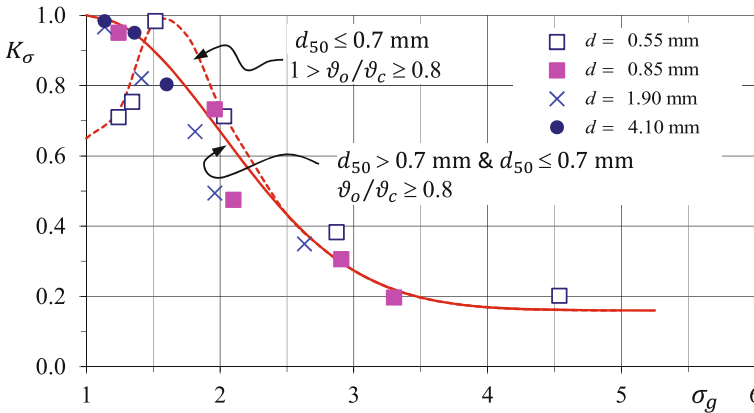
Fig. 8.13 Variation of coefficient K_σ with the standard geometric deviation of the particle-size curve of the material (Raudkivi and Ettema 1977)

Very often in order to reduce the scour depth, the bed is armored artificially around the pier. Should this be the case, Raudkivi and Ettema (1977) suggest to calculate the material size through the Shields criterion with regard to a bed shear stress τ_{max}, assessed with reference to the undisturbed value τ_o, with the following simple expression:

$$\tau_{max} = 4\tau_o \tag{8.37}$$

The thickness of the armoring layer must be at least equal to $2d_{50}$, even if a thicker armoring layer is more suitable. It is not advisable to rely only on the armoring layer without checking if the upstream or downstream conditions are able to undermine it. In order to reduce the secondary circulations, and therefore the scour, also some flow-altering countermeasures have been proposed. The installation of a collar with a $3D_p$ diameter attached to the pier was considered as especially effective (Chabert and Engeldinger 1956; Raudkivi and Sutherland 1981; Hoffmans and Verheij 1997) around $0.4D_p$ high from the bed. According to the authors, such a device would be able to reduce the scour by 60%.

Special attention must be paid to the case of a localized erosion when the armoring layer is broken by the localized effects around the pier. The case was studied in detail by Raudkivi and Ettema (1977), with reference to the collapse of the Rangitikei Bridge, at Bulls, in New Zealand in 1973. Ettema observed that the most dangerous case occurs when the breakage of the armoring layer initiates in the sections downstream the bridge, in particular if the breakage is not confined to a limited region around the pier but rather affects the whole transverse section. In this case, the bed downstream of the pier becomes mobile, while the bed upstream of the pier cannot be eroded thanks to the armoring layer.

Such a condition leads to the bed lowering y_{s1-2} (Fig. 8.14), assessable by means of the one-dimensional theory by imposing the liquid mass and momentum conservation
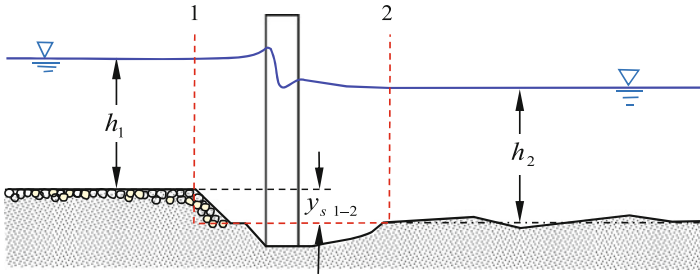
Fig. 8.14 Scour layout in the presence of armoring upstream of the pier (Raudkivi and Ettema 1977)

together with the incipient motion condition calculated with reference to the sub-layer grain size (i.e., the sediment below the armoring layer) in the downstream reach:

$$U_1 h_1 = U_2 h_2$$
$$\frac{1}{2}\rho g h_1^2 + \frac{1}{2}\rho g y_{s1-2}(h_1 + h_2) + \rho h_1 U_1^2 = \frac{1}{2}\rho g h_2^2 + \rho h_2 U_2^2$$
$$\theta_2 = \theta_c \tag{8.38}$$

Given that the downstream velocity can be expressed, in uniform flow, by means of the Chézy formula, $(U_2 = u_{*2}\chi/\sqrt{g})$, the system provides the following solution:

$$\frac{y_{s1-2}}{h_1} = F_{r1}A_{\theta2} - 1 + 2\frac{F_{r1}}{A_{\theta2}}\frac{1 - F_{r1}A_{\theta2}}{1 + F_{r1}A_{\theta2}} \tag{8.39}$$

where $F_{r1} = U_1/\sqrt{gh_1}$ represents the Froude number of the undisturbed flow and $A_{\theta2} = \sqrt{g}/\chi\sqrt{h_1/d\Delta\theta_c}$ is a parameter which considers the hydrodynamic and morphodynamic conditions of the downstream part. The value y_{s1-2} must be further increased with the scour produced by the secondary effects.

8.3.2 Local Scour at Pile Groups

Often the bridges are supported by two or multiple piles, more or less aligned with the flow direction. Although this case can be led to the previous one, some observations are to be added (Raudkivi and Sutherland 1981).

In general, the scour hole deepens in front of the upstream pier. The maximum scour depth (around 1.2 times the scour of a single pier) takes place when the distance between the two piers is around three times the diameter D_p of the single pile. The presence of the upstream pier produces a hiding effect on the downstream pier, thus reducing its upstream scour. The effect is also perceived downstream of the second
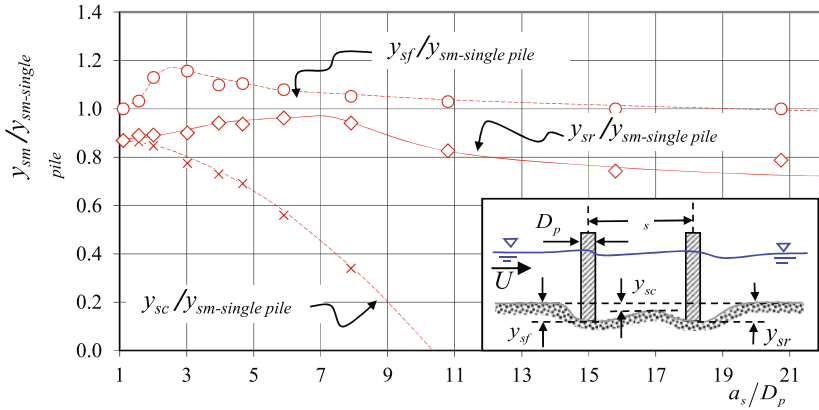
Fig. 8.15 Relative maximum scour depth for two in-line piles in function of the dimensionless pile spacing (Raudkivi and Sutherland 1981)
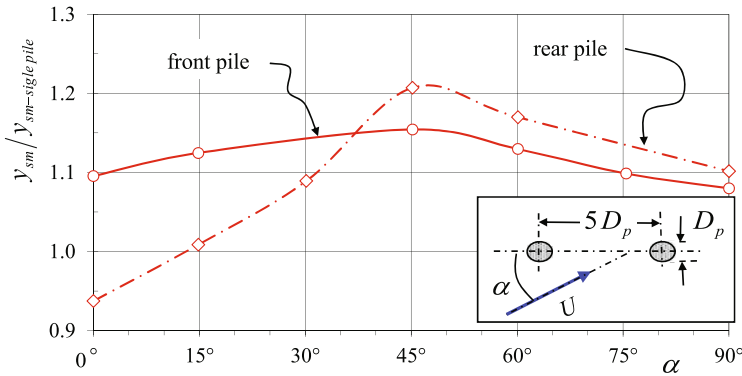
Fig. 8.16 Relative maximum scour depth for two in-line piles in function of the angle of attack (Raudkivi and Sutherland 1981)

pier, where the scour proves to be 20% lower than observed with a single pier (Fig. 8.15).

If the axis of the two piers is not aligned with the flow, each pier develops its own horseshoe vortex. Should the distance between the two piles be modest, the two internal arms of the vortex tend to be compressed, thus increasing their vorticity and consequently the erosive capacity.

The experiments carried out by Raudkivi and Sutherland (1981) on a pair of piles set at a distance $a_s = 5D_p$ show that the scour in front of the upstream pier varies very little with the hook angle when the maximum depth values are slightly higher (10−15%) than those observed in an isolated pier (Fig. 8.16).
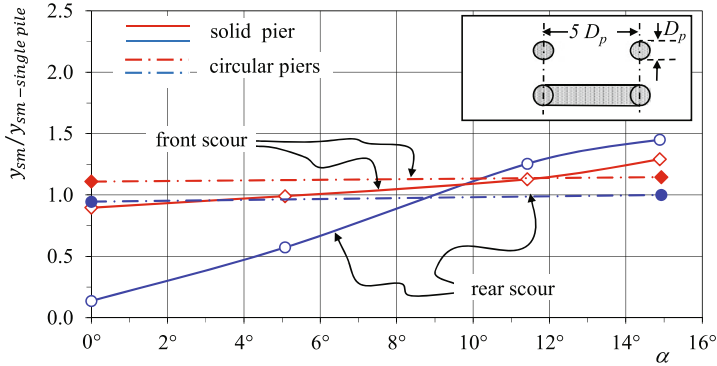
Fig. 8.17 Relative maximum scour depth for two in-line piles as a function of the dimensionless pile spacing and comparison with the equivalent solid pier (Raudkivi and Sutherland 1981)

The scour behind the second pier—which in aligned piers is slightly lower than the isolated pier—proves to increase as the attack angle increases and to reach its maximum value, equal to around 1.2 times the isolated pier, for ($\alpha = 45°$).

Still referring to the misalignment effect, Fig. 8.17 shows the comparison between two piers and one single pier occupying the same space as the two piers.

In case of misalignment to the flow direction, the front scour is slightly lower than that observed in the two in-line piles, while the rear scour is significantly more modest, 0.3 times the equivalent solid pier.

As the attack angle increases, there is an increase of both the front and rear scours, the latter even becomes larger with attack angles of around 8° and is 1.6 times larger than the scour of the solid pier with 15° attack angles.

8.3.3   Time Evolution of Scour

For safety's sake, applications are usually referred to the maximum scour depth in equilibrium conditions. However, in the cases characterized by small sediment mobility the time required to reach equilibrium conditions is much longer than the duration of the design flood. Consequently, the knowledge of the time evolution of the scour is particularly important (Froehlich 1988).

The observations on the time evolution of a local scour derive almost exclusively from laboratory experiments which, often being affected by scale effects, are less reliable when they are transferred into prototypes.

The scouring process can be described by the following relation (Hoffmans and Verheij 1997):

$$\frac{y_s(t)}{y_{sm}} = 1 - e^{\ln\left(1 - \frac{\lambda_z}{y_{sm}}\right)\left(\frac{t}{t_\lambda}\right)^\gamma} \tag{8.40}$$

in which $y_s(t)$ denotes the scour depth at time t; y_{sm}, the equilibrium scour depth ($t \to \infty$); λ_z, a reference length; and t_λ, the time when the scour reaches the value λ, that is $(y_s(t_\lambda) = \lambda_z)$. As for the exponent of Eq. (8.40), the authors suggest to set $\gamma = 0.2 \sim 0.4$.

The scour then proceeds with an exponential law, sometimes for very long periods of time. In the initial phase of the process ($t < t_\lambda$), Eq. (8.40) can be reduced to the following:

$$\frac{y_s(t)}{y_{sm}} = \left(\frac{t}{t_\lambda}\right)^\gamma \tag{8.41}$$

The authors suggest to assume as reference time t_λ the time required by the maximum scour to reach a value equal to the pier diameter:

$$t_\lambda = 29.2 \frac{b}{\sqrt{2}U_o} \left(\frac{\sqrt{g\Delta d_{50}}}{\sqrt{2}U_o - U_c}\right)^3 \left(\frac{b}{d_{50}}\right)^{1.9} \tag{8.42}$$

in which U_o and U_c are, respectively, the average velocity and the critical velocity of incipient motion of the undisturbed flow.

More complete than that is the expression, valid in the absence of upstream sediment transport (*clear water*), suggested by Oliveto and Hager (2002):

$$\frac{y_s(t)}{L_R} = 0.068 K'_{Sf} \sigma_g^{-1/2} \left(\frac{U_o}{\sqrt{g\Delta d}}\right)^{1.5} \log\left(\frac{t\sqrt{g\Delta d}}{L_R}\right) \tag{8.43}$$

Equation (8.43) can also be applied to bridge abutments and the like. L_R is a suitable reference scale, usually represented by the pier diameter D_p or by the abutment width b and, less frequently, by the water depth h_o or by a combination of these sizes with a length dimension:

$$L_R = D_p^\alpha h_o^\beta \quad \text{and} \quad L_R = b^\alpha h_o^\beta \quad \text{with} \quad \alpha + \beta = 1$$

The authors suggest to set $\alpha = 2/3$ and $\beta = 1/3$. K'_{Sf} is a shape factor: $K'_{Sf} = 1$ for circular piers and $K'_{Sf} = 1.25$ for rectangular piers or for abutments.

8.3.4   Design Considerations

As previously pointed out, the topic of local scours is still debated. From a design point of view, it is, therefore, advisable to see to the most disadvantageous conditions, which can be summed up as follows:

- the clear-water situation;
- the reduction effect in case of consistent reduction of the flow section;
- the effect of grain sorting to be neglected unless clearly evident;
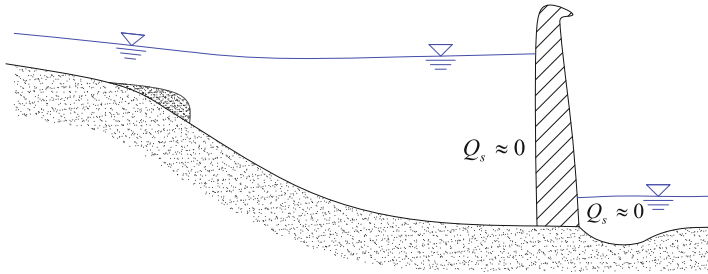
Fig. 8.18 Layout of the morphological process upstream of a dam

- as a precaution, the assumption of the value:

$$y_{sm} = (2.4 \sim 2.5)D_p \qquad (8.44)$$

- the shape effect on the basis of Table 8.2, especially for rectangular piers;
- the effect of any pier misalignment on multiple or non-circular piers;
- the sediment dimension assigned to the artificial armoring, if any, to be calculated with the Shields criterion applied to a bed shear stress τ_{max}, evaluated as:

$$\tau_{max} = 4\tau_o \qquad (8.45)$$

8.4 Local Scour Downstream of Structures

In general, falling jets downstream of some hydraulic structures (drops, check dams, sills, overfalls, spillways) or horizontal jets parallel to the bed (outflows downstream an open sluice gate, or an apron) induce extensive localized excavations caused by at least three mechanisms.

The first mechanism consists in the fact that very often upstream of these works the flow is so slowed to lose its transport capacity: the outgoing solid discharge is very small, or even null. This situation often occurs on the fluvial dams and barrages, in which the structures cause a backwater profile upstream of them. As schematically depicted in Fig. 8.18, and as it results from the analysis of the equation of conservation of the solid mass (Eq. 7.7 on page 135), these conditions induce a deposition process which, due to the reduced transport capacity of the incoming flow, evolves very slowly. In this case, the bed configuration upstream of the structure can be assumed as quasi-permanent within relatively long time intervals.

On the contrary, downstream of the structure the flow generally has a higher velocity and consequently a higher erosive capacity, thus triggering scour phenomena which tend to evolve over time if not inhibited, or be greatly slowed by possible self-armoring phenomena (see Sect. 3.3.6).
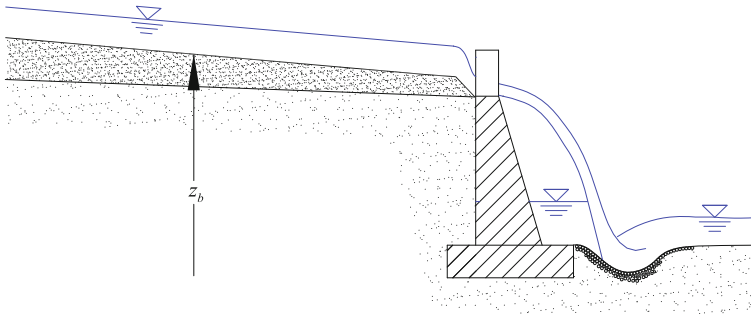
Fig. 8.19 Layout of the morphological process upstream of a check dam

A second mechanism triggering the local scour downstream a weir or a low-head dam or a drop is determined by the geometry of the flow field, represented by a plunging jet inclined with respect to the horizontal bed, as schematized in Fig. 8.19.

This is also the case of a check dam in mountain streams. Unlike the previous case, the morphologic adjustment processes are much faster, because of the more intense sediment transport rate.

In these cases, the morphological equilibrium is often rapidly achieved, especially during the single flood events. It means that the sediment flow rate is almost constant in the flow direction: we can assume the flow as a succession of uniform flows with the free surface almost parallel to the bed. The solid flow rate discharged by the structure in these conditions is significant (Armanini and Larcher 2001).

The third mechanism generating local scours occurs downstream a sluice gate or downstream an apron, induced either by the roughness variation or by strong velocity gradients like for jets issued from the vertical gate. In this situation, an erosion occurs immediately downstream of the apron. The initial erosion causes the flow direction to shift and deepen the scour up to an equilibrium condition. The flow field in equilibrium condition generally shows an extended region of flow separation with an intense recirculation area (Fig. 8.21).

8.4.1 Scour Produced by an Overfall Jet

As previously underlined, the impact of a jet overflowing a drop structure or a spillway tends to cause a localized erosion on the bed downstream of the structure.

Also in this case, a precise analytical prediction of the maximum scour is rather complicated. Instead, there are empirical formulae, beginning from the pioneering Schoklitsch (1932) equation that is widely used still today:

$$y_{sm} = 4.75 \frac{(h_u - h_d)^{0.2} q^{0.57}}{d_{90}^{0.32}} - h_d \tag{8.46}$$
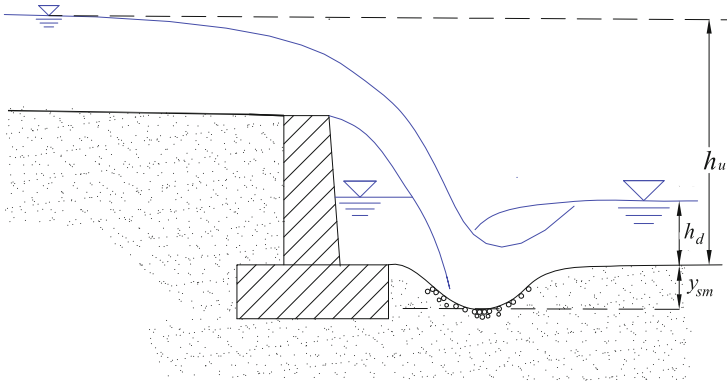
Fig. 8.20 Layout of the erosion downstream of a drop or a check dam

Table 8.3 Coefficients and exponents to utilize in Eq. (8.47) according to different authors. The different sizes (including d_{90}) are expressed in [MKS]; thus, c_w is in m$^{(1+m_3-m_1-2m_2-m_4)}$ s$^{-m_2}$]

	c_w	m_1	m_2	m_3	m_4
Schoklitsch (1932)	0.52	0.2	0.57	0.32	0
Veronese (1937)	0.2	0.225	0.54	0.42	0
Müller and Eggenberger (1944)	1.44	0.5	0.6	0.40	0
Mason and Arumugam (1985)	3.27	0.05	0.6	0.40(*)	0.15

(*) It refers to the mean diameter $\overline{d}$, and not to d_{90}

In the non-dimensionless relation, whose symbols are defined in Fig. 8.20, the height is expressed in meters, the bed sediment diameter, d_{90}, in [mm], the capacity per width unit q in [m^3/s/m].

The height difference between the upstream and downstream free surface levels $(h_u - h_d)$ is often replaced by the head difference, thus comprising the difference between the kinetic loads.

Other relations similar to Schoklitsch's have been proposed, e.g., by Veronese (1937), Müller and Eggenberger (1944), and Mason and Arumugam (1985):

$$y_{sm} = c_w \frac{(h_u - h_d)^{m_1} q^{m_2}}{d_{90}^{m_3}} h_d^{m_4} - h_d \qquad (8.47)$$

whose exponents and coefficients are shown in Table 8.3.

While the other formulae of Table 8.3 have been obtained from reduced-scale model tests, Mason and Arumugam (1985) verified their formula also on a prototype
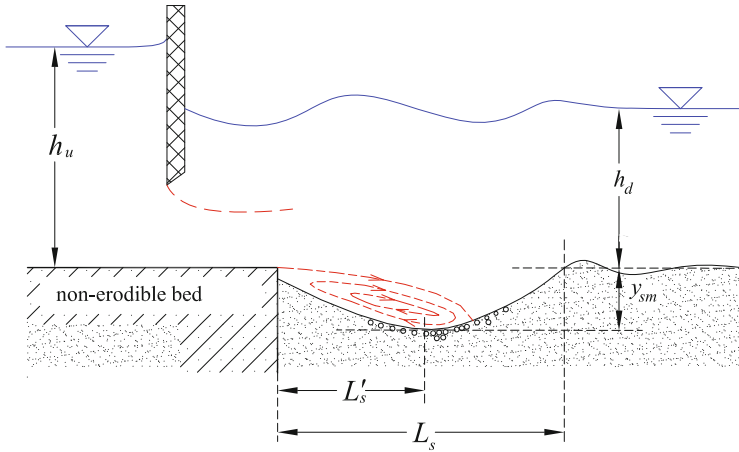
Fig. 8.21 Layout of erosion downstream of an outflow discharge

and found that the coefficient is better expressed as ($c_w = 6.42 - 3.1(h_u - h_d)^{0.1}$). The authors regard it as valid also for scours under jets, such as issues from a free dam, and *flip buckets*. Particularly, Meyer-Peter and Müller (1948) formula can be rewritten in a dimensionless form:

$$\frac{y_{sm}}{h_d} = -1 + \frac{3.6}{\Delta^{4/9}} \left(\frac{U_d}{g d_{90}} \right)^{0.3} \left(\frac{h_u}{h_d} - 1 \right)^{0.5} \left(\frac{h_d}{d_{90}} \right)^{0.1} \tag{8.48}$$

When the erosion formulae are applied downstream of dams, the maximum scour should be increased of $0.5-0.6$ m as a factor of safety.

8.4.2   Erosion Downstream of a Sluice Gate Opening

A type of erosion similar to the previous one is that induced by a horizontal jet issuing from a sluice gate opening on a mobile bed. The situation is sketched in Fig. 8.21. As depicted in the figure, in order to reduce the erosion, a non-erodible-bed protection is often inserted immediately downstream the gate to smooth the transition between the non-erodible and movable bed of the channel.

In this case, it is worth distinguishing between submerged jets and free jets, the latter situation being much more dangerous. In both cases, the scour is initially induced by the modified conditions between the non-erodible bottom and the mobile bed, mostly by the acceleration below the gate which makes the actual sediment transport rate of the outgoing flow much less than the sediment transport capacity of the whole flow. However, also the change of the roughness between the protection and the erodible bed has a certain influence on the erosion process.

Table 8.4 Coefficients and exponents to utilize in Eq. (8.49) according to various authors. The lengths (including d_{90}) are in [m], q in [m^{2}s^{-1}], c_w in [m$^{(1+m_3-m_1-2m_2-m_4)}$s$^{-m_2}$]

	c_w	m_1	m_2	m_3	m_4
Submerged jet					
Müller and Eggenberger (1944)	0.65	0.5	0.6	0.40	0
Mason and Arumugam (1985)	3.27	0.05	0.6	0.40(*)	0.15
Qayoum (1960)	2.78	0.22	0.4	0.22	0.4
Free jet					
Müller and Eggenberger (1944)	0.97	0.5	0.6	0.40	0

(*) It refers to the mean diameter $\overline{d}$, and not to d_{90}

The scour initiates immediately downstream the bed protection and rapidly develops up to form a flow separation region with kinematic characteristics more similar to the free turbulence (two-dimensional wall jet) than to the wall turbulence (Adami 1979).

Also in this case, there are a good number of detailed numerical analyses of the phenomenon, but they are quite complex tools and the results provided are not synthetic enough to be used in the design phase of the structures. In order to estimate the maximum scour depth, also in this case, expressions similar to (8.47) valid in the absence of the apron, are often adopted:

$$y_{sm} = c_w \frac{(h_u - h_d)^{m_1} q^{m_2}}{d_{90}^{m_3}} h_d^{m_4} - h_d \tag{8.49}$$

The exponents and coefficients suggested by different authors are shown in Table 8.4.

For its historical value, it is worth mentioning one formula of Schoklitsch (1932) expressed in MKS, which does not include the sediment diameter:

$$y_{sm} = 2.15a + 0.378(h_u - h_d)^{0.5} q^{0.35} \tag{8.50}$$

a denotes the difference between the elevation of the downstream bed and that of the apron. In case of submerged jets, Graf and Altinakar (1998) suggested the following expressions for the longitudinal dimension of the scour, experimented in the absence of the apron:

$$L_s' \simeq 3(y_{sm} + h_d) \quad \text{and} \quad L_s \simeq (5 \sim 7)(y_{sm} + h_d) \tag{8.51}$$

Fig. 8.22 Layout of erosion downstream of the combined effect of a headflow and an outflow jet
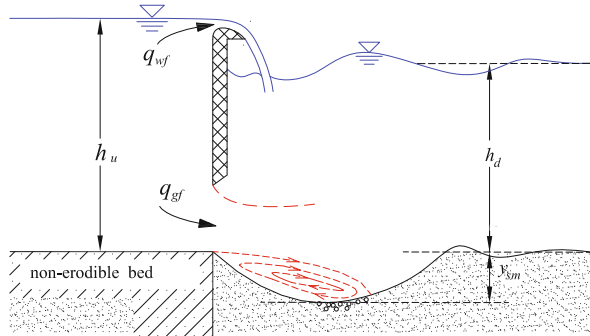
By analyzing the phenomenon, Adami (1979) observed that the asymptotic configuration of the scour profile upstream of the maximum scour section shows a similar geometry independently of the kinematic parameters. The scour shape downstream of the maximum depth point can have two layouts:

- if the mobility of the undisturbed flow downstream the reach is lower than the incipient critical mobility, the scour ends with a dune (Fig. 8.22) whose height depends on the difference between the undisturbed velocity and the incipient motion velocity;
- if, on the contrary, the water velocity is higher than that of incipient motion, downstream of the maximum depth point, the bed tends to increase monotonically up to the downstream undisturbed bed elevation. It goes without saying that in this case equilibrium conditions can be reached only in the presence of upstream sediment supply.

8.4.3   Combined Overflow and Underflow from a Gate Opening

Very often downstream of weirs or at low dams, especially in flood conditions, we find the combined effect of head- and outflow.

Such a complex case was studied by Müller (1944), who thought Eq. (8.49) by Müller and Eggenberger (1944) to be also suitable for this configuration:

$$y_{sm} = c_w \frac{(h_u - h_d)^{0.5} q^{0.6}}{d_{90}^{0.4}} - h_d \qquad (8.52)$$

in which the coefficient c_w is made dependent on the relationship between the outflowing discharge q_{wf} and the head overflow q_{gf}, according to Table 8.5.

Here, the d_{90} is expressed in [mm] and the discharge per width unit q is expressed in [m^3/s/m].

Table 8.5 Values of the coefficient c_w in Eq. (8.52), as a function of the ratio q_{wf}/q_{gf} between the headflow and outflow discharges

q_{gf}/q_{wf}	2	3	4	∞
c_w	6.3	6.9	7.7	10.4

8.5   Groyne Head Scours

The groynes are riverbank structures that project into the river, inclined with respect to the flow direction, which are built to protect the riverbank from erosion or to improve the river navigability.

The distance between two successive groynes must be such as to generate a secondary circulation with vertical axis between the two groynes (Fig. 8.23), which prevents the main flow of the river (the thalweg) from impacting the bank. The reduction in velocity in these areas (*groyne fields*) tends to favor the sedimentation of the finest material arriving there through a mechanism of lateral turbulent diffusion.

Quite clearly, in order to protect a riverbank the groynes must be placed at least in pairs, but more frequently they are in groups of more than two.

Groynes can be seen as constrictions of the transverse section, and consequently, they accelerate the flow and concentrate the main flow triggering a local erosion.

Groynes are, therefore, structures that cause the bed to deepen near the main flow bed, associated with a local scour near their heads. These local scours are similar to those produced by the bridge abutments described in Sect. 8.2.3.

The parameters that mostly affect the local scour near to the groyne heads are the orientation of the groyne with respect to the main flow direction (e.g., *normal*, *convergent* or *deflecting groynes* as sketched in Figs. 8.23 and 8.24), the groyne shape, and especially the inclination of the side slope of the groyne head. The curvature of the bend and the groynes' position inside the curve also influence the maximum excavation, even if to a lesser extent.

The same methodologies applied to the bridge abutment can be used for the scouring mechanisms induced by groynes on the bed, that is, the action due to the

Fig. 8.23 Layout of flow near groynes, oriented normally to the riverbank
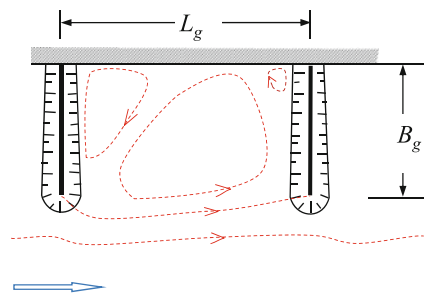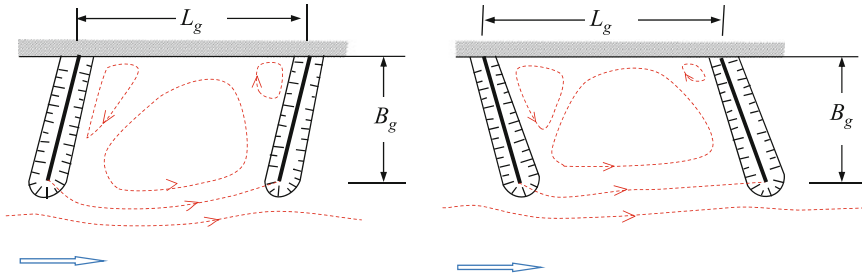
Fig. 8.24 Layouts of various groynes. Left: divergent groynes, pointing upstream. Right: deflecting groynes, pointing downstream
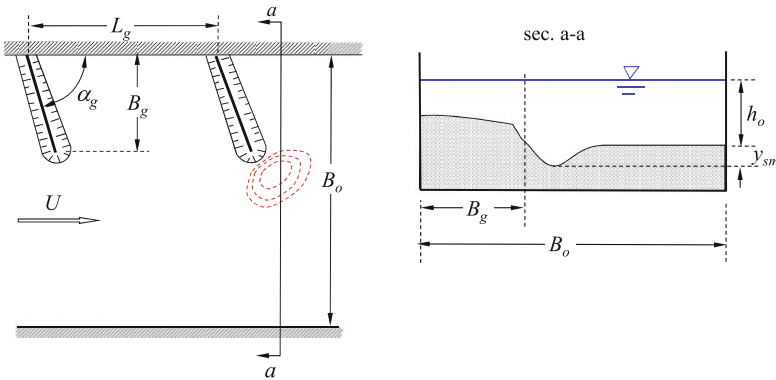
Fig. 8.25 Definition sketch of groyne scours

section contraction treated with Eq. (8.16) or (8.17) on page 177, and the action concentrated on the groyne head mainly imputable to secondary circulations.

Systematic studies on the local scour at the groyne head have been carried out since the 1950s (Inglis 1949; Ahmad 1953; Laursen 1962; Laursen et al. 1963; Richardson et al. 1975). All these formulations are basically empirical. Studies based on the numerical integration of the differential equations of the flow, together with the application of two-equation turbulence models, have been proposed in the last few years.

However, their complexity makes these schemes unsuitable for the design of proper structures. Therefore, the empirical formulations are still the most valid for immediate use. Following Ahmad (1953), we can write (Fig. 8.25):

$$y_{sm} + h_o = K_g \left(\frac{Q}{B_o - B_g} \right)^{2/3} \tag{8.53}$$

in which the lengths are expressed in [m] and the discharge in [m^3/s]. K_g proves to depend on the slope angle α_g and shape of the groyne, as well as on its position to

Table 8.6 Parameter K_1 in formulae (8.53) and (8.54), concerning the orientation of the groyne with respect to the flow direction

α_g	30°	45°	60°	90°	120°	150°
K_1	0.8	0.9	0.95	1.00	1.05	1.1

Table 8.7 Parameter K_2 in formulae (8.53) and (8.54) concerning the effect of the inclination of the side slope of the groyne head

Groyne shape	K_2
Vertical side walls	1.0
45° sloped side walls	0.85

Table 8.8 Parameter K_3 in formulae (8.53) and (8.54) concerning the effect of the inclination of the side slope of the groyne head

Groyne position in the bend	K_3
In rectilinear channels	1.0
On the concave bank	1.1
On the convex bank	0.8
On the concave bank toward the end of the bends:	1.1
• in moderately wide bends	1.1
• in narrow bends	1.4

the flow axis. It then results by multiplying three parameters:

$$K_g = 2K_1 K_2 K_3 \tag{8.54}$$

K_1, K_2, and K_3 are specified in Tables 8.6, 8.7, and 8.8, respectively.

Analogous to Ahmad's formulation is the expression proposed by Richardson et al. (1975) regarding the local scour near the groyne head, which is to be added to the constriction increase assessable with Eq. (8.16) or Eq. (8.13):

$$y_{sm} = 1.1 \, h_o \left(\frac{B_g}{h_o} \right)^{0.4} F_{ro}^{1/3} \quad \text{for} \quad \frac{B_g}{h_o} < 25$$

$$y_{sm} = 4 \, h_o F_{ro}^{1/3} \quad \text{for} \quad \frac{B_g}{h_o} > 25 \tag{8.55}$$
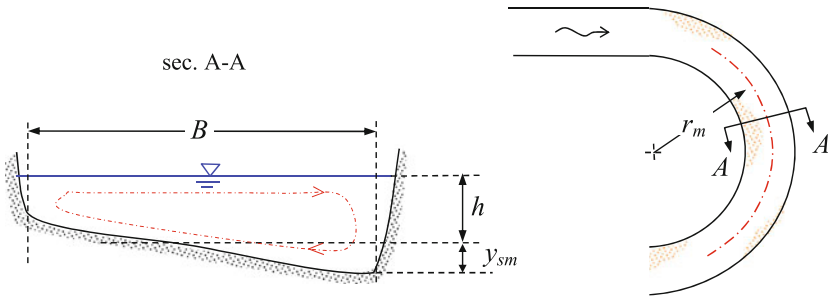
Fig. 8.26 Layout of local scours at the outer riverbank

8.6   Bend Scour

As previously said, in a channel flow bend we can observe the formation of secondary circulations, triggering shear stresses to the bed in the radial direction (Eq. 3.37 on page 67). These radial stresses induce a sediment transport in the radial direction from the outer bank toward the inner. In stationary conditions, an equilibrium bed configuration is then reached with a channel deepening near the outer bank.

In the literature, various expressions have been proposed to estimate the maximum scour depth in bends. Among these, the empirical formula proposed by Thorne et al. (1995) is of some use. This formula, however, does not make the scour directly dependent on either the grain size or on the kinematic conditions of the flow

$$\frac{y_{sm}}{h} = 1.07 - \log\left(\frac{r_m}{B} - 2\right) \tag{8.56}$$

The symbols are defined in Fig. 8.26.

The formulation is valid for $2 < r_m/B < 22$ and has been verified for grain sizes ranging between 0.3 and 17 mm and water depths up to 17 m.

An analogous relation was proposed by Maynord (1996). It is thought to be suitable for sandy beds, but it tends to overestimate the scour in gravel river beds.

$$\frac{y_{sm}}{h} = 0.8 - 0.051\frac{r_m}{B} + 0.0084\frac{B}{h} \tag{8.57}$$

The formulation was inferred by field observations on erosions due to floods with a return period less than 5 years. It is valid for $1.5 < r_m/B < 10$ and $20 < B/h < 125$.

An analytical expression of the maximum scour in a bend can also be obtained by applying the equilibrium theory of a particle on the outer bank of a curve (NEDECO 1959), already dealt with in Sect. 3.5.1 on the incipient motion (page 66). In this case, the bank slope is written as its local gradient, $\sin \alpha_l = -\partial h/\partial r$. By integrating the
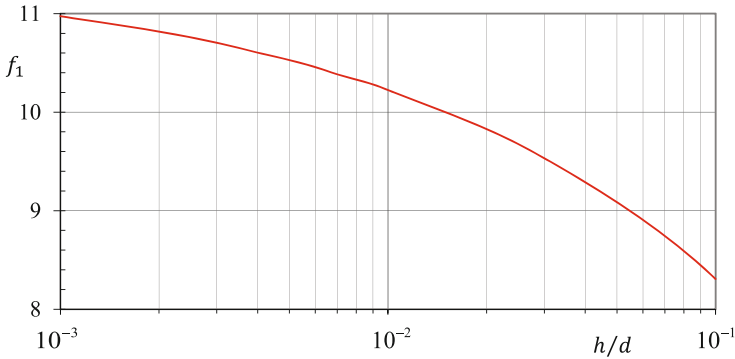
Fig. 8.27 Function f_1 of formula (8.60) for the maximum scour depth in curve (Seminara and Tubino 1989)

ensuing differential equation we obtain the bed profile in the bend:

$$\frac{1}{h} - \frac{1}{h_e} = \left(\frac{1}{r} - \frac{1}{r_e}\right) 1.5 A_\tau \frac{i_e r_e}{\Delta d} \tag{8.58}$$

h and h_e, respectively, denote (see Fig. 8.26) the water depths in the generic point and at the extrados; r and r_e the curvature radii of the curve in the generic point and at the extrados; and i_e is the longitudinal bed slope at the extrados. The authors assume that the product $i_r r = i_e r_e$ is constant along the radial direction. According to this hypothesis, the maximum scour at the extrados can be obtained from (8.58) as follows

$$\frac{y_{sm}}{h} = 3 A_\tau \frac{B}{r_m} \theta \frac{1}{\dfrac{4 r_m + 2 B}{r_m} - 3 A_\tau \dfrac{B}{r_m} \theta} \tag{8.59}$$

where $\theta = u_*^2/(g \Delta d)$ is the mobility parameter of the undisturbed flow. The parameter A_τ assumes values ranging between 7.30 and 8.16 for channel flows with sufficiently high Reynolds numbers, as underlined in Sect. 3.5.1 on page 67.

A similar expression, again inferred theoretically and valid for channels with a modest curvature and for uniform particle sizes, was proposed by Seminara and Tubino (1989):

$$\frac{y_{sm}}{h} = \frac{B}{r_m} \theta^{0.5} f_1 \tag{8.60}$$

the function f_1 depending on the relative roughness d/h is illustrated in Fig. 8.27.

The function f_1 can be approximated with the following expression:

$$f_1 = 12.716 - 65.658 \left(6 + 2.5 \ln \frac{h}{2.5d}\right)^{-1.2} \tag{8.61}$$
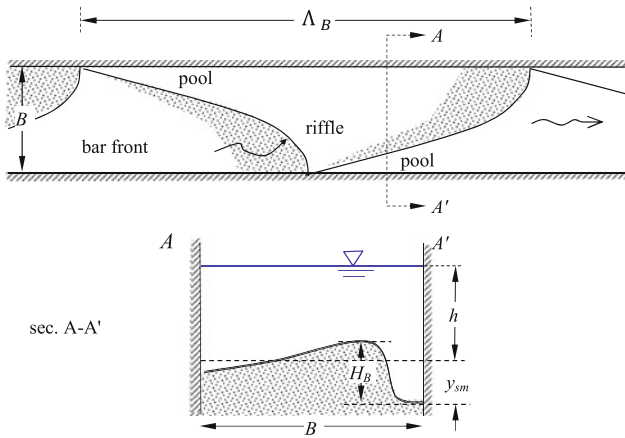
Fig. 8.28 Layout of an alternate bar (Ikeda 1984)

According to Seminara and Tubino (1989), should the curvature radius not be constant, the value of the maximum scour can be of an order of magnitude higher than that obtained with formulae (8.60) and (8.59) based on the local value of the curvature radius. The maximum scour depends on the intrinsic wavelength of the meander: the highest scour values are obtained with meanders of length between 10 and 15 times the channel width.

8.7   Bar Scours

The alternate bars are planar bed forms, which can be observed in sand or gravel bed rivers in their whole length.

In rectilinear or quasi-rectilinear channels, bars can slowly migrate downwards. Bars are planar forms with a vaguely semi-parabolic shape, as schematized in Fig. 8.28, with a steep front and a shallow-water lobe downstream. In the region near the bar tail, opposite the front, we can identify the area where the maximum scour depth is reached. Bars are quite important from the ecological viewpoint especially in low water conditions, in that the main wave flows along sections with a relatively high velocity (*chuts* or *riffles*), followed by others characterized by lower velocity (*pools*), thus favoring the habitat diversity and biodiversity.

The problem of the existence of river bars was theoretically dealt with by Colombini et al. (1987), by utilizing a perturbation technique for the weakly nonlinear flow equations. They showed the existence of stable perturbation modes in the river bed which can be assimilated to alternate bars.

According to this criterion, the conditions for incipient bar formation depend on the Shields mobility parameter $\theta = u_*^2/(g \Delta d)$ and on the relative roughness d/h.
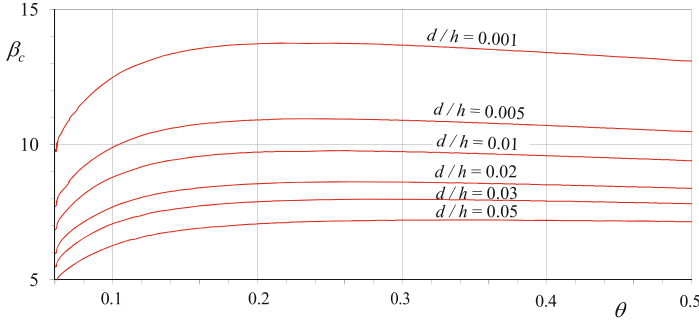
Fig. 8.29 Threshold level β_c of the semi-aspect ratio $\beta = B/2h$ for the existence of alternate bars in a rectangular channel (Colombini et al. 1987)

The parameter is the ratio $\beta = B/2h$ (*semi-aspect ratio*) between the half channel width $B/2$ and the water depth h. The existence condition is shown in Fig. 8.29 where β_c denotes the critical minimum value of the ratio $B/2h$ below which bars do not form.

The calculation of the maximum scour at the bar pool can be made through a series of experimental expressions provided by Ikeda (1984) concerning bar dimensions:

$$\Lambda_B = 5 \left(\frac{B\,h}{c_f} \right)^{0.5} \quad \text{for} \quad Fr < 0.8 \tag{8.62}$$

$$\frac{\Lambda_B}{B} = 181 c_f \left(\frac{B}{h} \right)^{0.55} \quad \text{for} \quad Fr > 0.8 \quad \text{and} \quad 4 < \frac{B}{h} < 70 \tag{8.63}$$

$$\frac{H_B}{h} = 0.0442 \left(\frac{B}{h} \right)^{1.45} \left(\frac{h}{d_{50}} \right)^{-0.45} = 0.0442 \left(\frac{B}{d_{50}} \right)^{-0.45} \left(\frac{B}{h} \right)^{1.9} \tag{8.64}$$

$$y_{sm} = 0.75\, H_B \tag{8.65}$$

where Λ_B and H_b denote the wavelength and total height of the bar, and c_f is the friction coefficient to be calculated through an adequate uniform flow formula. For instance,

$$c_f = \frac{ghi}{U^2} = \frac{g}{\chi^2} \tag{8.66}$$

in function of the Chézy friction coefficient. Alternatively, Ikeda (1983) also suggests the following logarithmic expression:

$$c_f = \left(\frac{1}{\kappa} \ln(11\, \frac{h}{2\,d_{90}}) \right)^{-2} \quad \text{valid for} \quad \frac{h}{d_{90}} \gg 1 \tag{8.67}$$

Equation (8.67) can be approximated by the following:
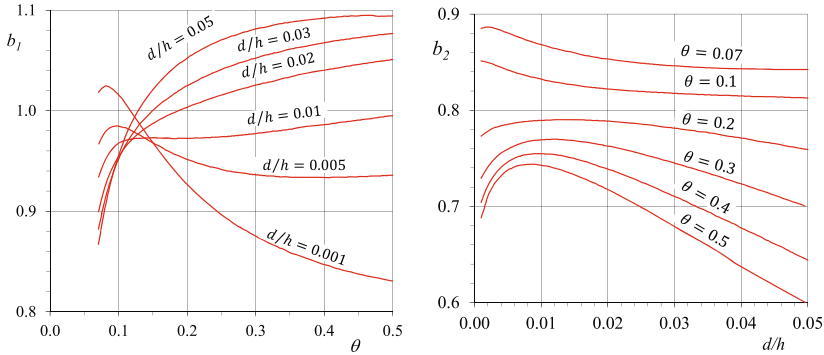
Fig. 8.30 Values of coefficients b_1 and b_2 to be inserted into Eq. (8.69) (Colombini et al. 1987)

$$c_f \simeq 0.0293 \left(\frac{h}{d_{90}}\right)^{-0.45} \tag{8.68}$$

Always according to Ikeda (1983), the presence of alternate bars produces an increase in the friction coefficient by about 20%, compared to the coefficient assessed with expression (8.67) or (8.68).

Also Colombini et al. (1987) proposed a theoretical expression for the maximum scour depth at a bar:

$$H_B = h \left(b_1 \left(\frac{\beta - \beta_c}{\beta_c}\right)^{1/2} + b_2 \left(\frac{\beta - \beta_c}{\beta_c}\right) \right) \tag{8.69}$$

where b_1 and b_2 are two coefficients depending on the mobility parameter θ and the relative roughness d/h after Fig. 8.30.

The maximum scour depth results to be:

$$y_{sm} = 0.57 \, H_B \tag{8.70}$$

For very large beds ($B > \sim 35h$), Ikeda (1984) observed the formation of multiple bars, which can be interpreted as a precursor to braiding.

References

A. Adami, Fenomeni localizzati ed erosione degli alvei, in *Atti del seminario: Moderne vedute sulla meccanica dei fenomeni fluviali* (Istituto di Idraulica dell'Univesrità di Padova, 1979)

M. Ahmad, Experiments on design and behavior of spur dikes, in *Proceeding of International Hydraulic Convention, ASCE, New York*. (ASCE, 1953), pp. 145–159

A. Armanini, M. Larcher, Rational criterion for designing opening of slit-check dam. J. Hydraul. Eng. **127**(2), 94–104 (2001)

V. Basak, Y. Baslamisli, O. Ergun, Local scour depths around circular pier groups aligned with the flow. Report (1977) p. 641

M. Bonasoundas, Strömungsvorgang und Kolkproblem am Pfeiler, in *Versuchsanstalt für Wasserbau* (Technischen Universität München, Oskar von Miller Institut, Bericht, 1973), p. 28

H. Breusers, *Conformity and Time Scale in Two-Dimensional Local Scour* (Delft Hydraulics Laboratory Delft, The Netherlands, 1965)

H. Breusers, A.J. Raudkivi, *Scouring* (Balkema Rotterdam, 1991)

H. Breusers, G. Nicollet, H. Shen, Local scour around cylindrical piers. J. Hydraul. Res. **15**(3), 211–252 (1977)

J. Chabert, P. Engeldinger, *Etude des affouillements autour des piles des ponts* (Laboratoire National d'Hydraulique, Chatou, France, 1956)

M. Colombini, G. Seminara, M. Tubino, Finite-amplitude alternate bars. J. Fluid Mech. **181**, 213–232 (1987)

D.C. Froehlich, Analysis of onsite measurements of scour at piers, in *Hydraulic Engineering: Proceedings of the 1988 National Conference on Hydraulic Engineering* (1988) pp. 534–539

W.H. Graf, M. Altinakar, *Fluvial Hydraulics: Flow and Transport Processes in Channels of Simple Geometry* (1998)

G.J. Hoffmans, H. Verheij, *Scour Manual*, vol. 96 (CRC Press, 1997)

S. Ikeda, Migration of alternate bars in straight channels. Rep. Dept. Found. Eng. Const. Eng. (13), 83–95 (1983)

S. Ikeda, Prediction of alternate bar wavelength and height. J. Hydraul. Eng. **110**(4), 371–386 (1984)

C.C. Inglis, *The Behaviour and Control of Rivers and Canals* (Yeravda Prison Press, 1949)

P.A. Johnson, Reliability-based pier scour engineering. J. Hydraul. Eng. **118**(10), 1344–1358 (1992)

E.M. Laursen, Scour at bridge crossings. Trans. Am. Soc. Civ. Eng. **127**(1), 166–179 (1962)

E.M. Laursen, A. Toch, *Scour Around Bridge Piers and Abutments*, vol. 4 (Iowa Highway Research Board Ames, IA, USA, 1956)

E.M. Laursen et al., An analysis of relief bridge scour. J. Hydraul. Div. ASCE **92**, 93–118 (1963)

P.J. Mason, K. Arumugam, Free jet scour below dams and flip buckets. J. Hydraul. Eng. **111**(2), 220–235 (1985)

S.T. Maynord, Toe-scour estimation in stabilized bendways. J. Hydraul. Eng. **122**(8), 460–464 (1996)

B. Melville, Local scour at bridge abutments. J. Hydraul. Eng. **118**(4), 615–631 (1992)

E. Meyer-Peter, R. Müller, Formulas for bedload transport, in *Proceedings of the 2nd Meeting of the International Association for Hydraulic Structures Research*, vol. 133 (IAHS, 1948), pp. 39–64

R. Müller, Die Kolkbildung beim reinen Unterströmen und allgemeinere Behandlung des Kolkproblems. *Mitt. der Versuchsanstalt für Wasserbau an der ETH*, vol. 5 (1944), pp. 12–15

R. Müller, W. Eggenberger, Experimentelle und theoretische Untersuchungen über das Kolkproblem. *Mitt. Versuchanstalt für Wasserbau an der ETH*, vol. 5 (1944)

NEDECO, *River Studies and Recommendations on Improvement of Niger and Benue [With illustrations, diagrams and maps]* (North Holland Publishing Company, 1959)

C. Neill, *Local Scour Around Bridge Piers* (Highway and River Engineering Division, Research Council of Alberta, Alberta, Canada, 1964)

G. Oliveto, W.H. Hager, Temporal evolution of clear-water pier and abutment scour. J. Hydraul. Eng. **128**(9), 811–820 (2002)

A. Qayoum. *Die Gesetzmäßigkeit der Kolkbildung hinter Unterströmten Wehren unter spezieller Berücksichtigung der Gestaltung eines beweglichen Sturzbettes* (Leichtweiß-Inst. f. Wasserbau u. Grundbau, Techn. Hochschule Braunschweig, 1960)

A. Raudkivi, R. Ettema, Effect of sediment gradation on clear water scour. J. Hydraul. Div. Am. Soc. Civ. Eng. **103** (1977)

A. Raudkivi, A.J. Sutherland, Scour at bridge crossings. Technical report (1981)

E. Richardson, M. Stevens, D. Simons, The design of spurs for river training, in *Proceeding of the 15th Congress of the International Assosiation for Hydraulic Research, IAHR, Basil*, vol. 2 (1975), pp. 382–388

A. Schoklitsch, Kolkbildung unter Überfallstrahlen. Die Wasserwirtsch. **24**, 341–343 (1932)

G. Seminara, M. Tubino, Alternate bars and meandering, in *River Meandering*. Water Resources Monograph (1989), pp. 267–320

H.W. Shen, V.R. Schneider, S. Karaki, Local scour around bridge piers. J. Hydraul. Div. (1969)

L.G. Straub, Approaches to the study of the mechanics of bed movement, in *Proceedings of the Hydraulics Conference, State University of Iowa* (1940)

C.R. Thorne, S. Abt, S. Maynord, Prediction of near-bank velocity and scour depth in meander bends for design of riprap revetments, in *River; Coastal and Shoreline Protection: Erosion Control Using Riprap and Armourstone* (1995), pp. 115–133

L. Tison, Erosion autour de piles de ponts en rivière. Ann. Trav. Publ. Belg. **41**, 813–817 (1940)

A. Veronese, Erosion de fond en aval d'une decharge, in *IAHR, Meeting for Hydraulic Works* (Berlin, 1937)

Index

213